

الجمهورية الجزائرية الديمقراطية الشعبية

République Algérienne Démocratique et Populaire

Ministère de L'Enseignement Supérieur et de la Recherche Scientifique



UNIVERSITÉ FERHAT ABBAS – SETIF-1

FACULTÉ DE TECHNOLOGIE

THÈSE

Présentée au Département de Génie des Procédés

Pour l'obtention du diplôme de

DOCTORAT

Domaine : Sciences et Technologie

Filière: Génie des Procédés

Option: Génie Chimique

Par

GUEDIRI ABDERRAOUF

THÈME

Optimisation de la synthèse de nouveaux matériaux : application à l'élimination des polluants organiques

Soutenue le 23/06/2022 devant le Jury:

GUELLAL Messaoud	Professeur	Univ. Sétif 1	Président
BOUGUETTOUCHA Abdallah	Professeur	Univ. Sétif 1	Directeur de thèse
CHEBLI Derradji	Professeur	Univ. Sétif 1	Co-Directeur
RIDA Kamel	Professeur	Univ. Jijel	Examineur
BOUREMMAD-BOUDJERDA Farida	Professeur	Univ. Jijel	Examineur

Catalogue

Catalogue

<i>Acknowledgement</i>	<i>I</i>
<i>Nomenclatures</i>	<i>II</i>
<i>List of figures</i>	<i>IV</i>
<i>List of tables</i>	<i>VIII</i>
<i>General introduction</i>	<i>1</i>
<i>References</i>	<i>6</i>

Chapter I: Bibliography

<i>1. Introduction</i>	<i>8</i>
<i>2. What does mean dye?</i>	<i>8</i>
<i>3. Dyes classification</i>	<i>8</i>
3.1. Azo dyes	<i>10</i>
<i>4. Health risk assessment on dyes</i>	<i>11</i>
4.1. Allergies from dyes:.....	<i>11</i>
4.2. Aquatic toxicity:	<i>11</i>
<i>5. Different ways for water decolorization</i>	<i>12</i>
<i>6. Low-cost adsorbents</i>	<i>13</i>
6.1. Adsorbent resources	<i>14</i>
6.1.1. Natural adsorbent.....	<i>14</i>
6.1.2. Industrial wastes	<i>15</i>
6.1.3. Agricultural and food wastes as adsorbents	<i>15</i>
6.1.3.1. Why should we use agricultural (food) wastes?	<i>16</i>
<i>7. Composite materials as alternative adsorbents</i>	<i>17</i>
7.1. Encapsulation history	<i>18</i>
7.2. Alginate as an encapsulating agent	<i>18</i>
7.3. Encapsulation methods	<i>20</i>
7.3.1. Encapsulation mechanism using alginate sodium through ionic gelation technique	<i>21</i>

Catalogue

7.3.1.1. External encapsulation	21
7.3.1.2. Internal encapsulation	22
7.4. Encapsulation benefits	22
8. Factors affecting adsorption of dye	22
8.1. Initial dye concentration	23
8.2. Initial solution pH.....	23
8.3. Effect of the pore volume of the adsorbent	24
8.4. Temperature effect	24
8.5. Ionic strength.....	24
8.6. Contact time effect.....	25
9. Molecular modeling for adsorption.....	25
10. References	25

Chapter II: Experimental protocols and analytical methods

1. Introduction.....	35
2. Materials and methods	35
2.1. Materials.....	35
2.2. Preparation of the adsorbents.....	36
2.2.1. Powdered adsorbent preparation	36
2.2.2. Beads adsorbent preparation (encapsulation).....	36
2.3. Materials characterization	37
2.4. Adsorption study	38
2.5. Kinetic adsorption	38
2.6. Adsorption isotherms	39
2.7. Initial pH effect on the MB adsorption	41
2.8. Effect of NaCl and Humic Acid on the MB adsorption.....	41
2.9. Effect of temperature and thermodynamic Parameters.....	41
2.10. Regeneration study of BZJS and BOP	41
3. Theoretical study	42
3.1. Density Function Theory (DFT) details	42
3.2. Molecular Dynamic Simulation (MDS) details.....	42
4. Statistical physical modeling	43

Catalogue

4.1. Monolayer model with single energy: MMSE	43
4.2. Monolayer model with two energies: MMTE	44
4.3. Double layer model with two energies: DMTE.....	44
4.4. Limited multilayer model (LMM)	45
4.5. Statistical physical modeling evaluation parameters	45
5. References	46

Chapter III: Insights on the statistical physics modeling of the methylene blue adsorption onto Ziziphus jujuba stones-treated ortho-phosphoric acid

1. Introduction.....	51
2.1. Materials characterization	52
2.2. Effect of the pH.....	56
2.3. Effect of the contact time and the initial concentration	57
2.4. Isotherms modeling	58
2.5. Kinetics modeling	61
2.6. Effect of the Temperature	63
2.7. Effect of the ionic strength and the humic acid on adsorption of MB onto ZJS-H ₃ PO ₄	63
3. Statistical physics models	64
3.1. Steric interpretation	65
3.1.1. Parameter n_m	65
3.1.3. Parameter Q_0	66
3.2. Energetic interpretation.....	67
4. Conclusion.....	67
7. References	68

Chapter IV: Molecular Dynamic Simulation and DFT computational studies on the adsorption performances of Methylene Blue in aqueous solutions by Orange peel-modified phosphoric acid

1. Introduction.....	74
2. Results and discussion.....	75
2.1. Materials Characterization	75
2.1.1. Physicochemical characterization of OP-H ₃ PO ₄	80
2.2. Initial Concentration and Contact Time effects	80

Catalogue

2.3. Kinetics modeling	81
2.4. Isotherms modeling	83
2.5. Orange peels as an adsorbent.....	85
2.6. Effect of the initial pH	87
2.7. Effect of ionic strength and humic acid on MB adsorption onto OP-H ₃ PO ₄	87
3. Density Function Theory (DFT) study	88
4. Molecular Dynamic Simulation (MDS) study.....	91
5. Proposed adsorption mechanism of MB onto OP-H₃PO₄.....	92
6. Conclusion.....	93
7. References	93
 <u>Chapter V: The use of encapsulation as a proposed solution to avoid problems encountered with conventional materials in powder form: application in methylene blue removal from aqueous solutions</u>	
1. Introduction.....	100
2. Results and discussion.....	101
2.1. Characterization of the materials	101
3.2. Effect of encapsulation on the MB adsorption capacity	107
2.3. MB adsorption isotherms Study	107
2.4. MB adsorption kinetics	111
2.4.1. Effect of the contact time and the MB initial concentration	111
2.4.2. Kinetics modeling.....	111
2.5. Initial pH effect.....	114
2.6. Ionic strength and humic acid effects	115
2.7. Regeneration study of BZJS1 and BZJS2.....	116
2.8. Temperature effect on MB adsorption onto BZJS1 and BZJS2	116
2.9. MB adsorption onto various adsorbents.....	117
3. Conclusion.....	118
4. References	119

Catalogue

Chapter VI: Statistical physics modeling and thermodynamic studies for methylene blue adsorption mechanism onto an eco-friendly composite adsorbent

1. Introduction	124
2. Results and discussion	125
2.1. Material characterization	125
2.2. Adsorption isotherm	129
2.3.1. Initial concentration and time effects	131
2.4. pH effect	135
2.5. NaCl and humic acid effects	135
2.6. Reuse of prepared beads	136
2.7. Statistical physical modeling	136
2.7.1. Choosing the best model	137
2.7.2. Steric interpretation for the adequate model (MMTE)	138
2.7.3. Energetic interpretations	141
2.7.4. Thermodynamic functions calculation.....	141
2.7.4.1. Entropy.....	141
2.7.4.2. Gibbs free enthalpy	143
2.7.4.3. Internal energy.....	144
3. Proposed mechanism for MB adsorption on BOP	145
5. References	146

Chapter VII: A short introduction on the employment of dynamic adsorption systems using fixed and semi-fluidized beds by using BZJS1 as an adsorbent

1. Introduction	154
2. Column adsorption process	155
3. Results and discussion	155
3.1. Bed height effect	155
3.2. Proposed solutions for the fixed bed experiments	156
3.3. Initial dye concentration effect for semi fluidized bed experiments	157

Catalogue

3.4. Advantages and disadvantages of MB continuous adsorption.....	158
5. Conclusion.....	159
6. References	159
General conclusion and prospects.....	160
Prospects for future applications	163
List of scientific works.....	164

Acknowledgement

Acknowledgement

Above all, thanks to Allah for guiding me, giving me the health, the patience, the courage, and the capacity to accomplish this work.

I am heartily thankful to all my supervisors, **Prof. BOUGUETTOUCHA Abdallah**, whose encouragement, guidance, and support enable me to finish my Ph.D study with a happy ending. I am grateful to my co-advisor, **Prof. CHEBLI Derradji**, whom I worked with and received good ideas and guidance from my experiments. Especially thank goes to **Prof. AMRANE Abdelatif** for his ideas and suggestion to improve my work. I always would like to thank **Dr. ATTOUT Hicham** and **Dr. MANAA Zoubir**, whom gave me endless help and support in my experiments. I would like to extend my gratitude to **Prof. BOUTAHALA Mokhtar**, who always helped me when I asked him for help. I also wish to express my special thanks to **Dr. CHAFAI Nadjib**, who helped me make the quantum chemical calculations.

A special thanks to my best friend **Mr. GUEDIRI Khalil** and **Ms. SID Dounia**, for their help with the lab material and the several fruitful discussions on this research topic.

I am also indebted to many of my colleagues. I will never forget their kind help.

I am eternally grateful to my parents, brothers, and sister for their unwavering love and their sacrifices to help me succeed in my education and research careers. They have always pushed me to achieve my dreams and have worked tirelessly to help me accomplish my objective

Also, no words can express my gratitude to my wife for her unwavering support, encouragement, and understanding throughout my PhD studies.

I also would like to be thankful for all the juries for their coming to participate in my defense and their good and useful suggestions and discussions of my thesis.

Finally, I want to thank all of my family members, friends, and everyone else who supported and encouraged me to complete this thesis.

Nomenclatures

Nomenclatures

AIC	Akaike Information Criterion.
BIC	Bayesian Information Criterion.
BOP	Beads of orange peels.
BOP1	Beads of orange peels with a OP-H ₃ PO ₄ /SA ratio equal to 1.
BOP2	Beads of orange peels with a OP-H ₃ PO ₄ /SA ratio equal to 2.
BZJS	Beads of <i>Ziziphus jujuba</i> stones.
BZJS1	Beads of <i>Ziziphus jujuba</i> stones with a ZJS-H ₃ PO ₄ /SA ratio equal to 1.
BZJS2	Beads of <i>Ziziphus jujuba</i> stones with a ZJS-H ₃ PO ₄ /SA ratio equal to 2.
C₀	MB initial concentration (mg/L).
C₁, C₂, C_{1/2}	Concentrations at half-saturation of the adsorbed layer (mg/L).
C_S	MB solubility (g/L).
C_e	The equilibrium concentration (mg/L).
C_t	MB concentration after time t (mg/L).
DMSE	Double Layer model with single energy.
DMTE	Double layer model with two energies.
E_{int}	System internal energy (J/mol)
E_R	Regeneration efficiency (%).
E_{HOMO}	The highest unoccupied molecular orbital energy (eV)
E_{LUMO}	The lowest unoccupied molecular orbital energy (eV)
F_L	Flow (ml/h).
G	Gibbs free enthalpy function (J/mol)
K	The number of parameters in the selective model.
h	Planck constant (J/s).
I	Intraparticle model constant (mg/g).
J	Grand statistical potential
K	The number of parameters in the selective model.
K₁	Pseudo first order (PFO) rate constant (min ⁻¹).
K₂	Pseudo second-order (PSO) adsorption rate constant (g/(mg min)).
K_n	Rate constant of Pseudo nth order (PNO) model.
k_{id}	Diffusion rate constant (mg/g min ^{-0.5}).
K_B	Boltzmann constant (J/K).
K_F	The Freundlich parameter (mg L/g).
K_L	The constant of equilibrium adsorption (L/mg).
K_S	The adsorption affinity constant (L/mg).
K_{RP}	Redlich-Peterson model constant (L/g).
LMM	Limited multilayer model.
m	Adsorbent mass (g)
MB	Methylene blue dye.
ms	System heterogeneity index of the Sips model.
MMSE	Monolayer model with single energy.
MMTE	Monolayer model with two energies.
n	Sorption reaction order.
N_{is}	Density of (i) Receptor sites (mg/g).

Nomenclatures

n_{im}, n_m	The number of MB molecules captured by the receptor sites.
n_f	Heterogeneity index of the Freundlich model.
OP-H₃PO₄	Orange peels treated with ortho-phosphoric acid.
P	The number of experimental points.
PFO	Pseudo first order.
PSO	Pseudo second order.
PNO	Pseudo nth order.
R	Ideal gas constant (J/mol K)
ROP	Raw orange peels.
R_E	BOP regeneration efficiency (%).
R²	Determination coefficient.
SA	Sodium alginate.
Sa	Entropy configuration (J/mol K)
T	Temperature (°C or °K).
t	Time (min).
V	Medium solution volume (L).
Q_e	The amount adsorbed at equilibrium (mg/g).
Q_m	The constant that expresses the recovery of the complete monolayer (mg/g).
Q_{sat}	Adsorbed quantity at saturation (mg/g).
Q_t	The amount adsorbed at instant t (mg/g).
Q_{ads}	The amount adsorbed at one cycle (mg/g).
Q_{des}	The amount desorbed at one cycle (mg/g).
x²	The chi-square of the fitted model.
ZJS	Raw <i>ziziphus jujuba</i> stones.
ZJS-H₃PO₄	<i>Ziziphus jujuba</i> stones treated with ortho-phosphoric acid
Z_v	Translation partition function per unit volume.
Z_{gc}	The grand canonical partition function of one site.
Z_{gtr}	The translation partition function.
Z_{gc} (Ns)	The grand canonical partition function relative to the density of receptor sites.
α	Redlich-Peterson model constant (L mg/g).
β_t	Mathematical function of “F” function.
β	Surface heterogeneity index of R-P model.
ΔH°	The change in enthalpy (J/mol).
ΔG°	The change in Gibbs free energy (J/mol).
ΔS°	The change in entropy (J/mol K).
ε, ΔE	Adsorption energy (J/mol).
ΔE_{GAP}	The energy gap (eV).
μ_c	The chemical potential of the adsorbed molecule (J/mol).
μ_m	The chemical potential of the dissolved molecule (J/mol).
π	Constant.
μ	Dipole moments (Debye).
σ	Global softness.
η	Global hardness (eV).
χ	Absolute electronegativity (eV).
Ω	Electrophilicity index (eV).

List of figures

List of figures

Chapter I

Figure 1. The most used techniques in wastewater treatment.

Figure 2. A simple comparison between chemisorption and physisorption.

Figure 3. Issues related to the conventional adsorbents and the characteristics of their alternative materials.

Figure 4. Representative alginate structure with G and M blocks.

Figure 5. Advantages and disadvantages of the most used encapsulation methods.

Figure 6. A simple proposed mechanism for alginate external encapsulation.

Figure 7. A simple proposed mechanism for alginate internal encapsulation.

Figure 8. Adsorption system's efficiency variation as function as various factors.

Chapter III

Figure 1. The change in final pH as a function of the initial pH for solutions of ZJS-H₃PO₄ adsorbent during the determination of the point of zero charge PZC.

Figure 2. FTIR spectra of samples: ZJS, ZJS-H₃PO₄ and ZJS-H₃PO₄+MB in the range of 4000–500 cm⁻¹.

Figure 3. XRD data of Treated and raw Ziziphus jujuba stones.

Figure 4. SEM images of ZJS-H₃PO₄.

Figure 5. Thermogravimetric analysis of ZJS and ZJS-H₃PO₄

Figure 6. Effect of pH on methylene blue biosorption onto ZJS-H₃PO₄.

Figure 7. Effect of the contact time and the initial MB concentration on the biosorption capacity.

Figure 8. Equilibrium isotherms for MB biosorption onto ZJS-H₃PO₄ at different temperatures.

Figure 9. Modeling by the Langmuir (a), Freundlich (b), Sips (c) and Redlich-Peterson (d) models of the MB biosorption isotherm onto ZJS-H₃PO₄ at different temperatures.

Figure 10. Experimental (symbols) and calculated data (continuous lines) by mean of pseudo-first-order (a), pseudo-second-order (b) and pseudo-nth order kinetics models (c) for MB biosorption onto ZJS-H₃PO₄ at various concentrations.

Figure 11. Experimental (symbols) and calculated data (continuous lines) by means intraparticle diffusion model for MB biosorption onto ZJS-H₃PO₄.

Figure 12. Effect of NaCl and Humic acid on methylene blue biosorption onto ZJS-H₃PO₄.

List of figures

Figure 13. Behavior of the steric parameters with the temperature: (a) parameter n , (b) parameter N_M , (c) parameter Q_0 .

Figure 14. Energy of biosorption at three temperatures (298K, 303K, and 313K).

Chapter IV

Figure 1. FTIR characterization of raw orange peels (ROP), treated (OP-H₃PO₄) and after MB adsorption (OP-H₃PO₄+MB).

Figure 2. Correlation diagram between the theoretical and experimental wavenumbers of OP-H₃PO₄.

Figure 3. XRD pattern of orange peels before (ROP), after treatment with phosphoric acid (OP-H₃PO₄), and after MB adsorption (OP-H₃PO₄+MB).

Figure 4. SEM images of OP-H₃PO₄.

Figure 5. EDS characterization of OP-H₃PO₄.

Figure 6. Thermogravimetric analysis of ROP, OP-H₃PO₄, and OP-H₃PO₄+MB.

Figure 7. Variations of the pH according to the initial pH for the isoelectric point determination of OP-H₃PO₄.

Figure 8. Time-courses of the MB adsorption for different initial concentrations of MB dye onto OP-H₃PO₄ (symbols) and Nonlinear adjustment of the pseudo-first-order, pseudo-second-order and pseudo-nth-order kinetic models (continuous lines).

Figure 9. Experimental (symbols) by means the intraparticle diffusion model for MB onto OP-H₃PO₄ at three concentrations.

Figure 10. Comparison between the experimental adsorption isotherms of MB onto OP-H₃PO₄ and the modeling curves by (a) Langmuir, (b) Freundlich, (c) Redlich Peterson and (d) Sips models.

Figure 11. Initial pH effect for the MB adsorption onto OP-H₃PO₄.

Figure 12. Ionic strength and humic acid effects for the MB adsorption onto OP-H₃PO₄.

Figure 13. (a) Optimized molecular structure, (b) HOMO, (c) LUMO and (d) MEP.

Figure 14. Equilibrium adsorption configuration of MB onto the OP-H₃PO₄ surface: (a) Side view, (b) Top view.

Chapter V

Figure 1. FTIR characterization of ZJS-H₃PO₄, BZJS1, BZJS2 and after adsorption of MB.

Figure 2. SEM captures of ZJS-H₃PO₄ (a), BZJS1 (b) and BZJS2 (c).

Figure 3. Elemental analysis by EDX of ZJS-H₃PO₄, BTS1 and BZJS2.

List of figures

- Figure 4.** Nitrogen adsorption-desorption curve of the best adsorbent (BZJS1).
- Figure 5.** TG curves of ZJS-H₃PO₄, BZJS1 and BZJS2.
- Figure 6.** Isoelectric points of ZJS-H₃PO₄, BZJS1, and BZJS2.
- Figure 7.** Encapsulation effect on the performance of the MB adsorption capacity.
- Figure 8.** Experimental data (points) of MB adsorption onto BZJS1 and BZJS2. Modeling Data (lines) by Langmuir, Freundlich, Sips, and Redlich-Peterson (R-P) models at different temperatures.
- Figure 9.** Kinetics data (symbol) of MB adsorption onto BZJS1 and BZJS2 and modeling data (lines) by PFO, PSO, and P^{nth}O with different initial concentrations.
- Figure 10.** Intraparticle diffusion modeling of MB adsorption onto BZJS1 and BZJS2
- Figure 11.** Boyd model data of MB adsorption onto BZJS1 and BZJS2.
- Figure 12.** pH effect of MB adsorption onto BZJS1 and BZJS2.
- Figure 13.** Ionic strength and humic acid effects on MB adsorption onto BZJS1 and BZJS2.
- Figure 14.** Regeneration study for BZJS1 and BZJS2.

Chapter VI

- Figure 1.** Isoelectric points of OP-H₃PO₄, BOP1 and BOP2.
- Figure 2.** SEM images of OP-H₃PO₄ (a) [22], BOP1 (b) and BOP2 (c).
- Figure 3.** Infrared spectra for ROP, OP-H₃PO₄, BOP1 and BOP2.
- Figure 4.** Thermogravimetric analysis of ROP, OP-H₃PO₄, BOP 1 and BOP2.
- Figure 5.** MB adsorption isotherms on BOP at varying temperatures
- Figure 6.** Langmuir and Freundlich modeling for MB adsorption isotherm onto BOP1 and BOP2 at various temperatures.
- Figure 7.** Time and initial concentration effects for MB adsorption on BOP1 and BOP2 .
- Figure 8.** PFO, PSO and PNO modeling curves for MB adsorption onto BOP1 and BOP2 at different initial concentrations.
- Figure 9.** Intraparticle model for MB adsorption onto BOP1 and BOP2 at different initial concentrations.
- Figure 10.** Boyd model for MB adsorption onto BOP1 and BOP2 at different initial concentrations.
- Figure 11.** Initial pH effect for MB adsorption onto BOP1 and BOP2.
- Figure 12.** Ionic strength and organic compounds effects for MB adsorption onto BOP1 and BOP2 at 25°C.

List of figures

Figure 13. Regeneration efficiency of BOP1 and BOP2 at 25°C.

Figure 14. MMSE, MMTE, and DMTE modeling curves for MB adsorption isotherms onto BOP1 and BOP2 at different temperatures.

Figure 15. The evolution of entropy as a function of equilibrium MB concentrations at different temperatures for BOP1 and BOP2.

Figure 16. Gibbs free enthalpy variation as a function of equilibrium MB concentrations at different temperatures for BOP1 and BOP2.

Figure 17. Internal energy variation as a function of equilibrium MB concentrations at different temperatures for BOP1 and BOP2.

Figure 18. Proposed mechanism for MB adsorption onto BOP.

Chapter VII

Figure1. The employed fixed bed design of MB continuous adsorption onto BZJS1.

Figure 2. Bed height effect for MB dynamic adsorption on BZJS1.

Figure 3. The relationship between the C/C_0 ratio and the BM discharge flow at column's outlet.

Figure 4. Initial dye concentrations effect for semi fluidized bed experiments

List of tables

List of tables

Chapter I

Table 1: Dyes classification based on their chemical structure.

Table 2: Classification of dyes based on their applications.

Table 3: Most natural adsorbents materials found in the literature.

Table 4: Some industrial wastes used as a precursor for adsorbents preparation.

Table 5: Some agricultural wastes used as a precursor for adsorbents preparation.

Table 6. Composite materials using sodium alginate as an encapsulating agent.

Chapter II

Table 1: Some characteristics of Methylene blue (MB) dye.

Chapter III

Table 1: Some Physical and chemical characteristics of ZJS and $ZJS-H_3PO_4$

Table 2: Comparison of some values of maximum biosorption amount of MB onto various adsorbents

Table 3: Langmuir, Freundlich, Sips and Redlich-Peterson constants for the biosorption of MB onto $ZJS-H_3PO_4$

Table 4: Kinetic parameters and correlation coefficients for nonlinear regression of PFO PSO and PNO models for the biosorption of MB onto $ZJS-H_3PO_4$

Table 5: Values of R^2 and AIC of fitting of MB on the $ZJS-H_3PO_4$

Table 6: Values of fitting parameters of MB on the $ZJS-H_3PO_4$ with monolayer model

Chapter IV

Table 1. Shared Absorption bands in FTIR characterization for raw orange peels (ROP), treated ($OP-H_3PO_4$) and after MB adsorption ($OP-H_3PO_4+MB$).

Table 2. Selected experimental and theoretical vibration frequencies of $OP-H_3PO_4$.

Table 3. Some physico-chemical characteristic found for $OP-H_3PO_4$.

Table 4. Kinetic parameters and correlation coefficients for nonlinear regression of PFO PSO and PNO models for the adsorption of MB onto $OP-H_3PO_4$ at $23 \pm 2^\circ C$.

Table 5. Langmuir, Freundlich, Sips, and Redlich-Peterson (R-P) constants for the adsorption of MB onto $OP-H_3PO_4$.

List of tables

Table 6. Comparative study for the used orange peels as an adsorbent for different adsorbates.

Table 7. The obtained values of the quantum chemical parameters of MB and OP-H₃PO₄ using DFT/B3LYP 6-31G (d,p) method.

Table 8. Calculated energies for the adsorption of the BM molecules on the OP-H₃PO₄ surface.

Chapter V

Table 1: Elemental analysis by XRF of ZJS-H₃PO₄, BTS1 and BZJS2.

Table 2: Textural properties of BZJS1 from N₂ adsorption-desorption isotherm.

Table 3: Isotherm modeling parameters of Langmuir, Freundlich, Sips and Redlich-Peterson models for MB adsorption onto BZJS1 and BZJS2 at different temperatures.

Table 4: kinetics modeling parameters of PFO, PSO and P^{nth}O models for MB adsorption onto BZJS1 and BZJS2.

Table 5: Thermodynamic parameters of MB adsorption onto BZJS1 and BZJS2.

Table 6: MB adsorption onto various beads with different precursors.

Chapter VI

Table 1: Observed similar peaks from FTIR analysis of ROP, OP-H₃PO₄, BOP1 and BOP2.

Table 2: XRF analysis of ROP, OP-H₃PO₄, BOP1 and BOP2.

Table 3: Langmuir and Freundlich modeling's parameters for MB adsorption on BOP at various temperatures.

Table 4: PFO, PSO, PNO and intraparticle modeling's parameters for MB adsorption onto BOP1 and BOP2.

Table 5: The comparative parameters (F error, R² and BIC) between the used statistical physics models.

Table 6: Obtained parameters of the best model (MMTE) for MB isotherm adsorption onto BOP1 and BOP2 at different temperatures.

Table 7: Calculated adsorption energies from MMSE model for MB adsorption onto BOP1 and BOP2 at different temperatures.

Chapter VII

Table 1: The observed advantages and disadvantages for dynamic and batch adsorption systems.

General introduction

General introduction

Since the mid-nineteenth century, economic activities have started to appear in exaggerated dimensions, leading the ecological system to get out of balance. The population increase leads to an extensive society with hopes for a diverse range of products (food, clothes, medicament, etc), and as a result, the imbalance was created. Despite the fact that sciences and contemporary technology have always sought to a better human living in terms of food, drink, clothing, communication, transport, and health, these discoveries have had severe repercussions on human life, particularly from an environmental standpoint.

One of the greatest problems that the world is facing today is environmental pollution which is increasing with every passing year and causing severe damage to the earth. Pollution is an undesirable change in the physical, chemical or biological characteristics of air, land, and water that makes the environment unhealthy and creates potential health hazards to living organisms.

In its third report, the US Royal Commission on Environmental Pollution defined pollution as "the introduction by man into the environment of a substance or energy capable of causing hazards to human health, harm to living resources and ecological systems, damage to structure or amenity, or interference with legitimate uses of the environment."

Water is a vital and unique natural resource on the planet, without which no life of any kind can exist [1]. Water is critical to preserving life's quality and the earth's ecology. Despite the fact that water covers 71 % of the earth's surface, salinity renders 97.5 % of it unsuitable for human consumption. Only 0.27 % of the remaining freshwater is available, as the rest is stuck in the ground, polar ice caps, and marshes [1]. Water scarcity is regarded as a major issue in the modern world because freshwater availability is insufficient to satisfy the requirements of the existing population [1,2]. According to the World Health Organization, 785 million people are concerned about access to healthy drinking water where this number is expected to rise to 6 billion by 2050 [3], World Health Organization report also that 2 million people drink polluted water, causing 502000 deaths each year [4]. Furthermore, based on a United Nations World Water Development report, more than 80% (In some of the world's poorest countries, the rate is as high as 95%) of all wastewater from various industries is discharged into the ecosystem without being

General introduction

appropriately treated [5,6]. As a result, a supply of high-quality water must be available for various activities [7].

Water pollution is a direct consequence of the unfavorable development of its chemical, physical and bacteriological properties. As it is known, there are many causes for water pollution where water can be polluted by many human, vegetable, mineral, industrial or chemical wastes. Although industrialization is seen as a cornerstone of development strategies due to its enormous contribution to economic growth and thus human wellbeing, it has resulted in serious environmental deterioration in the majority of developing countries. Therefore, sincere objectives are now aimed not only at the qualitative and quantitative treatment of industrial wastes but also at avoiding their hazards to human health and restoring the quality of the environment. In fact, industrial and agricultural effluents are frequently loaded with non-biodegradable contaminants, and their influence on biodiversity is highly harmful.

Since 2000 BC, dyes have grown significantly in the socioeconomic structure [8]. Nowadays, synthetic dyes are the foundation of many industries, including food, textile, pharmaceuticals, paper, leather, and cosmetics. However, because of its massive water consumption (up to 3000 m³/day for each process), the textile industry is one of the most polluting industries globally [9,10].

In the last decade, a lot of efforts have been put into identifying and addressing water pollution issues using chemical, physical, or biological approaches; as a result, many technologies have been used to remove contamination from water, such as membrane filtration, oxidation, coagulation, flocculation, photocatalysis, adsorption, ion exchange, and remediation by algae, enzymes or by bacteria, etc [7,10]. In addition to the many limitations of the different water treatments, unfortunately, water purification processes are currently prohibitively expensive in most countries, making them unattainable for many low and middle-income countries.

Although each process has its own set of advantages, the adsorption method has gotten a lot of attention because of its relative ease of operation, effectiveness, and especially its low cost, and many other advantages, in this context, according to Olasupo and Suah [11], adsorption was chosen as a purification process in 19.5 % of water treatment studies between 2010 and 2020.

General introduction

Furthermore, one of the most benefits of the adsorption process is the flexibility of the precursor choice, which can be used as an adsorbent or as a basis for the preparation of an adsorbent. So, if we look at the published researches, we can see that a vast range of adsorbents has been employed, including activated carbon, zeolites, biosorbents, clays [12], and so on; in this context, the main objective of this thesis is to valorize local by-products through the development of innovative low-cost adsorbent materials generated from agricultural and food wastes, where the prepared adsorbents must be subjected to certain specific characteristics, including:

- The raw materials (precursor) are available and easy to find.
- Adsorbents that are non-toxic and have no effect on the operators' health.
- Adsorbents with controllable preparation stages.
- A low-cost product.
- Adsorbents with high efficiency for water discoloration.
- Easy to regenerate after an adsorption phase.

In this thesis, we are interested in valorizing two local by-products, *Ziziphus jujuba* stones and orange peels.

The produced adsorbents will be used in two stages: the first is to test their performances in powder form; the second stage is to transform them into beads, in view of a future implementation at an industrial scale (to be closer to an industrial scale). Will we be able to accomplish our objectives? In the coming chapters, we'll answer this question.

Regarding the *Ziziphus jujuba*, it is a type of tree belonging to the genus *Ziziphus* of the Rhamnaceae family; it is a thorny tree that grows to be about 8 meters tall, its leaves are oblong, blunt and clusters of yellow-green flowers, its fruit is oval, brown to reddish, and sometimes black, similar to dates or olives, surrounding an elongated stone with two sharp ends, our choice was based on its wide availability in Algeria, as evidenced by the fact that the name of the Annaba city was derived from the name of this fruit, and Annaba has long been known for its abundant production of this fruit. This fruit is currently categorized as a wild fruit in Algeria and is known as “Bossofa” in Algerian dialect.

The jujuba tree can grow in all soil types, whether dry or watery or even in basal and highly saline soils. It also does not require much care and can be planted anywhere.

For at least 2500 years, jujuba has been used in traditional medication to cure nervous and psychological disorders, sore throats, asthma and coughs, various chest allergies,

General introduction

improving the liver and kidneys' performance, and generally improving the performance of the digestive system [13]. According to the Algerian Ministry of Agriculture and Rural Development, Algeria *Ziziphus jujuba* production can be more than 2 tons/0.1 hectares per year. In our study, *Ziziphus jujuba* stones have been used to produce an adsorbent for water treatment (especially dyes removal).

Moreover, Algeria is well-known for its orange fruit production (estimates say that Algeria is in 14th place in the world); according to the Algerian Ministry of Agriculture and Rural Development, orange production reached 11 million quintals in 2019, so just picture how many peels will be generated after orange fruit consumption. Because of their abundance and availability, these peels were valorized in our study by being used as a precursor to obtain novel adsorbent materials.

The results obtained during this PhD thesis will be presented under articles forms in the seven following chapters.

The first chapter will be devoted to a bibliographical study which will better position the problematic of this thesis. In this part, generalities on the types of dyes, their classification in relation to different criteria, as well as the risks associated with their use will be first reported. The studies on the different techniques of water discoloration will then be presented, of which the adsorption technique is more detailed. Furthermore, the different sources of low-cost adsorbents (natural, industrial, and agricultural residues) will be given and discussed, as well as comparison tables of different powder precursors used in literature and their adsorption performance with many pollutants. Moreover, composite materials recommended as alternative adsorbents to avoid problems with classical powdered materials will be presented. Encapsulation history and the use of alginate as gelation agent will also be provided, and the most known mechanisms of alginate encapsulation will be detailed; at the end of this chapter, many parameters, including adsorbent mass, initial dye concentration, time contact, pH, temperature, particle size, ionic strength, and so one, that can all have an impact on adsorption efficiency will be mentioned and discussed.

The characterization techniques employed in this thesis and the preparation procedures for the adsorbent materials will be described in detail in the second chapter. Additionally, all the protocols for performing the adsorption tests with various parameters will be presented in this chapter. Moreover, quantum chemical calculations (Density functional

General introduction

theory (DFT) and molecular dynamics simulations (MDS)) used in this work will also be described. Furthermore, the statistical physical modeling based on the grand canonical ensemble will be widely discussed at the end of this chapter.

The third and fourth chapters of this thesis will be concentrated on the use of the chosen precursors to prepare adsorbents in powder form; the third chapter supports the use of *Ziziphus jujuba* stones to chemically treat them with phosphoric acid in order to obtain a product suitable for water treatment, whereas the fourth chapter consists of using orange peels as a precursor and then following the same preparation steps as the third chapter. Moreover, the third chapter will differ from the fourth by employing physical statistical models. In contrast, the fourth chapter will contain an additional part of molecular modeling based on DFT.

Furthermore, the fifth and sixth chapters will be concentrated on encapsulating the powdered materials. The fifth chapter will be focused on the encapsulation of treated *Ziziphus jujuba* stones. The sixth chapter will be devoted to the encapsulation of orange peels.

The last chapter, the seventh, will be focused on developing a dynamic adsorption system in the form of a fixed bed, using the best adsorbent prepared throughout this thesis, and comparing its results to those obtained in the batch system; this chapter will be useful in evaluating the performances and advantages of the best adsorbent on dynamic adsorption systems, as well as, identifying and fixing any issues that may arise.

It is important to note that the characteristics of the prepared materials will be examined by different characterization techniques, such as Fourier transform infrared spectroscopy (FTIR), scanning electron microscopy (SEM), energy dispersive X-ray diffraction (EDX), *X-ray fluorescence* (XRF), thermogravimetric analysis (TGA). At the same time, their performances will be tested by the adsorption of methylene blue, which was used as a model molecule, with several parameters that can affect its adsorption, such as initial dye concentration, time contact, pH, temperature, and ionic strength. Therefore, the choice of methylene blue (MB) as a model molecule will be justified in the following chapters.

Finally, we conclude this thesis by summarizing the conducted investigations and the obtained results, as well as providing some prospects for future researches directions in this field of study.

References

- [1] P. Sirajudheen, N.C. Poovathumkuzhi, S. Vigneshwaran, B.M. Chelaveetil, S. Meenakshi, Applications of chitin and chitosan based biomaterials for the adsorptive removal of textile dyes from water — A comprehensive review, *Carbohydrate Polymers*. 273 (2021) 118604. <https://doi.org/10.1016/j.carbpol.2021.118604>.
- [2] P. Singh, P. Shandilya, P. Raizada, A. Sudhaik, A. Rahmani-Sani, A. Hosseini-Bandegharai, Review on various strategies for enhancing photocatalytic activity of graphene based nanocomposites for water purification, *Arabian Journal of Chemistry*. 13 (2020) 3498–3520. <https://doi.org/10.1016/j.arabjc.2018.12.001>.
- [3] K. Roa, E. Oyarce, A. Boulett, M. ALSamman, D. Oyarzún, G.D.C. Pizarro, J. Sánchez, Lignocellulose-based materials and their application in the removal of dyes from water: A review, *Sustainable Materials and Technologies*. 29 (2021) e00320. <https://doi.org/10.1016/j.susmat.2021.e00320>.
- [4] S. Fahimirad, Z. Fahimirad, M. Sillanpää, Efficient removal of water bacteria and viruses using electrospun nanofibers, *Science of The Total Environment*. 751 (2021) 141673. <https://doi.org/10.1016/j.scitotenv.2020.141673>.
- [5] S.H. Teo, C.H. Ng, A. Islam, G. Abdulkareem-Alsultan, C.G. Joseph, J. Janaun, Y.H. Taufiq-Yap, S. Khandaker, G.J. Islam, H. Znad, R. Awual, Sustainable toxic dyes removal with advanced materials for clean water production: A comprehensive review, *Journal of Cleaner Production*. (2021) 130039. <https://doi.org/10.1016/j.jclepro.2021.130039>.
- [6] M. Benjelloun, Y. Miyah, G. Akdemir Evrendilek, F. Zerrouq, S. Lairini, Recent Advances in Adsorption Kinetic Models: Their Application to Dye Types, *Arabian Journal of Chemistry*. 14 (2021) 103031. <https://doi.org/10.1016/j.arabjc.2021.103031>.
- [7] A. Bhatnagar, M. Sillanpää, Applications of chitin- and chitosan-derivatives for the detoxification of water and wastewater — A short review, *Advances in Colloid and Interface Science*. 152 (2009) 26–38. <https://doi.org/10.1016/j.cis.2009.09.003>.
- [8] C. Zhang, H. Chen, G. Xue, Y. Liu, S. Chen, C. Jia, A critical review of the aniline transformation fate in azo dye wastewater treatment, *Journal of Cleaner Production*. 321 (2021) 128971. <https://doi.org/10.1016/j.jclepro.2021.128971>.

- [9] M.T. ALSamman, J. Sánchez, Recent advances on hydrogels based on chitosan and alginate for the adsorption of dyes and metal ions from water, *Arabian Journal of Chemistry*. 14 (2021) 103455. <https://doi.org/10.1016/j.arabjc.2021.103455>.
- [10] A. Islam, S.H. Teo, Y.H. Taufiq-Yap, C.H. Ng, D.-V.N. Vo, M.L. Ibrahim, Md.M. Hasan, M.A.R. Khan, A.S.M. Nur, Md.R. Awual, Step towards the sustainable toxic dyes removal and recycling from aqueous solution- A comprehensive review, *Resources, Conservation and Recycling*. 175 (2021) 105849. <https://doi.org/10.1016/j.resconrec.2021.105849>.
- [11] A. Olasupo, F.B.M. Suah, Recent advances in the removal of pharmaceuticals and endocrine-disrupting compounds in the aquatic system: A case of polymer inclusion membranes, *Journal of Hazardous Materials*. 406 (2021) 124317. <https://doi.org/10.1016/j.jhazmat.2020.124317>.
- [12] A.E. Burakov, E.V. Galunin, I.V. Burakova, A.E. Kucherova, S. Agarwal, A.G. Tkachev, V.K. Gupta, Adsorption of heavy metals on conventional and nanostructured materials for wastewater treatment purposes: A review, *Ecotoxicol. Environ. Saf.* 148 (2018) 702–712. <https://doi.org/10.1016/j.ecoenv.2017.11.034>.
- [13] Z. Tahergorabi, M.R. Abedini, M. Mitra, M.H. Fard, H. Beydokhti, “Ziziphus jujuba”: A red fruit with promising anticancer activities, *Pharmacogn. Rev.* 9 (2015) 99–106. <https://doi.org/10.4103/0973-7847.162108>.

Chapter I: Bibliography

1. Introduction

This chapter is devoted to a bibliographical study which will allow to better position the problematic of this thesis. In this part, generalities on the types of dyes, their classification with different criteria, as well as the risks associated with their use are first reported. The studies on the different techniques of water discoloration are then presented, of which the adsorption technique is more detailed. Furthermore, the different sources of low-cost adsorbents (natural, industrial, and agricultural residues) are given and discussed, and comparison tables of different powder precursors used in literature and their adsorption performance with many pollutants. Moreover, composite materials recommended as alternative adsorbents to avoid problems with classical powdered materials are presented. Encapsulation history and the use of alginate as gelation agent are also provided, as well as the most known mechanisms of alginate encapsulation are detailed; at the end of this chapter, many parameters, including adsorbent mass, initial dye concentration, time contact, pH, temperature, ionic strength that can all have an impact on adsorption efficiency are mentioned and discussed.

2. What does mean dye?

Dyes are unsaturated aromatic compounds with special characteristics such as color intensity, solubility, and fastness. Dyes can be defined as the different types of coloring particles that differ in each type from the other in chemical composition that can be used for coloring fabrics in different colors and shades [1]. Natural dyes have often been manufactured on a small scale from naturally reachable sources such as insects or plants [2]. Synthetic dyes were discovered by accident by an English chemist named William Perkins [3].

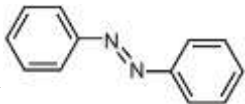
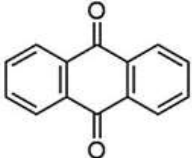
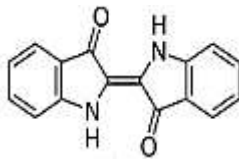
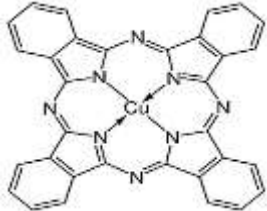
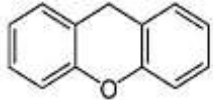
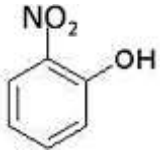
3. Dyes classification

Commercial dyes can be classified in a variety of ways. Structure, color, and application techniques may all be used to classify it [4]. However, because of the complexity of the chemical structure system's color nomenclature, classification based on application is frequently preferred [5]. Table 1 illustrates the classification of dyes based on chemical structure. While table 2 shows dyes classification based on their applications. Aside from the aforementioned, dyes are categorized as cationic (all basic dyes), anionic (direct, acid, and reactive dyes), and non-ionic (dispersed dyes) based on their particle charge upon dissolving in an aqueous application medium [6]. Dyes are utilized in a variety of fields,

Chapter I: Bibliography

including dyestuff, textile, paper, printing, carpet, plastic, food, and cosmetics. In addition, these dyes are constantly found in industrial wastes and, as a result, are frequently spilt into rivers and lakes [7].

Table 1: Dyes classification based on their chemical structure [8]

Dyes class	Description	Example
Azo	Its structure contains one or more azo groups -N=N-. The most used dyes in textile industry.	
Anthraquinone	its general formula is based on anthraquinone molecules	
Indigoid	These dyes give a large range of colors, from orange to turquoise	
Phthalocyanine	Its structure is based on complex structures with a central atom of metal (ex: Cu, Co, Pb, Fe, Mg)	
Xanthene	The compounds of this class provide intensive fluorescence. The most representative member is fluorescein	
Nitro and nitroso dyes.	They have a sample structure composed of a nitro group (-NO ₂) bonded with amine or hydroxyl group	

Chapter I: Bibliography

Table 2: Classification of dyes based on their applications [9]

Dyes class	Application
Acid	Wool, nylon, silk, inks, leather, and paper
Basic	Inks, paper, polyacrylonitrile, treated nylon, and polyester
Direct	Nylon, rayon, paper, leather, and cotton
Reactive	Wool, cotton, silk, and nylon
Sulfurous	Cotton and viscose polyamides and polyesters rarely silk
Vat	Wool and cotton.
Dispersive	Polyamide, acrylic polyester, acetate, and plastics
Mordant	Wool, silk
Pigments	Used in printing processes

3.1. Azo dyes

In their molecule structure, azo dyes are characterized by one or more azo groups ($-N=N-$). This dyes category is currently the most widely used in terms of applications, accounting for more than 50% of the world's dye production [7]. Azo dyes fall into several kinds of dyes, namely basic, acid, direct and reactive, dispersed, and mordant dyes [10].

The reactivity of azo dyes depends on different parameters. The first factor is the nature of the substituent in the molecular structure. They can be found in various forms: acid (if the functional groups are in protonated form), basic (deprotonated with free electron pair on nitrogen), or non-ionic depending on the pH values. Moreover, the basicity of dyes is influenced by additional factors; for example, the presence of acceptors substituents in aromatic rings such as $-Cl$ or $-NO_2$ groups decreases the basicity of the amino groups [11]. The azo dyes also have amphoteric properties if they contain additional acidic groups (hydroxyl) carboxyl or sulfonyl groups).

These dyes are used in the textile industry to color polyester, nylon, cellulose diacetate, triacetate, and acrylic fibers [12]. They are also used as additives in products derived from petroleum and dyeing leather, paints, plastics, papers, wood, oils, cosmetics, pharmaceuticals, metals, and food.

4. Health risk assessment on dyes

The term risk is defined as the combination of danger and possibility of hazard occurrence in a certain area. Grace Pavithra et al [13] covered several risk assessment techniques in their study work. Risk assessment research for the dye production industry is still in its early stages, and the specifics of dye exposure to people are mostly unknown. Bladder cancer is linked to dye precursor exposure. Textile dyes connected with aromatic amines can damage DNA in cells, increasing the risk of cancer [1]; because of that, textile coloring rules have been implemented in many nations. Long-term azo dye exposure results in a substantial amount of absorbed amines that exceeds the practically safe dosage limit when the azo dye is used repeatedly. In fact, the colors used in textiles pose a severe health danger. Acid Black 210 dye, for example, is used in the dyeing of cotton, leather, and wool, but according to a Dutch Health Council guideline, this dye is a human carcinogen that can harm the skin when humans are exposed to it by inhalation or dermal contact [1]. Moreover, Allergies, hyperactivity, irritability, and aggressiveness are all associated with food coloring use, where many people were reported with allergic reactions after food intake, and skin irritation symptoms were generally seen [14].

4.1. Allergies from dyes:

Allergic reactions to organic dyes clothing have been observed since 1868. By 1884, owing to the presence of modern synthetic dyes on the market, several reports were seen as excessive rashes caused by wearing underwear. In 1940, nylon stockings were introduced into the American market. Soon after their introduction, cases of nylon stockings dermatitis were reported; this was originally called “nylon allergy”. However, further investigation found that dermatitis was caused by dyes and not by nylon. Dobkevitch and Baer [14,15] reported eczema related to cross hypersensitivity between the azo dye disperse yellow and the p-phenylenediamine in nylon cloths. Moreover, patients with Allergic Contact Dermatitis (ACD) disease were detected in 1985 due to dark clothing, mainly due to contact reaction to other dyes such as blue 06 and blue 124 [15].

4.2. Aquatic toxicity:

Color can change the concentration of heavy metals and their toxicity to fish; besides all marine species, there are serious environmental issues as dyes increase aquatic life toxicity, affect the mechanism of self-purification and destroy the esthetic quality of the ecosystem. The main problem is that most synthetic dyes are resistant to light and oxidation.

Therefore, using dyes and pigments in the effluents causes collective pollution that impacts the aquatic ecosystem and the environment's esthetic nature. Because of that, dyes ought to attract a great deal of concern because of their ability to create many environmental issues [15,16].

5. Different ways for water decolorization

By the end of the 1990s, dye processing techniques used only preliminary water purification procedures, such as equalization and sedimentation, because of the absence of a dye effluent discharge limit [17]. After establishing appropriate coloring effluent release criteria, improvements have been made by implementing more efficient dye removal techniques, such as dye degrading filter beds and activated sludge techniques [18]. Currently, numerous works are underway to find the best dyes removal process to recover and treat dye wastewater appropriately [2,19]. Because of the adverse influence of pollutants generated from industrial activities on water quality and, as a result, on consumers, numerous wastewater treatment techniques have been developed, and their efficacy evaluated [20]. These methods can be classified into three categories, where the most used are illustrated in Fig.1. Although each of these processes has its own advantages, the adsorption method has gotten a lot of attention because of its low cost, relative ease of operation, effectiveness, and many other advantages.

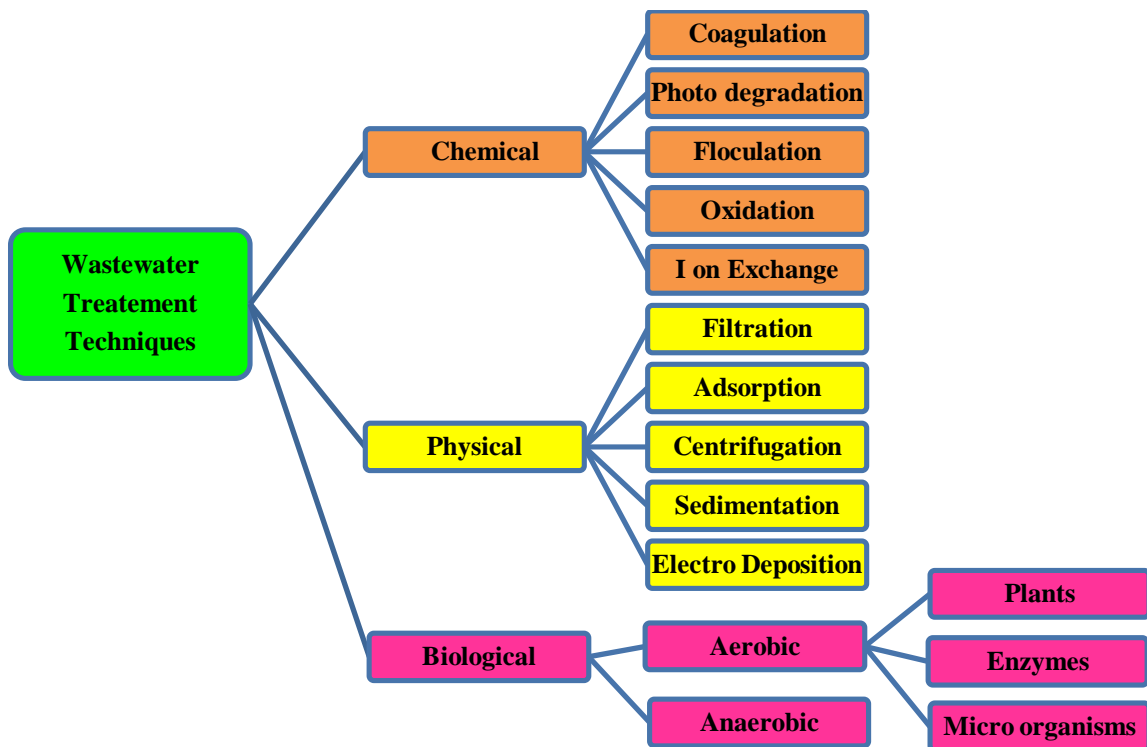


Figure 1. The most used techniques in wastewater treatment.

5.1. Adsorption

Adsorption is defined as the adherence of a substrate in a fluid phase to the functional group on the adsorbent's surface [21], resulting in the formation of an adsorbate layer on the adsorbent's surface (adsorption takes place at adsorbent/adsorbate interface). Adsorption, according to litterateurs, is the most widely employed procedure since it can manage pollutants at low concentrations, is low-cost, the adsorbent can be regenerated, and does not leave chemical residues [22]. Furthermore, it is a simple process that may be influenced by various parameters such as adsorbent specific area, temperature, pore structure, adsorbent surface chemistry, adsorbent form, adsorbate charge, the existence of competing adsorbates, and solution pH. Adsorption processes can be considered as either physical or chemical. Physical adsorption (physisorption) is reversible because it includes weak forces (van der Waals interaction, for example) [23]. It occurs at low temperatures and is typically exothermic. Chemical adsorption (chemisorption), on the other hand, occurs at high temperatures with considerable activation energy by strong interactions, and it is irreversible; this kind of adsorption generates high heat since it is created during a chemical reaction [23], Fig. 2 shows A simple comparison between chemisorption and physisorption.

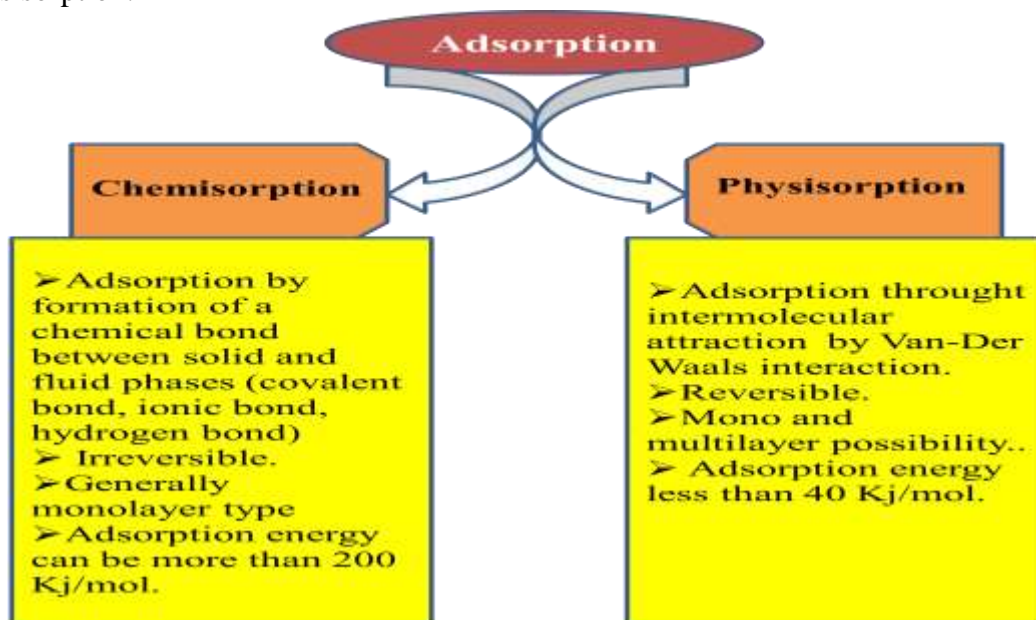


Figure 2. A simple comparison between chemisorption and physisorption.

6. Low-cost adsorbents

Generally, an adsorbent is "low cost" if it requires little processing, is abundant in nature, or is a by-product or wastes of a manufacturing process. Natural materials and certain industrial/agricultural wastes are the most well-known sources of low-cost adsorbents. In

Chapter I: Bibliography

most cases, these materials are readily available in huge quantities locally. So, they are cheap and have no economic use [24].

6.1. Adsorbent resources

6.1.1. Natural adsorbent

Water treatment is essential for the better life and health of humans and other organisms; as a result, many adsorbents have been used to be a solution. Therefore, Natural adsorbents have received a lot of attention in recent years, both environmentally and economically, as an alternative material to replace traditional adsorbents [25]. Natural materials are available in enormous quantities and may potentially be low-cost adsorbents [26,27]. These natural adsorbents can be used after being chemically treated or carbonized and then physically or chemically activated to produce chars. Chitin, zeolite, clay, wood, and coal are examples of natural adsorbents that have been effectively used to remove contaminants from water/wastewater (Table 3).

Table 3: Most natural adsorbents materials found in the literature.

Precursor	Prepared adsorbent	Pollutant	Adsorbed amount (mg/g)	Reference
Clay	Bentonite	Methylen blue	270	[28]
Clay	-Raw	Methylen blue	80 and 6.8	[29]
	-Calcined	Phenol	10 and 204	
Clay	Raw	Cu ²⁺ and Ni ²⁺	6.25 and 5.92	[30]
Zeolite	NKF-6 zeolite	Pb ²⁺ and Ni ²⁺	45.0 and 28.57	[31]
Zeolite	Na-X zeolite	-Reactive Black 5	25.3	[32]
		-Brilliant Green	24.13	
Chitin	Physically modified	Congo red	174.24	[33]
Wood	Activated carbon	Pb(II)	149.25	[34]
Acacia wood	Activated carbon	Methylen blue	338.29	[35]
Chitosan	Encapsulated	Anthocyanins	216.00	[36]
Lignin	Composite magnetic lignin	Titan yellow	192.51	[37]
Coal	Chemically treated	Humic acid	392.07	[38]
Lignin	Modified peanut Lignin	Pb(II)	269.0	[39]

Chapter I: Bibliography

6.1.2. Industrial wastes

Industrial wastes are defined as any undesired solids, liquids, gases, or mixtures of materials produced or evacuated from any manufacturing system [40]. These industrial wastes, such as red mud, coffee wastes, olive and oil industry wastes, and fly ash, have been employed to develop new adsorbents due to their low cost, wide distribution, and abundant sources [41]. Table 4 presents some examples of industrial wastes that have been used as a precursor to prepare adsorbents.

Table 4: Some industrial wastes used as a precursor for adsorbents preparation

Precursor	Prepared adsorbent	Pollutant	Adsorbed amount (mg/g)	Reference
Red mud	Calcined	U(VI)	59.45	[42]
Sunflower seed hulls	Chemically modified	Methylene blue	165.50	[43]
Fly ash	-Raw -Chemically modified	Phosphate	-6.28 -26.93	[44]
Olive oil factory wastes	Raw	Ni(II)	14.80	[45]
Phosphogypsum wastes	hydroxyapatite nanorods	Congo red (CR)	139.0	[46]
Coffee husk	Hydrochar	Methylene blue	416.68	[47]
Aerobic granular sludge	Composite	Methylen blue	106.00	[48]
palm-oil wastes	Raw	Reactive Red 120	376.41	[49]
sewage sludge	Activated carbon	Methylen blue	203.6	[50]

6.1.3. Agricultural and food wastes as adsorbents

Many attempts have been made to develop economical and easily available adsorbents to remove organic pollutants, especially solid residues. Agricultural wastes, fruits, and vegetable peels are abandoned wastes products that have no use [51], which may be highly promising adsorbents due to their physicochemical properties and low cost [52]. Because of their capability to remove a variety of organic contaminations, adsorbents derived from food leftover are getting prominence in the water treatment process [53]. Moreover, with a rising population, the consumption and demand for food and fruit have reached billions of tons each year; this signifies a high generation of fruit wastes such as peels, leaves, stalks, seeds, stones, and so on [54]. So with just a little processing, they can be exploited as a

Chapter I: Bibliography

low-cost adsorbent. Therefore, in recent years, many researchers have been interested in exploring new adsorbents based on natural materials alternative to those usually implemented in water treatment [55]. In fact, these wastes materials are less expensive, easier to find and use, and consequently appear as a topic of intensive research. For these reasons, several studies dealt with eliminating various pollutants using different precursors, as is shown in Table 5.

Table 5: Some agricultural wastes used as a precursor for adsorbents preparation.

Precursor	Prepared adsorbent	Pollutant	Adsorbed amount (mg/g)	Reference
Jackfruit peels	Biochar	Phosphate	7.95	[56]
Peach shell	Raw	Methylene blue	98.6	[57]
Ceiba pentandra Seeds	Physically/ chemically modified	Methylene blue	469.4	[58]
Stipa tenassicima	Raw	Congo red	7.93	[59]
Peanut husk	Raw	Pb ²⁺	27.03	[60]
Cones of pinus brutia	Raw	Congo red	102.8	[61]
Sugarcane bagasse	Raw	Lead and Nickel	1.61 and 123.46	[62]
Tea leaves	Activated carbon	Rhodamine B	757.6	[63]
Pistachio shells	Raw	basic blue 41	21.8	[64]
Orange peels	Magnetized	Crystal Violet	555.6	[65]
Pomegranate	Composite	Mn (VII)	477.38	[66]
Banana peels	Chemically Modified	Mn(II)	5.73	[67]
Pomegranate	Raw	Cd (II)	132.5	[68]
Date stones	Activated carbon	Malachite green	98	[69]
Corn cob husk	Biochar	As(III)	50	[70]

6.1.3.1. Why should we use agricultural (food) wastes?

Most solid wastes are not useful in their natural form without some pretreatment but are frequently subjected to physical or chemical modification processes; therefore, they are usually required to enhance the surface characteristics of the adsorbent materials produced [71]. According to several published works, the adsorption capacity and cations exchangeability of the produced adsorbent materials from agricultural wastes (food wastes)

Chapter I: Bibliography

can be greatly improved by chemical modifications with chemical agents containing oxygen, nitrogen, phosphate, sulfur, etc. Furthermore, these wastes may be physically modified into activated carbons through carbonization at high temperatures, which will provide additional benefits by allowing for more variety of pretreatment types. In addition, because of their eco-friendliness, renovation, availability, biodegradability, reuse, and efficiency, these wastes can be a promising way to be used as a precursor for adsorbents preparation.

7. Composite materials as alternative adsorbents

Much research on dyes removal has been published in the previous decade, with a wide range of powdered products currently in use, such as activated carbon [4], clays [5], biosorbents [6], and so on. Nevertheless, it is essential to point out some issues related to using these materials, such as the regeneration problems and the quantities of powder recovered after an adsorption test (see Fig. 3). Therefore, scientific studies have focused on the invention of alternative adsorbent materials to minimize the drawbacks of existing conventional materials.

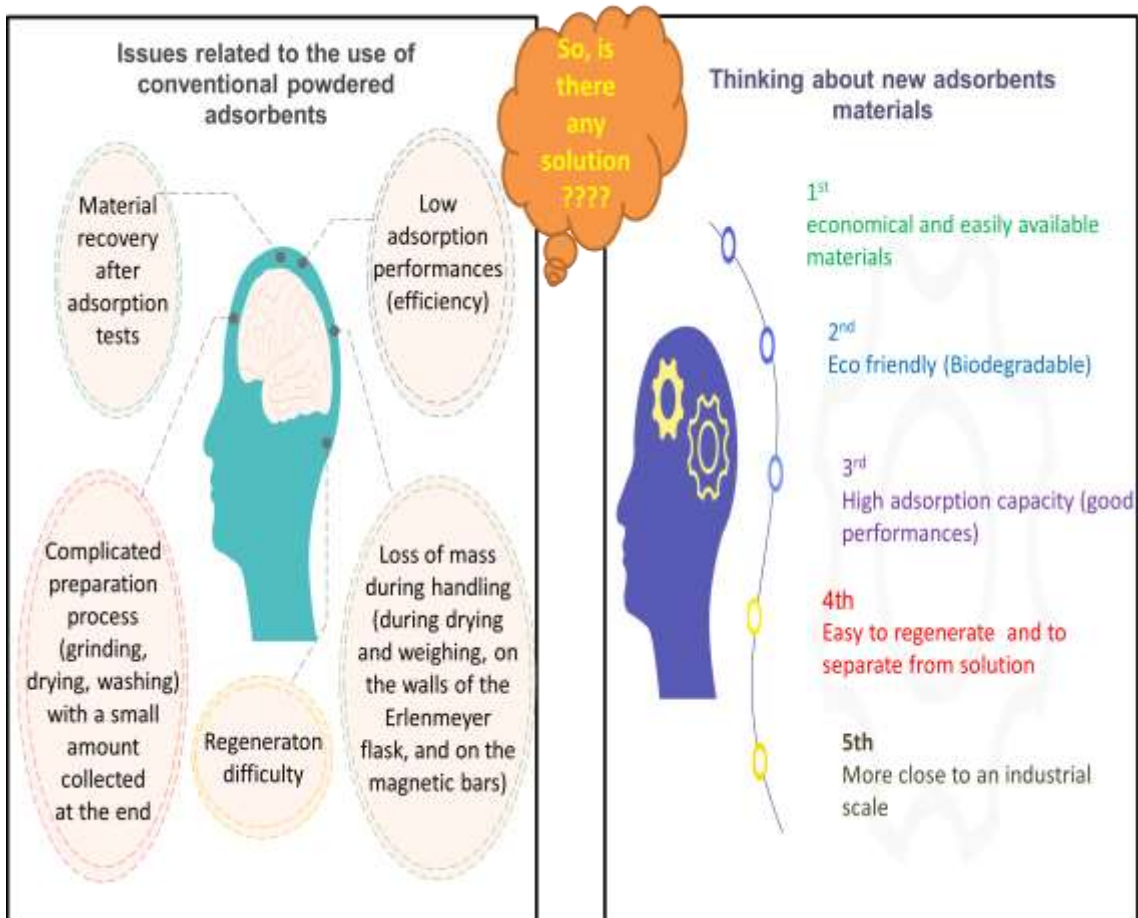


Figure 3. Issues related to the conventional adsorbents and the characteristics of their alternative materials.

Chapter I: Bibliography

Recently, composite materials outperformed other adsorbent materials due to their high porosity, ease of handling, variable morphology, and adjustable dimensions. Furthermore, hydrogels may also be easily made from natural and synthetic polymers, which is another significant benefit [72]. Moreover, the ability to entrap diverse precursors in the encapsulated agent matrix (e.g., clays, metals, biomass, carbon-based materials, etc.) provides composite materials with excellent and enhanced characteristics in terms of thermal stability, chemical and mechanical resistances, and adsorption capacity [73]. In this aim, encapsulation was proposed to skip these issues on the one hand and gain many benefits such as high adsorption capacity, high porosity, uniform size, ease of regeneration, and being closer to an industrial scale on the other hand. As a result, many polymers, such as alginate [74,75], chitosan [76], cellulose [77], and others, have been investigated for the encapsulation process. However, compared to alternative encapsulating agents, alginate was most used because of its various benefits, including its simplicity, biocompatibility, variety of resources, inexpensive cost, and non-toxicity [78].

7.1. Encapsulation history

Green and Schleicher first established microencapsulation technology in the 1950s with a patent submission to create capsules containing dyes that could be inserted into paper for copying operations [79]. Since then, it has been successfully used in a variety of manufacturing sectors such as pharmaceuticals (68%), food (13%), cosmetics (8%), and textiles (5%); nevertheless, its application in wastewater treatment has only lately been established [79,80], especially in this last decade.

7.2. Alginate as an encapsulating agent

Alginate called alginic acid is a carboxylated polysaccharide component with a characteristic structure composed of two uronic acids, β -D-mannuronic acid (M block) and α -L-guluronic acid (G block) (Fig. 4) [81,82] extracted especially from brown marine algae and also from some bacteria, such as *Pseudomonas aeruginosa* [83], because of the existence of carboxyl groups in its chains, alginate is known to be a good biosorbent [84]; it has the ability to form gels due to its easy crosslinking with divalent metal ions, where each divalent metal ion attaches to two carboxyl groups of adjacent alginate molecules.

Chapter I: Bibliography

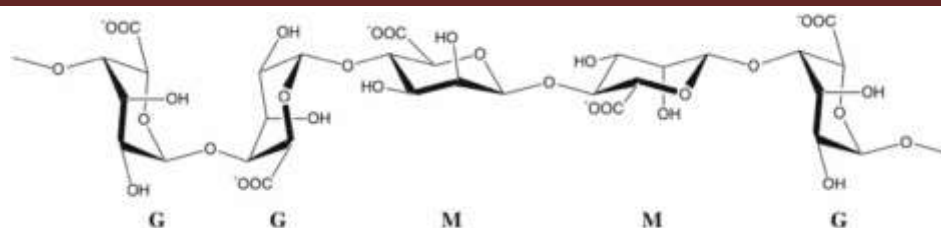


Figure 4. Representative alginate structure with G and M blocks [81,82].

Since its innovation, and because of its applicability in various fields, alginate has been used in a wide range of applications to encapsulate a variety of products, including living cells, protein drugs, enzymes, food ingredients, volatile compounds, and catalysts [85,86]. Furthermore, academic interests have largely motivated the use of alginate to produce composite materials suitable for water treatment. Table 6 presents some research papers that used alginate as an encapsulating agent.

Table 6. Composite materials using sodium alginate as an encapsulating agent.

Precursor	Encapsulating agent	Pollutants	Adsorbed amount (mg/g)	Reference
Bentonite	Sodium alginate	Methylene blue	2024	[87]
Lignin	Sodium alginate	Methylene blue	613.0	[88]
Cellulose nanofiber	Sodium alginate	Pb ²⁺	318.47	[89]
Graphene oxide	Sodium alginate	Methylene blue	357.14	[90]
Multiwall carbon nanotube	Sodium alginate	4-Nitro phenol	168.4	[91]
Functionalized iron oxide	Sodium alginate	Brilliant green	2.28	[92]
Organic montmorillonite	Sodium alginate	Phenanthrene	2.5	[93]
Polyamidoamine functionalized halloysite	Sodium alginate	Methyl green	113.64	[94]
Activated carbon from spent coffee grounds	sodium alginate	Methylene blue	710.2	[95]
Fibrous chitosan	Sodium alginate	Acid Black-172	817.0	[96]
Mesoporous nanocellulose	Sodium alginate	Pb ²⁺	472.59	[97]
Halloysite nanotube	sodium alginate	Methylene blue	250.0	[98]
Polyvinyl alcohol	Sodium alginate	Cd ²⁺	67.05	[99]
Activated carbon	sodium alginate	Methylene blue	502.5	[100]
MgO-loaded bentonite	sodium alginate	Phosphorus	70.5	[101]
PC@Fe₃O₄NPs	sodium alginate	Methylene blue	49.66	[102]
Polypyrrole-Chlorella	sodium alginate	Congo red	772.7	[103]

7.3. Encapsulation methods

Encapsulated products (especially beads) have been created using various methods. These techniques can be classified as physical (spray drying, spray chilling, spray cooling, extrusion, multi-hole centrifugal extrusion, co-crystallization, fluidized bed coating, and freeze drying), chemical (molecular inclusion by complexation and interfacial polymerization), or physicochemical (coacervation, organic phase separation, emulsion system, ionic gelation, and liposome formation) methods [104,105]. Each method has advantages and disadvantages according to the application fields. Among the encapsulation processes, ionic gelation has emerged as the most widely employed in water treatment, owing to several advantages, including [106–108]:

- Protocol's simplicity and ease of preparation.
- The product's effectiveness (especially in the adsorption field).
- Prepared beads are inexpensive (low cost).
- Beads with high porosity.

In order to compare different encapsulation processes, Fig. 5 depicts some of the benefits and drawbacks of the most commonly used encapsulation methods.

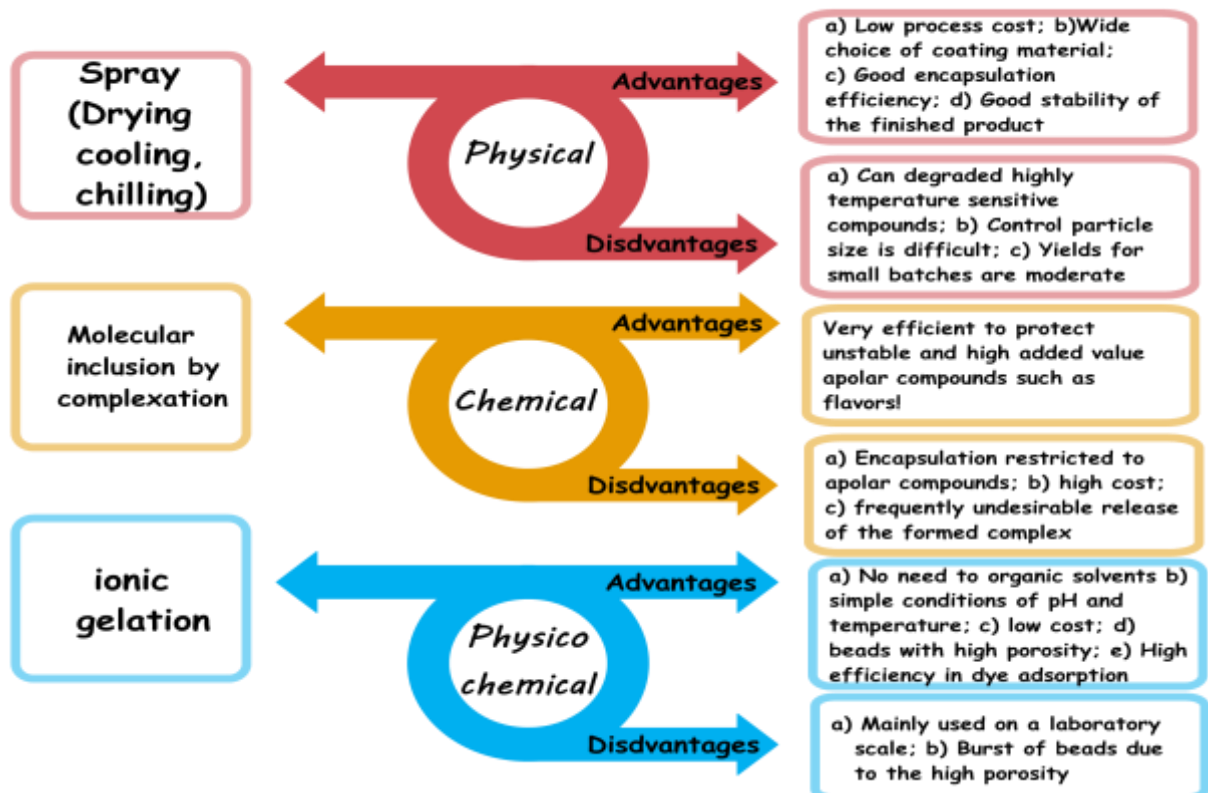


Figure 5. Advantages and disadvantages of the most used encapsulation methods.

7.3.1. Encapsulation mechanism using alginate sodium through ionic gelation technique

The alginate encapsulation is commonly achieved by crosslinking its chains with divalent cations that bind to the guluronic blocks, resulting in an ‘egg-box’ [109]; this egg-box structure is formed when divalent ions are coordinated with four-carboxyl groups by electrostatic interactions between the negatively charged carboxyl groups and the positively charged cations [110]. It's important to mention that alginate's affinity for the cations listed below decreases as $Pb > Cu > Cd > Ba > Sr > Ca > Co, Ni, Zn > Mn$. Calcium (Ca^{2+}) is the most often employed cation for alginate encapsulation since it is non-toxic compared to other cations [110,111]. Calcium chloride ($CaCl_2$) is the most widely utilized salt for encapsulation among the calcium sources available. $CaCl_2$ is very soluble in water; therefore, Ca^{2+} ions in solution may quickly cross-link with alginate droplets to create hydrogel beads; as a result, external and internal gelation are the two ways for obtaining alginate hydrogels.

7.3.1.1. External encapsulation

This method is also known as the encapsulation by diffusion process because it results in gel formation by calcium ions diffusion in an alginate solution. Droplets of alginate solution are typically extruded into a calcium bath (Fig. 6); this process is known as conventional or direct spherification, while an inverse spherification occurs when a calcium ions solution is dropped into an alginate solution [83]. Although this technique has several advantages of being a simple, low-cost process, it produces heterogeneous beads with weak mechanical characteristics due to the presence of calcium ions on the surface [112], in which the diffusion rate of the crosslinking agent controls the difference in concentration between the surface and the center of the beads [113].

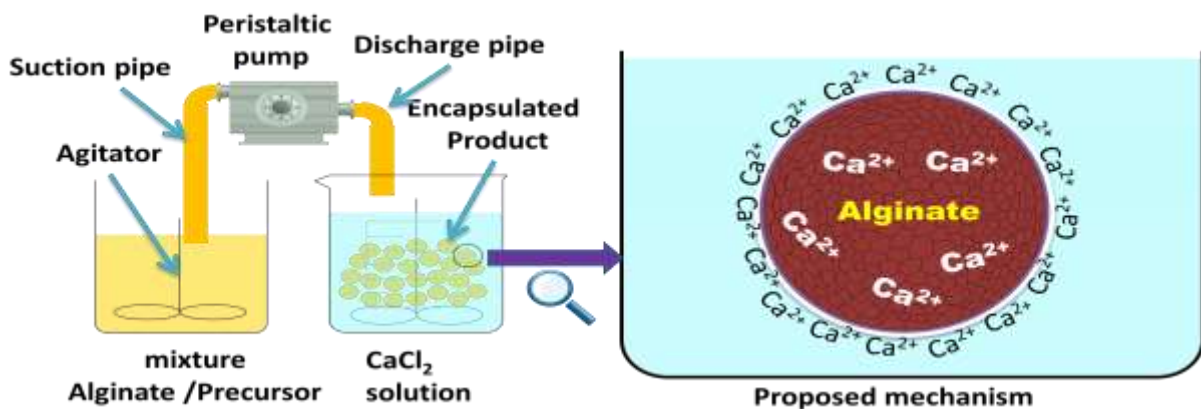


Figure 6. A simple proposed mechanism for alginate external encapsulation.

Chapter I: Bibliography

7.3.1.2. Internal encapsulation

Internal gelation can be realized throughout two steps; the first one consists in mixing an inactive calcium salt (CaCO_3 , CaSO_4) with alginate solution; the second one consists in releasing of Ca^{2+} in the interior of the alginate phase with an organic acid (glacial acetic acid) or using a lactone such as D-glucono- δ -lactone (GDL) (controlled release) [83,114] where the pH solution control the process kinetic.

Furthermore, internal encapsulation, as opposed to that external, provides for better control of gel kinetics and generates a homogeneous bead structure with pores; however, it took longer than external gelation due to the slow release of Ca^{+2} cations [115], Fig. 7 illustrate a simple proposed mechanism for internal alginate encapsulation.

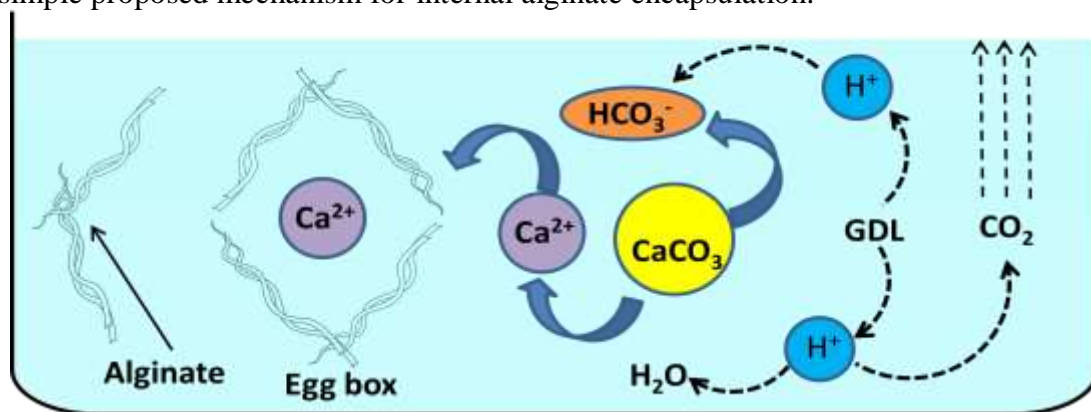


Figure 7. A simple proposed mechanism for alginate internal encapsulation.

7.4. Encapsulation benefits

Encapsulated particles can have different roles depending on the application for which they are designed, so they perform various functions such as:

- Masking a taste or odor.
- Improving the presentation of a product.
- Producing beads that are easier to separate from the solution.
- Protection and stabilization of an active ingredient in a formulation.
- Improving adsorption capacity.
- Obtaining a uniform size with high porosity.
- Generating a product that is easy to regenerate.

8. Factors affecting adsorption of dye

Adsorption is the attraction and retention of molecules from a fluid phase "adsorbate" by a solid phase "adsorbent" on its surface, resulting in a higher concentration of molecules

on the surface. While the pollutant molecule is transferred to the solid surface, it should be controlled by three physicochemical phenomena: thermodynamic equilibrium between the two phases, which defines the process's limit, adsorption kinetics, and competition between various adsorbates if there are more than one [116]; moreover, many parameters, including adsorbent mass, initial dye concentration, time contact, pH, temperature, particle size, ionic strength, and so one, can all have an impact on adsorption efficiency.

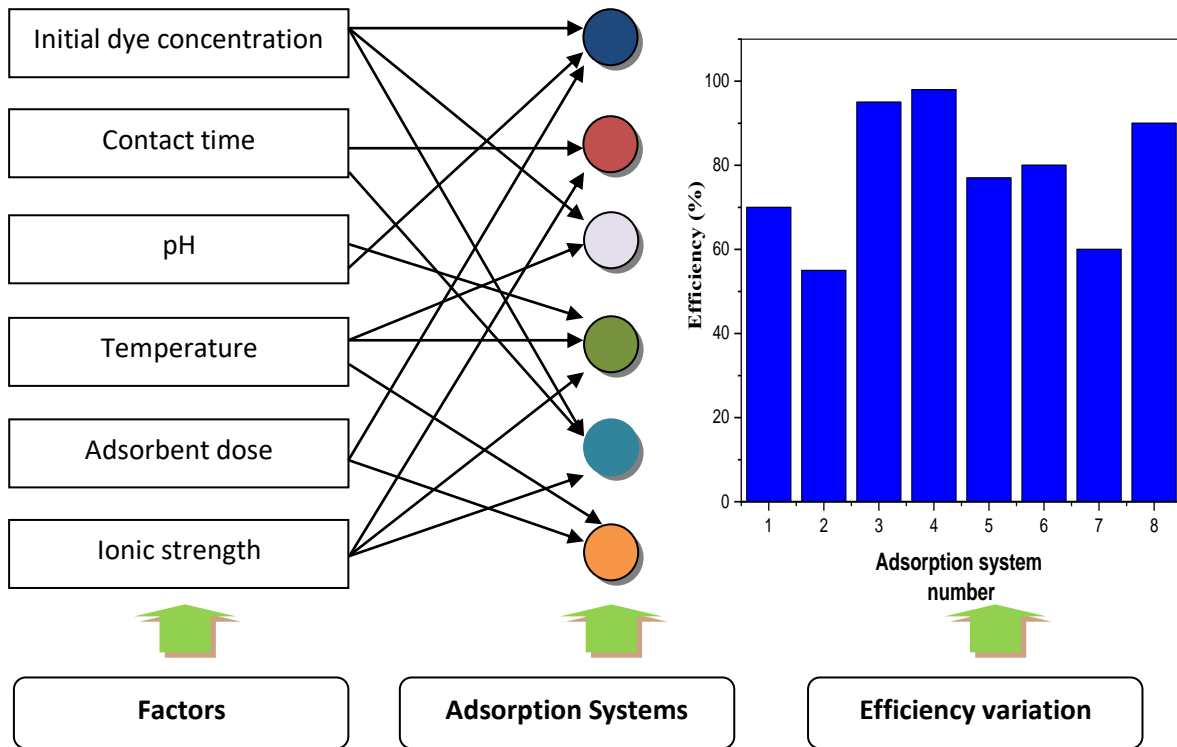


Figure 8. Adsorption system's efficiency variation as function as various factors.

8.1. Initial dye concentration

The initial dye concentration can impact dye adsorption capacity. The dye adsorption may not reach the saturation phase if the dye concentration is insufficient, and the adsorbent will be wasted. According to the literature, the dye adsorption capacity increases as the initial dye concentration rises until the free active sites at the adsorbent surface become saturated.

8.2. Initial solution pH

The adsorption of the organic dyes is often strongly influenced by the solution's pH, where examining its impact can be beneficial to understand the adsorption mechanism. For example, when dyes are attached by electrostatic interaction, the pH of the dye solution has a significant impact on dye adsorption, with maximum dye removal efficiency occurring at

the pH where the affinity between the adsorbent and dye molecules is highest [117]; this latter can be identified using the isoelectric point. Therefore, negatively charged adsorbents attract cationic dyes, whereas positively charged adsorbents attract anionic dyes. Furthermore, in other mechanisms (Van der Waal's force, hydrogen bonding, or hydrophobic-hydrophobic interactions), the initial pH may not be as important, and adsorption can occur over a wider range of pH.

8.3. Effect of the pore volume of the adsorbent

The pore volume of an adsorbent is critical in dye adsorption because it permits the maximum number of dye molecules to attach to it. According to literature, the repulsion between the adsorbate molecules substantially rises when the pore size of the adsorbent material is less than 1.7 times the size of the adsorbate molecule, necessitating greater adsorption energies [117,118]. Branton and Bradley [119] found that pore diameters 1.7–6 times larger than the adsorbate molecule size are the most effective.

8.4. Temperature effect

The temperature is one of the most important parameters affecting the adsorption process, the temperature at which the adsorption takes place has a significant impact on the dye adsorption capacity. Endothermic or exothermic reactions between dye molecules and adsorbents are possible; if low temperatures facilitate adsorption, it is exothermic; otherwise, it is endothermic [120]. Generally, the temperature effect is used to verify the adsorption process's reliability, understand the nature of the adsorption process, and perform a thermodynamic study; moreover, the adsorption temperature can affect the number of thermal collisions and mobility of dye molecules.

8.5. Ionic strength

Ionic strength is a significant factor that can impact adsorption processes. Dyes are mainly adsorbed by hydrophobic and electrostatic interactions, hydrogen bonding, and surface function group interactions between adsorbents and dyes. However, the impact of ionic strength on dye adsorption is complex and not well understood [121], where it can influence the electrostatic and hydrophobic interactions [122]. Generally, the ionic strength used to be closer to a real environment.

8.6. Contact time effect

To a certain extent, the rate of dye elimination increases with increasing contact time; however, any further increase in contact time will not affect the adsorption due to dye accumulation on the accessible adsorption site on the adsorbent surface; at this moment, the amount of free dye and the amount of dye being adsorbed are in a phase of dynamic equilibrium. The necessary time to reach this phase is referred to as the equilibrium time, and its dye adsorbed capacity represents the maximum adsorption capacity [123].

9. Molecular modeling for adsorption

Computational chemistry can give alternative and complementary information to understand the dye adsorption mechanism. Therefore, many computational chemistry approaches have been used. The density functional theory (DFT) and molecular dynamics simulations are the most commonly employed methods in molecular simulation research for dyes adsorption.

Density functional theory (DFT) is founded on the Hohenberg-Kohn theorem, claiming that all ground-state characteristics are functionals of the electronic density [124]. In these last years, the majority of DFT and MDS studies on dye adsorption are performed to get complementary information in addition to experimental results to define the type and orientation of the interactions between dyes and adsorbent using several parameters such as the highest occupied molecular orbital energy (E_{HOMO}), the lowest unoccupied molecular orbital energy (E_{LUMO}), the energy gap (ΔE_{GAP}), dipole moments (μ), global hardness (η), global softness (σ), absolute electronegativity (χ) and electrophilicity index (ω) [125].

10. References

- [1] K.G. Pavithra, S.K. P., J. V., S.R. P., Removal of colorants from wastewater: A review on sources and treatment strategies, *J. Ind. Eng. Chem.* 75 (2019) 1–19. <https://doi.org/10.1016/j.jiec.2019.02.011>.
- [2] V. Katheresan, J. Kandedo, S.Y. Lau, Efficiency of various recent wastewater dye removal methods: A review, *J. Environ. Chem. Eng.* 6 (2018) 4676–4697. <https://doi.org/10.1016/j.jece.2018.06.060>.
- [3] S. Madiraju, Color Removal and Treatment of Dye and Sugar Waste Water Using Low Cost Adsorbents, *ETD Arch.* (2018). <https://engagedscholarship.csuohio.edu/etdarchive/1098>.
- [4] E.A. Clarke, R. Anliker, *Organic Dyes and Pigments*, in: R. Anliker, G.C. Butler, E.A. Clarke, U. Förstner, W. Funke, C. Hyslop, G. Kaiser, C. Rappe, J. Russow, G. Tölg, M. Zander, V. Zitko (Eds.), *Anthropog. Compd.*, Springer, Berlin, Heidelberg, 1980: pp. 181–215. https://doi.org/10.1007/978-3-540-38522-6_7.

Chapter I: Bibliography

- [5] V.K. Gupta, Suhas, Application of low-cost adsorbents for dye removal – A review, *J. Environ. Manage.* 90 (2009) 2313–2342. <https://doi.org/10.1016/j.jenvman.2008.11.017>.
- [6] M.K. Purkait, S. DasGupta, S. De, Adsorption of eosin dye on activated carbon and its surfactant based desorption, *J. Environ. Manage.* 76 (2005) 135–142. <https://doi.org/10.1016/j.jenvman.2005.01.012>.
- [7] M.T. Yagub, T.K. Sen, S. Afroze, H.M. Ang, Dye and its removal from aqueous solution by adsorption: A review, *Adv. Colloid Interface Sci.* 209 (2014) 172–184. <https://doi.org/10.1016/j.cis.2014.04.002>.
- [8] D.R. Waring, G. Hallas, Classification of Dyes by Chemical Structure, in: *Chem. Appl. Dyes*, Springer Science & Business Media, 2013: pp. 17–47.
- [9] K. Hunger, R. Hamprecht, P. Miederer, C. Heid, A. Engel, K. Kunde, W. Mennicke, J. Griffiths, Dye Classes for Principal Applications, *Ind. Dyes.* (2002) 113–338. <https://doi.org/doi:10.1002/3527602011.ch3>.
- [10] H.Gao, K.Tastaskan, Removal of anionic Azo-dyes from aqueous solution, *J. Hazard. Mater.* 261 (2010) 83–90.
- [11] Z. Carmen, S. Daniela, Textile organic dyes—characteristics, polluting effects and separation/elimination procedures from industrial effluents—a critical overview, in: *Org. Pollut. Ten Years Stockh. Conv. - Environ. Anal. Update*, 2012.
- [12] C.R.L.D. Souza, P. Peralta-Zamora, Degradation of reactive dyes by the metallic iron/hydrogen peroxide system, *Quím. Nova.* 28 (2005) 226–228.
- [13] K. GracePavithra, V. Jaikumar, P.S. Kumar, P. SundarRajan, A review on cleaner strategies for chromium industrial wastewater: Present research and future perspective, *J. Clean. Prod.* 228 (2019) 580–593. <https://doi.org/10.1016/j.jclepro.2019.04.117>.
- [14] G. Feketea, S. Tsabouri, Common food colorants and allergic reactions in children: Myth or reality?, *Food Chem.* 230 (2017) 578–588. <https://doi.org/10.1016/j.foodchem.2017.03.043>.
- [15] S. Markandeya, P. Shukla, D. Mohan, Toxicity of disperse dyes and its removal from wastewater using various adsorbents: a review, *Res J Env. Toxicol.* 11 (2017) 72–89.
- [16] R. Orrego, G. Moraga-Cid, M. González, R. Barra, A. Valenzuela, A. Burgos, J.F. Gavilán, Reproductive, physiological, and biochemical responses in juvenile female rainbow trout (*oncorhynchus mykiss*) exposed to sediment from pulp and paper mill industrial discharge areas, *Environ. Toxicol. Chem.* 24 (2005) 1935–1943. <https://doi.org/10.1897/04-251R1.1>.
- [17] T. Robinson, G. McMullan, R. Marchant, P. Nigam, Remediation of dyes in textile effluent: a critical review on current treatment technologies with a proposed alternative, *Bioresour. Technol.* 77 (2001) 247–255. [https://doi.org/10.1016/S0960-8524\(00\)00080-8](https://doi.org/10.1016/S0960-8524(00)00080-8).
- [18] G. Mezohegyi, F.P. van der Zee, J. Font, A. Fortuny, A. Fabregat, Towards advanced aqueous dye removal processes: A short review on the versatile role of activated carbon, *J. Environ. Manage.* 102 (2012) 148–164. <https://doi.org/10.1016/j.jenvman.2012.02.021>.
- [19] M. Sarro, N.P. Gule, E. Laurenti, R. Gamberini, M.C. Paganini, P.E. Mallon, P. Calza, ZnO-based materials and enzymes hybrid systems as highly efficient catalysts for recalcitrant pollutants abatement, *Chem. Eng. J.* 334 (2018) 2530–2538. <https://doi.org/10.1016/j.cej.2017.11.146>.
- [20] A.A. Aryee, F.M. Mpatani, A.N. Kani, E. Dovi, R. Han, Z. Li, L. Qu, A review on functionalized adsorbents based on peanut husk for the sequestration of pollutants in

Chapter I: Bibliography

- wastewater: Modification methods and adsorption study, *J. Clean. Prod.* 310 (2021) 127502. <https://doi.org/10.1016/j.jclepro.2021.127502>.
- [21] D. Ewis, B.H. Hameed, A review on microwave-assisted synthesis of adsorbents and its application in the removal of water pollutants, *J. Water Process Eng.* 41 (2021) 102006. <https://doi.org/10.1016/j.jwpe.2021.102006>.
- [22] K.O. Iwuozor, J.O. Ighalo, L.A. Ogunfowora, A.G. Adeniyi, C.A. Igwegbe, An Empirical Literature Analysis of Adsorbent Performance for Methylene Blue Uptake from Aqueous Media, *J. Environ. Chem. Eng.* (2021) 105658. <https://doi.org/10.1016/j.jece.2021.105658>.
- [23] F.E. Titchou, H. Zazou, H. Afanga, J. El Gaayda, R.A. Akbour, M. Hamdani, Removal of Persistent Organic Pollutants (POPs) from water and wastewater by adsorption and electrocoagulation process, *Groundw. Sustain. Dev.* 13 (2021) 100575. <https://doi.org/10.1016/j.gsd.2021.100575>.
- [24] D. Mohan, C.U. Pittman, Arsenic removal from water/wastewater using adsorbents—A critical review, *J. Hazard. Mater.* 142 (2007) 1–53. <https://doi.org/10.1016/j.jhazmat.2007.01.006>.
- [25] G. Gupta, J. Khan, N.K. Singh, Application and efficacy of low-cost adsorbents for metal removal from contaminated water: A review, *Mater. Today Proc.* 43 (2021) 2958–2964. <https://doi.org/10.1016/j.matpr.2021.01.316>.
- [26] B. Ramaraju, P.M.K. Reddy, C. Subrahmanyam, Low cost adsorbents from agricultural waste for removal of dyes, *Environ. Prog. Sustain. Energy.* 33 (2014) 38–46. <https://doi.org/10.1002/ep.11742>.
- [27] M. Sulyman, J. Namiesnik, A. Gierak, Low-cost Adsorbents Derived from Agricultural By-products/Wastes for Enhancing Contaminant Uptakes from Wastewater: A Review, *Pol. J. Environ. Stud.* 26 (2017) 479–510. <https://doi.org/10.15244/pjoes/66769>.
- [28] M.U. Rehman, A. Manan, M. Uzair, A.S. Khan, A. Ullah, A.S. Ahmad, A.H. Wazir, I. Qazi, M.A. Khan, Physicochemical Characterization of Pakistani Clay for Adsorption of Methylene Blue: Kinetic, Isotherm and Thermodynamic Study, *Mater. Chem. Phys.* (2021) 124722. <https://doi.org/10.1016/j.matchemphys.2021.124722>.
- [29] Y. Dehmani, O.E. Khalki, H. Mezougane, S. Abouarnadasse, Comparative study on adsorption of cationic dyes and phenol by natural clays, *Chem. Data Collect.* 33 (2021) 100674. <https://doi.org/10.1016/j.cdc.2021.100674>.
- [30] H. Es-sahbany, R. Hsissou, M.L. El Hachimi, M. Allaoui, S. Nkhili, M.S. Elyoubi, Investigation of the adsorption of heavy metals (Cu, Co, Ni and Pb) in treatment synthetic wastewater using natural clay as a potential adsorbent (Sale-Morocco), *Mater. Today Proc.* (2021). <https://doi.org/10.1016/j.matpr.2020.12.1100>.
- [31] S. Khan, M. Idrees, M. Bilal, Revealing and elucidating chemical speciation mechanisms for lead and nickel adsorption on zeolite in aqueous solutions, *Colloids Surf. Physicochem. Eng. Asp.* 623 (2021) 126711. <https://doi.org/10.1016/j.colsurfa.2021.126711>.
- [32] H.A. Kiwaan, F.Sh. Mohamed, N.A. El-Ghamaz, N.M. Beshry, A.A. El-Bindary, Experimental and electrical studies of Na-X zeolite for the adsorption of different dyes, *J. Mol. Liq.* 332 (2021) 115877. <https://doi.org/10.1016/j.molliq.2021.115877>.
- [33] F. Hou, D. Wang, X. Ma, L. Fan, T. Ding, X. Ye, D. Liu, Enhanced adsorption of Congo red using chitin suspension after sonoenzymolysis, *Ultrason. Sonochem.* 70 (2021) 105327. <https://doi.org/10.1016/j.ultsonch.2020.105327>.
- [34] C.Q. Teong, H.D. Setiabudi, N.A.S. El-Arish, M.B. Bahari, L.P. Teh, Vatica rassak wood waste-derived activated carbon for effective Pb(II) adsorption: Kinetic,

Chapter I: Bibliography

- isotherm and reusability studies, *Mater. Today Proc.* 42 (2021) 165–171. <https://doi.org/10.1016/j.matpr.2020.11.270>.
- [35] M.F.M. Yusop, M.A. Ahmad, N.A. Rosli, M.E.A. Manaf, Adsorption of cationic methylene blue dye using microwave-assisted activated carbon derived from acacia wood: Optimization and batch studies, *Arab. J. Chem.* 14 (2021) 103122. <https://doi.org/10.1016/j.arabjc.2021.103122>.
- [36] C.P. Pinheiro, L.M.K. Moreira, S.S. Alves, T.R.S. Cadaval Jr, L.A.A. Pinto, Anthocyanins concentration by adsorption onto chitosan and alginate beads: Isotherms, kinetics and thermodynamics parameters, *Int. J. Biol. Macromol.* (2020). <https://doi.org/10.1016/j.ijbiomac.2020.10.250>.
- [37] L. Hu, C. Guang, Y. Liu, Z. Su, S. Gong, Y. Yao, Y. Wang, Adsorption behavior of dyes from an aqueous solution onto composite magnetic lignin adsorbent, *Chemosphere.* 246 (2020) 125757. <https://doi.org/10.1016/j.chemosphere.2019.125757>.
- [38] C. An, S. Yang, G. Huang, S. Zhao, P. Zhang, Y. Yao, Removal of sulfonated humic acid from aqueous phase by modified coal fly ash waste: Equilibrium and kinetic adsorption studies, *Fuel.* 165 (2016) 264–271. <https://doi.org/10.1016/j.fuel.2015.10.069>.
- [39] H. Yu, J. Wang, J. Yu, Y. Wang, R. Chi, Effects of surface modification on heavy metal adsorption performance and stability of peanut shell and its extracts of cellulose, lignin, and hemicellulose, *Environ. Sci. Pollut. Res.* 27 (2020) 26502–26510. <https://doi.org/10.1007/s11356-020-09055-x>.
- [40] N.K. Soliman, A.F. Moustafa, Industrial solid waste for heavy metals adsorption features and challenges; a review, *J. Mater. Res. Technol.* 9 (2020) 10235–10253. <https://doi.org/10.1016/j.jmrt.2020.07.045>.
- [41] J. Mo, Q. Yang, N. Zhang, W. Zhang, Y. Zheng, Z. Zhang, A review on agro-industrial waste (AIW) derived adsorbents for water and wastewater treatment, *J. Environ. Manage.* 227 (2018) 395–405. <https://doi.org/10.1016/j.jenvman.2018.08.069>.
- [42] W. Wu, Z. Chen, Y. Huang, J. Li, D. Chen, N. Chen, M. Su, Red mud for the efficient adsorption of U(VI) from aqueous solution: Influence of calcination on performance and mechanism, *J. Hazard. Mater.* 409 (2021) 124925. <https://doi.org/10.1016/j.jhazmat.2020.124925>.
- [43] G.B. Oguntimein, Biosorption of dye from textile wastewater effluent onto alkali treated dried sunflower seed hull and design of a batch adsorber, *J. Environ. Chem. Eng.* 3 (2015) 2647–2661. <https://doi.org/10.1016/j.jece.2015.09.028>.
- [44] Y. Wang, Y. Yu, H. Li, C. Shen, Comparison study of phosphorus adsorption on different waste solids: Fly ash, red mud and ferric–alum water treatment residues, *J. Environ. Sci.* 50 (2016) 79–86. <https://doi.org/10.1016/j.jes.2016.04.025>.
- [45] Y. Nuhoglu, E. Malkoc, Thermodynamic and kinetic studies for environmentally friendly Ni(II) biosorption using waste pomace of olive oil factory, *Bioresour. Technol.* 100 (2009) 2375–2380. <https://doi.org/10.1016/j.biortech.2008.11.016>.
- [46] H. Bensalah, S.A. Younssi, M. Ouammou, A. Gurlo, M.F. Bekheet, Azo dye adsorption on an industrial waste-transformed hydroxyapatite adsorbent: Kinetics, isotherms, mechanism and regeneration studies, *J. Environ. Chem. Eng.* 8 (2020) 103807. <https://doi.org/10.1016/j.jece.2020.103807>.
- [47] Adsorption isotherms and kinetic modeling of methylene blue dye onto a carbonaceous hydrochar adsorbent derived from coffee husk waste, *Sci. Total Environ.* 725 (2020) 138325. <https://doi.org/10.1016/j.scitotenv.2020.138325>.

Chapter I: Bibliography

- [48] S. Ladnorg, N.L. Junior, P. Dall' Agnol, D.G. Domingos, B.S. Magnus, M. Wichern, T. Gehring, R.H.R. da Costa, Alginate-like exopolysaccharide extracted from aerobic granular sludge as biosorbent for methylene blue: Thermodynamic, kinetic and isotherm studies, *J. Environ. Chem. Eng.* 7 (2019) 103081. <https://doi.org/10.1016/j.jece.2019.103081>.
- [49] B.H. Hameed, A.A. Ahmad, N. Aziz, Adsorption of reactive dye on palm-oil industry waste: Equilibrium, kinetic and thermodynamic studies, *Desalination*. 247 (2009) 551–560. <https://doi.org/10.1016/j.desal.2008.08.005>.
- [50] W. Deng, M. Hu, J. Ma, Y. Su, R. Ruan, Structural and functional relationships of activated char briquettes from pyrolysis of sewage sludge for methylene blue removal, *J. Clean. Prod.* 259 (2020) 120907. <https://doi.org/10.1016/j.jclepro.2020.120907>.
- [51] I. Anastopoulos, G.Z. Kyzas, Agricultural peels for dye adsorption: a review of recent literature, *J. Mol. Liq.* 200 (2014) 381–389.
- [52] M.A.M. Salleh, D.K. Mahmoud, W.A.W.A. Karim, A. Idris, Cationic and anionic dye adsorption by agricultural solid wastes: A comprehensive review, *Desalination*. 280 (2011) 1–13. <https://doi.org/10.1016/j.desal.2011.07.019>.
- [53] N.N. Rudi, M.S. Muhamad, L. Te Chuan, J. Alipal, S. Omar, N. Hamidon, N.H. Abdul Hamid, N. Mohamed Sunar, R. Ali, H. Harun, Evolution of adsorption process for manganese removal in water via agricultural waste adsorbents, *Heliyon*. 6 (2020) e05049. <https://doi.org/10.1016/j.heliyon.2020.e05049>.
- [54] N.H. Solangi, J. Kumar, S.A. Mazari, S. Ahmed, N. Fatima, N.M. Mubarak, Development of fruit waste derived bio-adsorbents for wastewater treatment: A review, *J. Hazard. Mater.* 416 (2021) 125848. <https://doi.org/10.1016/j.jhazmat.2021.125848>.
- [55] G. Crini, P. Badot, Traitement et épuration des eaux industrielles polluées: procédés membranaires, bioadsorption et oxydation chimique, (2007). [56] A. Nayak, B. Bhushan, V. Gupta, S. Kotnala, Fabrication of microwave assisted biogenic magnetite-biochar nanocomposite: A green adsorbent from jackfruit peel for removal and recovery of nutrients in water sample, *J. Ind. Eng. Chem.* (2021). <https://doi.org/10.1016/j.jiec.2021.05.028>.
- [57] S. Marković, A. Stanković, Z. Lopičić, S. Lazarević, M. Stojanović, D. Uskoković, Application of raw peach shell particles for removal of methylene blue, *J. Environ. Chem. Eng.* 3 (2015) 716–724. <https://doi.org/10.1016/j.jece.2015.04.002>.
- [58] M. G., S.K. P., S. A., Modelling and analysis on the removal of methylene blue dye from aqueous solution using physically/chemically modified Ceiba pentandra seeds, *J. Ind. Eng. Chem.* 62 (2018) 446–461. <https://doi.org/10.1016/j.jiec.2018.01.028>.
- [59] D. Chebli, A. Bouguettoucha, T. Mekhalef, S. Nacef, A. Amrane, Valorization of an agricultural waste, *Stipa tenassicima* fibers, by biosorption of an anionic azo dye, Congo red, *Desalination Water Treat.* 54 (2015) 245–254. <https://doi.org/10.1080/19443994.2014.880154>.
- [60] I. Abdelfattah, A.A. Ismail, F.A. Sayed, A. Almedolab, K.M. Aboelghait, Biosorption of heavy metals ions in real industrial wastewater using peanut husk as efficient and cost effective adsorbent, *Environ. Nanotechnol. Monit. Manag.* 6 (2016) 176–183. <https://doi.org/10.1016/j.enmm.2016.10.007>.
- [61] A. Bouguettoucha, D. Chebli, T. Mekhalef, A. Noui, A. Amrane, The use of a forest waste biomass, cone of *Pinus brutia* for the removal of an anionic azo dye Congo red from aqueous medium, *Desalination Water Treat.* 55 (2015) 1956–1965. <https://doi.org/10.1080/19443994.2014.928235>.

Chapter I: Bibliography

- [62] B.A. Ezeonuegbu, D.A. Machido, C.M.Z. Whong, W.S. Japhet, A. Alexiou, S.T. Elazab, N. Qusty, C.A. Yaro, G.E.-S. Batiha, Agricultural waste of sugarcane bagasse as efficient adsorbent for lead and nickel removal from untreated wastewater: Biosorption, equilibrium isotherms, kinetics and desorption studies, *Biotechnol. Rep.* 30 (2021) e00614. <https://doi.org/10.1016/j.btre.2021.e00614>.
- [63] M. Goswami, P. Phukan, Enhanced adsorption of cationic dyes using sulfonic acid modified activated carbon, *J. Environ. Chem. Eng.* 5 (2017) 3508–3517. <https://doi.org/10.1016/j.jece.2017.07.016>.
- [64] İ. Şentürk, M. Alzein, Adsorptive removal of basic blue 41 using pistachio shell adsorbent - Performance in batch and column system, *Sustain. Chem. Pharm.* 16 (2020) 100254. <https://doi.org/10.1016/j.scp.2020.100254>.
- [65] M. Ahmed, F. Mashkoo, A. Nasar, Development, characterization, and utilization of magnetized orange peel waste as a novel adsorbent for the confiscation of crystal violet dye from aqueous solution, *Groundw. Sustain. Dev.* 10 (2020) 100322. <https://doi.org/10.1016/j.gsd.2019.100322>.
- [66] M.K. Seliem, M. Mobarak, A.Q. Selim, E.A. Mohamed, R.A. Halfaya, H.K. Gomaa, I. Anastopoulos, D.A. Giannakoudakis, E.C. Lima, A. Bonilla-Petriciolet, G.L. Dotto, A novel multifunctional adsorbent of pomegranate peel extract and activated anthracite for Mn(VII) and Cr(VI) uptake from solutions: Experiments and theoretical treatment, *J. Mol. Liq.* 311 (2020) 113169. <https://doi.org/10.1016/j.molliq.2020.113169>.
- [67] A. Ali, Removal of Mn(II) from water using chemically modified banana peels as efficient adsorbent, *Environ. Nanotechnol. Monit. Manag.* 7 (2017) 57–63. <https://doi.org/10.1016/j.enmm.2016.12.004>.
- [68] Y. Chen, H. Wang, W. Zhao, S. Huang, Four different kinds of peels as adsorbents for the removal of Cd (II) from aqueous solution: Kinetics, isotherm and mechanism, *J. Taiwan Inst. Chem. Eng.* 88 (2018) 146–151. <https://doi.org/10.1016/j.jtice.2018.03.046>.
- [69] M. Hijab, P. Parthasarathy, H.R. Mackey, T. Al-Ansari, G. McKay, Minimizing adsorbent requirements using multi-stage batch adsorption for malachite green removal using microwave date-stone activated carbons, *Chem. Eng. Process. - Process Intensif.* (2021) 108318. <https://doi.org/10.1016/j.cep.2021.108318>.
- [70] J.I.Z. Montero, A.S.C. Monteiro, E.S.J. Gontijo, C.C. Bueno, M.A. de Moraes, A.H. Rosa, High efficiency removal of As(III) from waters using a new and friendly adsorbent based on sugarcane bagasse and corncob husk Fe-coated biochars, *Ecotoxicol. Environ. Saf.* 162 (2018) 616–624. <https://doi.org/10.1016/j.ecoenv.2018.07.042>.
- [71] P.N. Omo-Okoro, A.P. Daso, J.O. Okonkwo, A review of the application of agricultural wastes as precursor materials for the adsorption of per- and polyfluoroalkyl substances: A focus on current approaches and methodologies, *Environ. Technol. Innov.* 9 (2018) 100–114. <https://doi.org/10.1016/j.eti.2017.11.005>.
- [72] A.G.B. Pereira, F.H.A. Rodrigues, A.T. Paulino, A.F. Martins, A.R. Fajardo, Recent advances on composite hydrogels designed for the remediation of dye-contaminated water and wastewater: A review, *J. Clean. Prod.* 284 (2021) 124703. <https://doi.org/10.1016/j.jclepro.2020.124703>.
- [73] K. Kabiri, H. Omidian, M.J. Zohuriaan-Mehr, S. Doroudiani, Superabsorbent hydrogel composites and nanocomposites: A review, *Polym. Compos.* 32 (2011) 277–289. <https://doi.org/10.1002/pc.21046>.
- [74] M.A. Dominguez, M. Etcheverry, G.P. Zanini, Evaluation of the adsorption kinetics of brilliant green dye onto a montmorillonite/alginate composite beads by the

Chapter I: Bibliography

- shrinking core model, *Adsorption*. 25 (2019) 1387–1396. <https://doi.org/10.1007/s10450-019-00101-w>.
- [75] S. Biswas, T.K. Sen, A.M. Yeneneh, B.C. Meikap, Synthesis and characterization of a novel Ca-alginate-biochar composite as efficient zinc (Zn^{2+}) adsorbent: Thermodynamics, process design, mass transfer and isotherm modeling, *Sep. Sci. Technol.* 54 (2019) 1106–1124. <https://doi.org/10.1080/01496395.2018.1527353>.
- [76] S. Dandil, D. Akin Sahbaz, C. Acikgoz, Adsorption of Cu(II) ions onto crosslinked chitosan/Waste Active Sludge Char (WASC) beads: Kinetic, equilibrium, and thermodynamic study, *Int. J. Biol. Macromol.* 136 (2019) 668–675. <https://doi.org/10.1016/j.ijbiomac.2019.06.063>.
- [77] Y. Pan, H. Xie, H. Liu, P. Cai, H. Xiao, Novel cellulose/montmorillonite mesoporous composite beads for dye removal in single and binary systems, *Bioresour. Technol.* 286 (2019) 121366. <https://doi.org/10.1016/j.biortech.2019.121366>.
- [78] N. Fiol, J. Poch, I. Villaescusa, Grape Stalks Wastes Encapsulated in Calcium Alginate Beads for Cr(VI) Removal from Aqueous Solutions, *Sep. Sci. Technol.* 40 (2005) 1013–1028. <https://doi.org/10.1081/SS-200048041>.
- [79] F. Paulo, L. Santos, Design of experiments for microencapsulation applications: A review, *Mater. Sci. Eng. C*. 77 (2017) 1327–1340. <https://doi.org/10.1016/j.msec.2017.03.219>.
- [80] S.P. Dhakal, J. He, Microencapsulation of vitamins in food applications to prevent losses in processing and storage: A review, *Food Res. Int.* 137 (2020) 109326. <https://doi.org/10.1016/j.foodres.2020.109326>.
- [81] A. Mohammadi, A.H. Doctorsafaei, K.M. Zia, Alginate/calix[4]arenes modified graphene oxide nanocomposite beads: Preparation, characterization, and dye adsorption studies, *Int. J. Biol. Macromol.* 120 (2018) 1353–1361. <https://doi.org/10.1016/j.ijbiomac.2018.09.136>.
- [82] B. Boukoussa, A. Mokhtar, A. El Guerdaoui, M. Hachemaoui, H. Ouachtak, S. Abdelkrim, A.A. Addi, S. Babou, B. Boudina, A. Bengueddach, R. Hamacha, Adsorption behavior of cationic dye on mesoporous silica SBA-15 carried by calcium alginate beads: Experimental and molecular dynamics study, *J. Mol. Liq.* 333 (2021) 115976. <https://doi.org/10.1016/j.molliq.2021.115976>.
- [83] C. Bennacef, S. Desobry-Banon, L. Probst, S. Desobry, Advances on alginate use for spherification to encapsulate biomolecules, *Food Hydrocoll.* 118 (2021) 106782. <https://doi.org/10.1016/j.foodhyd.2021.106782>.
- [84] N. Marzban, A. Moheb, S. Filonenko, S.H. Hosseini, M.J. Nouri, J.A. Libra, G. Farru, Intelligent modeling and experimental study on methylene blue adsorption by sodium alginate-kaolin beads, *Int. J. Biol. Macromol.* 186 (2021) 79–91. <https://doi.org/10.1016/j.ijbiomac.2021.07.006>.
- [85] C. Hu, W. Lu, A. Mata, K. Nishinari, Y. Fang, Ions-induced gelation of alginate: Mechanisms and applications, *Int. J. Biol. Macromol.* 177 (2021) 578–588. <https://doi.org/10.1016/j.ijbiomac.2021.02.086>.
- [86] Y. Deng, A. Shavandi, O.V. Okoro, L. Nie, Alginate modification via click chemistry for biomedical applications, *Carbohydr. Polym.* 270 (2021) 118360. <https://doi.org/10.1016/j.carbpol.2021.118360>.
- [87] Ravi, L.M. Pandey, Enhanced adsorption capacity of designed bentonite and alginate beads for the effective removal of methylene blue, *Appl. Clay Sci.* 169 (2019) 102–111. <https://doi.org/10.1016/j.clay.2018.12.019>.
- [88] J.C. Kim, J. Kim, J. Park, J.K. Oh, I.G. Choi, H.W. Kwak, Highly efficient and sustainable alginate/carboxylated lignin hybrid beads as adsorbent for cationic dye

Chapter I: Bibliography

- removal, *React. Funct. Polym.* 161 (2021) 104839. <https://doi.org/10.1016/j.reactfunctpolym.2021.104839>.
- [89] H. Zhao, X.K. Ouyang, L.Y. Yang, Adsorption of lead ions from aqueous solutions by porous cellulose nanofiber–sodium alginate hydrogel beads, *J. Mol. Liq.* 324 (2021) 115122. <https://doi.org/10.1016/j.molliq.2020.115122>.
- [90] X. Liu, B. Cui, S. Liu, Q. Ma, Methylene Blue Removal by Graphene Oxide/Alginate Gel Beads, *Fibers Polym.* 20 (2019) 1666–1672. <https://doi.org/10.1007/s12221-019-9011-z>.
- [91] S.D. Ashrafi, G.H. Safari, K. Sharafi, H. Kamani, J. Jaafari, Adsorption of 4-Nitrophenol on calcium alginate-multiwall carbon nanotube beads: Modeling, kinetics, equilibriums and reusability studies, *Int. J. Biol. Macromol.* 185 (2021) 66–76. <https://doi.org/10.1016/j.ijbiomac.2021.06.081>.
- [92] Adsorption of cationic dyes, drugs and metal from aqueous solutions using a polymer composite of magnetic/ β -cyclodextrin/activated charcoal/Na alginate: Isotherm, kinetics and regeneration studies, *J. Hazard. Mater.* 409 (2021) 124840. <https://doi.org/10.1016/j.jhazmat.2020.124840>.
- [93] W.J. Dai, P. Wu, D. Liu, J. Hu, Y. Cao, T.Z. Liu, C.P. Okoli, B. Wang, L. Li, Adsorption of Polycyclic Aromatic Hydrocarbons from aqueous solution by Organic Montmorillonite Sodium Alginate Nanocomposites, *Chemosphere.* 251 (2020) 126074. <https://doi.org/10.1016/j.chemosphere.2020.126074>.
- [94] J. Kurczewska, M. Cegłowski, G. Schroeder, Alginate/PAMAM dendrimer – Halloysite beads for removal of cationic and anionic dyes, *Int. J. Biol. Macromol.* 123 (2019) 398–408. <https://doi.org/10.1016/j.ijbiomac.2018.11.119>.
- [95] K.W. Jung, B.H. Choi, M.J. Hwang, T.U. Jeong, K.H. Ahn, Fabrication of granular activated carbons derived from spent coffee grounds by entrapment in calcium alginate beads for adsorption of acid orange 7 and methylene blue, *Bioresour. Technol.* 219 (2016) 185–195. <https://doi.org/10.1016/j.biortech.2016.07.098>.
- [96] X. Zhao, X. Wang, T. Lou, Preparation of fibrous chitosan/sodium alginate composite foams for the adsorption of cationic and anionic dyes, *J. Hazard. Mater.* 403 (2021) 124054. <https://doi.org/10.1016/j.jhazmat.2020.124054>.
- [97] W. Li, L. Zhang, D. Hu, R. Yang, J. Zhang, Y. Guan, F. Lv, H. Gao, A mesoporous nanocellulose/sodium alginate/carboxymethyl-chitosan gel beads for efficient adsorption of Cu²⁺ and Pb²⁺, *Int. J. Biol. Macromol.* 187 (2021) 922–930. <https://doi.org/10.1016/j.ijbiomac.2021.07.181>.
- [98] L. Liu, Y. Wan, Y. Xie, R. Zhai, B. Zhang, J. Liu, The removal of dye from aqueous solution using alginate-halloysite nanotube beads, *Chem. Eng. J.* 187 (2012) 210–216. <https://doi.org/10.1016/j.cej.2012.01.136>.
- [99] Fabrication of nanofibers using sodium alginate and Poly(Vinyl alcohol) for the removal of Cd²⁺ ions from aqueous solutions: adsorption mechanism, kinetics and thermodynamics, *Heliyon.* 5 (2019) e02941. <https://doi.org/10.1016/j.heliyon.2019.e02941>.
- [100] H.W. Kwak, Y. Hong, M.E. Lee, H.-J. Jin, Sericin-derived activated carbon-loaded alginate bead: An effective and recyclable natural polymer-based adsorbent for methylene blue removal, *Int. J. Biol. Macromol.* 120 (2018) 906–914. <https://doi.org/10.1016/j.ijbiomac.2018.08.116>.
- [101] H. Xi, H. Jiang, D. Zhao, A.H. Zhang, B. Fan, Y. Yang, J. Zhang, Highly selective adsorption of phosphate from high-salinity water environment using MgO-loaded and sodium alginate-immobilized bentonite beads, *J. Clean. Prod.* 313 (2021) 127773. <https://doi.org/10.1016/j.jclepro.2021.127773>.

Chapter I: Bibliography

- [102] Z. Anfar, A. Amedlous, A.A. El Fakir, M. Zbair, H. Ait Ahsaine, A. Jada, N. El Alem, High extent mass recovery of alginate hydrogel beads network based on immobilized bio-sourced porous carbon@Fe₃O₄-NPs for organic pollutants uptake, *Chemosphere*. 236 (2019) 124351. <https://doi.org/10.1016/j.chemosphere.2019.124351>.
- [103] M. Maqbool, S. Sadaf, H.N. Bhatti, S. Rehmat, A. Kausar, S.A. Alissa, M. Iqbal, Sodium alginate and polypyrrole composites with algal dead biomass for the adsorption of Congo red dye: Kinetics, thermodynamics and desorption studies, *Surf. Interfaces*. 25 (2021) 101183. <https://doi.org/10.1016/j.surfin.2021.101183>.
- [104] N.T.T. Uyen, Z.A.A. Hamid, N.X.T. Tram, N. Ahmad, Fabrication of alginate microspheres for drug delivery: A review, *Int. J. Biol. Macromol.* 153 (2020) 1035–1046. <https://doi.org/10.1016/j.ijbiomac.2019.10.233>.
- [105] J.S. Ribeiro, C.M. Veloso, Microencapsulation of natural dyes with biopolymers for application in food: A review, *Food Hydrocoll.* 112 (2021) 106374. <https://doi.org/10.1016/j.foodhyd.2020.106374>.
- [106] H. Song, W. Yu, M. Gao, X. Liu, X. Ma, Microencapsulated probiotics using emulsification technique coupled with internal or external gelation process, *Carbohydr. Polym.* 96 (2013) 181–189. <https://doi.org/10.1016/j.carbpol.2013.03.068>.
- [107] G. Ozkan, P. Franco, I. De Marco, J. Xiao, E. Capanoglu, A review of microencapsulation methods for food antioxidants: Principles, advantages, drawbacks and applications, *Food Chem.* 272 (2019) 494–506. <https://doi.org/10.1016/j.foodchem.2018.07.205>.
- [108] V. Suganya, V. Anuradha, Microencapsulation and Nanoencapsulation: A Review, *Int. J. Pharm. Clin. Res.* 9 (2017). <https://doi.org/10.25258/ijpcr.v9i3.8324>.
- [109] J.Y. Leong, W.-H. Lam, K.W. Ho, W.P. Voo, M.F.X. Lee, H.P. Lim, S.L. Lim, B.T. Tey, D. Poncelet, E.S. Chan, Advances in fabricating spherical alginate hydrogels with controlled particle designs by ionotropic gelation as encapsulation systems, *Particuology*. 24 (2016) 44–60. <https://doi.org/10.1016/j.partic.2015.09.004>.
- [110] A.C. Hernández-González, L. Téllez-Jurado, L.M. Rodríguez-Lorenzo, Alginate hydrogels for bone tissue engineering, from injectables to bioprinting: A review, *Carbohydr. Polym.* 229 (2020) 115514. <https://doi.org/10.1016/j.carbpol.2019.115514>.
- [111] K.Y. Lee, D.J. Mooney, Alginate: Properties and biomedical applications, *Prog. Polym. Sci.* 37 (2012) 106–126. <https://doi.org/10.1016/j.progpolymsci.2011.06.003>.
- [112] N.D.A. Arriola, P.I. Chater, M. Wilcox, L. Lucini, G. Rocchetti, M. Dalmina, J.P. Pearson, R.D. de Mello Castanho Amboni, Encapsulation of stevia rebaudiana Bertoni aqueous crude extracts by ionic gelation – Effects of alginate blends and gelling solutions on the polyphenolic profile, *Food Chem.* 275 (2019) 123–134. <https://doi.org/10.1016/j.foodchem.2018.09.086>.
- [113] B. Reig-Vano, B. Tytkowski, X. Montané, M. Giamberini, Alginate-based hydrogels for cancer therapy and research, *Int. J. Biol. Macromol.* 170 (2021) 424–436. <https://doi.org/10.1016/j.ijbiomac.2020.12.161>.
- [114] S.A. Strobel, K. Hudnall, B. Arbaugh, J.C. Cunniffe, H.B. Scher, T. Jeoh, Stability of Fish Oil in Calcium Alginate Microcapsules Cross-Linked by In Situ Internal Gelation During Spray Drying, *Food Bioprocess Technol.* 13 (2020) 275–287. <https://doi.org/10.1007/s11947-019-02391-y>.
- [115] L. Cao, W. Lu, A. Mata, K. Nishinari, Y. Fang, Egg-box model-based gelation of alginate and pectin: A review, *Carbohydr. Polym.* 242 (2020) 116389. <https://doi.org/10.1016/j.carbpol.2020.116389>.

Chapter I: Bibliography

- [116] M. Benjelloun, Y. Miyah, G. Akdemir Evrendilek, F. Zerrouq, S. Lairini, Recent Advances in Adsorption Kinetic Models: Their Application to Dye Types, *Arab. J. Chem.* 14 (2021) 103031. <https://doi.org/10.1016/j.arabjc.2021.103031>.
- [117] M.M. Hassan, C.M. Carr, Biomass-derived porous carbonaceous materials and their composites as adsorbents for cationic and anionic dyes: A review, *Chemosphere.* 265 (2021) 129087. <https://doi.org/10.1016/j.chemosphere.2020.129087>.
- [118] Y.S. Al-Degs, M.I. El-Barghouthi, M.A. Khraisheh, M.N. Ahmad, S.J. Allen, Effect of Surface Area, Micropores, Secondary Micropores, and Mesopores Volumes of Activated Carbons on Reactive Dyes Adsorption from Solution, *Sep. Sci. Technol.* 39 (2005) 97–111. <https://doi.org/10.1081/SS-120027403>.
- [119] P. Branton, R.H. Bradley, Effects of active carbon pore size distributions on adsorption of toxic organic compounds, *Adsorption.* 2 (2011) 293–301. <https://doi.org/10.1007/s10450-010-9284-4>.
- [120] H. Wang, Z. Li, S. Yahyaoui, H. Hanafy, M.K. Seliem, A. Bonilla-Petriciolet, G. Luiz Dotto, L. Sellaoui, Q. Li, Effective adsorption of dyes on an activated carbon prepared from carboxymethyl cellulose: Experiments, characterization and advanced modelling, *Chem. Eng. J.* 417 (2021) 128116. <https://doi.org/10.1016/j.cej.2020.128116>.
- [121] Q. Li, Q.Y. Yue, H.J. Sun, Y. Su, B.Y. Gao, A comparative study on the properties, mechanisms and process designs for the adsorption of non-ionic or anionic dyes onto cationic-polymer/bentonite, *J. Environ. Manage.* 91 (2010) 1601–1611. <https://doi.org/10.1016/j.jenvman.2010.03.001>.
- [122] Y. Hu, T. Guo, X. Ye, Q. Li, M. Guo, H. Liu, Z. Wu, Dye adsorption by resins: Effect of ionic strength on hydrophobic and electrostatic interactions, *Chem. Eng. J.* 228 (2013) 392–397. <https://doi.org/10.1016/j.cej.2013.04.116>.
- [123] M.A.M. Razi, M.N.A.M. Hishammudin, R. Hamdan, Factor Affecting Textile Dye Removal Using Adsorbent From Activated Carbon: A Review, *MATEC Web Conf.* 103 (2017) 06015. <https://doi.org/10.1051/mateconf/201710306015>.
- [124] C.E. Ibarra Torres, T.E. Serrano Quezada, O.V. Kharissova, B.I. Kharisov, Ma.I. Gómez de la Fuente, Carbon-based aerogels and xerogels: Synthesis, properties, oil sorption capacities, and DFT simulations, *J. Environ. Chem. Eng.* 9 (2021) 104886. <https://doi.org/10.1016/j.jece.2020.104886>.
- [125] C. Osagie, A. Othmani, S. Ghosh, A. Malloum, Z. Kashitarash Esfahani, S. Ahmadi, Dyes adsorption from aqueous media through the nanotechnology: A review, *J. Mater. Res. Technol.* 14 (2021) 2195–2218. <https://doi.org/10.1016/j.jmrt.2021.07.085>.

Chapter II: Experimental protocols and analytical methods

1. Introduction

This chapter describes all of the characterization techniques used in this thesis as well as the adsorbent material synthesis methods. This chapter also provides all of the protocols for performing the adsorption experiments with various parameters. Moreover, quantum chemical calculations (Density functional theory and molecular dynamics simulations) employed in this work will be discussed. Moreover, the statistical physical modeling based on the grand canonical ensemble will be discussed at the end of this chapter.

2. Materials and methods

2.1. Materials

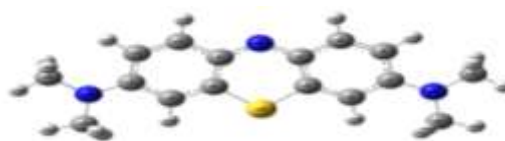
The *Ziziphus jujuba stones* (ZJS) used in this study were collected from forests (in the town of Setif, in northeastern Algeria). The orange peels used in this study were collected after consuming orange. All the chemicals used in this work were obtained from Sigma-Aldrich, namely methylene blue ($C_{16}H_{18}N_3SCl$) (MB), sodium hydroxide (NaOH), hydrochloric acid (HCl), ortho-phosphoric acid (H_3PO_4), humic acid and sodium alginate, a glass column with 600 mm in length and a diameter of 8 mm. Peristaltic pump (Master Flex C/L, 77122-24 model).

Table 1 summarizes the main characteristics of the model dye, methylene blue (MB).

Table 1: Some characteristics of Methylene blue (MB) dye.

Methylene Blue dye (MB)	
Category	Basic cationic dye
Brute formula	$C_{16}H_{18}N_3SCl$
Chemical name	Tetramethylthionine hydrochloride
Molar mass (g /mol)	320
Diametre (Å°)	15
Maximum wavelength (nm)	654
pKa	3.8
Solubility at 20 °C (g/L)	40

Structure



2.2. Preparation of the adsorbents

2.2.1. Powdered adsorbent preparation

The preparation protocol comprised several stages: drying, grinding, sieving, washing and finally, a modification with phosphoric acid. Briefly, about 4 kg of the precursors (orange peels or *Ziziphus jujuba* stones) were collected, dried to a constant mass using an oven at 50 °C, then crushed until a homogeneous material was obtained; the particle sizes used for the adsorption tests were mechanically isolated by means of sieves with a mesh size between 0.2 and 0.4 mm. Only the retained powder on the sieves was used. Before the treatment step, tap and distilled water were used to wash the powder. This operation was aimed at both the elimination of the grinding residues and the removal of the impurities; the material was again dried at a temperature of 50 °C before being modified by phosphoric acid.

The treatment step consisted in mixing a mass of the powder of the raw materials (ROP or ZJS) with a solution of H₃PO₄ (1M) with a ratio of (1/1). The mixture was kept stirring for one day using a magnetic stirrer at a well-controlled temperature (≈ 25 C°). For drying, the mixture was put in an oven at 50 °C for 48 hours. The product obtained underwent the same steps of grinding, sieving and washing mentioned above to obtain a powder applicable for adsorption tests. The obtained powders were abbreviated as ZJS-H₃PO₄ and OP-H₃PO₄ for *ziziphus jujuba* stones and orange peels respectively, and stored in desiccators.

2.2.2. Beads adsorbent preparation (encapsulation)

Once the treated powder (ZJS-H₃PO₄ or OP-H₃PO₄) was ready, the beads of *Ziziphus jujuba* stones (BZJS) and orange peels (BOP) were prepared by encapsulation using sodium alginate, which shows the ability of forming hydrogels in the presence of divalent cations [1–3]. To this end, the encapsulation method used in this chapter consisted of mixing a mass of ZJS-H₃PO₄ or OP-H₃PO₄ with a sodium alginate solution (2 percent) and then keeping them in agitation, where the ratio of treated powder/Alginate varied between 1 and 2. When the blend treated powder/Alginate became homogeneous, it was added by means of a peristaltic pump into a divalent solution of CaCl₂ to allow the formation of beads by a quick reaction between the alginate and the crosslinking agent at the surface; this must be accomplished under agitation to avoid the consumption of Ca²⁺ cations. The beads obtained were stirred with the CaCl₂ solution for 12 hours; next, dried at room

temperature and then stored under the abbreviations BZJS1 and BZJS2 for ZJS-H₃PO₄, and BOP1 and BOP2 for OP-H₃PO₄, respectively, for the ratios 1:1 and 1:2 to carry out the adsorption tests.

2.3. Materials characterization

An Agilent technologies Fourier transform spectrophotometer (FTIR) (cary 600 series FTIR spectrometer) was used to examine the surface chemistry of BZJS1 and BZJS2, where the infrared spectra ranged from 4000 cm to 550 cm⁻¹.

The micromorphology of the prepared adsorbent was examined by scanning electron spectroscopy, where the captures were made by a Hitachi S-3000N SEM. In addition, using the same apparatus, the elemental analysis was examined with energy dispersive X-ray diffraction (EDX), as well as X-ray fluorescence (XRF) using a ZSX Primus IV-Rigaku device.

The nitrogen adsorption and desorption isotherms were considered to examine the porous structure. Before starting the characterization, a vacuum degassing at a temperature of 130 °C must be carried out on the sample; next, specific surface, size, and pore volume were calculated.

The adsorbent in powder form were analyzed by a PW3071/xx diffractometer at a voltage of 45 KV and an intensity of 35 mA using a copper anticathode emitting Ka radiation ($\lambda = 1.5405 \text{ \AA}$). The XRD diagrams were carried out in a 2θ angle range between 4 and 90 degrees with a step of 0.02 degree and 6.985 seconds per step

Moreover, thermogravimetric analysis (TGA) of the prepared materials was carried out using SDT Q600 V20.9 Build 20 thermal gravimetric, at temperatures ranging from 40 to 900 °C with a heating flow of 10 °C/minute.

The zero charge point (pHpzc) for each material corresponds to a zero charge potential on the adsorbent surface; it is very helpful for understanding the interaction mechanism between the liquid and solid phases. A simple protocol was followed, which consisted of using a series of 11 beakers of 50 ml containing a suspension of 50 mg of adsorbent with 50 ml of distilled water where the initial pHs of water were adjusted from 2 to 12 using HCl or NaOH. These suspensions were kept under stirring for 48 h, and then the final pH of each beaker was measured. Finally, the results obtained are displayed on a graph according to the following expression $\Delta\text{pH} = f(\text{pHi})$. For the purpose of physicochemical

characterization of powder adsorbents, porosity, moisture, acidity, basicity, ash content, and apparent density were determined.

2.4. Adsorption study

Batch system was chosen to carry out adsorption experiments of MB onto ZJS-H₃PO₄, OP-H₃PO₄, BZJS and BOP whose contact time effect, initial concentration, pH, temperature, ionic strength, and humic acid were examined.

2.5. Kinetic adsorption

The objectives were to evaluate the adsorbed amount of MB onto the prepared adsorbent as a function of time, as well as the effect of the initial concentration on the maximum amount adsorbed. MB adsorption kinetics were studied at room temperature (approximately 25 °C) with different initial dye concentrations (50,100, 150 and 200 mg/L) and at a constant stirring speed of 250 rpm until equilibrium was reached. The adsorbed amounts of MB were determined using the relation [4] (1)

$$Q_t = (C_0 - C_t) * V/m \dots \dots \dots (1)$$

Kinetics modeling is an important and effective step that can help determine the mechanism that controls the adsorption process [5]. In this context, experimental data of MB adsorption onto all adsorbents were modeled by some models reported in the literature.

The pseudo-first-order equation proposed by Lagergren and Sven in 1898 [6] is given in the following form:

$$dQ_t/dt = K_1(Q_e - Q_t) \dots \dots \dots (2)$$

Lagergren's equation can be written in nth order according to Eq. (3):

$$dQ_t/dt = K(Q_e - Q_t)^n \dots \dots \dots (3)$$

The integration of Eq. (8) under the conditions (Q = 0 to Q = Q_t and t = 0 to t = t) at the boundaries leads to pseudo-first-order and pseudo-second-order models according to the relations (4) and (5) respectively:

If n = 1, the integration leads to the pseudo-first-order model according to the following Eq. (4):

$$Q_t = Q_e(1 - e^{-K_1t}) \dots \dots \dots (4)$$

And if n=2, the integration leads to the pseudo-second-order model in the following form:

$$Q_t = K_2 Q_e^2 t / (1 + K_2 Q_e t) \dots \dots \dots (5)$$

To approach to the experimental data, Ozer [7] used the model of nth order for the determination of the rate constant and the order of the reaction of the kinetics data without setting a priori the value of n; by integrating Eq. (6), he obtained the following formula:

$$Q_t = Q_e - \left[(n - 1) K_n t + Q_e^{(1-n)} \right]^{1/(1-n)} \dots \dots \dots (6)$$

The intraparticle diffusion model was also applied; it was proposed by Weber and Morris [8] and is commonly used in the literature. In this model, the adsorbed quantity varies almost proportionally with $t^{0.5}$ [8,9] according to Eq. (7):

$$Q_t = K_{id} t^{0.5} + I \dots \dots \dots (7)$$

Otherwise, the Boyd and Weber-Morris models were considered to better understand the diffusion mechanism as well as the limiting step that controls the adsorption process [10,11]. The Boyd model (Eq. 8) was applied to discriminate between two mechanisms and determine what step controls the adsorption process, between the diffusion into the pores and the diffusion film [12,13]. In this model, the formula of β_t is given according to the fraction value ($F = Q_e / Q_t$).

$$F = \frac{Q_t}{Q_e} = 1 - \left(\frac{6}{\pi^2} \right) \sum_{n=1}^{\infty} \left(\frac{1}{n^2} \right) e^{(-n^2 \beta_t)} \dots \dots \dots (8)$$

If $F > 0.85$ then

$$\beta_t = -0.04977 - \ln(1 - F) \dots \dots \dots a$$

If $F < 0.85$ then

$$\beta_t = \left[\sqrt{\pi} - \sqrt{\pi - \left(\frac{\pi^2 F}{3} \right)} \right]^2 \dots \dots \dots b$$

2.6. Adsorption isotherms

The adsorption isotherm tests were performed by contacting the MB solutions at different concentrations (between 50 and 500 mg/L for powder; between 50 and 1200 mg/L for beads) with adsorbent masses added to have a ratio of m/v equal to 1. These mixtures were kept under constant stirring equal to 250 rpm for 24 h (48 h for beads) with a well-controlled temperature (10, 25, 30 and 40 °C). Once the equilibrium was reached, the solutions were separated, then analyzed, and the adsorbed quantities were calculated using Eq. 1.

To understand the reaction mechanism and describe the adsorption process suitably, the correlations between the adsorbed quantity and the initial MB concentration were tested with Langmuir, Freundlich (two-parameter models) and Sips, Redlich-Peterson models (three-parameter models).

In an adsorption phenomenon, if the surface of the solid can be considered homogeneous, the Langmuir model can be applied. This model is based on the assumption of the similarity of the active sites with independent energies; the adsorption is monolayer without lateral interactions or steric hindrance between the adsorbed molecules [14]. The Langmuir equation is the following [15,16]:

$$Q_e/Q_m = K_L C_e / (1 + K_L C_e) \dots \dots \dots (9)$$

Whether the Langmuir modeling is favorable or not, a dimensionless separation factor under the abbreviation R_L , which can be calculated by the following relation (Eq. 10), has been proposed by Weber and Chakravorti, [17]:

$$R_L = 1 / (1 + K_L C_0) \dots \dots \dots (10)$$

Among the most used models, the oldest one, Freundlich model, that describes non-ideal and reversible adsorption. This empirical model is based on the formation of multilayer adsorbate, a non-uniform distribution, with a heterogeneity of the surface of the solid, and hence an adsorbent/adsorbate affinity [14,18]. Freundlich's empirical equation is defined as follows [14,15]:

$$Q_e = K_F C_e^{1/n_f} \dots \dots \dots (11)$$

Besides two-parameter models, three-parameter models are also available, such as the Redlich-Peterson model [19], which constitutes a compromise between the two above models; it is described by Eq. (12):

$$Q_e = K_{RP} C_e / (1 + \alpha C_e^\beta) \dots \dots \dots (12)$$

The adsorbate concentration in the Redlich-Peterson model plays an essential role because if it is high, the model approaches the Freundlich one. On the other hand, when it is low, the model becomes closer to the Langmuir model [14,20].

Our experimental results were also tested by one other three-parameter model, which has been proposed by Sips [4,14] according to the Eq. (13) as follows:

$$Q_e/Q_m = (K_S C_e)^{ms} / (1 + (K_S C_e)^{ms}) \dots \dots \dots (13)$$

2.7. Initial pH effect on the MB adsorption

In an adsorption study, the adsorbent surface charge is a dominant factor that cannot be ignored because the pH acts on both the surface charges of the material and the distribution of the anions and cations. Then, it has a considerable influence on the adsorption of MB. In 100 ml Erlenmeyer flasks, the effect of pH on the adsorption of MB was investigated by contacting at ambient temperature 50 ml of MB at an initial concentration of 100 mg/L with 50 mg of adsorbent, the agitation rate was 250 rpm, and the initial pH range investigated was between 2 and 12. The adjustment of the pH was insured by sodium hydroxide or hydrochloric acid. After shaking for 24 hours, the suspensions were centrifuged and analyzed by visible UV.

2.8. Effect of NaCl and Humic Acid on the MB adsorption

Inorganic salt NaCl and humic acid were used to quantify their impact on the adsorption performances. Constant concentrations of the used agents (0.1 mol/L for NaCl and 50 mg/L for humic acid) with different dye concentrations ranging from 50 up to 1200 mg/L were considered. After the dissolution of NaCl and humic acid in 50 ml of MB dye, 50 mg of adsorbent were added at room temperature; the mixtures were stirred with a multi-post magnetic stirrer for 24 h and then centrifuged and analyzed.

2.9. Effect of temperature and thermodynamic Parameters

The effect of the temperature was carried out in the range of 10 to 40°C, and the experiments were carried out similarly to adsorption isotherms. Therefore, considering Eq. 14 and 15, the feasibility of the MB adsorption process was checked [21].

$$\ln \left(\frac{Q_e}{C_e} * 1000 \right) = \Delta S^\circ - \frac{\Delta H^\circ}{T} \dots \dots \dots (14)$$

$$\Delta G^\circ = \Delta H^\circ - T * \Delta S^\circ \dots \dots \dots (15)$$

2.10. Regeneration study of BZJS and BOP

Achieving an efficient regeneration is among the objectives of the encapsulation to minimize treatment costs in view of subsequent industrial applications [22]. For this purpose, 100 mg of beads was introduced in a MB solution at 100 mg/L initial concentration and at natural pH (6.2). The mixture was kept under agitation for 48 h; once equilibrium was reached, the used beads were separated, cleaned several times with distilled water, and then dried at atmospheric temperature. Next, these dried beads were introduced again into a distilled water solution adjusted to the minimum pH of adsorption

by adding droplets of HCl; the suspension was stirred for 48 hours. This cycle was repeated six times, and the regeneration efficiency was calculated using Eq. 16.

$$E_R = \frac{Q_{des}}{Q_{ads}} * 100 \dots \dots \dots (16)$$

3. Theoretical study

3.1. Density Function Theory (DFT) details

All quantum chemical parameters presented in this study were calculated by the Gaussian 09W program package. The DFT method used involved B3LYP hybrid functional at 6-31G (d, p) basis set to optimize geometrically the molecular structures of BM and OP-H₃PO₄ [23]. In addition, at the obtained optimised structures, some quantum chemical parameters, such as the highest occupied molecular orbital energy (E_{HOMO}), the lowest unoccupied molecular orbital energy (E_{LUMO}), the energy gap (ΔE_{GAP}), dipole moments (μ), global hardness (η), global softness (σ), absolute electronegativity (χ) and electrophilicity index (Ω) were calculated by applying the following relationships [24,25] :

$$\Delta E_{GAP} = E_{LUMO} - E_{HOMO} \dots \dots \dots (17)$$

$$\eta = \frac{E_{LUMO} - E_{HOMO}}{2} \dots \dots \dots (18)$$

$$\sigma = \frac{1}{\eta} \dots \dots \dots (19)$$

$$\chi = \frac{-(E_{HOMO} + E_{LUMO})}{2} \dots \dots \dots (20)$$

$$\Omega = \frac{\chi^2}{2\eta} \dots \dots \dots (21)$$

3.2. Molecular Dynamic Simulation (MDS) details

The Materials Studio 7.0 software was used to carry out all the molecular dynamics simulations (MDS) performed in this work. The OP-H₃PO₄ (110) surface to study the adsorption of MB onto the OP-H₃PO₄ surface was chosen in these simulations. The dimensions of the chosen simulation box were (30 Å × 15 Å × 25 Å), using the periodic boundary conditions. In addition, the OP-H₃PO₄ slab, the MB molecule, and a vacuum slab were included in this simulation box. The MB molecular structure and the OP-H₃PO₄ (110) surface were geometrically optimized by minimizing the energy. The MDS were performed at 298K, NVT ensemble we applied the COMPASS force field model with a time step of 0.1 fs and a simulation period of 50 ps.

4. Statistical physical modeling

To provide deeper and more precise interpretations for the MB adsorption mechanism on adsorbents [26], physical modeling was considered using statistical physics models based on applying the grand canonical partition function in statistical physics. The three models applied are detailed in the following subsection.

4.1. Monolayer model with single energy: MMSE

This model assumes that the adsorption occurred in a monolayer with only one energy [27]. The demonstration of the applied physical models needs to go through the use of the grand canonical partition function in statistical physics; for this purpose, the grand canonical partition function of one site is given as follows (Eq. 22) [28] :

$$Z_{gc} = 1 + e^{\beta_s(\varepsilon_1 + \mu)} \dots \dots \dots (22)$$

Where β_s is defined $1/k_B T$.

Then, Eq. 23 presents the grand canonical partition function relative to the density of receptor sites, which is assumed to be identical and independent.

$$Z_{gc}(Ns) = (Z_{gc})^{Ns} \dots \dots \dots (23)$$

As a result, it is possible to write that:

$$Z_{gc}(Ns) = (1 + e^{\beta_s(\varepsilon_1 + \mu)})^{Ns} \dots \dots \dots (24)$$

As a consequence, the average site occupation number is given according to Eq. 25 [29] :

$$N_0 = \frac{N_s \partial \ln Z_{gc}}{\beta_s \partial \mu} \dots \dots \dots (25)$$

Furthermore, in an adsorption process of a binary system (for example, the adsorption of MB on BOP), it is possible to write that:



At thermodynamic equilibrium, Eq. 25 provides the relationship between the chemical potentials of dissolved molecules μ_m and that of adsorbed molecules μ as a function of the translational partition function, as seen in Eq. 26 [30] :

$$\mu_m = \frac{\mu}{n_m} = k_B T \ln(Ns/Z_{gr}) \dots \dots \dots (26)$$

Eq. 27 can be used to express the translation partition function [31]:

$$Z_{gtr} = V \left(\frac{2\pi m}{\beta_s h^2} \right)^{3/2} \dots \dots \dots (27)$$

Furthermore, the adsorbed quantity at saturation is given by Eq. 28 [32,33]:

$$Q_{sat} = n_{im} N_{iS} \dots \dots \dots (28)$$

Taking all previous equations into consideration, the monolayer model with single energy (MMSE) is given by Eq.29 [32,33]:

$$Q = \frac{Q_0}{\left(1 + \left(\frac{C_{1/2}}{C_e} \right)^{n_m} \right)} \dots \dots \dots (29)$$

It is worth noting that MMSE can provide a number of adsorbates equal to or greater than unity on a single adsorption site [34].

4.2. Monolayer model with two energies: MMTE

For this model, the demonstration carried out for the MMSE is the same, except that its grand canonical partition function and that related to the receptor sites are given according to Eqs.30 and 31, respectively [35]:

$$Z_{gc} = 1 + e^{\beta_s(\varepsilon_1+\mu)} + e^{\beta_s(\varepsilon_2+2\mu)} \dots \dots \dots (30)$$

$$Z_{gc}(N_S) = \left(1 + e^{\beta_s(\varepsilon_1+\mu)} + e^{\beta_s(\varepsilon_2+2\mu)} \right)^{N_S} \dots \dots \dots (31)$$

As the name implies, the MMTE assumes that the adsorption was carried out on a monolayer with two types of receptor sites, which have two deferent energies (ΔE_1 and ΔE_2), and that the receptor site can capture a variable number of adsorbate [36], the change in the adsorbed amount as a function of the equilibrium concentration is given by Eq. 32 [37]:

$$Q_e = \frac{n_{1m} N_{1S}}{1 + \left(\frac{C_1}{C_e} \right)^{n_1}} + \frac{n_{2m} N_{2S}}{1 + \left(\frac{C_2}{C_e} \right)^{n_2}} \dots \dots \dots (32)$$

4.3. Double layer model with two energies: DMTE

For this last used model, the adsorption is carried out in double layers with two energies; the first energy is considered to ensure the solid-liquid interaction (adsorbent, adsorbate) and the second energy to ensure the interaction between the two liquid phases (adsorbate first layer and that of the second layer) [37,38]. The grand canonical partition

function (Z_{gc}) and the one related to the density of receptor sites ($Z_{gc}(N_s)$) representative of DMTE are given by Eqs. 32 and 33, respectively.

$$Z_{gc} = 1 + e^{\beta_s(\varepsilon_1+\mu)} + e^{\beta_s(\varepsilon_1+\varepsilon_2+2\mu)} \dots \dots \dots (32)$$

$$Z_{gc}(N_s) = (1 + e^{\beta_s(\varepsilon_1+\mu)} + e^{\beta_s(\varepsilon_1+\varepsilon_2+2\mu)})^{N_s} \dots \dots \dots (33)$$

As a result, the empirical expression of DMTE is given by Eq. 34:

$$Q = Q_0 \frac{\left(\frac{C_e}{C_1}\right)^{n_m} + 2\left(\frac{C_e}{C_2}\right)^{n_m}}{1 + \left(\frac{C_e}{C_1}\right)^{n_m} + \left(\frac{C_e}{C_2}\right)^{n_m}} \dots \dots \dots (34)$$

4.4. Limited multilayer model (LMM)

The last model used in this part is the limited multilayer model (LMM). In this model, it is assumed that adsorption occurs in multilayer, with the adsorption energy of the molecules in the first layer is higher than that of the second layer and so on [39]. The adsorbed amount in this model varies according to the following equation [39,40]:

$$Q = \frac{\left[Q_0 \left[\frac{\left(\frac{C}{C_1}\right)^{n_m} + 2\left(\frac{C}{C_1}\right)^{n_m} \left(\frac{C}{C_2}\right)^{n_m} \left(1 - \left(\frac{C}{C_2}\right)^{n_m N_2}\right)}{1 - \left(\frac{C}{C_2}\right)^{n_m}} - \frac{N_2 \left(\frac{C}{C_1}\right)^{n_m} \left(\frac{C}{C_2}\right)^{n_m} \left(\frac{C}{C_2}\right)^{n_m N_2}}{1 - \left(\frac{C}{C_2}\right)^{n_m}} + \frac{\left(\frac{C}{C_1}\right)^{n_m} \left(\frac{C}{C_2}\right)^{2n_m} \left(1 - \left(\frac{C}{C_2}\right)^{n_m N_2}\right)}{\left(1 - \left(\frac{C}{C_2}\right)^{n_m}\right)^2} \right] \right]}{\left[1 + \frac{\left(\frac{C}{C_1}\right)^{n_m} + \frac{\left(\frac{C}{C_1}\right)^{n_m} \left(\frac{C}{C_2}\right)^{n_m} \left(1 - \left(\frac{C}{C_2}\right)^{n_m N_2}\right)}{1 - \left(\frac{C}{C_2}\right)^{n_m}} \right]} \dots \dots (35)$$

4.5. Statistical physical modeling evaluation parameters

The error function (F error), the adjusted determination coefficient R^2 and the Bayesian information criterion (BIC) were used to select the appropriate statistical model for the experimental results; the concept of the error function is to compare the experimental points with those generated by the model; F error is defined as follows [36]:

$$F_{error} = \sqrt{\sum_1^p \left(\frac{1}{p-1}\right) \left(\frac{Q_{i,mod} - Q_{i,exp}}{Q_{i,exp}}\right)^2} \dots \dots \dots (36)$$

Further, the Bayesian Information Criterion (BIC) is given by Eq. 37 [41]:

$$BIC = K * \ln(n) + p * \ln \left[\frac{\sum (Q_{e,exp} - Q_{e,mod})^2}{p} \right] \dots \dots \dots (37)$$

An adjustment method based on the Levenberg-Marquardt iteration algorithm that uses statistical weighting and nonlinear regression was considered to correlate the experimental

- [7] A. Özer, Removal of Pb(II) ions from aqueous solutions by sulphuric acid-treated wheat bran, *J. Hazard. Mater.* 141 (2007) 753–761. <https://doi.org/10.1016/j.jhazmat.2006.07.040>.
- [8] A. Bouguettoucha, D. Chebli, T. Mekhalef, A. Noui, A. Amrane, The use of a forest waste biomass, cone of *Pinus brutia* for the removal of an anionic azo dye Congo red from aqueous medium, *Desalination Water Treat.* 55 (2015) 1956–1965. <https://doi.org/10.1080/19443994.2014.928235>.
- [9] M.C. Somasekhara Reddy, L. Sivaramakrishna, A. Varada Reddy, The use of an agricultural waste material, Jujuba seeds for the removal of anionic dye (Congo red) from aqueous medium, *J. Hazard. Mater.* 203–204 (2012) 118–127. <https://doi.org/10.1016/j.jhazmat.2011.11.083>.
- [10] S. Li, Z. Zeng, W. Xue, Adsorption of lead ion from aqueous solution by modified walnut shell: kinetics and thermodynamics, *Environ. Technol.* 40 (2019) 1810–1820. <https://doi.org/10.1080/09593330.2018.1430172>.
- [11] G. Polat, Y.S. Açikel, Synthesis and Characterization of Magnetic Halloysite–Alginate Beads for the Removal of Lead(II) Ions from Aqueous Solutions, *J. Polym. Environ.* 27 (2019) 1971–1987. <https://doi.org/10.1007/s10924-019-01489-w>.
- [12] B. Choudhary, D. Paul, Isotherms, kinetics and thermodynamics of hexavalent chromium removal using biochar, *J. Environ. Chem. Eng.* 6 (2018) 2335–2343. <https://doi.org/10.1016/j.jece.2018.03.028>.
- [13] S.U. Din, T. Mahmood, A. Naeem, M. Hamayun, N.S. Shah, Detailed kinetics study of arsenate adsorption by a sequentially precipitated binary oxide of iron and silicon, *Environ. Technol.* 40 (2019) 261–269. <https://doi.org/10.1080/09593330.2017.1385649>.
- [14] K.Y. Foo, B.H. Hameed, Insights into the modeling of adsorption isotherm systems, *Chem. Eng. J.* 156 (2010) 2–10. <https://doi.org/10.1016/j.cej.2009.09.013>.
- [15] K.V. Kumar, K. Porkodi, F. Rocha, Isotherms and thermodynamics by linear and non-linear regression analysis for the sorption of methylene blue onto activated carbon: Comparison of various error functions, *J. Hazard. Mater.* 151 (2008) 794–804. <https://doi.org/10.1016/j.jhazmat.2007.06.056>.
- [16] I. Langmuir, THE ADSORPTION OF GASES ON PLANE SURFACES OF GLASS, MICA AND PLATINUM., *J. Am. Chem. Soc.* 40 (1918) 1361–1403. <https://doi.org/10.1021/ja02242a004>.

- [17] N. Sivarajasekar, R. Baskar, Adsorption of Basic Magenta II onto H₂SO₄ activated immature *Gossypium hirsutum* seeds: Kinetics, isotherms, mass transfer, thermodynamics and process design, *Arab. J. Chem.* (2014). <https://doi.org/10.1016/j.arabjc.2014.10.040>.
- [18] M. Bounaas, A. Bouguettoucha, D. Chebli, A. Reffas, I. Harizi, F. Rouabah, A. Amrane, High efficiency of methylene blue removal using a novel low-cost acid treated forest wastes, *Cupressus sempervirens* cones: Experimental results and modeling, *Part. Sci. Technol.* 0 (2018) 1–10. <https://doi.org/10.1080/02726351.2017.1401569>.
- [19] O. Redlich, D.L. Peterson, A Useful Adsorption Isotherm, *J. Phys. Chem.* 63 (1959) 1024–1024. <https://doi.org/10.1021/j150576a611>.
- [20] M. Baghdadi, UT (University of Tehran) isotherm as a novel and useful adsorption isotherm for investigation of adsorptive removal of pollutants, *J. Environ. Chem. Eng.* 5 (2017) 1906–1919. <https://doi.org/10.1016/j.jece.2017.03.037>.
- [21] T. Benhalima, H. Ferfera-Harrar, Eco-friendly porous carboxymethyl cellulose/dextran sulfate composite beads as reusable and efficient adsorbents of cationic dye methylene blue, *Int. J. Biol. Macromol.* 132 (2019) 126–141. <https://doi.org/10.1016/j.ijbiomac.2019.03.164>.
- [22] F. Ogata, T. Nakamura, N. Kawasaki, Adsorption capability of virgin and calcined wheat bran for molybdenum present in aqueous solution and elucidating the adsorption mechanism by adsorption isotherms, kinetics, and regeneration, *J. Environ. Chem. Eng.* 6 (2018) 4459–4466. <https://doi.org/10.1016/j.jece.2018.06.047>.
- [23] R.G. Parr, Y. Weitao, *Density-Functional Theory of Atoms and Molecules*, Oxford University Press, 1994.
- [24] W. Kohn, L.J. Sham, Quantum Density Oscillations in an Inhomogeneous Electron Gas, *Phys. Rev.* 137 (1965) A1697–A1705. <https://doi.org/10.1103/PhysRev.137.A1697>.
- [25] M. Arivazhagan, V.P. Subhasini, Quantum chemical studies on structure of 2-amino-5-nitropyrimidine, *Spectrochim. Acta. A. Mol. Biomol. Spectrosc.* 91 (2012) 402–410. <https://doi.org/10.1016/j.saa.2012.02.018>.
- [26] M. Mobarak, E.A. Mohamed, A.Q. Selim, L. Sellaoui, A.B. Lamine, A. Erto, A. Bonilla-Petriciolet, M.K. Seliem, Surfactant–modified serpentine for fluoride and Cr(VI) adsorption in single and binary systems: Experimental studies and theoretical

- modeling, Chem. Eng. J. 369 (2019) 333–343. <https://doi.org/10.1016/j.cej.2019.03.086>.
- [27] A. Yazidi, L. Sellaoui, G.L. Dotto, A. Bonilla-Petriciolet, A.C. Fröhlich, A.B. Lamine, Monolayer and multilayer adsorption of pharmaceuticals on activated carbon: Application of advanced statistical physics models, J. Mol. Liq. 283 (2019) 276–286. <https://doi.org/10.1016/j.molliq.2019.03.101>.
- [28] A.H. Almuqrin, S. Wjihi, F. Aouaini, A.B. Lamine, New insights on physico-chemical investigation of bisphosphonate adsorption isotherm into apatite substrate using statistical physics treatment, J. Mol. Liq. 310 (2020) 113230. <https://doi.org/10.1016/j.molliq.2020.113230>.
- [29] B. Mohamed, Z. Qingyu, G. D. Moggridge, B.L. Abdelmottaleb, New insight in adsorption of pyridine on the two modified adsorbents types MN200 and MN500 by means of grand canonical ensemble, J. Mol. Liq. 263 (2018) 413–421. <https://doi.org/10.1016/j.molliq.2018.05.008>.
- [30] A.Q. Selim, L. Sellaoui, M. Mobarak, Statistical physics modeling of phosphate adsorption onto chemically modified carbonaceous clay, J. Mol. Liq. 279 (2019) 94–107. <https://doi.org/10.1016/j.molliq.2019.01.100>.
- [31] M. Khalfaoui, A.E. Ghali, C. Aguir, Z. Mohamed, M.H.V. Baouab, A.B. Lamine, Study on adsorption of herbicide onto functionalized cellulose extracted from *Juncus acutus* L. plant: Experimental results and theoretical modeling, Ind. Crops Prod. 67 (2015) 169–178. <https://doi.org/10.1016/j.indcrop.2015.01.032>.
- [32] F. Dhaouadi, L. Sellaoui, H.E. Reynel-Ávila, V. Landín-Sandoval, D.I. Mendoza-Castillo, J.E. Jaime-Leal, E.C. Lima, A. Bonilla-Petriciolet, A.B. Lamine, Adsorption mechanism of Zn²⁺, Ni²⁺, Cd²⁺, and Cu²⁺ ions by carbon-based adsorbents: interpretation of the adsorption isotherms via physical modelling, Environ. Sci. Pollut. Res. 28 (2021) 30943–30954. <https://doi.org/10.1007/s11356-021-12832-x>.
- [33] A. Gómez-Avilés, L. Sellaoui, M. Badawi, A. Bonilla-Petriciolet, J. Bedia, C. Belver, Simultaneous adsorption of acetaminophen, diclofenac and tetracycline by organo-sepiolite: Experiments and statistical physics modelling, Chem. Eng. J. 404 (2021) 126601. <https://doi.org/10.1016/j.cej.2020.126601>.
- [34] S. Wjihi, F. Aouaini, A.H. Almuqrin, A.B. Lamine, Physicochemical assessment of prednisone adsorption on two molecular composites using statistical physics formalism in cosmetics, Arab. J. Chem. 13 (2020) 6876–6886. <https://doi.org/10.1016/j.arabjc.2020.06.040>.

- [35] M.B. Manaa, N. Issaoui, N. Bouaziz, A.B. Lamine, Combined statistical physics models and DFT theory to study the adsorption process of paprika dye on TiO₂ for dye sensitized solar cells, *J. Mater. Res. Technol.* 9 (2020) 1175–1188. <https://doi.org/10.1016/j.jmrt.2019.11.045>.
- [36] C. Djama, D. Chebli, A. Bouguettoucha, I. Doudou, A. Amrane, Statistical physics modelling of azo dyes biosorption onto modified powder of *Acorus calamus* in batch reactor, *Biomass Convers. Biorefinery.* (2021). <https://doi.org/10.1007/s13399-020-01190-2>.
- [37] F. Dhaouadi, L. Sellaoui, G.L. Dotto, A. Bonilla-Petriciolet, A. Erto, A.B. Lamine, Adsorption of methylene blue on comminuted raw avocado seeds: Interpretation of the effect of salts via physical monolayer model, *J. Mol. Liq.* 305 (2020) 112815. <https://doi.org/10.1016/j.molliq.2020.112815>.
- [38] L. Sellaoui, S. Knani, A. Erto, M.A. Hachicha, A. Ben Lamine, Equilibrium isotherm simulation of tetrachlorethylene on activated carbon using the double layer model with two energies: Steric and energetic interpretations, *Fluid Phase Equilibria.* 408 (2016) 259–264. <https://doi.org/10.1016/j.fluid.2015.09.022>.
- [39] L. Sellaoui, H. Guedidi, S. Knani, L. Reinert, L. Duclaux, A. Ben Lamine, Application of statistical physics formalism to the modeling of adsorption isotherms of ibuprofen on activated carbon, *Fluid Phase Equilibria.* 387 (2015) 103–110. <https://doi.org/10.1016/j.fluid.2014.12.018>.
- [40] F. Aouaini, S. Knani, M.B. Yahia, N. Bahloul, N. Kechaou, A.B. Lamine, Application of Statistical Physics on the Modeling of Water Vapor Desorption Isotherms, *Dry. Technol.* 32 (2014) 1905–1922. <https://doi.org/10.1080/07373937.2014.924131>.
- [41] D.R. Lima, E.C. Lima, C.S. Umpierres, P.S. Thue, G.A. El-Chaghaby, R.S. da Silva, F.A. Pavan, S.L.P. Dias, C. Biron, Removal of amoxicillin from simulated hospital effluents by adsorption using activated carbons prepared from capsules of cashew of Para, *Environ. Sci. Pollut. Res.* 26 (2019) 16396–16408. <https://doi.org/10.1007/s11356-019-04994-6>.
- [42] M.B. Yahia, S. Knani, L.B.H. Hsan, M.B. Yahia, H. Nasri, A. Ben Lamine, Statistical studies of adsorption isotherms of iron nitrate and iron chloride on a thin layer of porphyrin, *J. Mol. Liq.* 248 (2017) 235–245. <https://doi.org/10.1016/j.molliq.2017.10.073>.

Chapter III: Insights on the statistical physics modeling of the methylene blue adsorption onto *Ziziphus jujuba* stones-treated ortho-phosphoric acid

1. Introduction

During the last decade, biosorbents have been widely used to eliminate dyes from textiles effluents [1,2], to treat effluents from the pharmaceutical industry [3,4], as well as for the removal of toxic metal ions [5,6], in order to benefit from their low cost, their availability in nature, their porosity, their active sites and their richness in different hetero-elements, such as O, N, S, Fe [7]. Statistics show that world dyes production is about 100,000 dyes with a flux of 7×10^5 - 1×10^6 tons per year [8], and 2% of this annual production is released directly into aqueous effluents [5]. These synthetic dyes are both toxic (usually not biodegradable) and responsible for water coloration; they constitute a real problem that needs to be solved. Consequently, and to clean up wastewater before its return to the natural environment or its reuse, coagulation and flocculation [9], chemical oxidation [10,11], filtration [12,13], adsorption [14–16], among other techniques, have been used for wastewater treatment. Each of these processes shows advantages and disadvantages (efficiency, cost and environmental impact etc). Because of its performance, low cost, simplicity of design, and ease of use, adsorption is considered the most efficient technique that meets the requirements of rejection [17,18].

In this aim, in recent years, many researchers have been interested in exploring new adsorbents based on natural materials alternative to those usually implemented in water treatment. These materials are less expensive, easier to find and use, and consequently appear as a topic of intensive research. For these reasons, several studies dealt with eliminating various pollutants using different precursors. Among them, the adsorption of congo red on the Seeds of *Jujuba* [19], the removal of cationic dyes onto raw peach shell [20], the adsorption of methylene blue on modified seeds of a tree called *Ceibapentandra* [21], the elimination of congo red onto *Stipa tenassicima* [22], as well as on cones of *Pinus brutia* [23], the removal of rhodamine B (RhB), methylene blue, brilliant green, crystal violet and orange G from aqueous solutions on activated carbon made from tea leaves [24], and the adsorption of methylene blue using nut shells [25] can be for instance cited.

Intending to promote local by-products, and from economic and environmental terms, the objective of this chapter was to prepare a low-cost adsorbent from biomass. For this

purpose, stones of *Ziziphus jujuba*, commonly encountered in northern Algeria, were used as a precursor for the preparation of the biosorbent. These stones were chemically treated with ortho-phosphoric acid and then characterized by scanning electron microscopy (SEM), Fourier transform infrared spectroscopy (FTIR), *X-ray fluorescence* (XRF) and thermogravimetric analysis (TGA). The performances of our material were tested by the adsorption of methylene blue (MB), which is considered a model of cationic dyes [26]. In addition, pH effect, initial concentration, contact time, temperature, the impact of the presence of salts, and humic acids were also examined.

Moreover, to more deeply understand the adsorption process and to obtain new physico-chemical interpretations at the molecular level [27,28], and based on the grand canonical ensemble in statistical physics, our experimental results were correlated by few statistical physics models, where the monolayer with single energy (MMSE), double layer with single energy (DMSE), double layer with two energies (DMTE) and the limited multi-layer (LMM) models were considered.

2. Results and Discussions

2.1. Materials characterization

Regarding the physicochemical characteristics of ZJS- H_3PO_4 , the zero charge point (pH_{PZC}), humidity, porosity, ash content, acidity, basicity and apparent density were determined. In this context, the XRF analysis was used to quantify the elemental composition of ZJS before and after treatment; all the results obtained are summarized in Table 1.

Table 1: Some Physical and chemical characteristics of ZJS and *ZJS-H₃PO₄*

	Porosity (%)	Apparent density (g ml ⁻¹)	Moisture content (%)	ash content (%)	Acidity (m eq g g ⁻¹)	Basicity (m eq g g ⁻¹)	pH _{PCZ}	pH in water solution
<i>ZJS</i>	80.21	0.031	0.15	33.12	0.31	0.32	7.4	6.5
<i>ZJS-H₃PO₄</i>	87.29	0.034	0.12	31.42	0.35	0.30	6.8	6.1
Elemental Composition by XRF								
Element	C (%)	O (%)	Mg (%)	Al (%)	Si (%)	P (%)	Others	
<i>ZJS</i>	48.700	50.400	0.131	0.048	0.044	0.030	0.647	
<i>ZJS-H₃PO₄</i>	47.500	51.700	0.022	0.106	0.150	0.110	0.412	

The pH_{PZC} is a dominant parameter for understanding the adsorption mechanism of MB onto ZJS- H_3PO_4 ; it corresponds to the point for which the ZJS- H_3PO_4 has a zero charge potential on its surface. It also gives an idea about the charge of the material surface based on the presence or the absence of H^+ protons and OH^- ions.

Fig. 1 shows the plot ΔpH as a function of the initial pH_i , showing pH_{PZC} values of approximately 7.4 for ZJS and 6.8 for ZJS- H_3PO_4 , which means that:

- The material surface functional groups are protonated by an excess of H^+ protons when the pH is below pH_{PZC} .
- The ZJS- H_3PO_4 surface functional groups are deprotonated by the presence of excess OH^- ions in the solution when the pH is greater than pH_{PZC} .

Table 1 shows that ZJS- H_3PO_4 had an acidic character compared to ZJS, owing to more acidic sites than alkaline sites. However, table 1 also indicates that the porosity and apparent density after treatment were improved from 80.21 to 87.29 % and 0.031 to 0.034 $g\ ml^{-1}$, respectively. Consequently, these improvements may be attributed to integrating ortho-phosphoric acid into the material structure, where the washing of the final product to extract the incorporated acid led to create an extreme porosity.

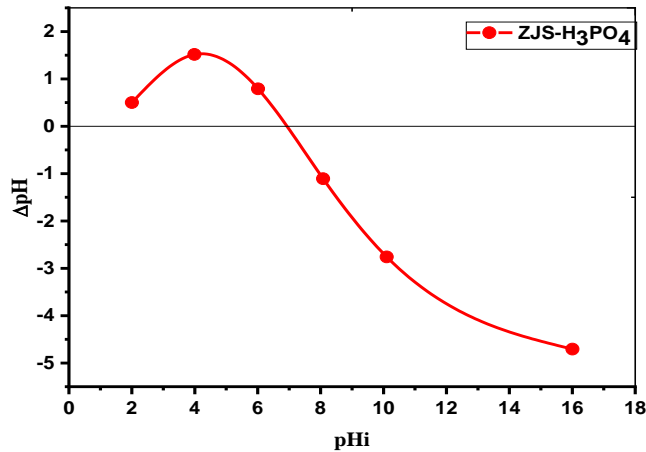


Figure 1. The change in final pH as a function of the initial pH for solutions of ZJS- H_3PO_4 adsorbent during the determination of the point of zero charge PZC.

The elemental composition analysis XRF indicates that carbon and oxygen were the main elements in ZJS- H_3PO_4 . XRF also showed an increase in phosphorus due to the influence of ortho-phosphoric acid during treatment. Fourier transform infrared spectroscopy is a very useful technique to determine the functional groups present on the surface of a material, allowing to improve the understanding of the mechanism of MB

adsorption onto ZJS-H₃PO₄, as well as the interactions between MB and ZJS-H₃PO₄. The FTIR spectra of ZJS, ZJS-H₃PO₄, and ZJS-H₃PO₄ after the adsorption of methylene blue (ZJS-H₃PO₄ + MB) are illustrated in Fig. 2, showing very similar spectra for the three samples. The valence vibrations of the hydroxyl groups (of carboxyl, phenol, or alcohol) and the adsorbed water were represented by the broadband located at 3421 cm⁻¹ [29]. The two small absorption bands at 2850 and 2932 cm⁻¹ resulted mainly from the aliphatic C-H elongation vibrations. However, olefinic vibrations (C = C) caused the band appearing at about 1644 cm⁻¹. The carboxylic groups (C = O) were represented by the absorption band at 1735cm⁻¹. The band at 1381 cm⁻¹ can be attributed to the N-O elongation vibration [19]. The small absorption bands at 1517 and 1444 cm⁻¹ were due to the elongation vibrations of the C = C bonds in aromatic rings; the small bands between 600 and 900 cm⁻¹ can be attributed to the mode of deformation outside the C-H plane in the aromatic rings [30].

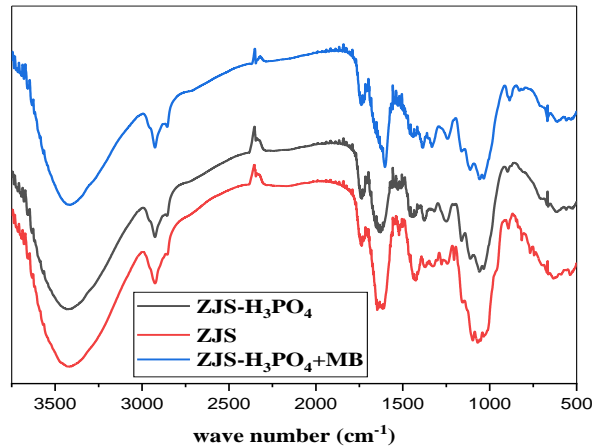


Figure 2. FTIR spectra of samples: ZJS, ZJS-H₃PO₄ and ZJS-H₃PO₄ +MB in the range of 4000–500 cm⁻¹.

Fig. 2 shows the existence of several bands between 900 and 1200 cm⁻¹, which may be due to the presence of phosphorus and phosphocarbon compounds in the samples [31,32], whose three bands appeared at 1163, 1118 and 1045 cm⁻¹ and are generally attributed to P-O-P elongation vibrations of polyphosphates or P⁺-O⁻ ionized bonds in ortho-phosphoric acid esters [32,33]. Fig. 2 also shows certain variations in the intensity of some peaks and shifting of other peaks, which led us to conclude that the treatment by ortho-phosphoric acid was modified the surface chemistry of ZJS, maybe by the formation of acidic oxygen-contained complexes by strong oxidation [34]; this promotes the absorption of basic compounds such as methylene blue.

The XRD of *Ziziphus jujuba* stones before (ZJS) and after treatment (ZJS-H₃PO₄) are shown in Fig. 3. The diffractograms showed an amorphous structure for both samples,

which confirmed that the treatment with ortho-phosphoric acid did not act on the crystalline structure. Fig. 3 also shows a broad and intense peak around $2\theta=22^\circ$ which can be attributed to cellulose [20]. The amorphous structure was confirmed by the presence of lignin and hemicelluloses, which were represented by a small peak at $2\theta = 15^\circ$ [3].

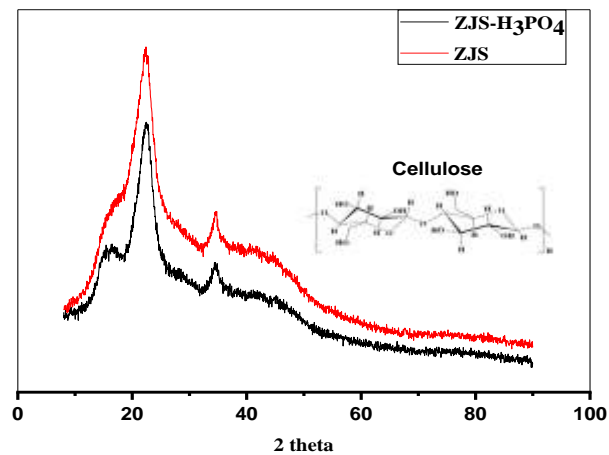


Figure 3. XRD data of Treated and raw Ziziphus jujuba stones.

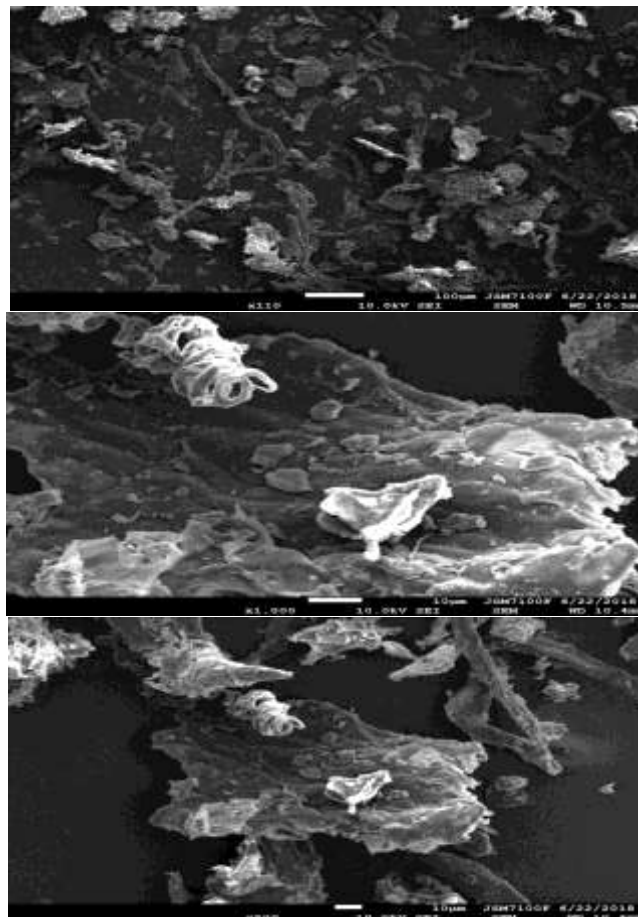


Figure 4. SEM images of ZJS-H₃PO₄.

The micromorphology of ZJS- H_3PO_4 was examined, and the obtained results are displayed in Fig. 4, showing that the ZJS- H_3PO_4 had a non-uniform structure with a heterogeneity of the pores size [19], which favors its use as an adsorbent.

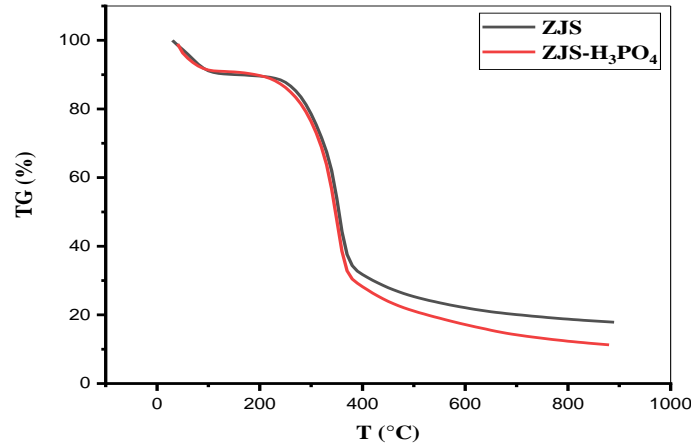


Figure 5. Thermogravimetric analysis of ZJS and ZJS- H_3PO_4

Thermogravimetric analysis for ZJS and ZJS- H_3PO_4 was performed in a temperature range from 30 to 890 °C and the results obtained are given in Fig.5. It is obvious from this figure that the two samples showed similar results characterized by four stages. The first stage (from 30 to 100 °C) is defined by a 9% mass loss, which may be attributed to the elimination of the product's humidity. The second phase was characterized by an equilibrium stage between 100 and 230 °C, with no weight loss. Then, from 230 up to 370°C, the third stage, showed a significant weight loss of about 77%, which may be due to gaseous compounds (CO_2 , CH_4 , CO , H_2) or to the degradation of the hemicelluloses [35]. Finally, in the last stage (370 °C up to the end of analysis), the mass loss reached 83% for ZJS and 89% for ZJS- H_3PO_4 ; these losses can be attributed to the degradation of cellulose which was the main compound of the products as indicated by the XRD analysis.

2.2. Effect of the pH

The influence of the pH on the adsorption of MB onto ZJS- H_3PO_4 was examined. Fig. 6 illustrates the results obtained, showing a noticeable increase in the amount adsorbed in the range of 2 to 8. In contrast, no significant variation of the adsorbed amount of MB was observed in the range of 8 to 12. This variation can be explained by the pH_{PZC} of ZJS- H_3PO_4 , which was about 6.8. Indeed, since MB is a cationic dye, its adsorption is favored at pH higher than the pH_{PZC} by electrostatic interactions between the dye that is positively charged and the ZJS- H_3PO_4 that is deprotonated by the surplus of (OH^-) ions, owing to the significant impact of the pH, the optimal pH (10) was selected and considered thereafter.

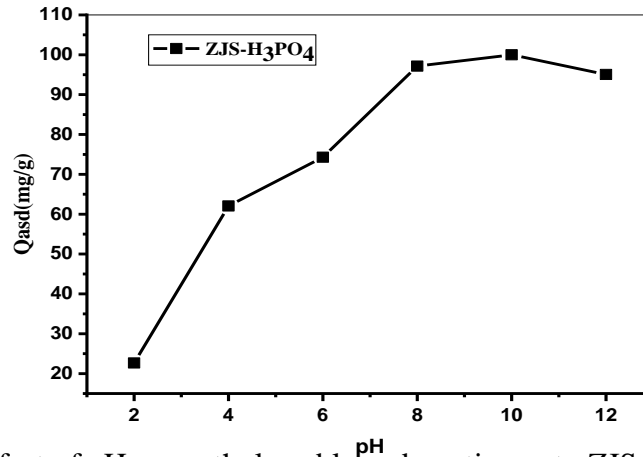


Figure 6. Effect of pH on methylene blue adsorption onto ZJS-H₃PO₄. (agitation Speed=250 rpm, m=50 mg, V =50 ml, T =25°C).

2.3. Effect of the contact time and the initial concentration

The results obtained regarding the adsorption kinetics are illustrated in Fig. 7, showing several steps in the adsorption kinetics of MB onto ZJS-H₃PO₄, which unrolled starting with a rapid adsorption step on the external surface of the solid, which may be due to the difference between the concentration of MB in the solution and the solid surface [36]. The second step can be defined by a decrease in the number of available adsorption sites, which slowed down the adsorption rate as the MB was adsorbed. Finally, the equilibrium time was achieved in the third step, when there were no more free or accessible adsorption sites (after 20 min for the lowest concentration and 60 min for the highest concentration). The results also show that when the initial concentration increased, the adsorbed quantity also increased, and the amounts adsorbed at equilibrium were 50, 93 and 128 mg g⁻¹ for 50, 100, and 150 mg L⁻¹ dye concentrations, respectively.

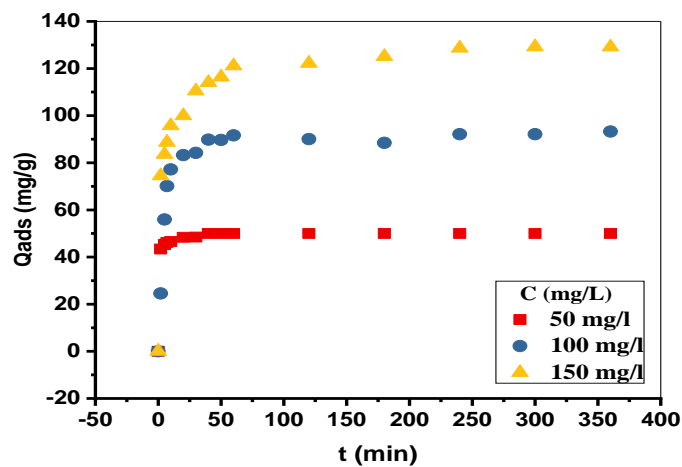


Figure 7. Effect of the contact time and the initial MB concentration on the adsorption capacity. (T = 25°C, agitation speed= 250 rpm, pH=10).

2.4. Isotherms modeling

The adsorption isotherm is represented by the variation of the adsorbed quantity as a function of the equilibrium concentration at a given temperature. In this work, the adsorption isotherms of MB onto ZJS-H₃PO₄ were carried out at different temperatures (25, 30, and 40 °C). Fig. 8 illustrates that the obtained isotherms were of type-I for the three considered temperatures, according to the classification of the UPAC [37]. Such a type of isotherm is commonly encountered; it characterizes both an adsorption monolayer and the existence of micropores.

According to Fig. 8, it can be observed that for 30 and 40°C, the adsorption isotherms were almost similar. This phenomenon may be due to several factors, including the solubility of the MB molecules, which does not change in this temperature range, or the morphology of ZJS-H₃PO₄, which can be distorted when the temperature increases to 40°C and causes a decrease in the adsorption performance of the ZJS-H₃PO₄.

Moreover, adsorption capacity deduced from adsorption isotherms clearly shows the potential of ZJS-H₃PO₄ to be used as an adsorbent for organic dyes. Indeed, its maximum adsorption capacity is compared to some other adsorbents tested for MB adsorption in Table 2, showing that its capacity was almost similar to the most efficient ones, peach shells, 179.8 and 183.6 mg g⁻¹, respectively (Table 2).

Table 2: Comparison of some values of maximum biosorption amount of MB onto various adsorbents

Adsorbent	Q _{ads} (mg g ⁻¹)	References
ZJS-H ₃ PO ₄	179.83	This work
Peach shells	183.6	[20]
Mango seed kernel	142.9	[38]
S. tenassicima fiber	5.35	[22]
Pine cone biomass	109.89	[18]
Treated Macauba palm cake	33.06	[39]
treated lignocellulosic	769	[40]

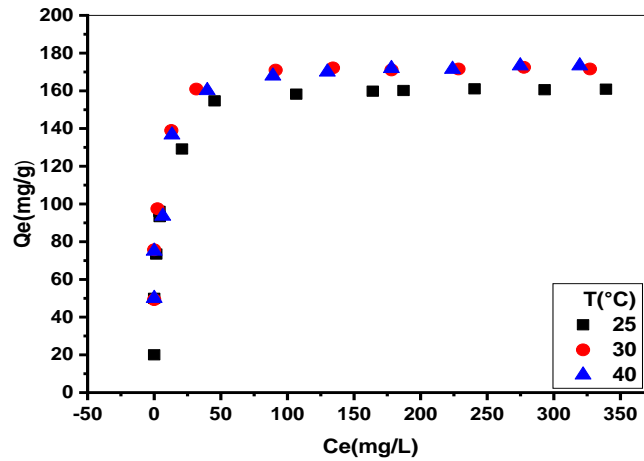


Figure 8. Equilibrium isotherms for MB adsorption onto ZJS-H₃PO₄ at different temperatures.(agitation speed= 250 rpm, pH=10).

Besides, experimental data were fitted by the non-linear models of Langmuir and Freundlich (2 parameters), Sips and Redlich-Peterson (three-parameters). The corresponding data are displayed in Fig. 9, and the related constants are collected in Table 3. As observed, the adsorption isotherms for the three temperatures were well described by the Langmuir model compared to the other models, with coefficients of correlation between 0.968 and 0.981. In addition, the adsorbed quantities calculated by the Langmuir model were very close to the adsorbed quantities found experimentally. Therefore, it can be concluded that the Langmuir model was the most reliable irrespective of the temperature.

Furthermore, the R_L factor values were between 0 and 1, confirming that the Langmuir modeling was favorable for the three temperatures [41].

Table 3: Langmuir, Freundlich, Sips and Redlich-Peterson constants for MB adsorption onto ZJS-H₃PO₄

Material	Models	Parameters	25 °C		30 °C		40 °C	
ZJS-H ₃ PO ₄	Langmuir	Q _{exp} (mg/g)	160.85	173.45	179.83			
		Q _m (mg/g)	160.57	172.71	176.99			
		K _L (L/mg)	0.391	0.467	0.189			
		R ²	0.977	0.968	0.981			
		R _L	50	500	50	500	50	500
			mg/L	mg/L	mg/L	mg/L	mg/L	mg/L
			0.056	0.006	0.093	0.010	0.519	0.098
	Freundlich	1/n _f	0.125	0.116	0.123			
		K _F (mg/g)(L/mg) ^{1/n}	82.710	90.734	91.973			
		R ²	0.853	0.517	0.542			
	Sips	Q _m (mg/g)	170.50	177.16	176.37			
		K _S (L/mg)	0.369	0.017	0.180			
		M _S	0.645	0.223	1.18778			
		R ²	0.976	0.958	0.949			
Redlich-Peterson	k _{RP} (L/g)	87.166	95.14	30.40				
	α _R (L/ mg)	0.680	0.609	0.146				
	β _R	0.956	0.980	1.03				
	R ²	0.972	0.958	0.928				

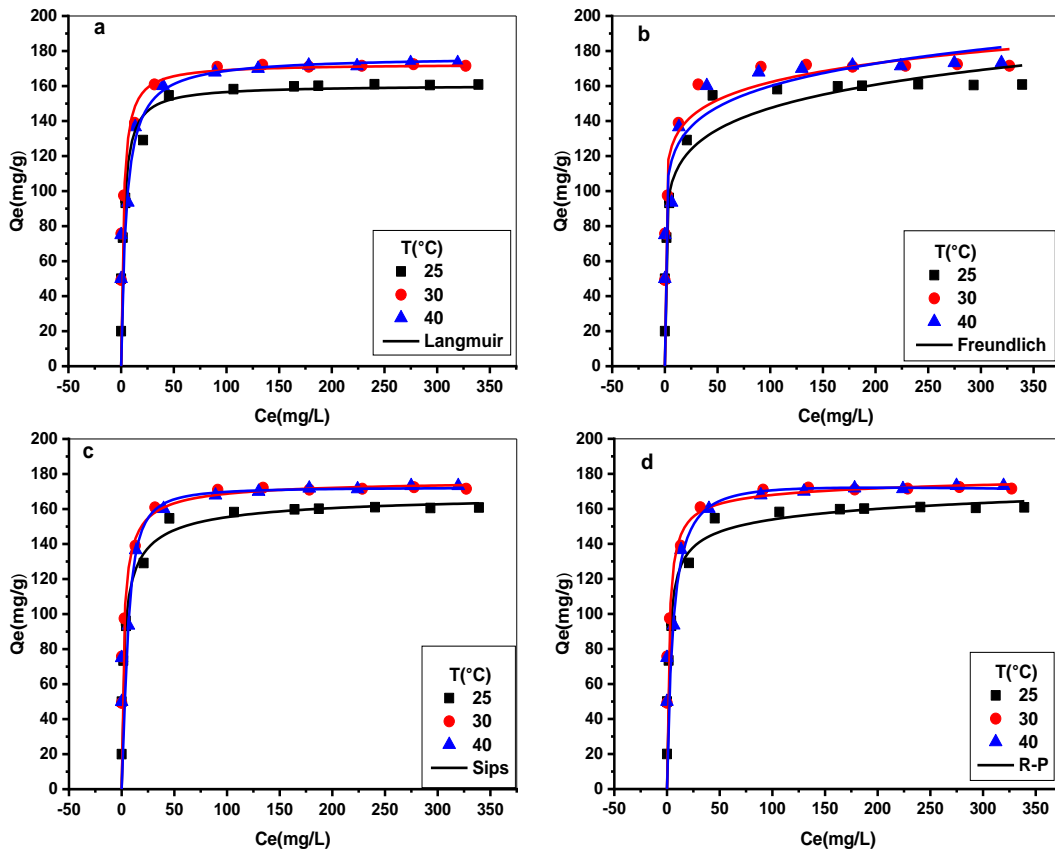


Figure 9. modeling by the Langmuir (a), Freundlich (b), Sips (c) and Redlich-Peterson (d) models of the MB adsorption isotherm onto ZJS-H₃PO₄ at different temperatures.

(Agitation speed=250 rpm, pH=10).

2.5. Kinetics modeling

The modeling results are shown in Fig. 10, and the obtained constants from the adsorption models, namely the rate constants K , the theoretical maximum adsorbed quantities, and the correlation coefficients R^2 are given in Table 4. As observed, for both the pseudo-first and the pseudo-second-order models, the calculated adsorbed quantities were close to those obtained experimentally. However, correlation coefficients R^2 for the pseudo-first-order model were low, in the range 0.903 to 0.993, while they were in the range 0.975 to 0.996 for the pseudo-second-order model.

Table 4: Kinetic parameters and correlation coefficients for nonlinear regression of PFO PSO and PNO models for the biosorption of MB onto *ZJS-H₃PO₄*

Material	Model	Parameters	C ₀ (mg/L)		
			50	100	150
ZJS-H₃PO₄	PFO	Q _{exp} , (mg g ⁻¹)	50.00	93.27	129.14
		Q _{ecal} , (mg g ⁻¹)	48.89	90.86	116.10
		K ₁ , (min ⁻¹)	1.06	0.188	0.289
		R²	0.984	0.993	0.903
	PSO	Q _{ecal} , (mg g ⁻¹)	49.75	95.69	121.01
		K ₂ *10 ⁺⁴ , (g mg ⁻¹ min ⁻¹)	0.055	0.004	0.003
		R²	0.996	0.978	0.975
		Q _{ecal} , (mg g ⁻¹)	51.19	91.21	135.54
	PNO	k _n , (min ⁻¹) (mg g ⁻¹) ¹⁻ⁿ	0.0022	0.115	1.64E-06
		n	3.20	1.12	3.74
		R²	0.998	0.993	0.991

It can also be seen that rate constants decreased as the concentration increased, which may be due to a competition on the active sites. Regarding the pseudo-nth-order model, the correlation coefficients R^2 were 0.998, 0.993, and 0.991 for 50, 100, and 150 mg L⁻¹ dye, respectively, with adsorbed quantities of 51.19, 91.21, and 135.54 mg g⁻¹, and the order of the reaction was between 1.12 and 3.74. In conclusion, and according to the calculations carried out, it can be considered that the pseudo-second-order model is the most adequate to describe the adsorption kinetics of MB onto ZJS-H₃PO₄; it led to the most accurate fit of experimental data.

The intraparticle diffusion model was also applied (Fig. 11), showing two linear parts. The first one can be attributed to the adsorption at the surface or the external diffusion, and the second part represents the intraparticle diffusion [23]. The results show that the curve $q_t = f(t^{0.5})$ does not cross the origin, and hence the intraparticle diffusion occurs but is not the limiting step [19].

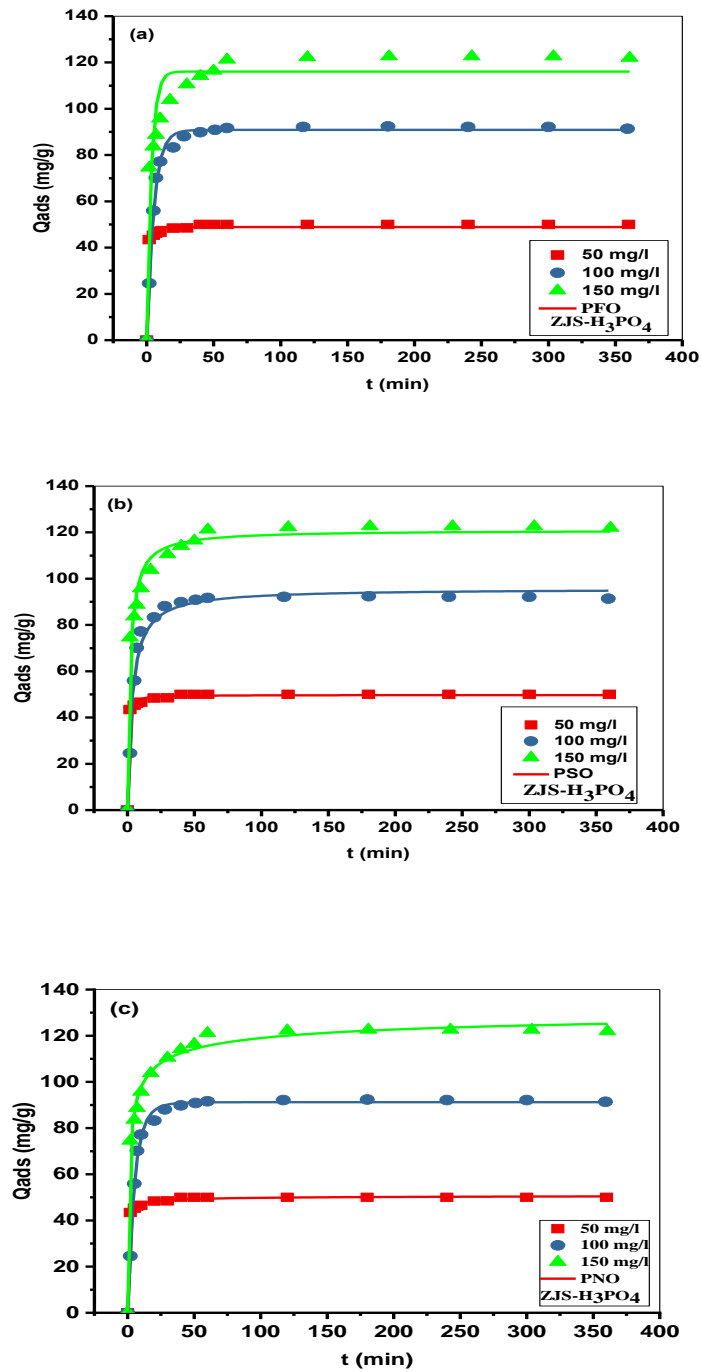


Figure 10. Experimental (symbols) and calculated data (continuous lines) by mean of pseudo-first-order (a), pseudo-second-order (b) and pseudo-nth order kinetics models (c) for MB adsorption onto ZJS- H_3PO_4 at various concentrations. ($T = 25^\circ C$, agitation speed =250 rpm, pH 10).

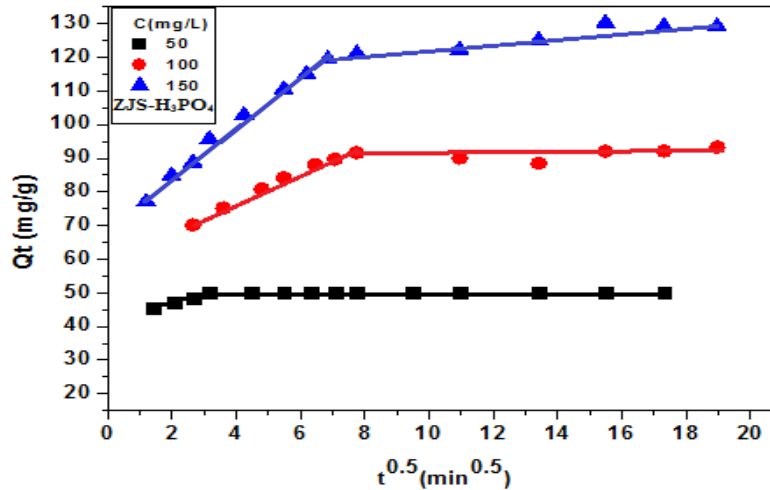


Figure 11. Experimental (symbols) and calculated data (continuous lines) by means intraparticle diffusion model for MB adsorption onto ZJS- H_3PO_4 . ($T = 25^\circ C$, agitation speed =250 rpm, pH 10).

2.6. Effect of the Temperature

The effect of temperature on MB adsorption onto ZJS- H_3PO_4 was investigated at temperatures ranging from 25 to 40 °C. Contrarily to the usual case, adsorption was not exothermic, according to the finding (see Fig. 8). Indeed, an increase in the temperature from 25 to 40 °C caused an increase in the adsorbed amount of MB, from 160.85 mg g⁻¹ to 174.31mg g⁻¹; this increase can be due to the diffusion of MB in the micropores, which accelerates with the rise of the temperature [42].

2.7. Effect of the ionic strength and the humic acid on adsorption of MB onto ZJS- H_3PO_4

Ionic strength is known as a significant factor in the adsorption of organic and inorganic compounds. To be closer to real conditions, NaCl salt and humic acid were considered to examine their impact on the adsorption of MB onto ZJS- H_3PO_4 . As shown in Fig. 12, humic acid did not affect the MB adsorption since the adsorbed quantity did not vary after its addition, while the adsorbed amount almost doubled after the addition of NaCl. This increase may be due to the increase in ionic strength, which promotes the adsorption of MB onto the ZJS- H_3PO_4 .

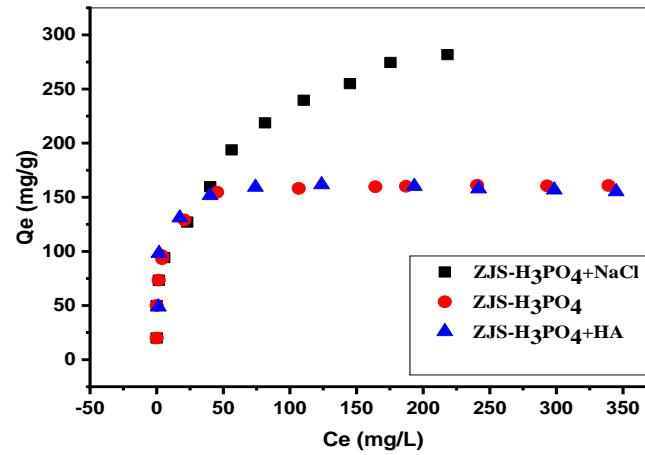


Figure 12. Effect of NaCl and Humic acid on methylene blue adsorption onto ZJS-H₃PO₄ (T=25°C, agitation speed=250 rpm, pH 10).

3. Statistical physics models

The ideal fitting is obtained when the R^2 is high, without exceeding 1, while the AIC reaches their minimum values. The results of the fitting are presented in table 5.

Table 5 indicates the highest R^2 and AIC values in the limited multilayer; however, the monolayer model provides the highest R^2 value and the lowest AIC value. In a general way, an adsorption process is better described when the number of physical parameters of the model increases [43]. Thus, minimizing information loss requires having a minimum AIC [44]. Therefore, the monolayer model was selected and considered to describe the experimental values of isotherms for the three temperatures.

Table 5: Values of R^2 and AIC of fitting of MB on the ZJS-H₃PO₄

T(°C)	25°C		30°C		40°C	
Model	R^2	AIC	R^2	AIC	R^2	AIC
Monolayer	0.99126	6.01	0.99417	6.00	0.99721	6.00
Double layer model with two energies	0.99109	8.01	0.99353	8.00	0.99811	8.00
Double layer model with one energy	0.99109	6.01	0.99353	6.00	0.99811	6.00
Limited multilayer	0.999317	10.02	0.99447	10.00	0.99879	10.00

The values of fitting parameters of MB onto the ZJS-H₃PO₄ using the monolayer model are consequently given in Table 6.

Table 6: Values of fitting parameters of MB on the ZJS-H₃PO₄ with monolayer model

	N _s (mg/g)	Q ₀ (mg/g)	C _{1/2} (mg/L)	n _m	R ²
T=25°	282.25	172.17	2.76	0.61	0.99126
T=30°	236.67	177.50	1.97	0.75	0.99417
T=40°	115.53	172.14	5.69	1.49	0.99721

3.1. Steric interpretation

The number of molecules per site (n_m), the density of receptor sites (N_s), and the adsorbed amount at saturation (Q₀) are the basis parameters for the steric interpretation. The variation of the steric parameters according to temperature is shown in Fig. 13.

3.1.1. Parameter n_m

The n_m parameter is a critical factor in the adsorption mechanism elucidation; it provides information on the molecule's orientation towards the adsorbent surface [45]. This parameter can be higher or less than 1. If n_m is higher than 1, it reflects the number of anchored molecules at one site, corresponding to multi-molecular adsorption [46,47]. In this particular instance, it gives information on the number of molecules attached to a receptor site as an aggregate [47]. In the case where the number "n_m" is less than unity, the adsorbed molecules take a parallel position to the surface of the adsorbent material [28]. In this scenario, it may be related to the number of sites occupied by the adsorbate (anchorage number) defined as n'_m=1/n_m [27,28,48]. Fig. 13a illustrates an increase in the number of adsorbed MB molecules per site (n_m); this can be due to the thermal collision [27].

Knani and co-workers [43] show that the percentage of pollutant molecules anchored by 1 or 2 free sites can be calculated. However, suppose we put x the rate of molecules with one anchorage. In that case, the percentage of molecules having two anchorages is then (1-x), as a result, Knani and co-workers [43] also show that n_m = x+ 0.5*(1-x), for example, where n_m= 0.61 at 25°C, which mean that almost 22% of MB molecules were anchored with a single anchorage and 78% were adsorbed with two free active sites.

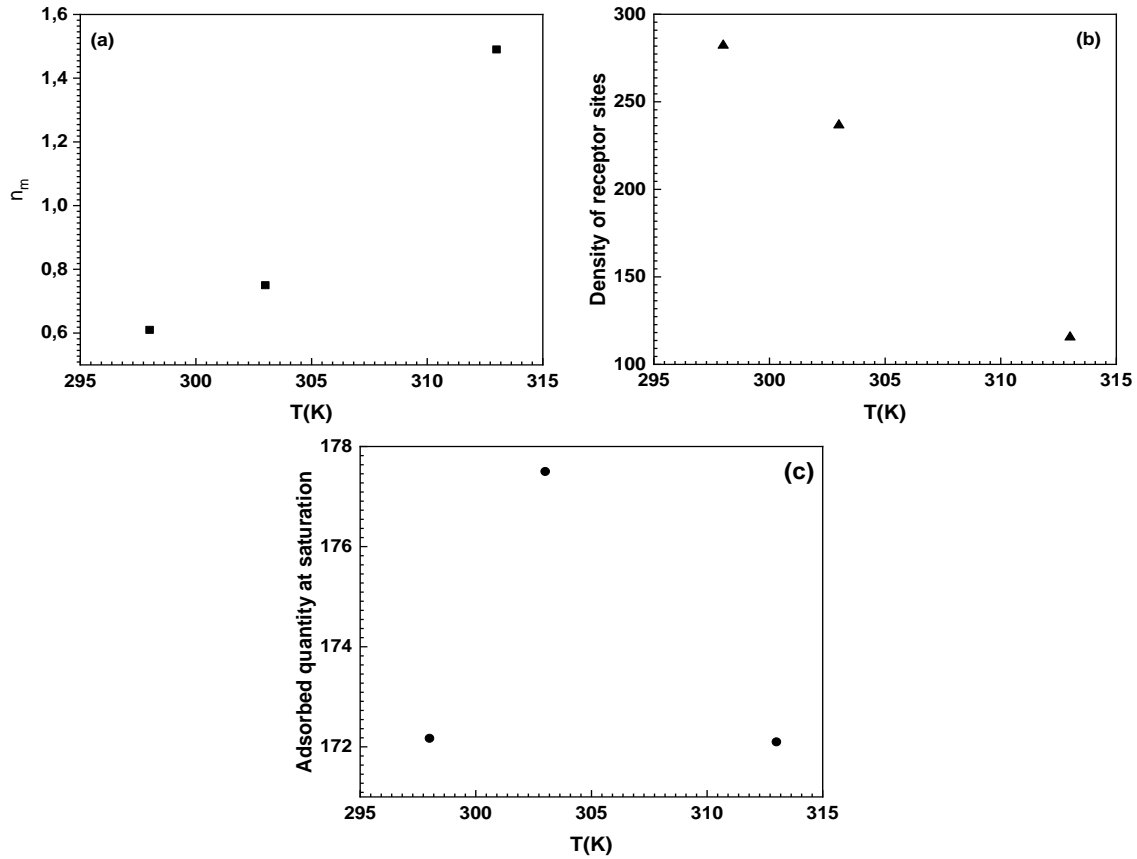


Figure 13. Behavior of the steric parameters with the temperature: (a) parameter n_m , (b) parameter N_s , (c) parameter Q_0 .

3.1.2. Parameter N_s

The receptor site density (N_s) variation according to the temperature is shown in Fig. 13 b. It is clear from this figure that the receptor sites density of the ZJS- H_3PO_4 decreased with temperature. This finding can be explained by the solubility of MB, which increases with increasing temperature, making the interactions of the liquid phase (between water and dye molecules) stronger than that between MB molecules and the surface of ZJS- H_3PO_4 [27]. These interpretations show that temperature is a dominant factor in the adsorption process.

3.1.3. Parameter Q_0

The adsorption amount at saturation depends on various variables such as (n_m) and (N_s) parameters, representing the potential of the ZJS- H_3PO_4 surface to adsorb MB molecules. In Fig. 13c, the Q_0 is reported according to temperature; it can be seen that the increase in the initial temperature caused an increase in the adsorbed quantity and then a decrease. From this, $T=30^\circ C$ can be considered an optimum temperature for the adsorption process.

3.2. Energetic interpretation

The adsorption energy $-\Delta E$ is a parameter representing the depth of good potentials at the receptor site on the ZJS- H_3PO_4 surface [44,46]. Therefore, this parameter can help to make an energetic interpretation where it is calculated according to the following relation:

$$-\Delta E = RT \ln \left(\frac{C_{1/2}}{C_s} \right) \dots \dots \dots (39)$$

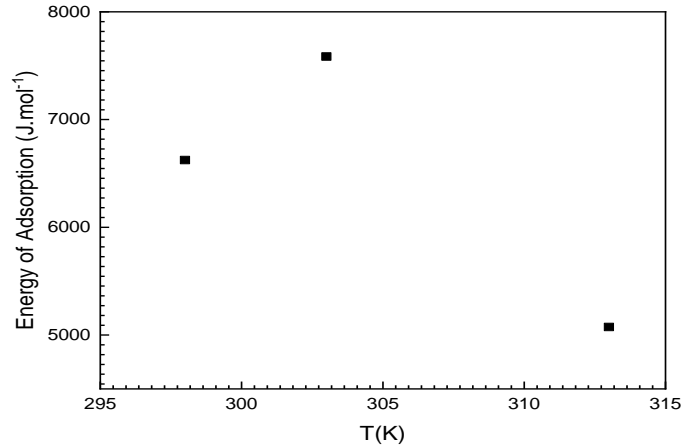


Figure 14. Energy of adsorption at three temperatures (298K, 303K, and 313K)

The temperature-based adsorption energy variation is shown in Fig. 14. The (5–8 kJ mol⁻¹) range observed in Fig. 14 corresponds to physical interactions, generally electrostatic interactions and hydrogen bonds [27]. In addition, the adsorption energy obtained at 30°C, which was identical to that of the adsorbed quantity at saturation, confirmed that this temperature was optimal.

4. Conclusion

The study of the adsorption of MB onto the *Ziziphus jujuba* stones treated with ortho-phosphoric acid was the subject of this chapter. The results obtained related to adsorption kinetics, adsorption isotherms, thermodynamics and ionic strength were analyzed to explain the adsorption mode of MB onto ZJS- H_3PO_4 . The study of adsorption kinetics showed that the adsorption process followed the pseudo-second-order model. Intraparticle diffusion seemed to be a significant step in the adsorption process but was not the limiting step. Moreover, the nonlinear Langmuir model was the most convincing to describe experimental data. The study of the effect of ionic strength showed that NaCl had a positive impact on adsorption. Regarding statistical models, the monolayer model with single energy (MMSE) was selected to describe the experimental isotherms. Furthermore, at 25°C 22% of MB molecules were adsorbed by a single site and 78% were adsorbed with two sites. The (5–8 kJ mol⁻¹) range corresponds to physical interactions, generally

electrostatic and hydrogen bonds. Moreover, the adsorption energy behavior was the same as the adsorbed saturation quantity, which confirmed that the temperature of 30 °C can be regarded as the optimum adsorption temperature of MB onto ZJS-H₃PO₄.

7. References

- [1] F. Deniz, R.A. Kepekci, Dye biosorption onto pistachio by-product: A green environmental engineering approach, *J. Mol. Liq.* 219 (2016) 194–200. <https://doi.org/10.1016/j.molliq.2016.03.018>.
- [2] F. Temesgen, N. Gabbiye, O. Sahu, Biosorption of reactive red dye (RRD) on activated surface of banana and orange peels: Economical alternative for textile effluent, *Surf. Interfaces.* 12 (2018) 151–159. <https://doi.org/10.1016/j.surfin.2018.04.007>.
- [3] E.F. Lessa, M.L. Nunes, A.R. Fajardo, Chitosan/waste coffee-grounds composite: An efficient and eco-friendly adsorbent for removal of pharmaceutical contaminants from water, *Carbohydr. Polym.* 189 (2018) 257–266. <https://doi.org/10.1016/j.carbpol.2018.02.018>.
- [4] T.R. Moro, F.R. Henrique, L.C. Malucelli, C.M.R. de Oliveira, M.A. da Silva Carvalho Filho, E.C. de Vasconcelos, Adsorption of pharmaceuticals in water through lignocellulosic fibers synergism, *Chemosphere.* 171 (2017) 57–65. <https://doi.org/10.1016/j.chemosphere.2016.12.040>.
- [5] A.B. Albadarin, S. Solomon, T.A. Kurniawan, C. Mangwandi, G. Walker, Single, simultaneous and consecutive biosorption of Cr(VI) and Orange II onto chemically modified masau stones, *J. Environ. Manage.* 204 (2017) 365–374. <https://doi.org/10.1016/j.jenvman.2017.08.042>.
- [6] M. Torab-Mostaedi, M. Asadollahzadeh, A. Hemmati, A. Khosravi, Equilibrium, kinetic, and thermodynamic studies for biosorption of cadmium and nickel on grapefruit peel, *J. Taiwan Inst. Chem. Eng.* 44 (2013) 295–302. <https://doi.org/10.1016/j.jtice.2012.11.001>.
- [7] G. Lin, R. Ma, Y. Zhou, Q. Liu, X. Dong, J. Wang, KOH activation of biomass-derived nitrogen-doped carbons for supercapacitor and electrocatalytic oxygen reduction, *Electrochimica Acta.* 261 (2018) 49–57.
- [8] S. Rangabhashiyam, S. Lata, P. Balasubramanian, Biosorption characteristics of methylene blue and malachite green from simulated wastewater onto *Carica papaya*

- wood biosorbent, *Surf. Interfaces.* 10 (2018) 197–215. <https://doi.org/10.1016/j.surfin.2017.09.011>.
- [9] C.Y.P. Ayekoe, D. Robert, D.G. Lanciné, Combination of coagulation-flocculation and heterogeneous photocatalysis for improving the removal of humic substances in real treated water from Agbô River (Ivory-Coast), *Catal. Today.* 281 (2017) 2–13. <https://doi.org/10.1016/j.cattod.2016.09.024>.
- [10] J. Ke, J. Liu, H. Sun, H. Zhang, X. Duan, P. Liang, X. Li, M.O. Tade, S. Liu, S. Wang, Facile assembly of Bi₂O₃/Bi₂S₃/MoS₂ n-p heterojunction with layered n-Bi₂O₃ and p-MoS₂ for enhanced photocatalytic water oxidation and pollutant degradation, *Appl. Catal. B Environ.* 200 (2017) 47–55. <https://doi.org/10.1016/j.apcatb.2016.06.071>.
- [11] T.S. Natarajan, K.R. Thampi, R.J. Tayade, Visible light driven redox-mediator-free dual semiconductor photocatalytic systems for pollutant degradation and the ambiguity in applying Z-scheme concept, *Appl. Catal. B Environ.* 227 (2018) 296–311. <https://doi.org/10.1016/j.apcatb.2018.01.015>.
- [12] A. Aghigh, V. Alizadeh, H.Y. Wong, Md.S. Islam, N. Amin, M. Zaman, Recent advances in utilization of graphene for filtration and desalination of water: A review, *Desalination.* 365 (2015) 389–397. <https://doi.org/10.1016/j.desal.2015.03.024>.
- [13] J.M. Dickhout, J. Moreno, P.M. Biesheuvel, L. Boels, R.G.H. Lammertink, W.M. de Vos, Produced water treatment by membranes: A review from a colloidal perspective, *J. Colloid Interface Sci.* 487 (2017) 523–534. <https://doi.org/10.1016/j.jcis.2016.10.013>.
- [14] Z. Huang, Y. Li, W. Chen, J. Shi, N. Zhang, X. Wang, Z. Li, L. Gao, Y. Zhang, Modified bentonite adsorption of organic pollutants of dye wastewater, *Mater. Chem. Phys.* 202 (2017) 266–276. <https://doi.org/10.1016/j.matchemphys.2017.09.028>.
- [15] W. Konicki, M. Aleksandrak, E. Mijowska, Equilibrium, kinetic and thermodynamic studies on adsorption of cationic dyes from aqueous solutions using graphene oxide, *Chem. Eng. Res. Des.* 123 (2017) 35–49. <https://doi.org/10.1016/j.cherd.2017.03.036>.
- [16] M. Ngabura, S.A. Hussain, W.A.W.A. Ghani, M.S. Jami, Y.P. Tan, Utilization of renewable durian peels for biosorption of zinc from wastewater, *J. Environ. Chem. Eng.* 6 (2018) 2528–2539. <https://doi.org/10.1016/j.jece.2018.03.052>.
- [17] M. Bounaas, A. Bouguettoucha, D. Chebli, A. Reffas, I. Harizi, F. Rouabah, A. Amrane, High efficiency of methylene blue removal using a novel low-cost acid

- treated forest wastes, *Cupressus semperirens* cones: Experimental results and modeling, *Part. Sci. Technol.* 0 (2018) 1–10. <https://doi.org/10.1080/02726351.2017.1401569>.
- [18] T.K. Sen, S. Afroze, H.M. Ang, Equilibrium, Kinetics and Mechanism of Removal of Methylene Blue from Aqueous Solution by Adsorption onto Pine Cone Biomass of *Pinus radiata*, *Water. Air. Soil Pollut.* 218 (2011) 499–515. <https://doi.org/10.1007/s11270-010-0663-y>.
- [19] M.C. Somasekhara Reddy, L. Sivaramakrishna, A. Varada Reddy, The use of an agricultural waste material, Jujuba seeds for the removal of anionic dye (Congo red) from aqueous medium, *J. Hazard. Mater.* 203–204 (2012) 118–127. <https://doi.org/10.1016/j.jhazmat.2011.11.083>.
- [20] S. Marković, A. Stanković, Z. Lopičić, S. Lazarević, M. Stojanović, D. Uskoković, Application of raw peach shell particles for removal of methylene blue, *J. Environ. Chem. Eng.* 3 (2015) 716–724. <https://doi.org/10.1016/j.jece.2015.04.002>.
- [21] G. Manikandan, A. Saravanan, Modelling and analysis on the removal of methylene blue dye from aqueous solution using physically/chemically modified *Ceiba pentandra* seeds, *J. Ind. Eng. Chem.* 62 (2018) 446–461. <https://doi.org/10.1016/j.jiec.2018.01.028>.
- [22] D. Chebli, A. Bouguettoucha, T. Mekhalef, S. Nacef, A. Amrane, Valorization of an agricultural waste, *Stipa tenassicima* fibers, by biosorption of an anionic azo dye, Congo red, *Desalination Water Treat.* 54 (2015) 245–254. <https://doi.org/10.1080/19443994.2014.880154>.
- [23] A. Bouguettoucha, D. Chebli, T. Mekhalef, A. Noui, A. Amrane, The use of a forest waste biomass, cone of *Pinus brutia* for the removal of an anionic azo dye Congo red from aqueous medium, *Desalination Water Treat.* 55 (2015) 1956–1965. <https://doi.org/10.1080/19443994.2014.928235>.
- [24] M. Goswami, P. Phukan, Enhanced adsorption of cationic dyes using sulfonic acid modified activated carbon, *J. Environ. Chem. Eng.* 5 (2017) 3508–3517. <https://doi.org/10.1016/j.jece.2017.07.016>.
- [25] Y. Miyah, A. Lahrichi, M. Idrissi, A. Khalil, F. Zerrouq, Adsorption of methylene blue dye from aqueous solutions onto walnut shells powder: Equilibrium and kinetic studies, *Surf. Interfaces.* 11 (2018) 74–81. <https://doi.org/10.1016/j.surfin.2018.03.006>.

- [26] N. Belhouchat, H. Zaghouane-Boudiaf, C. Viseras, Removal of anionic and cationic dyes from aqueous solution with activated organo-bentonite/sodium alginate encapsulated beads, *Appl. Clay Sci.* 135 (2017) 9–15. <https://doi.org/10.1016/j.clay.2016.08.031>.
- [27] G.L. Dotto, L.A.A. Pinto, M.A. Hachicha, S. Knani, New physicochemical interpretations for the adsorption of food dyes on chitosan films using statistical physics treatment, *Food Chem.* 171 (2015) 1–7. <https://doi.org/10.1016/j.foodchem.2014.08.098>.
- [28] S. Knani, M. Khalfaoui, M.A. Hachicha, A. Ben Lamine, M. Mathlouthi, Modelling of water vapour adsorption on foods products by a statistical physics treatment using the grand canonical ensemble, *Food Chem.* 132 (2012) 1686–1692. <https://doi.org/10.1016/j.foodchem.2011.11.065>.
- [29] P. Liao, Z. Malik Ismael, W. Zhang, S. Yuan, M. Tong, K. Wang, J. Bao, Adsorption of dyes from aqueous solutions by microwave modified bamboo charcoal, *Chem. Eng. J.* 195–196 (2012) 339–346. <https://doi.org/10.1016/j.cej.2012.04.092>.
- [30] H.N. Tran, Y.F. Wang, S.J. You, H.P. Chao, Insights into the mechanism of cationic dye adsorption on activated charcoal: The importance of π - π interactions, *Process Saf. Environ. Prot.* 107 (2017) 168–180. <https://doi.org/10.1016/j.psep.2017.02.010>.
- [31] A. Kumar, H.M. Jena, Preparation and characterization of high surface area activated carbon from Fox nut (*Euryale ferox*) shell by chemical activation with H₃PO₄, *Results Phys.* 6 (2016) 651–658. <https://doi.org/10.1016/j.rinp.2016.09.012>.
- [32] M.A. Nahil, P.T. Williams, Pore characteristics of activated carbons from the phosphoric acid chemical activation of cotton stalks, *Biomass Bioenergy.* 37 (2012) 142–149. <https://doi.org/10.1016/j.biombioe.2011.12.019>.
- [33] S. Basu, G. Ghosh, S. Saha, Adsorption characteristics of phosphoric acid induced activation of bio-carbon: Equilibrium, kinetics, thermodynamics and batch adsorber design, *Process Saf. Environ. Prot.* 117 (2018) 125–142. <https://doi.org/10.1016/j.psep.2018.04.015>.
- [34] J. Guo, A.C. Lua, Textural and chemical properties of adsorbent prepared from palm shell by phosphoric acid activation, *Mater. Chem. Phys.* 80 (2003) 114–119. [https://doi.org/10.1016/S0254-0584\(02\)00383-8](https://doi.org/10.1016/S0254-0584(02)00383-8).
- [35] C. Paduraru, L. Tofan, C. Teodosiu, I. Bunia, N. Tudorachi, O. Toma, Biosorption of zinc(II) on rapeseed waste: Equilibrium studies and thermogravimetric investigations,

- Process Saf. Environ. Prot. 94 (2015) 18–28.
<https://doi.org/10.1016/j.psep.2014.12.003>.
- [36] B.H. Hameed, A.A. Ahmad, Batch adsorption of methylene blue from aqueous solution by garlic peel, an agricultural waste biomass, *J. Hazard. Mater.* 164 (2009) 870–875. <https://doi.org/10.1016/j.jhazmat.2008.08.084>.
- [37] M.D. Donohue, G.L. Aranovich, Classification of Gibbs adsorption isotherms, *Adv. Colloid Interface Sci.* 76–77 (1998) 137–152. [https://doi.org/10.1016/S0001-8686\(98\)00044-X](https://doi.org/10.1016/S0001-8686(98)00044-X).
- [38] K.V. Kumar, A. Kumaran, Removal of methylene blue by mango seed kernel powder, *Biochem. Eng. J.* 27 (2005) 83–93. <https://doi.org/10.1016/j.bej.2005.08.004>.
- [39] S.S. Vieira, Z.M. Magriotis, N.A.V. Santos, M. das G. Cardoso, A.A. Saczk, Macauba palm (*Acrocomia aculeata*) cake from biodiesel processing: An efficient and low cost substrate for the adsorption of dyes, *Chem. Eng. J.* 183 (2012) 152–161. <https://doi.org/10.1016/j.cej.2011.12.047>.
- [40] S. Manna, D. Roy, P. Saha, D. Gopakumar, S. Thomas, Rapid methylene blue adsorption using modified lignocellulosic materials, *Process Saf. Environ. Prot.* 107 (2017) 346–356. <https://doi.org/10.1016/j.psep.2017.03.008>.
- [41] N. Sivarajasekar, R. Baskar, Adsorption of Basic Magenta II onto H₂SO₄ activated immature *Gossypium hirsutum* seeds: Kinetics, isotherms, mass transfer, thermodynamics and process design, *Arab. J. Chem.* (2014). <https://doi.org/10.1016/j.arabjc.2014.10.040>.
- [42] N.E. Messaoudi, A. Dbik, M.E. Khomri, A. Sabour, S. Bentahar, A. Lacherai, Date stones of *Phoenix dactylifera* and jujube shells of *Ziziphus lotus* as potential biosorbents for anionic dye removal, *Int. J. Phytoremediation.* 19 (2017) 1047–1052. <https://doi.org/10.1080/15226514.2017.1319331>.
- [43] S. Knani, F. Aouaini, N. Bahloul, M. Khalfaoui, M.A. Hachicha, A. Ben Lamine, N. Kechaou, Modeling of adsorption isotherms of water vapor on Tunisian olive leaves using statistical mechanical formulation, *Phys. Stat. Mech. Its Appl.* 400 (2014) 57–70. <https://doi.org/10.1016/j.physa.2014.01.006>.
- [44] M.B. Yahia, S. Knani, L.B.H. Hsan, M.B. Yahia, H. Nasri, A. Ben Lamine, Statistical studies of adsorption isotherms of iron nitrate and iron chloride on a thin layer of porphyrin, *J. Mol. Liq.* 248 (2017) 235–245. <https://doi.org/10.1016/j.molliq.2017.10.073>.

- [45] Z. Li, L. Sellaoui, G.L. Dotto, A.B. Lamine, A. Bonilla-Petriciolet, H. Hanafy, H. Belmabrouk, M.S. Netto, A. Erto, Interpretation of the adsorption mechanism of Reactive Black 5 and Ponceau 4R dyes on chitosan/polyamide nanofibers via advanced statistical physics model, *J. Mol. Liq.* 285 (2019) 165–170. <https://doi.org/10.1016/j.molliq.2019.04.091>.
- [46] L. Sellaoui, S. Knani, A. Erto, M.A. Hachicha, A. Ben Lamine, Equilibrium isotherm simulation of tetrachlorethylene on activated carbon using the double layer model with two energies: Steric and energetic interpretations, *Fluid Phase Equilibria.* 408 (2016) 259–264. <https://doi.org/10.1016/j.fluid.2015.09.022>.
- [47] L. Sellaoui, H. Guedidi, S. Knani, L. Reinert, L. Duclaux, A. Ben Lamine, Application of statistical physics formalism to the modeling of adsorption isotherms of ibuprofen on activated carbon, *Fluid Phase Equilibria.* 387 (2015) 103–110. <https://doi.org/10.1016/j.fluid.2014.12.018>.
- [48] M. Khalfaoui, S. Knani, M.A. Hachicha, A.B. Lamine, New theoretical expressions for the five adsorption type isotherms classified by BET based on statistical physics treatment, *J. Colloid Interface Sci.* 263 (2003) 350–356. [https://doi.org/10.1016/S0021-9797\(03\)00139-5](https://doi.org/10.1016/S0021-9797(03)00139-5).

Chapter IV: Molecular Dynamic Simulation and DFT computational studies on the adsorption performances of Methylene Blue in aqueous solutions by Orange peel-modified phosphoric acid

1. Introduction

Due to the progress of civilization and population growth, many imbalances have emerged, making people constantly anxious and eager to find appropriate solutions to reduce these imbalances. Unfortunately, the high exploitation of water produces an intense and continuous decrease of the water reserves [1]. In this dispute and for several years, much effort should be made to explore alternative resources for water supply; in this aim, the treatment of industrial wastewater should be considered as a proposed solution that can not be ignored. Indeed, high amounts of water are used in industry, leading to the release of polluted water, and particularly water loaded with dyes [2], which are widely used in manufacturing industries, including textiles, cosmetics, leather, pharmaceuticals, food processing, petroleum, rubber and printing [3,4]. Often, the carcinogenicity, mutagenicity and high toxicity of these dyes make them very harmful to human health and the aquatic environment [5]. Indeed, the development of industrial wastewater treatment processes has become a topic subject that can not be ignored. In this context, several techniques have been exploited for water treatment, such as adsorption, which is a topical issue in eliminating dyes [6–8] because of its advantages, namely speed of operation, high efficiency, ease of operation [9]. In recent years, many research teams have focused on the development of new alternative absorbent materials, displaying a low cost of preparation, effectiveness, easy to find and to use. A wide range of conventional and unconventional adsorbent materials has been proposed for dyes removal [10], such as activated carbon [11], clays [12], chitosan [13], as well as agricultural residues [14,15], which are the subject of present work. The possibility of valorizing residues of agriculture (fruits peels) through their use as biosorbents of organic pollutants such as dyes was consequently the purpose of this study. Methylene blue was considered as a model dye compound to examine the adsorptive performance of OP-H₃PO₄, since it is a basic dye [16], which is in favor of its adsorption on an acidic adsorbent such as OP-H₃PO₄; it is stable over a wide range of pH, which makes its degradation very difficult; it is highly soluble in water (40 g/L), and it can be easily analyzed, in UV, is widely used in different industrial fields such as textiles where it is used to tint cotton, silk, and wood; it is also used in medicine and

biology [17]. However, this kind of dye is very dangerous in the case of direct contact with the eyes, causing permanent lesions; its inhalation can cause difficulties breathing for humans. In case of ingestion, several possible symptoms may occur, for example, nausea, vomiting, and methemoglobinemia [18]. Orange peels were considered as a raw material for the adsorbent preparation. These peels were modified by phosphoric acid and then characterized by scanning electron microscopy (SEM), X-ray diffraction (XRD), Fourier transform Infra-red spectroscopy (FTIR), and elemental analysis by Energy Dispersive X-Ray Spectroscopy (EDS) as well as thermogravimetric analysis (TGA). In a batch system, the methylene blue (BM) dye was chosen to carry out adsorption tests, and some operating parameters were investigated, namely pH, initial concentration, contact time, temperature, and the impact of salts and humic acid. Furthermore, the experimental results were correlated with quantum chemical parameters using DFT method. Finally, molecular dynamic simulations study was realized to examine the adsorption mode and the energy of MB molecule onto the OP-H₃PO₄ (110) surface.

2. Results and discussion

2.1. Materials Characterization

The FT-IR characterization was used to quantify the functional groups present on the surface of the samples of the raw orange peels (ROP), treated (OP-H₃PO₄) and after adsorption of MB (OP-H₃PO₄+ MB) to allow a comparison between them. The results obtained are illustrated in Fig. 1.

These spectra show on the one hand that the three samples comprised several similar functional groups, which are summarized in Table 1 and that our materials contained cellulosic compounds with significant peaks of cellulose (≈ 1020 and 1156 cm^{-1}) [19]. This finding was confirmed by the results of the XRD. On the other hand, a comparison between the three spectra shows variations in the location and intensity of some peaks, especially in the range of 900 to 1840 cm^{-1} .

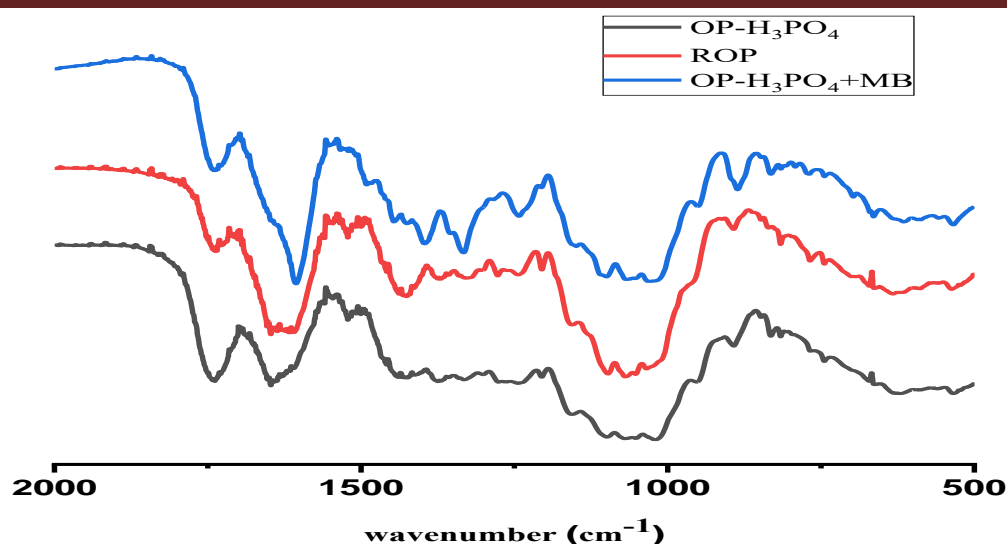


Figure 1. FTIR characterization of raw orange peels (ROP), treated (OP-H₃PO₄) and after MB adsorption (OP-H₃PO₄+MB).

Table 1: Shared Absorption bands in FTIR characterization for raw orange peels (ROP), treated (OP-H₃PO₄) and after MB adsorption (OP-H₃PO₄+MB).

	ROP	OP-H ₃ PO ₄	OP-H ₃ PO ₄ +MB	Attribution
	3424	3423	3423	- COOH, -N-H, and -O-H
Absorption bands (cm⁻¹)	2925 and 2858	2925 and 2858	2925 and 2858	-C-H _{Alph}
	1737	1740	1740	C=O
	1647	1645	1606	C=C
	1380	1376	1393	N-O and C-O
	1427 and 1522	1430 and 1520	1424 and 1491	C=C in aromatic rings [20]

The spectra also show that after treatment with phosphoric acid, some peaks were vanished or shifted to 1017, 1100 and 1159 cm⁻¹ which can be attributed to phosphorus or polyphosphate compounds [20,21], confirming that the chemical modification by phosphoric acid was efficiently carried out. Regarding the spectrum of OP-H₃PO₄ after MB adsorption, a significant increase in the C=C peak intensity can be observed with another increase in the intensity of peak at about 1335 cm⁻¹ which may be due to the adsorption of MB onto OP-H₃PO₄.

Additionally, the selected experimental and theoretical vibration frequencies of the characteristic functional groups of OP-H₃PO₄ are summarized in Table 2. Moreover, the calculated frequencies via DFT method are scaled using a scaling factor of 0.9614 [22]. As a result, we observe from Fig. 2 that the scaling theoretical frequencies are in good correlation with the experimental frequencies.

Table 2: Selected experimental and theoretical vibration frequencies of OP-H₃PO₄.

Assignment	Vibrational frequency (cm ⁻¹)		
	Experimental	Theoretical (DFT)	
		Unscaled	Scaled
O–H	3423	3584	3445
C–H _{Alph}	2925	3106	2986
C–H _{Alph}	2858	3006	2889
C=O	1740	1822	1751
C=C	1645	1701	1635
C=C _{Ar}	1520	1601	1539
C=C _{Ar}	1430	1512	1453
C–O	1376	1438	1382

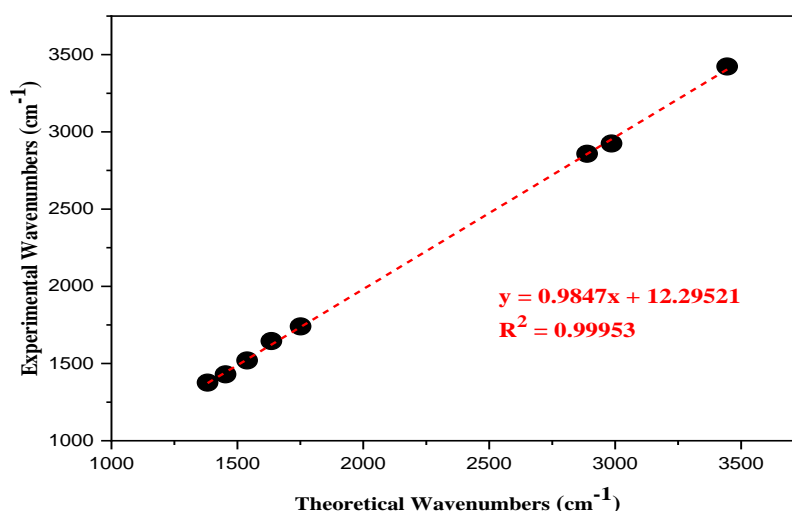


Figure 2. Correlation diagram between the theoretical and experimental wave numbers of OP-H₃PO₄.

Fig. 3 shows the results obtained by the X-Ray Diffraction for the orange peels before and after treatment with phosphoric acid. The two diffractograms show the same pattern with very similar peaks, indicating that the structural integrity of ROP was maintained and was not disrupted due to modification of ROP with phosphoric acid. The XRD patterns also indicate that the ROP material becomes more amorphous after treatment with phosphoric acid; this observation may be due to the integration of the phosphoric acid towards the internal surface of the ROP, which makes its structure more amorphous; this phenomenon was also observed after MB adsorption, OPH₃PO₄+MB, where the MB dye

integrated into the OPH_3PO_4 pores make its structure more amorphous. Similar interpretations were reported by another research team [23]. Fig. 3 also shows that ROP, $\text{OP-H}_3\text{PO}_4$, and $\text{OP-H}_3\text{PO}_4+\text{MB}$ displayed an intense peak at $2\theta = 22^\circ$ and a weak one at $2\theta = 15^\circ$, which can be attributed to the typical structure of cellulose I [24–26]. This observation confirms the results of the FTIR characterization.

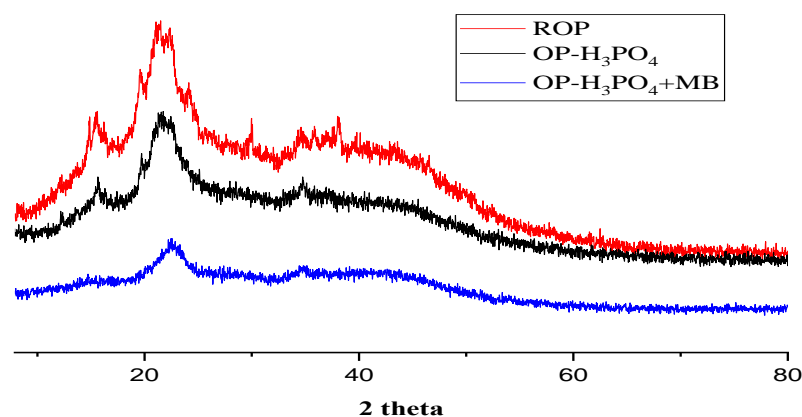


Figure 3. XRD pattern of orange peels before (ROP), after treatment with phosphoric acid ($\text{OP-H}_3\text{PO}_4$), and after MB adsorption ($\text{OP-H}_3\text{PO}_4+\text{MB}$).

Scanning electron microscopy (Fig. 4) shows that $\text{OP-H}_3\text{PO}_4$ had an irregular and heterogeneous structure [27] with different pore sizes [28], indicating that orange peels treated with phosphoric acid are promising to be used as an adsorbent [29].

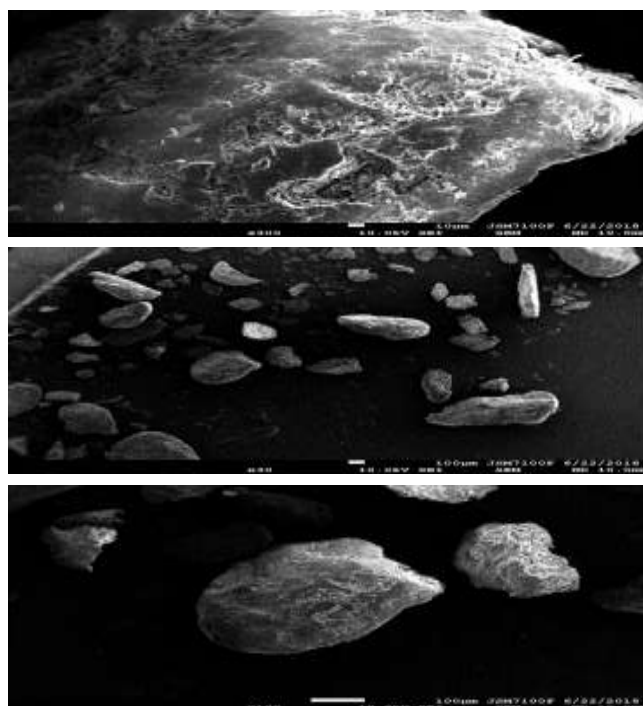


Figure 4. SEM images of $\text{OP-H}_3\text{PO}_4$.

The results of the elemental analysis (EDS) of the OP-H₃PO₄ are shown in Fig. 5. Two significant peaks of carbon and oxygen can be observed, indicating that C and O were the dominant elements in the composition of the OP-H₃PO₄ with also traces of calcium.

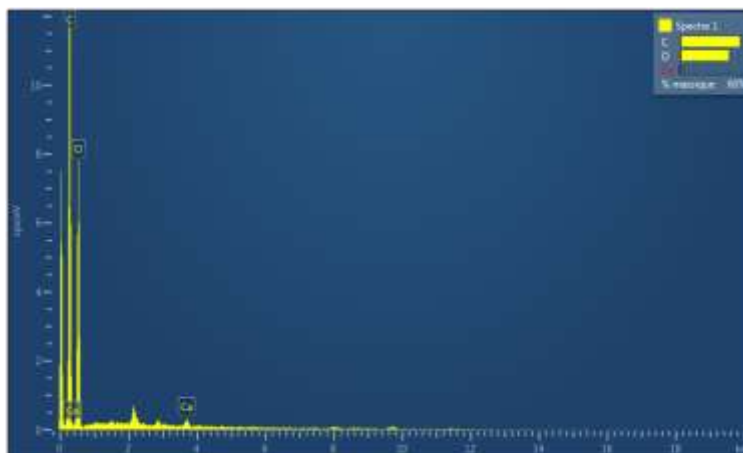


Figure 5. EDS characterization of OP-H₃PO₄.

Fig. 6 illustrates the results obtained from the thermogravimetric analysis (TGA) of ROP, OP-H₃PO₄, and OP-H₃PO₄+MB; from these results, it is clear that the three curves demonstrate a similar pattern for the three samples where they show two stages, the first one from the beginning of the analysis up to 220 °C, which is due to the removal of the adsorbed water onto the surface materials [30], the second phase starts from 220 °C until the end of the analysis, which may be due to the decomposition of cellulose [31] (cellulose is the main component of our materials as indicated in the XRD characterization). In order to establish a comparison between the three samples, Fig. 6 also shows that there is a weight loss of 91% for ROP, 76% for OP-H₃PO₄ and finally 83% OP-H₃PO₄+MB; these values indicate that the modification by phosphoric acid was well achieved and the MB was adsorbed onto OP-H₃PO₄.

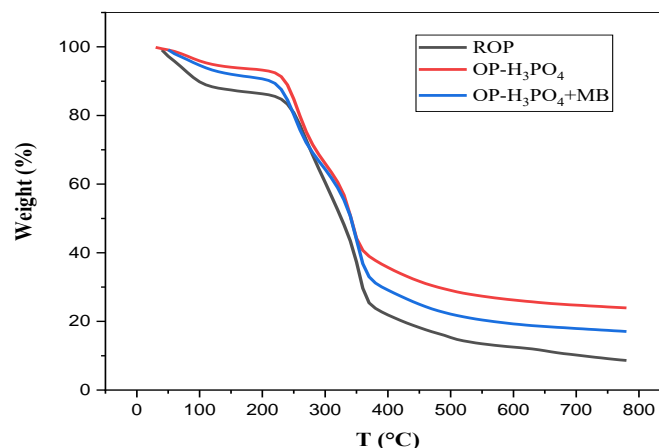


Figure 6. Thermogravimetric analysis of ROP, OP-H₃PO₄, and OP-H₃PO₄+MB.

2.1.1. Physicochemical characterization of OP-H₃PO₄

Table 3 represents some physicochemical characteristics of the OP-H₃PO₄. As observed, the OP-H₃PO₄ had a very high porosity of about 79%, in agreement with the SEM characterization (Fig.4). Furthermore, according to Table 4, it is clear that the OP-H₃PO₄ had an organic nature with a low ash content of about 18.43%.

Table 4 also shows the acidic character of OP-H₃PO₄ with acidity equal to 0.85. Furthermore, it is indicated in table 3 and Fig. 7 that the OP-H₃PO₄ had an isoelectric point equal to 3.34, which means that at the pH of the solution (6.2), the OP-H₃PO₄ was negatively charged, which facilitated the adsorption of MB because it was positively charged.

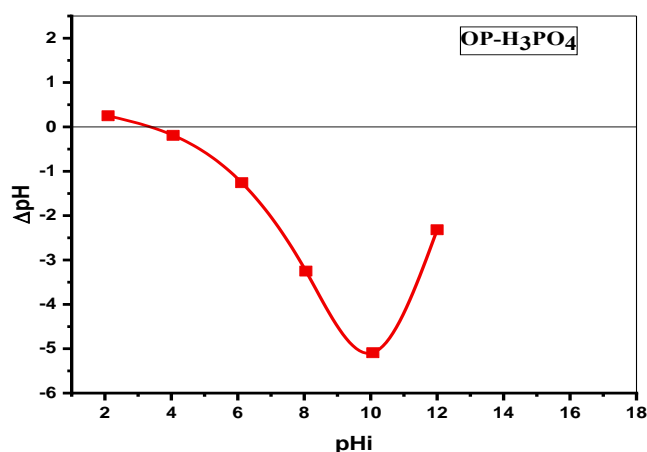


Figure 7. Variations of the pH according to the initial pH for the isoelectric point determination of OP-H₃PO₄.

Table 3. Some physico-chemical characteristic found for OP-H₃PO₄.

OP-H ₃ PO ₄	Porosity	Apparent	Moisture	ash	Acidity	Basicity	pH _{PHZ}	pH
	(%)	density (g ml ⁻¹)	content (%)	content (%)	(m eq g g ⁻¹)	(m eq g g ⁻¹)		
	79	0.026	0.067	18.43	0.8	0.35	3.34	6.1

2.2. Initial Concentration and Contact Time effects

In an adsorption phenomenon, contact time is a crucial parameter that can give important information about the optimal efficiency of absorption [32]. In this context, the initial concentration and contact time effects for the adsorption of MB onto OP-H₃PO₄ are illustrated in Fig. 8. As observed, the adsorption of MB onto OP-H₃PO₄ was very fast during the first minutes, and then it slowed down until reaching equilibrium after 30 min

for the low dye concentration and 60 min for the high concentration. This can be explained by the availability and the location of the free adsorption sites at the beginning of adsorption compared to the end of adsorption, leading to a fast adsorption at the beginning of the process, located in external adsorption sites which are available and easy to access; and at lower rates in internal sites which are less available and difficult to access in a second step [33]. Fig. 8 also shows that there was a direct correlation relation between the initial concentration and the adsorbed quantity, due to the motor force between the solution and the OP-H₃PO₄, which increases when the initial concentration increases, and which reduces the resistance to the mass transfer inducing a significant increase in the adsorbed amount [34].

2.3. Kinetics modeling

The nonlinear pseudo-first-order (PFO), the pseudo-second-order (PSO) and the pseudo-nth-order (PNO) models were applied to model the experimental results. The low R² correlation coefficients obtained for the pseudo-first-order model for the three concentrations considered indicate that this model was not appropriate. On the contrary, Fig. 8 and Table 4 show that for the three concentrations, the PSO and PNO models led to high R² correlation factors. In addition, the adsorbed quantities found by the PSO model for all concentrations were close to those found experimentally. Therefore, the PSO model was the most adequate to describe the MB adsorption process onto OP-H₃PO₄.

Table 4: Kinetic parameters and correlation coefficients for nonlinear regression of PFO, PSO and PNO models for the adsorption of MB onto OP-H₃PO₄ at 25 °C.

Material	Model	Parameters	C ₀ (mg/L)		
			50	100	150
OP-H ₃ PO ₄	PFO	Q _{exp} , (mg g ⁻¹)	48.04	95.70	142.29
		Q _{ecal} , (mg g ⁻¹)	47.59	92.29	136.90
		K ₁ , (min ⁻¹)	0.154	0.212	0.163
		F _{error}	0.185	0.130	0.175
		R ²	0.962	0.961	0.935
		Q _{ecal} , (mg g ⁻¹)	50.19	96.99	144.40
	PSO	K ₂ *10 ⁺⁴ , (gmg ⁻¹ min ⁻¹)	0.005	0.004	0.002
		F _{error}	0.256	0.523	0.245
		R ²	0.973	0.995	0.974
		Q _e , (mg g ⁻¹)	49.20	98.68	150.28
	PNO	k _n , (min ⁻¹) (mg g ⁻¹) ¹⁻ⁿ	0.014	0.001	1.83E-04
		N	1.72	2.24	2.50
		F _{error}	0.232	0.217	0.586
		R ²	0.972	0.994	0.974

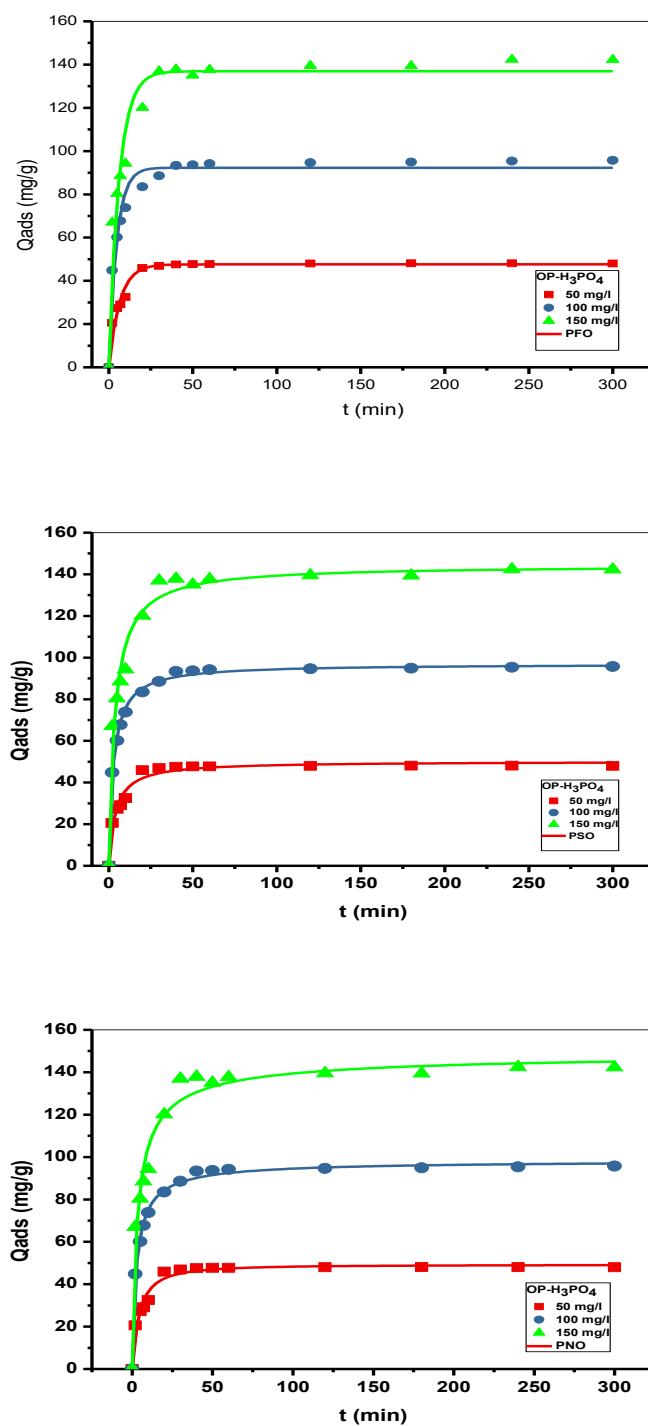


Figure 8. Time-courses of the MB adsorption for different initial concentrations of MB dye onto OP- H_3PO_4 (symbols) and nonlinear adjustment of the pseudo-first-order, pseudo-second-order and pseudo-nth-order kinetic models (continuous lines). (pH=6.2, agitation speed = 250 rpm, T=25°C)

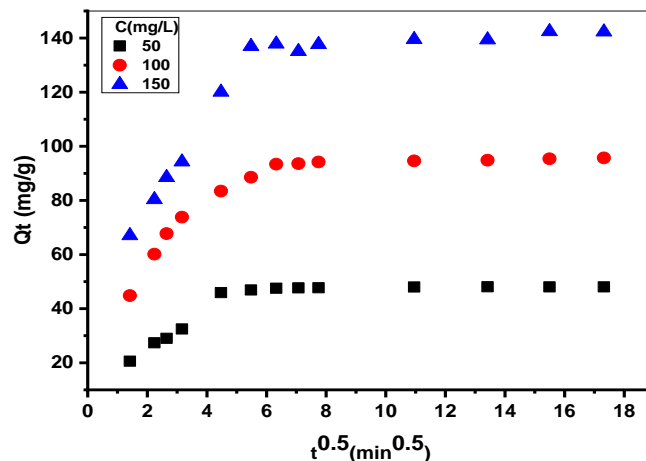


Figure 9. Experimental (symbols) by means the intraparticle diffusion model for MB onto OP-H₃PO₄ at three concentrations. (Agitation speed=250 rpm, pH=6.2).

Moreover, the intraparticle diffusion model was used to examine the mass transfer mechanism between the liquid and the solid phases [35]. The obtained plots are illustrated in Fig.9, showing two stages; the first one can be attributed to diffusion in the macropores [36] and the second to diffusion in the micropores. These results show that intraparticle diffusion occurred, but it was not the rate-limiting step [35,36].

2.4. Isotherms modeling

The adsorption isotherms of MB onto OP-H₃PO₄ at different temperatures are shown in Fig. 10. As observed, the isotherms had the same shape; they are characterized by a significant increase in the amount adsorbed until reaching equilibrium. The increase in the initial concentration of MB from 50 to 500 mg/L leads to improve the motor force of the mass transfer of MB between the liquid and the solid phase [37]. Fig. 10 also shows that the amounts adsorbed at equilibrium were 307.63, 301.37, 293.663 mg/g for 25, 30 and 40 °C, respectively, showing the negative impact of the temperature on the adsorption of MB onto OP-H₃PO₄.

Using Origin software, the modeling parameters of the experimental isotherm data by the above-mentioned models are summarized in Table 5, and the corresponding curves are represented in Fig. 10.

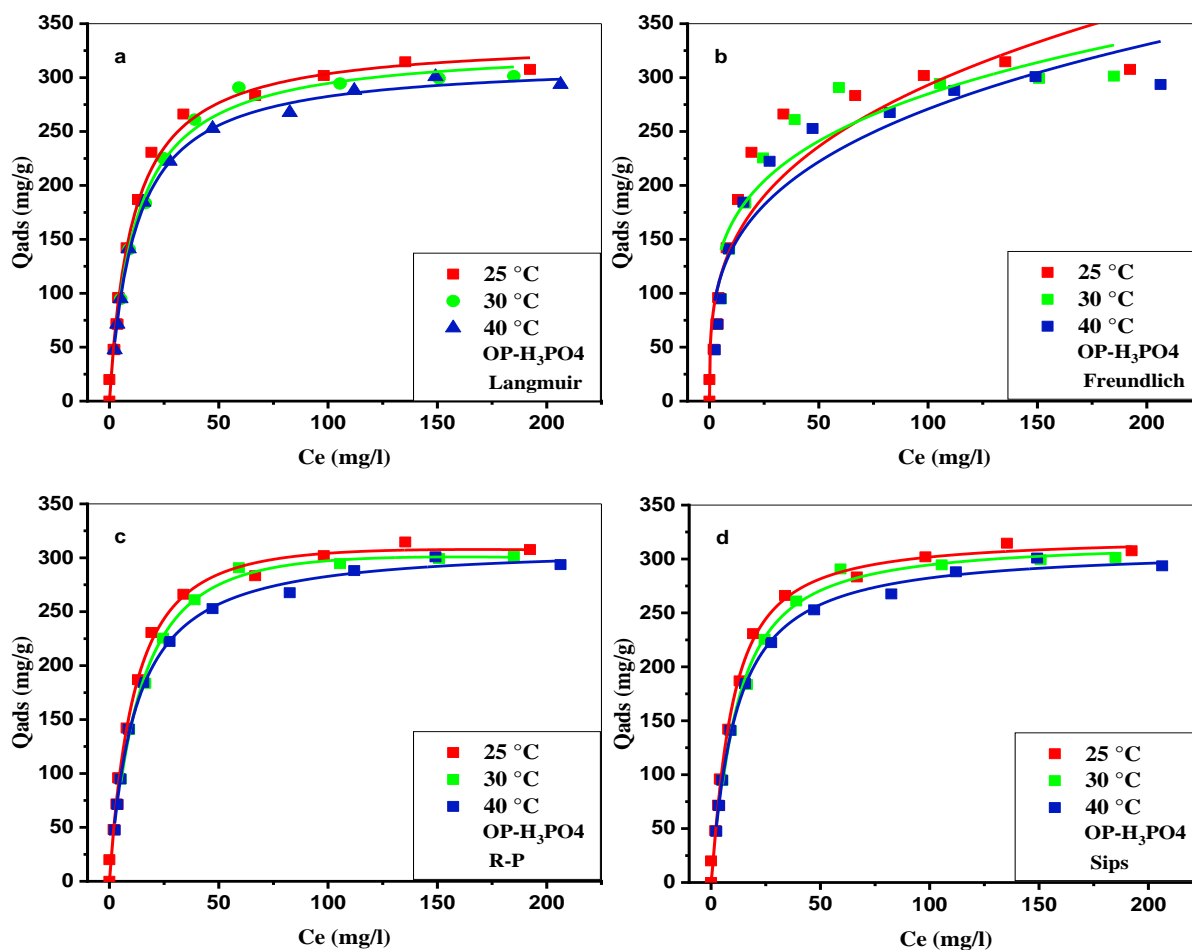


Figure 10. Comparison between the experimental adsorption isotherms of MB onto OP-H₃PO₄ and the modeling curves by (a) Langmuir, (b) Freundlich, (c) Redlich Peterson and (d) Sips models. (Agitation speed=250 rpm, pH=6.2).

Regarding the two-parameter models, the adsorbed quantities calculated by the Langmuir model led to the best fit of experimental data, with good correlation coefficients R^2 , between 0.986 and 0.996; while the low correlation coefficients (R^2) obtained for the Freundlich model showed that it was not appropriate to describe MB adsorption isotherms onto OP-H₃PO₄. In addition, the values of the K_L constant of the Langmuir model were very low (between 0.084×10^{-3} and 0.096×10^{-3} L/mg), showing the affinity between the MB molecules and the active sites of OP-H₃PO₄, because more the K_L values are low, more the adsorbate-adsorbent affinity is high [33]. Regarding the three-parameter models, for the whole temperatures range considered, both the sips and the Redlich-Peterson models gave high correlation factors. However, the adsorbed quantities calculated by the Sips model were very close to those found experimentally, suggesting that MB adsorption occurs on both homogeneous and heterogeneous surfaces of OP-H₃PO₄ [38].

Table 5: Langmuir, Freundlich, Sips, and Redlich-Peterson (R-P) constants for the adsorption of MB onto OP-H₃PO₄.

Material	Models	Parameters	25 °C	30 °C	40 °C
OP-H₃PO₄	Langmuir	Q_{exp}(mg/g)	307.635	301.376	293.663
		Q_m(mg/g)	336.33	329.817	315.472
		K_L (L/mg)x 10³	0.093	0.084	0.086
		R²	0.992	0.986	0.996
	Freundlich	1/n	0.312	0.240	0.288
		K_F(mg/g)(L/mg)^{1/n}	69.572	94.222	72.021
		R²	0.906	0.836	0.893
	Sips	Q_m(mg/g)	319.870	316.191	309.716
		K_S (L/mg)	0.107	0.089	0.090
		M	1.184	1.191	1.062
		R²	0.995	0.991	0.996
	Redlich-Peterson	k_R(L/g)	27.346	22.015	26.350
		α_R (L/ mg)	0.057	0.042	0.079
		β_R	1.072	1.093	1.010
		R²	0.994	0.995	0.996

Nevertheless, the values of the system heterogeneity index in the Sips model were 1.118, 1.191 and 1.062 for 25, 30 and 40 °C respectively, namely close to 1 and hence close to the Langmuir equation. In conclusion, the Sips and the Langmuir models led to the most accurate fit of experimental data; and it should be noted that at high concentrations, the Sips equation tends towards the Langmuir equation [39].

2.5. Orange peels as an adsorbent

For the purpose of comparison with other research studies that used orange peels as a precursor to prepare different adsorbents, Table 6 summarizes the literature data, including the adsorbent and the adsorbate considered, as well as the maximum amount adsorbed and the modeling results. As shown in Table 6, it is clear that the OP-H₃PO₄ is in an excellent position to be used as an adsorbent since the obtained results were similar to those gathered in the Table.

Table 6. Comparative study for the used orange peels as an adsorbent for different adsorbates.

Adsorbent	Adsorbate	Maximal amount (mg/g)	Isotherm modeling	Kinetic modeling	References
Modified orange peels (KOP)	Cu ²⁺	59.77	non-linear Langmuir	non-linear PSO	[40]
Modified Orange Peels Powder (CMOPP)	Congo Red	163	non-linear Langmuir	non-linear PSO	[41]
OP-derived biochar	Cadmium	114.69	non-linear Langmuir	non-linear PSO	[42]
Pectin from orange Industry residues	MB	398.40	Linear Langmuir	linear PSO	[43]
	Indigo Carmine	130.89	Linear Langmuir	linear PSO	[43]
Sulfuric acid-treated orange peels (STOP)	MB	50	Linear Freundlich	linear PSO	[44]
Orange peels	Reactive Gray BF-2R	11.4	non-linear Freundlich and Fritz-Schlunder	non-linear PSO	[45]
Activated carbon	Violet B	49.2	linear Langmuir	linear PSO	[46]
Orange peels (COP)	Violet 5R	87.26	linear Langmuir	liner PSO	[46]
OP-H₃PO₄	MB	307.63	non-linear Sips and Langmuir	non-linear PSO	This study

2.6. Effect of the initial pH

The impact of the initial pH is displayed in Fig. 11. As observed, the plot can be divided into two parts; the first one is defined by a significant increase in the adsorbed amount from 0 to 91 mg/g in the pH range of 2 to 4, while in a second step, the amount of adsorbed MB remained almost stable in the range of pH 4 to 12.

This variation can be explained by the fact that for a pH increase, the negative charges on the surface of the OP-H₃PO₄ also increased because the p_Hpzc of the OP-H₃PO₄ was equal to 3.34. Consequently, when the pH of the solution varied towards alkaline pH, negative charges became more available on the OP-H₃PO₄ surface; this availability of negative charges on the adsorbent surface makes the adsorption of MB easier and more favorable since the latter is a cationic dye.

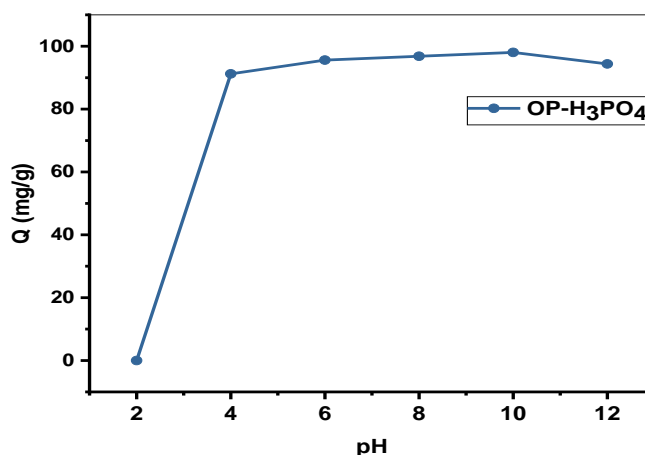


Figure 11. Initial pH effect for the MB adsorption onto OP-H₃PO₄. (Agitation speed = 250 rpm, T=25°C).

2.7. Effect of ionic strength and humic acid on MB adsorption onto OP-H₃PO₄

The results obtained (Fig. 12) show that the performances of the OP-H₃PO₄ decreased after the addition of NaCl; this finding can be explained by the competitive adsorption between the Na⁺ ions and the MB dye [47], which makes the accessibility of the active sites more difficult for MB, in agreement with others findings [48,49]. Contrarily, the adsorption efficiency increased after the addition of humic acid, from 314.0 to 358.5 mg/g.

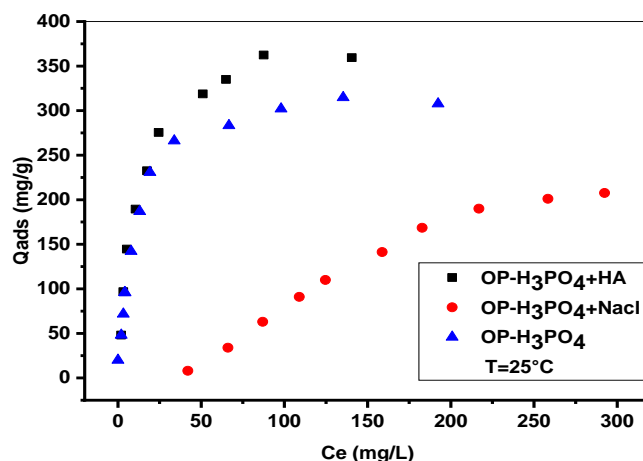


Figure 12. Ionic strength and humic acid effects for the MB adsorption onto OP-H₃PO₄. (pH=6.2, agitation speed = 250 rpm, T=25°C)

3. Density Function Theory (DFT) study

In this study, the quantum chemical calculations employing DFT theorem were carried out to investigate the effect of these molecular structure on the adsorption process of MB molecules onto the OP-H₃PO₄ surface. The optimized molecular structures, the HOMO orbitals, the LUMO orbitals and the molecular electrostatic potential maps of MB and OP-H₃PO₄ are shown in Fig. 13. It can be observed from Figs. 13 (b) and 13 (c) that both HOMO and LUMO orbitals were widely distributed on the area of the MB molecule, and on the oxygen atoms of the OP-H₃PO₄, which indicates that these sites are probably the active sites of adsorption. This result was confirmed by the molecular electrostatic potential maps (MEP). Generally, the molecular electrostatic potential gives a visual scheme to understand the relative polarity and the reactive sites of the molecules [50,51]. Additionally, the charges distribution of molecules in three dimensions can be illustrated by the electrostatic potential maps. In this context, the MEP maps of MB and OP-H₃PO₄ were calculated using the DFT method and the obtained results are displayed in Fig. 13 (d). From Fig. 13 (d), it can be seen that the negative regions of the MEP, red and yellow colors, were located on the oxygen, nitrogen and sulfur atoms which are the most appropriate for electrophilic attacks.

On the other hand, to better understand the effect of MB adsorption on the electrical and structural properties of OP-H₃PO₄, the values of E_{HOMO} , E_{LUMO} , ΔE_{GAP} , μ , η , σ , χ and ω for the MB and OP-H₃PO₄ molecules were determined, and the obtained results are summarized in Table 7. Generally, the reactivity and the stability of a molecule can be

determined by the value of the total energy (E_{Tot}); a high value of E_{Tot} characterizes a high stability of the molecule and hence a small value of its affinity to the adsorption capacity.

As known, the highest occupied molecular orbital energy (E_{HOMO}) is usually related to the ability of a molecule to lose electrons [52], while the lowest unoccupied molecular orbital energy (E_{LUMO}) indicates the capacity of the molecule to capture electrons and it is associated to electron affinity [53]. Consequently, an elevated value of E_{HOMO} designates the affinity of electrons transfer to a suitable acceptor molecule which hence favors the adsorption of the MB molecules onto the OP- H_3PO_4 surface. Moreover, a low value of ΔE_{GAP} characterizes a high reactivity of the molecule, which is also in favor of the adsorption of MB onto the OP- H_3PO_4 surface, indicating that the adsorption process is very stable.

Usually, the dipole moment (μ) is due to a molecule's polarity and is associated to the adsorptive capacity. An elevated value of μ can enhance the adsorption between MB molecules and the OP- H_3PO_4 surface. Therefore, the high dipole moment obtained can cause electrons transfer from the MB molecule to the OP- H_3PO_4 surface. Additionally, when the MB is adsorbed on the surface of OP- H_3PO_4 , the size and the direction of the dipole moment vector are modified depending on the adsorption configuration. Furthermore, the stability and the reactivity of molecules can be determined by the values of the global hardness and softness. The global hardness indicates the resistance of a molecule towards the deformation or polarization under a small perturbation of the chemical reaction. Generally, small values of the global hardness and elevated values of the global softness of molecules can help their adsorption process to an appropriate surface. Also, the electrophilicity index (Ω) shows the capability of molecules to capture electrons; the adsorption process can increase with the decrease of the Ω value [54].

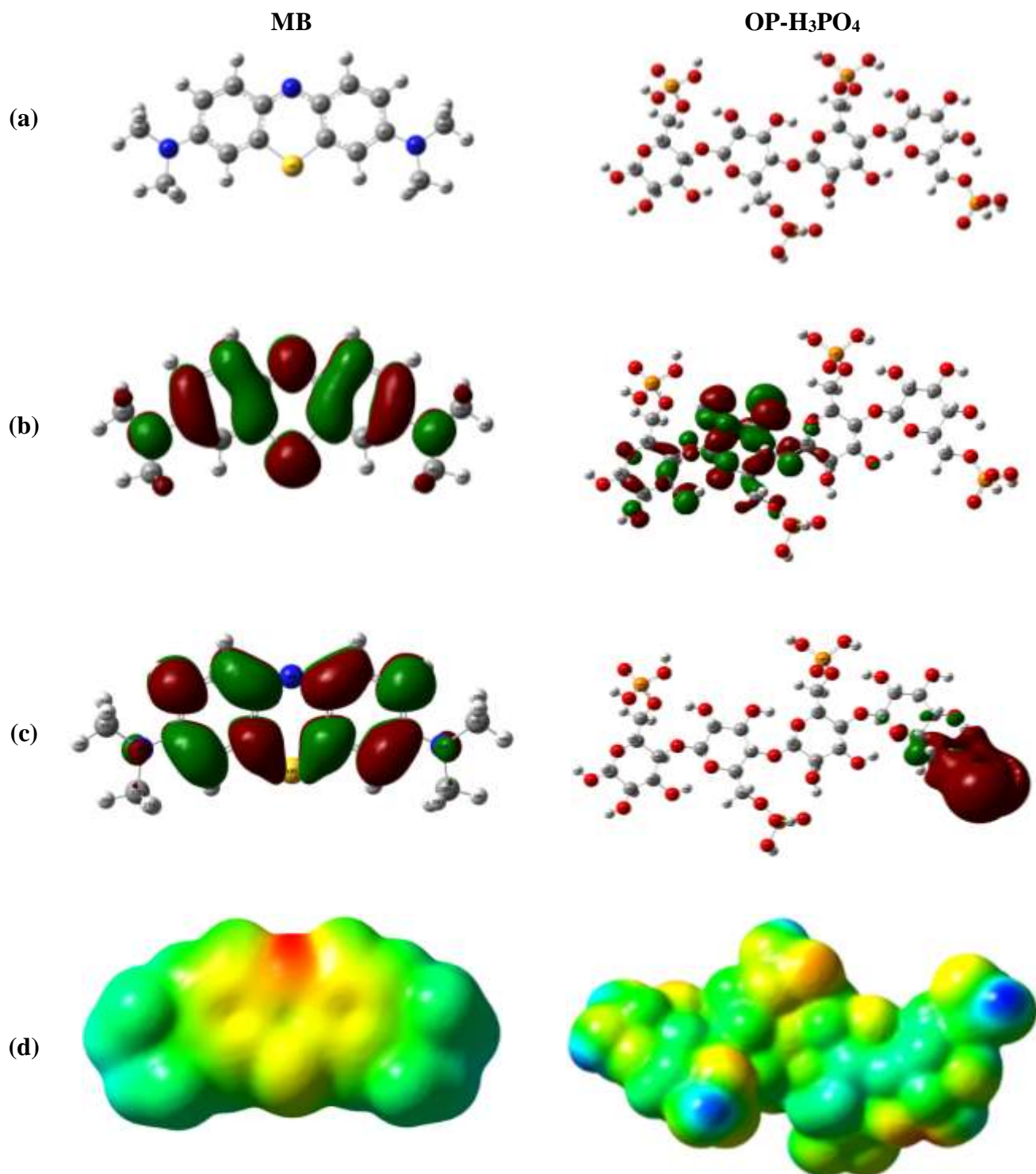


Figure 13. (a) Optimized molecular structure, (b) HOMO, (c) LUMO and (d) MEP.

Table 7: The obtained values of the quantum chemical parameters of MB and OP-H₃PO₄ using DFT/B3LYP 6-31G (d,p) method.

Quantum chemical parameters	MB	OP-H ₃ PO ₄
E_{Tot} (eV)	- 32190.5915	- 130380.854
E_{HOMO} (eV)	- 3.66347078	- 7.07795725
E_{LUMO} (eV)	- 0.08544379	- 0.26041309
ΔE_{GAP} (eV)	3.57802699	6.81754415
μ (Debye)	2.5589	9.5981
η (eV)	1.78901349	3.40877208
Σ	0.55896728	0.29336077
χ (eV)	1.874457285	3.66918517
Ω	0.981990950	1.97474626

4. Molecular Dynamic Simulation (MDS) study

The use of the molecular dynamic simulations (MDS) is an important way to understand and interpret the interactions between the MB molecules and the OP-H₃PO₄ surface. Fig. 14 shows the most stable equilibrium configuration of the adsorption of MB molecule onto the OP-H₃PO₄ (110) surface. From Fig. 14, it can be observed that the MB molecule adsorbs on the OP-H₃PO₄ (110) surface following a parallel mode, which confirms the strong interactions between the MB and OP-H₃PO₄ surface atoms. Analysis of the molecular structures of MB and OP-H₃PO₄ shows that the adsorption of MB onto the OP-H₃PO₄ surface can be related to the contribution of the electrons of sulfur, nitrogen, and oxygen (chemical adsorption). Furthermore, the Van Der Waals dispersion forces can also contribute to catch the MB molecules towards the cellulose surface (physical adsorption), which confirm the results obtained in the isoelectric point characterization. The calculated values of the different energies of the adsorption of MB onto the OP-H₃PO₄ surface are summarized in Table 8. The negative value of the adsorption energy (-37.117 kcal/mol) indicates the spontaneity of the adsorption process. The high value of the binding energy (37.117 kcal/mol) can be assigned to the best and most stable adsorption process [54]. The deformation energy of the molecule suggests that the conformational rearrangement induced by the MB adsorption provides both the MB and the OP-H₃PO₄ surface less stable.

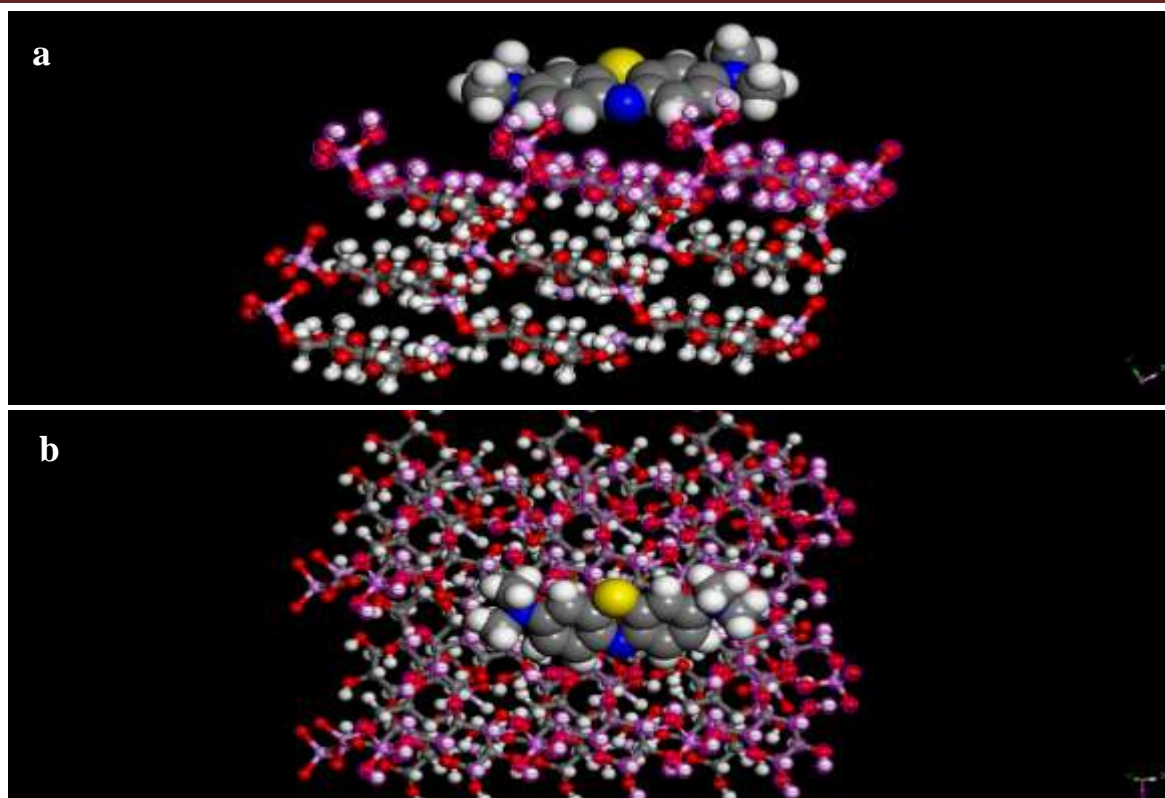


Figure 14. Equilibrium adsorption configuration of MB onto the OP-H₃PO₄ surface: (a) Side view, (b) Top view.

Table 8: Calculated energies for the adsorption of the MB molecules on the OP-H₃PO₄ surface.

Adsorption energy	Rigid adsorption energy	Deformation energy	Binding energy
-37,117 kcal/mol	-38,162 kcal/mol	1,045 kcal/mol	37.117 kcal/mol

5. Proposed adsorption mechanism of MB onto OP-H₃PO₄

From the isoelectric point, the pH effect and the MDS results, it is assumed that the MB adsorption onto OP-H₃PO₄ mechanism is globally driven by electrostatic interactions (physical adsorption) between the adsorbent, which is negatively charged at the pH of the solution (6.2) and the dye that is positively charged. Furthermore, the MDS results confirm that physical adsorption exists with Van Der Waals electrostatic interactions. Otherwise, the MDS shows that chemical adsorption can also exist because of the electrons of sulfur, nitrogen and oxygen contribution or the π - π interactions between the aromatic rings in dye and those of the OP-H₃PO₄. To conclude, by combining the obtained results, it is assumed that the MB molecules adsorb onto OP-H₃PO₄ (110) surface with parallel position by

electrostatic interactions, while the chemical adsorption is also involved at a low extent compared to the physical adsorption.

6. Conclusion

In this study, raw orange peels (ROP) was used as a precursor and then modified using phosphoric acid for the preparation of our adsorbent material (OP-H₃PO₄). The adsorption tests were carried out in a batch system using methylene blue (MB) as a model dye. The results obtained showed a high adsorption potential of OP-H₃PO₄, 307.63 mg/g at 25 °C. The modeling of the adsorption kinetics shows that the pseudo-second-order model was the most reliable to describe experimental data. Moreover, the equilibrium data indicates that both Sips and Langmuir models could represent the MB uptake onto OP-H₃PO₄. The results of the ionic strength effect showed that the competition between the MB dye and the Na⁺ ions led to a decrease in the amount adsorbed. The experimental results were well correlated with the calculated quantum chemical parameters. Also, molecular dynamics simulations indicate that the MB molecule adsorbs on the OP-H₃PO₄ (110) surface in a nearby horizontal position.

7. References

- [1] G. Vilar, L. Di Palma, N. Verdone, Heavy metals adsorption by banana peels micro-powder: Equilibrium modeling by non-linear models, *Chin. J. Chem. Eng.* 26 (2018) 455–464. <https://doi.org/10.1016/j.cjche.2017.06.026>.
- [2] A.B. Albadarin, S. Solomon, T.A. Kurniawan, C. Mangwandi, G. Walker, Single, simultaneous and consecutive biosorption of Cr(VI) and Orange II onto chemically modified masau stones, *J. Environ. Manage.* 204 (2017) 365–374. <https://doi.org/10.1016/j.jenvman.2017.08.042>.
- [3] L. Wang, Z. Chen, H. Wen, Z. Cai, C. He, Z. Wang, W. Yan, Microwave assisted modification of activated carbons by organic acid ammoniums activation for enhanced adsorption of acid red 18, *Powder Technol.* 323 (2018) 230–237. <https://doi.org/10.1016/j.powtec.2017.10.021>.
- [4] S. Rangabhashiyam, S. Lata, P. Balasubramanian, Biosorption characteristics of methylene blue and malachite green from simulated wastewater onto Carica papaya wood biosorbent, *Surf. Interfaces.* 10 (2018) 197–215. <https://doi.org/10.1016/j.surfin.2017.09.011>.

- [5] W. Li, Q. Ma, Y. Bai, D. Xu, M. Wu, H. Ma, Facile fabrication of gelatin/bentonite composite beads for tunable removal of anionic and cationic dyes, *Chem. Eng. Res. Des.* 134 (2018) 336–346. <https://doi.org/10.1016/j.cherd.2018.04.016>.
- [6] X. Wang, C. Jiang, B. Hou, Y. Wang, C. Hao, J. Wu, Carbon composite lignin-based adsorbents for the adsorption of dyes, *Chemosphere.* 206 (2018) 587–596. <https://doi.org/10.1016/j.chemosphere.2018.04.183>.
- [7] T.N.V. de Souza, S.M.L. de Carvalho, M.G.A. Vieira, M.G.C. da Silva, D. do S.B. Brasil, Adsorption of basic dyes onto activated carbon: Experimental and theoretical investigation of chemical reactivity of basic dyes using DFT-based descriptors, *Appl. Surf. Sci.* 448 (2018) 662–670. <https://doi.org/10.1016/j.apsusc.2018.04.087>.
- [8] A. Kausar, M. Iqbal, A. Javed, K. Aftab, Z.-H. Nazli, H.N. Bhatti, S. Nouren, Dyes adsorption using clay and modified clay: A review, *J. Mol. Liq.* 256 (2018) 395–407. <https://doi.org/10.1016/j.molliq.2018.02.034>.
- [9] F. Ogata, T. Nakamura, N. Kawasaki, Adsorption capability of virgin and calcined wheat bran for molybdenum present in aqueous solution and elucidating the adsorption mechanism by adsorption isotherms, kinetics, and regeneration, *J. Environ. Chem. Eng.* 6 (2018) 4459–4466. <https://doi.org/10.1016/j.jece.2018.06.047>.
- [10] G. Crini, Non-conventional low-cost adsorbents for dye removal: A review, *Bioresour. Technol.* 97 (2006) 1061–1085. <https://doi.org/10.1016/j.biortech.2005.05.001>.
- [11] M. Danish, T. Ahmad, R. Hashim, N. Said, M.N. Akhtar, J. Mohamad-Saleh, O. Sulaiman, Comparison of surface properties of wood biomass activated carbons and their application against rhodamine B and methylene blue dye, *Surf. Interfaces.* 11 (2018) 1–13. <https://doi.org/10.1016/j.surfin.2018.02.001>.
- [12] T.S. Anirudhan, M. Ramachandran, Adsorptive removal of basic dyes from aqueous solutions by surfactant modified bentonite clay (organoclay): Kinetic and competitive adsorption isotherm, *Process Saf. Environ. Prot.* 95 (2015) 215–225. <https://doi.org/10.1016/j.psep.2015.03.003>.
- [13] M. Vakili, M. Rafatullah, B. Salamatinia, A.Z. Abdullah, M.H. Ibrahim, K.B. Tan, Z. Gholami, P. Amouzgar, Application of chitosan and its derivatives as adsorbents for dye removal from water and wastewater: A review, *Carbohydr. Polym.* 113 (2014) 115–130. <https://doi.org/10.1016/j.carbpol.2014.07.007>.

- [14] N. Gupta, A.K. Kushwaha, M.C. Chattopadhyaya, Application of potato (*Solanum tuberosum*) plant wastes for the removal of methylene blue and malachite green dye from aqueous solution, *Arab. J. Chem.* 9 (2016) S707–S716. <https://doi.org/10.1016/j.arabjc.2011.07.021>.
- [15] A. Bhatnagar, M. Sillanpää, A. Witek-Krowiak, Agricultural waste peels as versatile biomass for water purification – A review, *Chem. Eng. J.* 270 (2015) 244–271. <https://doi.org/10.1016/j.cej.2015.01.135>.
- [16] J. Fu, Z. Chen, M. Wang, S. Liu, J. Zhang, J. Zhang, R. Han, Q. Xu, Adsorption of methylene blue by a high-efficiency adsorbent (polydopamine microspheres): Kinetics, isotherm, thermodynamics and mechanism analysis, *Chem. Eng. J.* 259 (2015) 53–61. <https://doi.org/10.1016/j.cej.2014.07.101>.
- [17] A.B. Albadarin, M.N. Collins, M. Naushad, S. Shirazian, G. Walker, C. Mangwandi, Activated lignin-chitosan extruded blends for efficient adsorption of methylene blue, *Chem. Eng. J.* 307 (2017) 264–272. <https://doi.org/10.1016/j.cej.2016.08.089>.
- [18] Mohd. Rafatullah, O. Sulaiman, R. Hashim, A. Ahmad, Adsorption of methylene blue on low-cost adsorbents: A review, *J. Hazard. Mater.* 177 (2010) 70–80. <https://doi.org/10.1016/j.jhazmat.2009.12.047>.
- [19] T.L. Silva, A.L. Cazetta, P.S.C. Souza, T. Zhang, T. Asefa, V.C. Almeida, Mesoporous activated carbon fibers synthesized from denim fabric waste: Efficient adsorbents for removal of textile dye from aqueous solutions, *J. Clean. Prod.* 171 (2018) 482–490. <https://doi.org/10.1016/j.jclepro.2017.10.034>.
- [20] M.A. Nahil, P.T. Williams, Pore characteristics of activated carbons from the phosphoric acid chemical activation of cotton stalks, *Biomass Bioenergy.* 37 (2012) 142–149. <https://doi.org/10.1016/j.biombioe.2011.12.019>.
- [21] A.N.A. El-Hendawy, Variation in the FTIR spectra of a biomass under impregnation, carbonization and oxidation conditions, *J. Anal. Appl. Pyrolysis.* 75 (2006) 159–166. <https://doi.org/10.1016/j.jaap.2005.05.004>.
- [22] J.P. Merrick, D. Moran, L. Radom, An Evaluation of Harmonic Vibrational Frequency Scale Factors, *J. Phys. Chem. A.* 111 (2007) 11683–11700. <https://doi.org/10.1021/jp073974n>.
- [23] C. Namasivayam, D. Kavitha, IR, XRD and SEM studies on the mechanism of adsorption of dyes and phenols by coir pith carbon from aqueous phase, *Microchem. J.* 82 (2006) 43–48. <https://doi.org/10.1016/j.microc.2005.07.002>.

- [24] W. Chen, H. Yu, Y. Liu, P. Chen, M. Zhang, Y. Hai, Individualization of cellulose nanofibers from wood using high-intensity ultrasonication combined with chemical pretreatments, *Carbohydr. Polym.* 83 (2011) 1804–1811. <https://doi.org/10.1016/j.carbpol.2010.10.040>.
- [25] A. Kumar, Y.S. Negi, N.K. Bhardwaj, V. Choudhary, Synthesis and characterization of methylcellulose/PVA based porous composite, *Carbohydr. Polym.* 88 (2012) 1364–1372. <https://doi.org/10.1016/j.carbpol.2012.02.019>.
- [26] A. Kumar, Y.S. Negi, V. Choudhary, N.K. Bhardwaj, Characterization of Cellulose Nanocrystals Produced by Acid-Hydrolysis from Sugarcane Bagasse as Agro-Waste, *J. Mater. Phys. Chem.* 2 (2014) 1–8. <https://doi.org/10.12691/jmpc-2-1-1>.
- [27] S. Banerjee, M.C. Chattopadhyaya, Adsorption characteristics for the removal of a toxic dye, tartrazine from aqueous solutions by a low cost agricultural by-product, *Arab. J. Chem.* 10 (2017) S1629–S1638. <https://doi.org/10.1016/j.arabjc.2013.06.005>.
- [28] F. Marrakchi, M. Auta, W.A. Khanday, B.H. Hameed, High-surface-area and nitrogen-rich mesoporous carbon material from fishery waste for effective adsorption of methylene blue, *Powder Technol.* 321 (2017) 428–434. <https://doi.org/10.1016/j.powtec.2017.08.023>.
- [29] S.E.A. Elhafez, H.A. Hamad, A.A. Zaatout, G.F. Malash, Management of agricultural waste for removal of heavy metals from aqueous solution: adsorption behaviors, adsorption mechanisms, environmental protection, and techno-economic analysis, *Environ. Sci. Pollut. Res.* 24 (2017) 1397–1415. <https://doi.org/10.1007/s11356-016-7891-7>.
- [30] B. Tural, E. Ertaş, B. Enez, S.A. Fincan, S. Tural, Preparation and characterization of a novel magnetic biosorbent functionalized with biomass of *Bacillus Subtilis*: Kinetic and isotherm studies of biosorption processes in the removal of Methylene Blue, *J. Environ. Chem. Eng.* 5 (2017) 4795–4802. <https://doi.org/10.1016/j.jece.2017.09.019>.
- [31] D.L. Postai, C.A. Rodrigues, Adsorption of Cationic Dyes Using Waste from Fruits of *Eugenia umbelliflora* Berg (Myrtaceae), *Arab. J. Sci. Eng.* 43 (2018) 2425–2440. <https://doi.org/10.1007/s13369-017-2819-1>.
- [32] A.A. Sharipova, S.B. Aidarova, N.E. Bekturganova, A. Tleuova, M. Schenderlein, O. Lygina, S. Lyubchik, R. Miller, Triclosan as model system for the adsorption on recycled adsorbent materials, *Colloids Surf. Physicochem. Eng. Asp.* 505 (2016) 193–196. <https://doi.org/10.1016/j.colsurfa.2016.04.049>.

- [33] L.A. Romero-Cano, H. García-Rosero, L.V. Gonzalez-Gutierrez, L.A. Baldenegro-Pérez, F. Carrasco-Marín, Functionalized adsorbents prepared from fruit peels: Equilibrium, kinetic and thermodynamic studies for copper adsorption in aqueous solution, *J. Clean. Prod.* 162 (2017) 195–204. <https://doi.org/10.1016/j.jclepro.2017.06.032>.
- [34] G.B. Oguntimein, Biosorption of dye from textile wastewater effluent onto alkali treated dried sunflower seed hull and design of a batch adsorber, *J. Environ. Chem. Eng.* 3 (2015) 2647–2661. <https://doi.org/10.1016/j.jece.2015.09.028>.
- [35] D. Chebli, A. Bouguettoucha, T. Mekhalef, S. Nacef, A. Amrane, Valorization of an agricultural waste, *Stipa tenassicima* fibers, by biosorption of an anionic azo dye, Congo red, *Desalination Water Treat.* 54 (2015) 245–254. <https://doi.org/10.1080/19443994.2014.880154>.
- [36] A. Bouguettoucha, D. Chebli, T. Mekhalef, A. Noui, A. Amrane, The use of a forest waste biomass, cone of *Pinus brutia* for the removal of an anionic azo dye Congo red from aqueous medium, *Desalination Water Treat.* 55 (2015) 1956–1965. <https://doi.org/10.1080/19443994.2014.928235>.
- [37] B. Tanhaei, A. Ayati, M. Lahtinen, M. Sillanpää, Preparation and characterization of a novel chitosan/Al₂O₃/magnetite nanoparticles composite adsorbent for kinetic, thermodynamic and isotherm studies of Methyl Orange adsorption, *Chem. Eng. J.* 259 (2015) 1–10. <https://doi.org/10.1016/j.cej.2014.07.109>.
- [38] E. Daneshvar, A. Vazirzadeh, A. Niazi, M. Kousha, Mu. Naushad, A. Bhatnagar, Desorption of Methylene blue dye from brown macroalga: Effects of operating parameters, isotherm study and kinetic modeling, *J. Clean. Prod.* 152 (2017) 443–453. <https://doi.org/10.1016/j.jclepro.2017.03.119>.
- [39] Y. Wang, L. Shi, L. Gao, Q. Wei, L. Cui, L. Hu, L. Yan, B. Du, The removal of lead ions from aqueous solution by using magnetic hydroxypropyl chitosan/oxidized multiwalled carbon nanotubes composites, *J. Colloid Interface Sci.* 451 (2015) 7–14. <https://doi.org/10.1016/j.jcis.2015.03.048>.
- [40] S. Liang, X. Guo, N. Feng, Q. Tian, Isotherms, kinetics and thermodynamic studies of adsorption of Cu²⁺ from aqueous solutions by Mg²⁺/K⁺ type orange peel adsorbents, *J. Hazard. Mater.* 174 (2010) 756–762. <https://doi.org/10.1016/j.jhazmat.2009.09.116>.

- [41] V.S. Munagapati, D.S. Kim, Adsorption of anionic azo dye Congo Red from aqueous solution by Cationic Modified Orange Peel Powder, *J. Mol. Liq.* 220 (2016) 540–548. <https://doi.org/10.1016/j.molliq.2016.04.119>.
- [42] H.N. Tran, S.J. You, H.P. Chao, Effect of pyrolysis temperatures and times on the adsorption of cadmium onto orange peel derived biochar, *Waste Manag. Res.* 34 (2016) 129–138. <https://doi.org/10.1177/0734242X15615698>.
- [43] M. Kebaili, S. Djellali, M. Radjai, N. Drouiche, H. Lounici, Valorization of orange industry residues to form a natural coagulant and adsorbent, *J. Ind. Eng. Chem.* 64 (2018) 292–299. <https://doi.org/10.1016/j.jiec.2018.03.027>.
- [44] P.S. Kumar, P.S.A. Fernando, R.T. Ahmed, R. Srinath, M. Priyadharshini, A.M. Vignesh, A. Thanjiappan, Effect of Temperature on the Adsorption of Methylene Blue Dye Onto Sulfuric Acid-Treated Orange Peel, *Chem. Eng. Commun.* 201 (2014) 1526–1547. <https://doi.org/10.1080/00986445.2013.819352>.
- [45] G.E. do Nascimento, M.M.M.B. Duarte, N.F. Campos, O.R.S. da Rocha, V.L. da Silva, Adsorption of azo dyes using peanut hull and orange peel: a comparative study, *Environ. Technol.* 35 (2014) 1436–1453. <https://doi.org/10.1080/09593330.2013.870234>.
- [46] S. Hashemian, K. Salari, H. Salehifar, Z. Atashi Yazdi, Removal of Azo Dyes (Violet B and Violet 5R) from Aqueous Solution Using New Activated Carbon Developed from Orange Peel, *J. Chem.* (2013). <https://doi.org/10.1155/2013/283274>.
- [47] C.H. Weng, Y.T. Lin, T.W. Tzeng, Removal of methylene blue from aqueous solution by adsorption onto pineapple leaf powder, *J. Hazard. Mater.* 170 (2009) 417–424. <https://doi.org/10.1016/j.jhazmat.2009.04.080>.
- [48] R. Han, J. Zhang, P. Han, Y. Wang, Z. Zhao, M. Tang, Study of equilibrium, kinetic and thermodynamic parameters about methylene blue adsorption onto natural zeolite, *Chem. Eng. J.* 145 (2009) 496–504. <https://doi.org/10.1016/j.cej.2008.05.003>.
- [49] Y. Liu, Y. Zheng, A. Wang, Enhanced adsorption of Methylene Blue from aqueous solution by chitosan-g-poly (acrylic acid)/vermiculite hydrogel composites, *J. Environ. Sci.* 22 (2010) 486–493. [https://doi.org/10.1016/S1001-0742\(09\)60134-0](https://doi.org/10.1016/S1001-0742(09)60134-0).
- [50] A.E. Reed, F. Weinhold, Natural localized molecular orbitals, *J. Chem. Phys.* 83 (1985) 1736–1740. <https://doi.org/10.1063/1.449360>.
- [51] F.J. Luque, J.M. López, M. Orozco, Perspective on “Electrostatic interactions of a solute with a continuum. A direct utilization of ab initio molecular potentials for the

- prevision of solvent effects,” in: C.J. Cramer, D.G. Truhlar (Eds.), *Theor. Chem. Acc. New Century Issue*, Springer Berlin Heidelberg, Berlin, Heidelberg, 2001: pp. 343–345. https://doi.org/10.1007/978-3-662-10421-7_56.
- [52] L. Herrag, B. Hammouti, S. Elkadiri, A. Aouniti, C. Jama, H. Vezin, F. Bentiss, Adsorption properties and inhibition of mild steel corrosion in hydrochloric solution by some newly synthesized diamine derivatives: Experimental and theoretical investigations, *Corros. Sci.* 52 (2010) 3042–3051. <https://doi.org/10.1016/j.corsci.2010.05.024>.
- [53] K.F. Khaled, Studies of iron corrosion inhibition using chemical, electrochemical and computer simulation techniques, *Electrochimica Acta.* 55 (2010) 6523–6532. <https://doi.org/10.1016/j.electacta.2010.06.027>.
- [54] N. Chafai, S. Chafaa, K. Benbouguerra, D. Daoud, A. Hellal, M. Mehri, Synthesis, characterization and the inhibition activity of a new α -aminophosphonic derivative on the corrosion of XC48 carbon steel in 0.5M H₂SO₄: Experimental and theoretical studies, *J. Taiwan Inst. Chem. Eng.* 70 (2017) 331–344. <https://doi.org/10.1016/j.jtice.2016.10.026>.

Chapter V: The use of encapsulation as a proposed solution to avoid problems encountered with conventional materials in powder form: application in methylene blue removal from aqueous solutions

1. Introduction

During their manufacturing activities, the petroleum, petrochemical, chemical and pharmaceutical industries produce huge amounts of polluted water, where its toxicity and its carcinogenicity have serious consequences on human health, as well as on the environment even at very low concentrations [1], leading to a systematic ecological disorder. It is therefore necessary to treat these waters before their recycling or rejection in the environment. In this background, and over the last decades, the treatment of these waters has always been a very important area of research and a topical subject for which thousands of research studies have been carried out, and huge budgets have been established in order to discover appropriate solutions to treat industrial water at reasonable costs.

As it is known, industrial water treatment is defined as the process of removing contaminants from industrial water, whether inorganics, such as heavy metals (arsenic, lead, cadmium), nitrates, phosphates, or organics, such as pharmaceutical effluents, detergents, acids, oils, diluents and dyes.

In fact, all industries that use dyes in their processes, such as textiles production, discharge more than 10^9 kg tons of dye, including 8000 associated molecules [1], to the natural environment, making their biodegradation impossible, hence human intervention is necessary. In this context, several classical and modern methods have been used to treat these polluted waters. Among these techniques, adsorption is one of the most widely used in wastewater treatment processes worldwide [2] due to its rapidity, performances and economic efficiency [3].

Therefore, much researches has recently been released on dye removal with a wide range of convenient powdered products already in use, such as activated carbon [4], clays [5], biosorbents [6]...etc. Nevertheless, it is essential to point out some issues related to the use of these materials, such as the regeneration problems and the quantities of powder recovered after an adsorption test. Indeed, in the last decade, scientific researches has focused on the development of new adsorbent materials aimed at avoiding the

disadvantages of these conventional materials. In this aim, encapsulation is proposed in this study to skip these issues on the one hand and to gain a number of benefits such as high adsorption capacity, high porosity, uniform size and ease of regeneration on the other hand. As a result, several polymers have been considered to perform the encapsulation step, such for example alginate [7,8], chitosan [9,10], cellulose [11,12], etc. In this study, sodium alginate was chosen with regards to its numerous advantages, such as its simplicity, biocompatibility and low cost [13,14] compared to other encapsulating agents.

This study focused on preparing a treated powdered material from *Ziziphus jujuba* stones (ZJS-H₃PO₄) and its encapsulation with sodium alginate, considering ratios in the range from 1 to 2. The efficiency of the prepared materials was evaluated in a batch system by adsorption of methylene blue dye, which was chosen as a model molecule of basic dye.

In addition, the characteristics of the prepared beads were also examined by different techniques of characterization, such as Fourier transform infrared spectroscopy (FTIR), scanning electron microscopy (SEM), X-ray fluorescence (XRF), thermogravimetric analysis (TGA), Brunauer–Emmett–Teller method (BET) and the point of zero charges (pH_{PZC}). In addition, the reusability of the prepared beads was also assessed.

2. Results and discussion

2.1. Characterization of the materials

In order to quantify the different functional groups present on the surface of the prepared materials and after MB adsorption, an FTIR analysis was carried out; the results obtained are shown in Fig. 1. A broad band was observed at about 3425 cm⁻¹, which can be attributed to vibrations of OH, NH, and COOH present on the surface of materials, in agreement with the related literature [15]. The vibrations of CH₂ and CH₃ were represented by small bands at 2853 and 2923 cm⁻¹, respectively. The peak at 1624 cm⁻¹ can be assigned to asymmetric and symmetric elongations of C=O in carboxylic groups, and the peak at approximately 1262 cm⁻¹ can be demonstrated by stretching vibrations of C-O. Moreover, Fig. 1 demonstrates the presence of C-N amines, C-H in aromatic rings and some phosphorus compounds owing to the existence of certain peaks between 1267 and 700 cm⁻¹ [16]. The BZJS curves show small bands at 1055 and 1031 cm⁻¹, which can be attributed to the C-O, C-O-H and C-C vibration modes on alginate carbohydrate rings [17]. These findings indicate that BZJS1 and BZJS2 have similar functional groups with some

variations in the intensity of some peaks, owing to the different ratios between *Ziziphus jujuba* powder and sodium alginate during the preparation step.

These results also show that after encapsulation, some peaks are shifted or reduced in intensity, and others have disappeared, which indicates that the encapsulation was efficiently done; the same remark after MB adsorption confirming that MB adsorption onto BZJS was efficiently achieved.

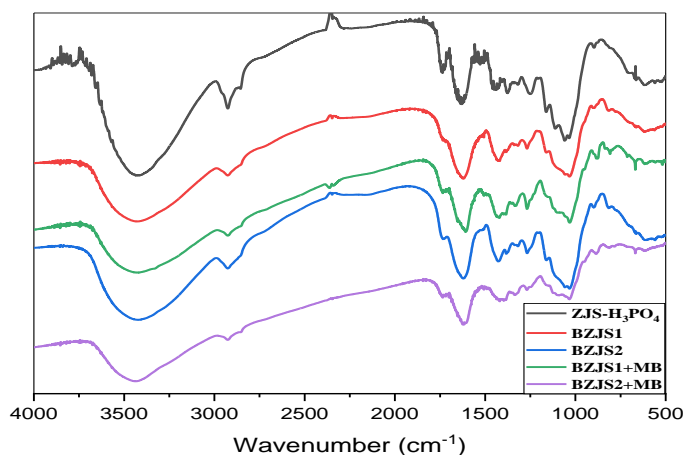


Figure 1. FTIR characterization of ZJS-H₃PO₄, BZJS1, BZJS2 and after adsorption of MB.

ZJS-H₃PO₄, BZJS1, and BZJS2 micromorphologies are displayed in Fig. 2 (a, b, c), showing a heterogeneous surface before encapsulation for the treated *Ziziphus jujuba* stones in powder form [18]. According to Fig. 2 (b and c), BZJS1 and BZJS2 had a spherical structure, with a more radiated (rigorous) structure for BZJS1 compared to BZJS2; this finding may be due to a higher alginate ratio for BZJS1, which promotes the proper integration of ZJS-H₃PO₄ into the alginate matrix.

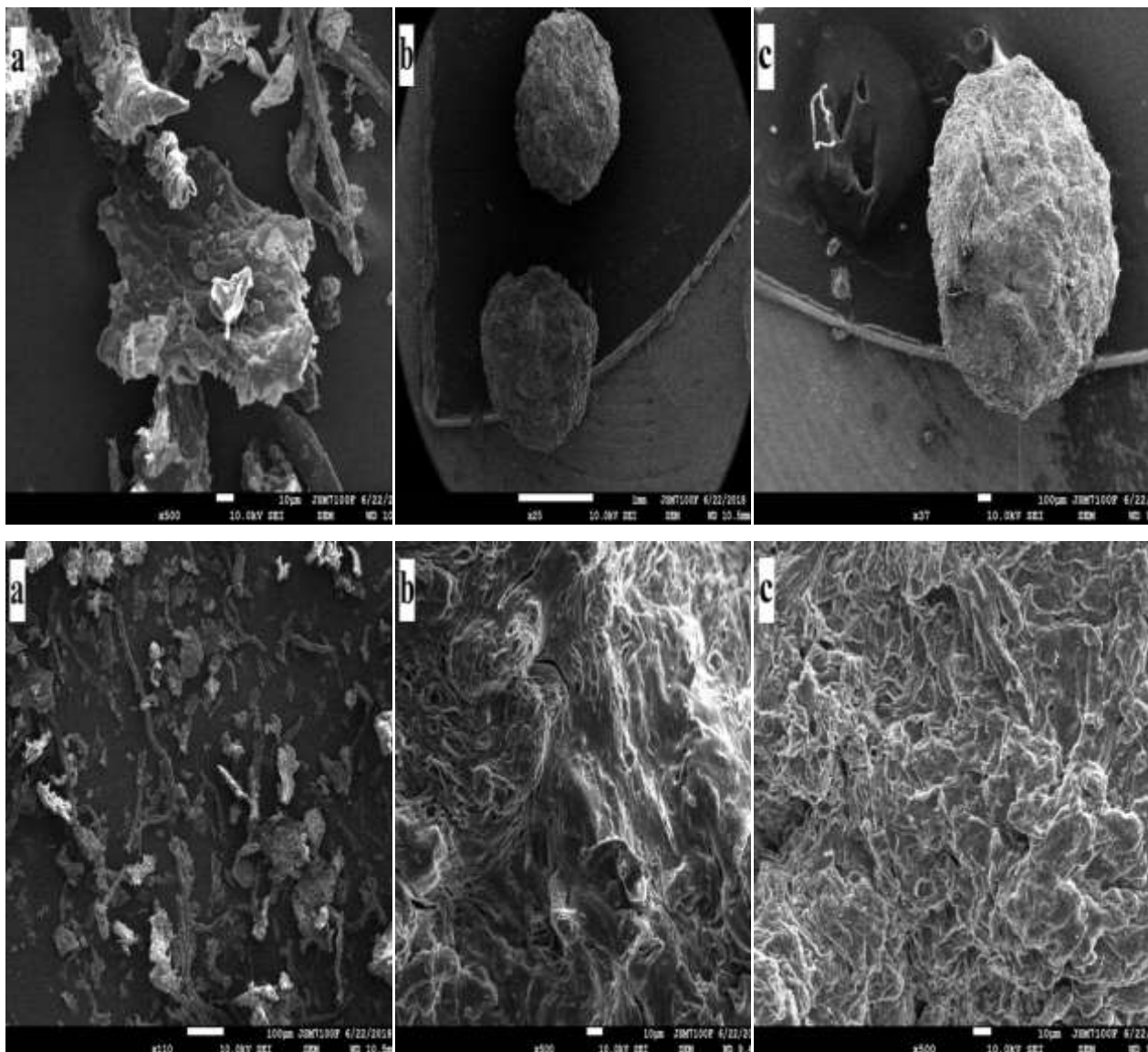


Figure 2. SEM captures of ZJS-H₃PO₄ (a), BZJS1 (b) and BZJS2 (c).

With the aim to realize a quantitative comparison between ZJS-H₃PO₄, BZJS1, and BZJS2, an elementary analysis using XRF and EDX characterizations were performed, and the obtained results are collected in Fig. 3 and Table 1. Both techniques show that the elemental composition was changed after the encapsulation of ZJS-H₃PO₄; this change can be seen in the decrease of certain elements percentages, such as carbon, as well as the increase in the percentage of some other elements, such as oxygen and the appearance of calcium which can characterize the efficiency of encapsulation. Furthermore, the XRF results show that the percentage of Ca for BZJS1 was higher than that for BZJS2; this finding must be related to the considered ratio in the bead preparation step.

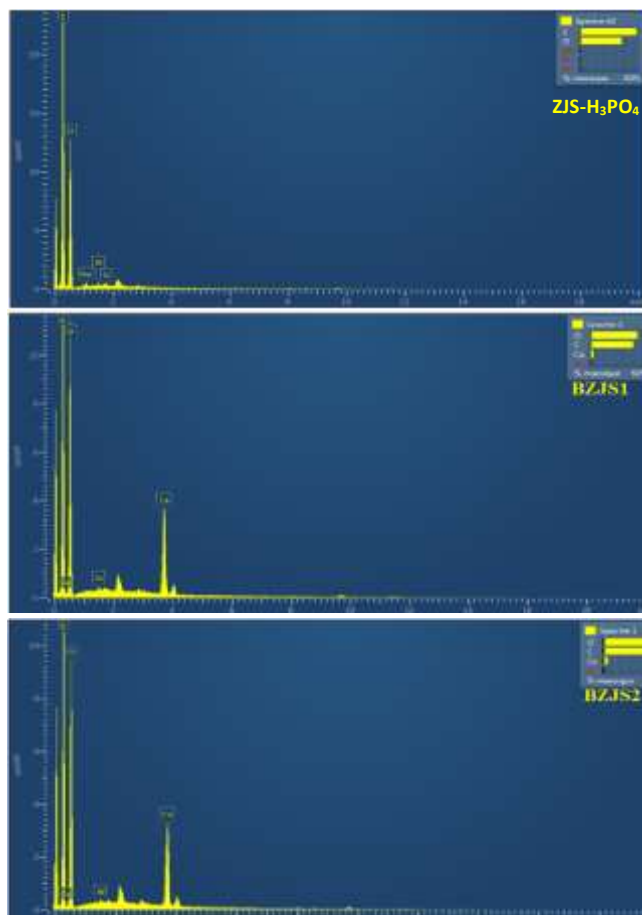


Figure 3. Elemental analysis by EDX of ZJS-H₃PO₄, BZJS1 and BZJS2.

Table 1: Elemental analysis by XRF of ZJS-H₃PO₄, BZJS1 and BZJS2.

Adsorbent	ZJS-H₃PO₄	BZJS1	BZJS2
Element	% Weight	% Weight	% Weight
C	47.5	41.6	40.6
O	51.7	52.8	54.3
Ca	0.05	5.19	4.73
Si	0.15	0.08	0.12
Al	0.11	0.03	0.03
P	0.11	0.02	0.02
Zn	0.11	0.08	0.08
Others	0.27	0.19	0.13
Total	100.00	100.00	100.00

The porous structure of an adsorbent material is characterized by the measurement of its specific surface and its pore volume. In this context, the textural properties of BZJS1 (Best adsorbent) were examined, and hence the 77 K nitrogen adsorption-desorption isotherm onto BZJS1 is shown in Fig. 4, and the corresponding parameters are reported in Table 2. As observed, the BZJS1 had a specific area of 15.685 m²/g, a pore volume of 0.032 cm³/g and a pore diameter of 4.11 nm, showing its low porosity; this can be due to the effect of alginate that hinders or damages the creation of porosity [19].

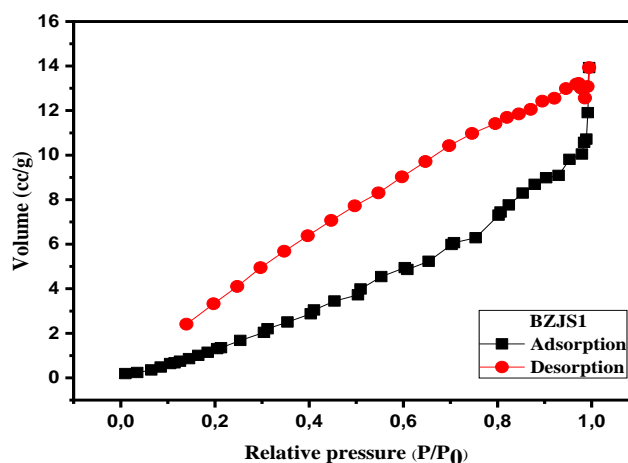


Figure 4. Nitrogen adsorption-desorption curve of the best adsorbent (BZJS1).

Table 2: Textural properties of BZJS1 from N₂ adsorption-desorption isotherm.

Material	BET surface area (m ² /g)	Totale pores volume (cm ³ /g)	Pore diameter (nm)
BZJS1	15.68	0.032	4.11

Thermogravimetric analysis was carried out for ZJS-H₃PO₄, BZJS1, and BZJS2 at temperatures ranging from 40 to 900 °C. The obtained data are shown in Fig. 5. The three samples show curves characterized by 3 stages. The first stage (from 40 °C to 230 °C for ZJS-H₃PO₄ and from 30 °C to 200 °C for BZJS) is defined by a weight loss of approximately 12%, which can be attributed to the removal of the adsorbed water and the volatile matter attached to the surface [20]; the second stage (from 230 °C to 380 °C for ZJS-H₃PO₄ and from 200 °C to 380 °C for BZJS) was due to the decomposition of the cellulosic elements [21]; the last stage (from 380 °C to the end of the analysis) corresponded to decomposition reactions of organic carbon and inorganic oxygen as well as by further degradation of the alginate [22,23]. This final phase can also be defined by the cracking of the C-H and C-O bands [24]. At the end of the analysis, we notice that

there is a weight loss of 88.74, 76.07 and 74.78, respectively, for ZJS- H_3PO_4 , BZJS1, and BZJS2, which indicates that the encapsulation may slightly increase the thermal stability.

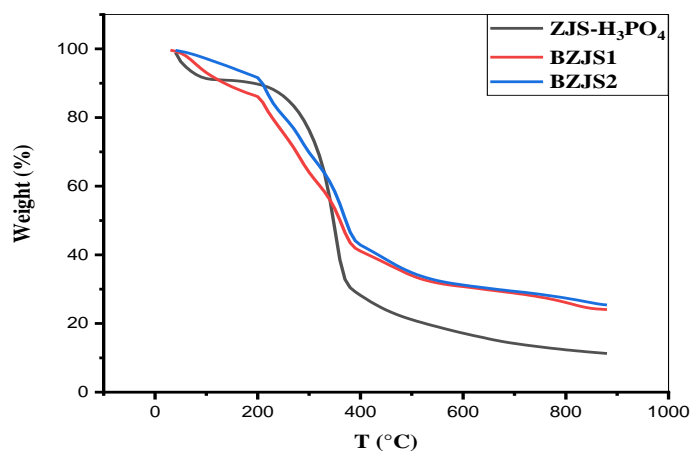


Figure 5. TG curves of ZJS- H_3PO_4 , BZJS1 and BZJS2.

Fig. 6 shows that the isoelectric points obtained were 6.8, 7.41 and 7.22 for ZJS- H_3PO_4 , BZJS1, and BZJS2, respectively, indicating that the encapsulation makes the surface character of the materials more alkaline. This finding shows that in the case where the pH of the solution is below the isoelectric point value (7.41 for BZJS1 and 7.22 for BZJS2), the BZJS surface functional groups are protonated by an excess of H^+ protons, and in the opposite case (solution pH is greater the isoelectric point value) the BZJS surface functional groups are deprotonated by the excess of OH^- ions.

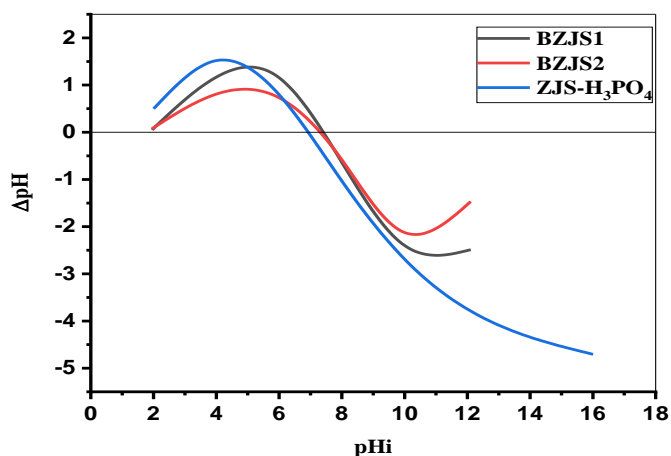


Figure 6. Isoelectric points of ZJS- H_3PO_4 , BZJS1, and BZJS2. (T=25 °C, stirring speed= 250 rpm)

3.2. Effect of encapsulation on the MB adsorption capacity

In an attempt to investigate the impact of the encapsulation process on the MB adsorption efficiency, the maximum adsorbed quantity of MB onto the ZJS-H₃PO₄, BZJS1 and BZJS2 obtained from the 25°C adsorption isotherms are shown in Fig. 7. As observed, the encapsulation strongly and positively affected the performances since the adsorbed quantity increased from 160.85 (ZJS-H₃PO₄) to 737.13 mg/g (BZJS1) and 660.12 mg/g (BZJS2), respectively.

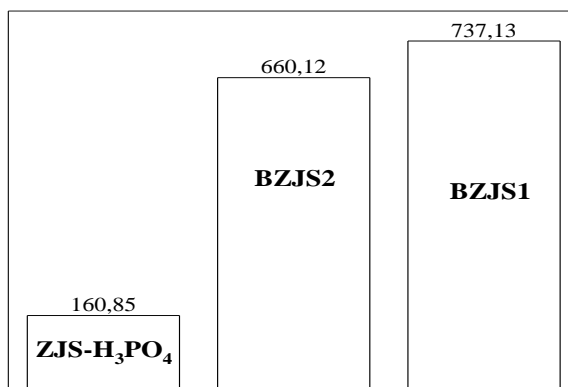


Figure 7. Encapsulation effect on the performance of the MB adsorption capacity. (T=25 °C, stirring speed= 250 rpm, pH=6.2)

2.3. MB adsorption isotherms Study

Adsorption isotherms are usually considered to establish an adsorbent-adsorbate relationship and to give insight with regards to the adsorption mode in order to achieve a pilot design [25].

The results obtained from the adsorption isotherms of MB onto BZJS1 and BZJS2 at different temperatures (10, 25, 30 and 40 °C) are illustrated in Fig. 8, showing isotherms of type L according to the GILL classification; such form of isotherm is characterized by a strong affinity between the adsorbent-adsorbate duo with a monolayer adsorption mode [26]. Moreover, the adsorbed quantities decreased from 768.10 to 627.55 mg/g for the BZJS1, and from 680.10 to 493.26 for the BZJS2 for temperatures increasing from 10 to 40 °C; these high values show the efficiency of the prepared materials for the adsorption of cationic organic pollutants.

Otherwise, the results of the modeling of experimental data for MB adsorption isotherms onto BZJS1 and BZJS2 are shown in Fig. 8, and the corresponding data are collected in Table 3. The selection of the best model is generally based on the high value of

the R^2 correlation factor, as well as the small delta between the experimentally adsorbed quantity values and that found theoretically by the considered model [27].

From Table 3, Langmuir, Sips, and Redlich Peterson's models showed high correlation coefficients for the four temperatures tested (10, 25, 30, and 40 °C); however, the Sips and Langmuir models demonstrated theoretical adsorbed amounts a little far from that found experimentally. To conclude this part, it can be assumed that the Redlich Peterson model is the most appropriate to describe the MB adsorption process onto BZJS1 and BZJS. The Redlich Peterson model can describe both mono and multilayer adsorption. However, whatever the temperature, the β coefficient of this latter model was very close to 1, showing that the Redlich Peterson model approached the Langmuir model, indicating a monolayer mode for the MB adsorption onto both materials.

Chapter V: The use of encapsulation as a proposed solution to avoid problems encountered with conventional materials in powder form: application in methylene blue removal from aqueous solutions

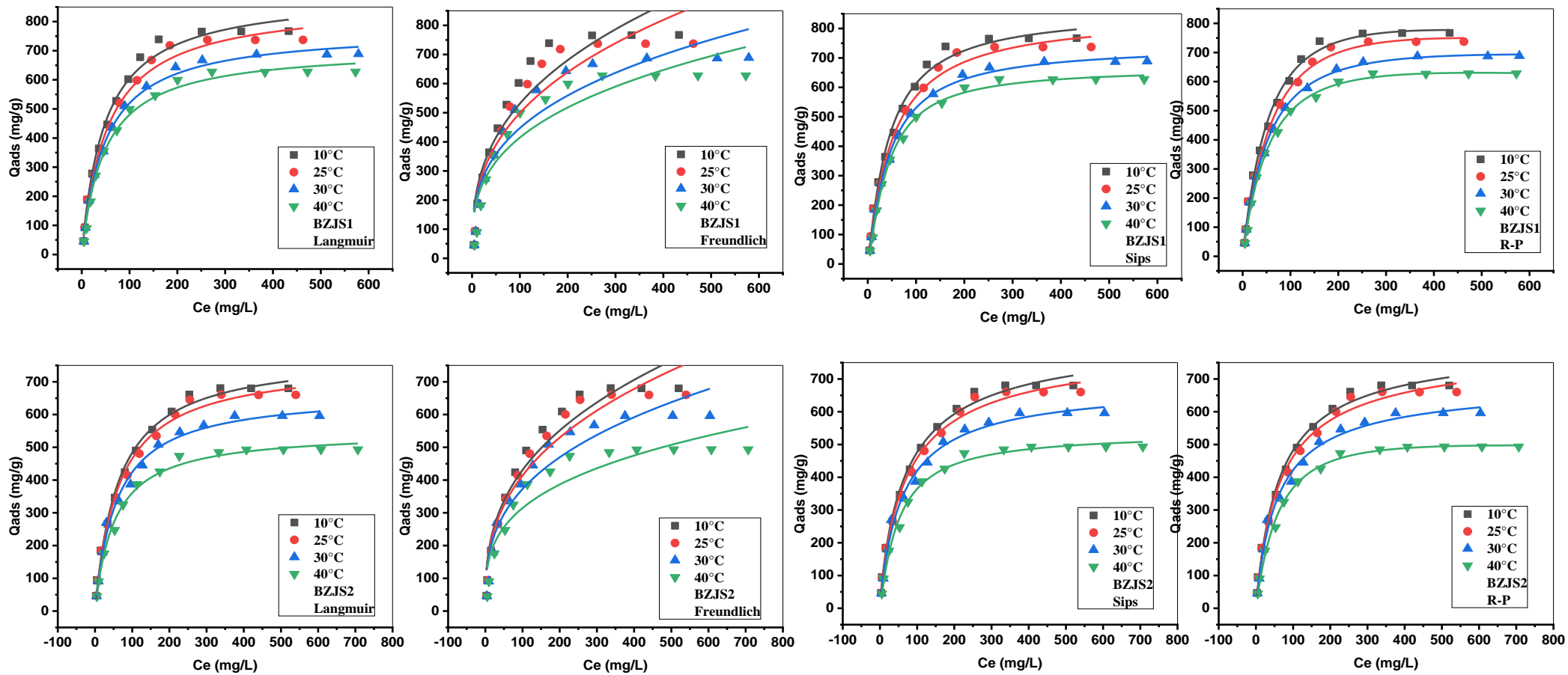


Figure 8. Experimental data (points) of MB adsorption onto BZJS1 and BZJS2. Modeling Data (lines) by Langmuir, Freundlich, Sips, and Redlich-Peterson (R-P) models at different temperatures. (stirring speed= 250 rpm, pH=6.2)

Chapter V: The use of encapsulation as a proposed solution to avoid problems encountered with conventional materials in powder form: application in methylene blue removal from aqueous solutions

Table 3: Isotherm modeling parameters of Langmuir, Freundlich, Sips and Redlich-Peterson models for MB adsorption onto BZJS1 and BZJS2 at different temperatures.

Models	Materials Parameters	BZJS1				BZJS2			
		10 °C	25 °C	30 °C	40 °C	10 °C	25 °C	30 °C	40 °C
Langmuir	Q_{exp} (mg/g)	768.102	737.126	687.266	627.551	680.098	660.120	596.124	493.258
	Q_m (mg/g)	897.416	866.694	773.612	711.251	786.868	760.919	667.623	549.604
	K_L (L/mg)	0.020	0.019	0.020	0.021	0.016	0.016	0.017	0.019
	R^2	0.989	0.987	0.994	0.9911	0.992	0.991	0.991	0.992
	n_F	2.81	2.80	3.10	3.12	2.80	2.80	2.99	3.36
Freundlich	$K_F(mg/g)(L/mg)^{1/n}$	102.59	96.24	101.36	94.65	83.32	79.97	80.10	79.93
	R^2	0.893	0.899	0.884	0.871	0.943	0.938	0.920	0.884
Sips	Q_m (mg/g)	859.91	845.78	742.59	665.82	836.71	806.	687.21	536.54
	K_S (L/mg)	0.023	0.019	0.022	0.024	0.014	0.014	0.016	0.020
	ms	1.11	1.06	1.13	1.24	0.881	0.888	0.935	1.086
	R^2	0.990	0.986	0.996	0.996	0.993	0.9914	0.991	0.992
	k_R (L/g)	14.68	12.77	13.19	11.78	13.11	12.93	12.24	8.7
Redlich-Peterson	α_R (L/ mg)	0.007	0.006	0.010	0.008	0.019	0.021	0.021	0.008
	β_R	1.136	1.138	1.091	1.123	0.980	0.968	0.978	1.091
	R^2	0.993	0.989	0.9978	0.997	0.991	0.990	0.990	0.995

2.4. MB adsorption kinetics

2.4.1. Effect of the contact time and the MB initial concentration

As observed (Fig. 9), for both materials, especially in the case of high initial concentrations, the equilibrium time was slowly achieved. Fig. 9 also shows that the adsorbed quantity increased with the initial concentration, from 45.80 to 182.59 mg/L for BZJS1 and from 45.86 to 177.88 mg/L for BZJS2 for initial concentrations increasing from 50 to 200 mg/L. It is due to the driving force that increases with the initial concentration. It can also be seen that the adsorption of MB onto both materials was characterized by three stages, fast adsorption in the first stage compared to the two others. It is due to the availability of free adsorption sites at the beginning of the experiment and occurring on the external surface of BZJS1 and BZJS2, facilitating the adsorption of MB. The second stage of slower adsorption appears when the free sites are occupied, making MB adsorption more difficult. The third stage is defined by a saturation of the available adsorption sites, which makes the MB adsorption close to impossible; this stage is illustrated graphically by the equilibrium phase.

2.4.2. Kinetics modeling

Results of MB adsorption kinetics modeling onto BZJS1 and BZJS2 are shown in Fig. 9 and Table 4. Regardless of the initial concentration, both materials showed excellent correlation factors for all three models (Table 4). Moreover, when comparing the adsorbed experimental quantities with those found theoretically by each model, it was obvious that the PFO model was the most appropriate to describe MB's adsorption kinetics onto BZJS1 and BZJS2 compared to the two other (PSO, PNO) models.

Chapter V: The use of encapsulation as a proposed solution to avoid problems encountered with conventional materials in powder form: application in methylene blue removal from aqueous solutions

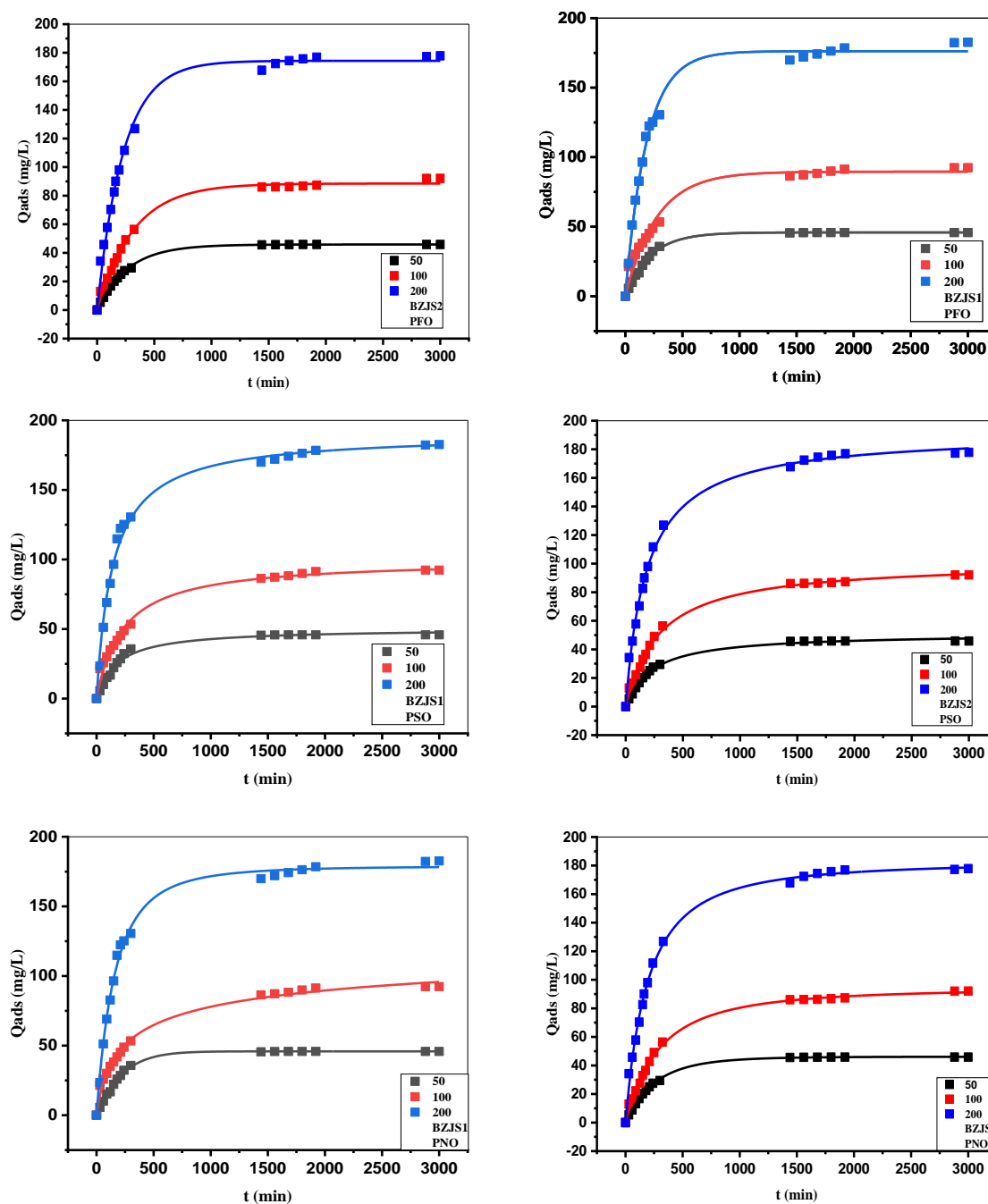


Figure 9. Kinetics data (symbol) of MB adsorption onto BZJS1 and BZJS2 and modeling data (lines) by PFO, PSO, and PNO with different initial concentrations. (T=25 °C, stirring speed= 250 rpm, pH=6.2)

Chapter V: The use of encapsulation as a proposed solution to avoid problems encountered with conventional materials in powder form: application in methylene blue removal from aqueous solutions

Table 4: kinetics modeling parameters of PFO, PSO and PNO models for MB adsorption onto BZJS1 and BZJS2.

Materials	Models	Parameters	50 mg/L	100 mg/L	200 mg/L
BZJS1	PFO	Q _{exp} (mg/g)	45.80	92.36	182.59
		Q _e (mg/g)	45.89	89.56	176.16
		K ₁ , (min ⁻¹)	0.004	0.004	0.005
		R ²	0.997	0.976	0.994
	PSO	Q _e (mg/g)	50.37	100.10	190.77
		K ₂ *10 ⁺⁴ (g/(mg*min))	1.117	0.433	0.368
		R ²	0.984	0.988	0.992
	PNO	Q _e (mg/g)	45.88	156.66	178.88
		k _n , (mg/g) ¹⁻ⁿ /min	0.006	3.471*10 ⁻¹²	9.024*10 ⁻⁴
		n	0.92	5.12	1.37
		R ²	0.997	0.992	0.995
	BZJS2	PFO	Q _{exp} (mg/g)	45.86	92.10
Q _e (mg/g)			45.83	88.49	174.37
K ₁ , (1/min)			0.004	0.003	0.004
R ²			0.999	0.996	0.994
PSO		Q _e (mg/g)	51.33	101.67	191.93
		K ₂ *10 ⁺⁴ (g/(mg*min))	0.843	0.336	0.280
		R ²	0.996	0.997	0.997
PNO		Q _e (mg/g)	46.115	94.250	182.796
		k _n , (mg/g) ¹⁻ⁿ /min	0.002	2.800*10 ⁻⁴	1.969*10 ⁻⁴
		n	1.137	1.549	1.626
		R ²	0.999	0.997	0.997

The curves of intra-particle modeling are shown in Fig. 10. Whatever the initial concentration multi-line curves were observed for both materials, meaning that MB adsorption onto BZJS1 and BZJS2 occurred in three stages. These stages can be defined as follows: the first step is the fastest one due to the diffusion of MB molecules from the boundary layer to the external surface of the adsorbent. After that, the adsorption rate decreases and the MB molecules of the external surface are transported to the internal layer of the BZJS in the second step; the third phase starts when the equilibrium is reached [28].

The data obtained by the Boyd model are shown in Fig. 11. A linear curve that passes through the zero suggests that the diffusion into the pores is the limiting step that controls the adsorption process; while a non-linear curve $\beta = f(t)$ means that the film diffusion is the limiting step that controls the process [28,29], as it is the case in this study where the curves were not linear for BZJS1 and BZJS2.

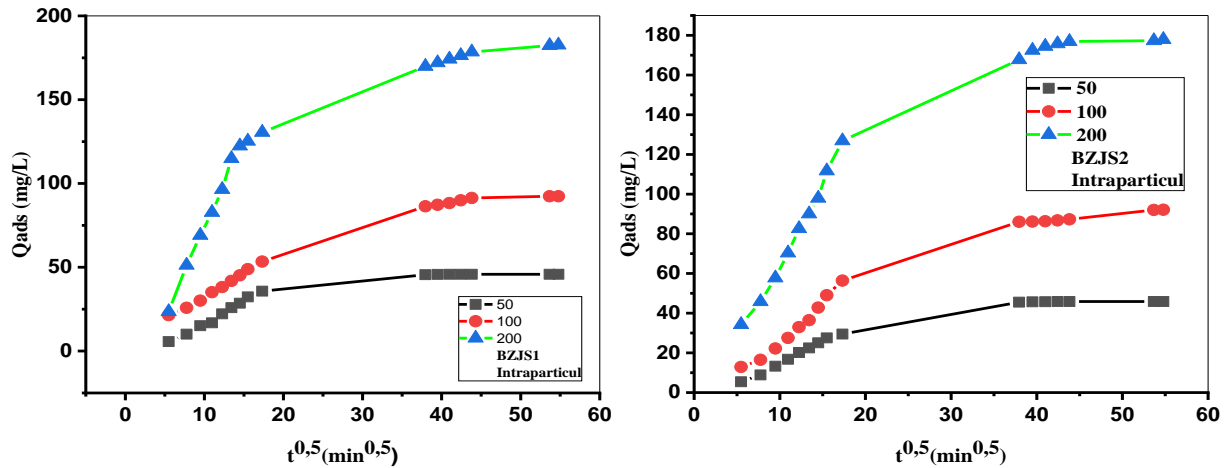


Figure 10. Intraparticle diffusion modeling of MB adsorption onto BZJS1 and BZJS2.

(T=25 °C, stirring speed= 250 rpm, pH=6.2)

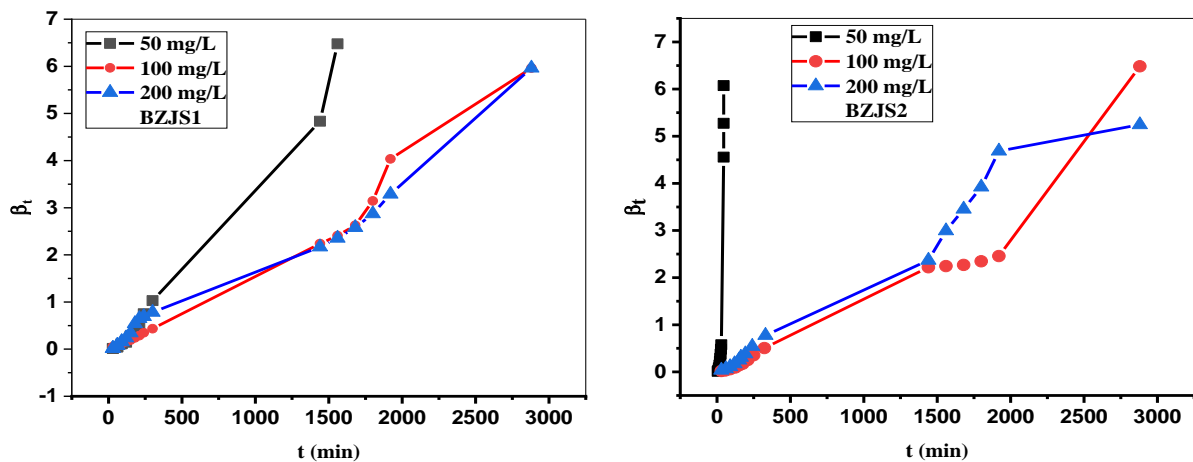


Figure 11. Boyd model data of MB adsorption onto BZJS1 and BZJS2. (T=25 °C, stirring speed= 250 rpm, pH=6.2)

2.5. Initial pH effect

It is evident from Fig. 12 that the pH had a significant impact on dye adsorption. It can be noted the efficient adsorption for pH in the range 6 to 12, while efficiency decreased at acidic pH. This can be explained by considering the pH_{pzc} values (7.4 for BZJS1 and 7.3 for BZJS2), which can be related to the cations and anions distribution on the adsorbent

surface. When the pH varies towards alkaline values, the OH^- anions become more available, facilitating the MB adsorption by electrostatic interactions, while the opposite occurs when the pH varies towards acidic pH. Fig. 12 also shows that even if the adsorbents were positively charged in the pH range between 4 and 6, there was a significant adsorbed quantity; this indicates that electrostatic interactions are not the only mode of adsorption involved in the MB adsorption onto BZJS1 and BZJS2, where the adsorption can be achieved by the contribution of sulfur, nitrogen and oxygen electrons or by the π - π interactions between the aromatic cycles of MB and those of BZJS, this interpretation has recently been assumed by our research group [21].

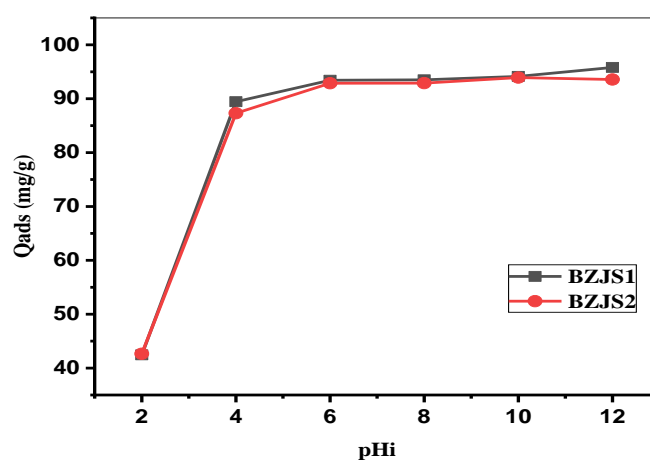


Figure 12. pH effect of MB adsorption onto BZJS1 and BZJS2. (T=25 °C, stirring speed= 250 rpm)

2.6. Ionic strength and humic acid effects

Fig. 13 shows the effect of the ionic strength and the presence of organic compounds onto BZJS1 and BZJS22 adsorption of MB. Regarding the ionic strength, the amount adsorbed strongly decreased for both materials, from 737.13 to 268.95 mg/g for BZJS1 and from 660.12 to 261.82 mg/g for BZJS2, indicating a negative impact of NaCl on the adsorption process, most likely due to the decomposition of the inorganic salt into Na^+ and Cl^- creating competitiveness between MB molecules and Na^+ cations for adsorption onto the adsorbents. A similar impact was observed in the case of humic acid, since the adsorbed quantities decreased to 375.22 and 297.48 mg/g for BZJS1 and BZJS2, respectively

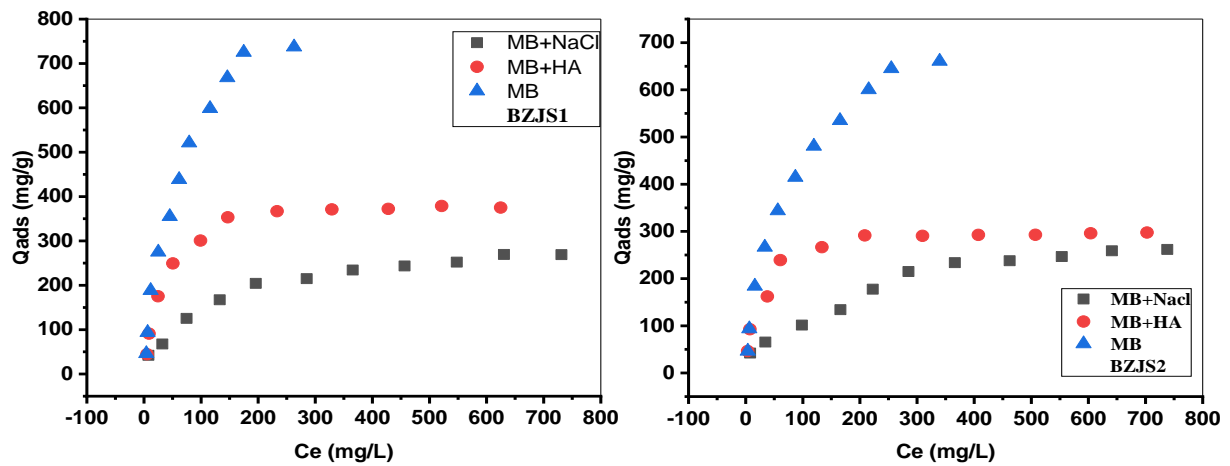


Figure 13. Ionic strength and humic acid effects on MB adsorption onto BZJS1 and BZJS2. (T=25 °C, stirring speed= 250 rpm, pH=6.2)

2.7. Regeneration study of BZJS1 and BZJS2

In view of a future implementation at industrial scale, a regeneration study of the prepared beads was performed (Fig. 14), showing a higher reusability for BZJS1 if compared to BZJS2. Indeed, its adsorption performances decreased only slightly, from 99.08% for the first cycle to 92.01% for the sixth cycle.

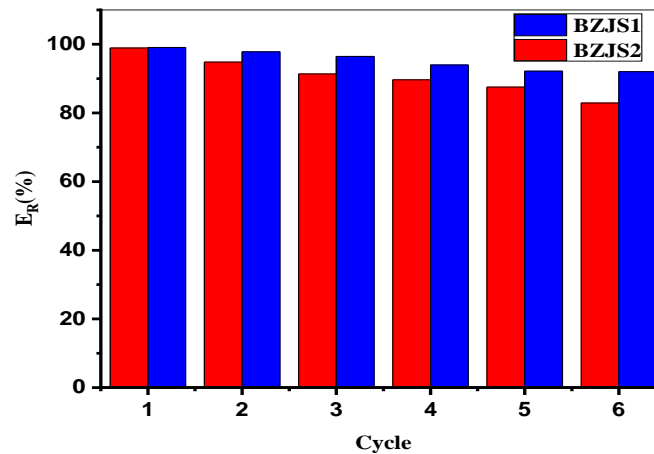


Figure 14. Regeneration study for BZJS1 and BZJS2. (T=25 °C, stirring speed= 250 rpm, pH=2)

2.8. Temperature effect on MB adsorption onto BZJS1 and BZJS2

Fig. 8 shows that the temperature had a negative impact on the adsorption of MB onto each material, indicating that the adsorption process was exothermic. Furthermore, with the help of the Q_e/C_e plot as a function of the reverse of the temperature and after the necessary calculations carried out according to Van't Hoff and Gibbs free energy

equations, the thermodynamic parameters were determined and reported in Table 5. As shown, the free Gibbs energy was negative, proving that the MB adsorption onto the prepared beads was spontaneous. Negative enthalpies suggest that the adsorption process was exothermic. In addition, on the basis of enthalpies parameters, it can be deduced that MB adsorption onto both materials was achieved in physisorption mode because the values were within the range of 0 to -20 kJ/mol [5]. Table 5 also shows the positive entropy values, which indicate that the BM molecules have a random character at the liquid-solid interface during their adsorption onto BZJS1 and BZJS2 [30].

Table 5: Thermodynamic parameters of MB adsorption onto BZJS1 and BZJS2.

Adsorbent	T(°K)	ΔG° (KJ/mol)	ΔH° (KJ/mol)	ΔS° (J/mol*K)
BZJS1	283	-17.708	-11.655	21.389
	298	-18.023		
	303	-18.136		
	313	-18.350		
BZJS2	283	-17.096	-14.813	8.065
	298	-17.217		
	303	-17.257		
	313	-17.340		

2.9. MB adsorption onto various adsorbents

In this part, a comparison of the performances of the prepared beads (BZJS1 and BZJS2) to those also considered in the available literature for the removal of methylene blue is displayed in Table 6, which summarizes the maximum adsorbent capacity of each material as well as the number of regeneration cycles with a variety of precursors and encapsulating agents. As observed, BZJS1 displays interesting performances and hence its relevance must be subsequently confirmed at a larger scale.

Table 6: MB adsorption onto various beads with different precursors.

Precursor	Encapsulating agent	Adsorbed amount	Regeneration cycle	Reference
Bentonite	Sodium alginate	2024	More than 2	[31]
Fe ₃ O ₄ particle	Chitosan	20.40	--	[32]
graphene oxide	Sodium alginate	357.14	5	[33]
Activated carbon from Mangosteen fruit peels	sodium alginate	230	--	[34]
Halloysite	Chitosan	270.27	5	[35]
Activated carbon from spent coffee grounds	sodium alginate	710.2	7	[36]
Halloysite nanotube	sodium alginate	250.0	10	[37]
Activated carbon from silk sericin	sodium alginate	502.5	5	[38]
PC@Fe ₃ O ₄ NPs	sodium alginate	49.66	--	[39]
<i>Ziziphus jujuba</i> stones (BZJS1)	Sodium alginate	737.13	6	This study
<i>Ziziphus jujuba</i> stones (BZJS2)	Sodium alginate	660.12	6	This study

3. Conclusion

In this chapter, encapsulation by sodium alginate was used as a proposed solution to avoid some problems encountered with conventional materials in powder form, such as the difficulty of regeneration. For this purpose, *Ziziphus jujuba* stones were used as a precursor. The performances of the prepared materials (BZJS1 and BZJS2) were examined in a batch system by adsorption of a cationic dye, methylene blue (MB). The results obtained confirmed that the encapsulation was efficiently carried out since the adsorption potential of the prepared beads strongly increased from 160.85 mg/g for ZJS-H₃PO₄ to 768.10 and 660.12 mg/g for BZJS1 and BZJS2 respectively at 25 °C. Furthermore, the modeling of MB adsorption isotherms showed that whatever the temperature, the Redlich Peterson model led to the most accurate fitting of experimental data. Regarding the adsorption kinetics, the nonlinear models of pseudo-first-order (PFO), pseudo-second-order (PSO), and pseudo nth order (PNO) were considered, and the PFO model was found to be the most suitable model to describe the kinetic results. In addition, the Intra particle diffusion model showed that the MB adsorption was performed in three steps, and the Boyd model suggested that film diffusion is the limiting step that controlled the MB adsorption process onto both materials. Otherwise, the effects of ionic strength and organic

compounds have shown that NaCl and humic acid had a negative impact on the adsorption of MB on both materials. The temperature effect and thermodynamic parameters showed that the adsorption of MB onto BZJS1 and BZJS1 was spontaneous and exothermic. The regeneration study concluded on the reusability of the beads since the MB removal yields were 92.01 and 82.88% for BZJS1 and BZJS2, even at the sixth cycle.

4. References

- [1] A.B. Albadarin, S. Solomon, T.A. Kurniawan, C. Mangwandi, G. Walker, Single, simultaneous and consecutive biosorption of Cr(VI) and Orange II onto chemically modified masau stones, *J. Environ. Manage.* 204 (2017) 365–374. <https://doi.org/10.1016/j.jenvman.2017.08.042>.
- [2] L. Zhao, J.-P. Basly, M. Baudu, Macroporous alginate/ferrhydrite hybrid beads used to remove anionic dye in batch and fixed-bed reactors, *J. Taiwan Inst. Chem. Eng.* 74 (2017) 129–135. <https://doi.org/10.1016/j.jtice.2017.02.006>.
- [3] F. Ogata, T. Nakamura, N. Kawasaki, Adsorption capability of virgin and calcined wheat bran for molybdenum present in aqueous solution and elucidating the adsorption mechanism by adsorption isotherms, kinetics, and regeneration, *J. Environ. Chem. Eng.* 6 (2018) 4459–4466. <https://doi.org/10.1016/j.jece.2018.06.047>.
- [4] Z. Noorimotlagh, S.A. Mirzaee, S.S. Martinez, S. Alavi, M. Ahmadi, N. Jaafarzadeh, Adsorption of textile dye in activated carbons prepared from DVD and CD wastes modified with multi-wall carbon nanotubes: Equilibrium isotherms, kinetics and thermodynamic study, *Chem. Eng. Res. Des.* 141 (2019) 290–301. <https://doi.org/10.1016/j.cherd.2018.11.007>.
- [5] I. Chaari, E. Fakhfakh, M. Medhioub, F. Jamoussi, Comparative study on adsorption of cationic and anionic dyes by smectite rich natural clays, *J. Mol. Struct.* 1179 (2019) 672–677. <https://doi.org/10.1016/j.molstruc.2018.11.039>.
- [6] C.E. de F. Silva, B.M.V. da Gama, A.H. da S. Gonçalves, J.A. Medeiros, A.K. de S. Abud, Basic-dye adsorption in albedo residue: Effect of pH, contact time, temperature, dye concentration, biomass dosage, rotation and ionic strength, *J. King Saud Univ. - Eng. Sci.* (2019) S1018363918304501. <https://doi.org/10.1016/j.jksues.2019.04.006>.
- [7] M.A. Dominguez, M. Etcheverry, G.P. Zanini, Evaluation of the adsorption kinetics of brilliant green dye onto a montmorillonite/alginate composite beads by the

- shrinking core model, Adsorption. 25 (2019) 1387–1396. <https://doi.org/10.1007/s10450-019-00101-w>.
- [8] S. Biswas, T.K. Sen, A.M. Yeneneh, B.C. Meikap, Synthesis and characterization of a novel Ca-alginate-biochar composite as efficient zinc (Zn^{2+}) adsorbent: Thermodynamics, process design, mass transfer and isotherm modeling, Sep. Sci. Technol. 54 (2019) 1106–1124. <https://doi.org/10.1080/01496395.2018.1527353>.
- [9] S. Dandil, D. Akin Sahbaz, C. Acikgoz, Adsorption of Cu(II) ions onto crosslinked chitosan/Waste Active Sludge Char (WASC) beads: Kinetic, equilibrium, and thermodynamic study, Int. J. Biol. Macromol. 136 (2019) 668–675. <https://doi.org/10.1016/j.ijbiomac.2019.06.063>.
- [10] T.T.N. Le, V.T. Le, M.U. Dao, Q.V. Nguyen, T.T. Vu, M.H. Nguyen, D.L. Tran, H.S. Le, Preparation of magnetic graphene oxide/chitosan composite beads for effective removal of heavy metals and dyes from aqueous solutions, Chem. Eng. Commun. 206 (2019) 1337–1352. <https://doi.org/10.1080/00986445.2018.1558215>.
- [11] Y. Pan, H. Xie, H. Liu, P. Cai, H. Xiao, Novel cellulose/montmorillonite mesoporous composite beads for dye removal in single and binary systems, Bioresour. Technol. 286 (2019) 121366. <https://doi.org/10.1016/j.biortech.2019.121366>.
- [12] H. Xie, Y. Pan, H. Xiao, H. Liu, Preparation and characterization of amphoteric cellulose–montmorillonite composite beads with a controllable porous structure, J. Appl. Polym. Sci. 136 (2019) 47941. <https://doi.org/10.1002/app.47941>.
- [13] J. Kurczewska, M. Cegłowski, G. Schroeder, Alginate/PAMAM dendrimer – Halloysite beads for removal of cationic and anionic dyes, Int. J. Biol. Macromol. 123 (2019) 398–408. <https://doi.org/10.1016/j.ijbiomac.2018.11.119>.
- [14] N. Fiol, J. Poch, I. Villaescusa, Grape Stalks Wastes Encapsulated in Calcium Alginate Beads for Cr(VI) Removal from Aqueous Solutions, Sep. Sci. Technol. 40 (2005) 1013–1028. <https://doi.org/10.1081/SS-200048041>.
- [15] P. Tiwari, Adsorption of Pb (II), Cu (II), and Zn (II) Ions onto Urtica dioica Leaves (UDL) as a Low Cost Adsorbent: Equilibrium and Thermodynamic Studies, Mod. Chem. 5 (2017) 11. <https://doi.org/10.11648/j.mc.20170501.13>.
- [16] M.A. Nahil, P.T. Williams, Pore characteristics of activated carbons from the phosphoric acid chemical activation of cotton stalks, Biomass Bioenergy. 37 (2012) 142–149. <https://doi.org/10.1016/j.biombioe.2011.12.019>.

- [17] M.A. Khan, S.M. Wabaidur, M.R. Siddiqui, A.A. Alqadami, A.H. Khan, Silico-manganese fumes waste encapsulated cryogenic alginate beads for aqueous environment de-colorization, *J. Clean. Prod.* 244 (2020) 118867. <https://doi.org/10.1016/j.jclepro.2019.118867>.
- [18] S. Marković, A. Stanković, Z. Lopičić, S. Lazarević, M. Stojanović, D. Uskoković, Application of raw peach shell particles for removal of methylene blue, *J. Environ. Chem. Eng.* 3 (2015) 716–724. <https://doi.org/10.1016/j.jece.2015.04.002>.
- [19] A. Oussalah, A. Boukerroui, A. Aichour, B. Djellouli, Cationic and anionic dyes removal by low-cost hybrid alginate/natural bentonite composite beads: Adsorption and reusability studies, *Int. J. Biol. Macromol.* 124 (2019) 854–862. <https://doi.org/10.1016/j.ijbiomac.2018.11.197>.
- [20] A. Nasrullah, B. Saad, A.H. Bhat, A.S. Khan, M. Danish, M.H. Isa, A. Naem, Mangosteen peel waste as a sustainable precursor for high surface area mesoporous activated carbon: Characterization and application for methylene blue removal, *J. Clean. Prod.* 211 (2019) 1190–1200. <https://doi.org/10.1016/j.jclepro.2018.11.094>.
- [21] A. Guediri, A. Bouguettoucha, D. Chebli, N. Chafai, A. Amrane, Molecular dynamic simulation and DFT computational studies on the adsorption performances of methylene blue in aqueous solutions by orange peel-modified phosphoric acid, *J. Mol. Struct.* (2019) 127290. <https://doi.org/10.1016/j.molstruc.2019.127290>.
- [22] N. Belhouchat, H. Zaghouane-Boudiaf, C. Viseras, Removal of anionic and cationic dyes from aqueous solution with activated organo-bentonite/sodium alginate encapsulated beads, *Appl. Clay Sci.* 135 (2017) 9–15. <https://doi.org/10.1016/j.clay.2016.08.031>.
- [23] M. Lezehari, J.-P. Basly, M. Baudu, O. Bouras, Alginate encapsulated pillared clays: removal of a neutral/anionic biocide (pentachlorophenol) and a cationic dye (safranine) from aqueous solutions, *Colloids Surf. Physicochem. Eng. Asp.* 366 (2010) 88–94. <https://doi.org/10.1016/j.colsurfa.2010.05.021>.
- [24] R. Ahmad, R. Kumar, Synthesis and Properties of Cellulose Carbon Encapsulated ZnO for Dye Removal, *J. Dispers. Sci. Technol.* 32 (2011) 737–740. <https://doi.org/10.1080/01932691.2010.480869>.
- [25] O. Moradi, M. Aghaie, K. Zare, M. Monajjemi, H. Aghaie, The study of adsorption characteristics Cu²⁺ and Pb²⁺ ions onto PHEMA and P(MMA-HEMA) surfaces

- from aqueous single solution, *J. Hazard. Mater.* 170 (2009) 673–679. <https://doi.org/10.1016/j.jhazmat.2009.05.012>.
- [26] A. Gil, L. Santamaría, S.A. Korili, Removal of Caffeine and Diclofenac from Aqueous Solution by Adsorption on Multiwalled Carbon Nanotubes, *Colloid Interface Sci. Commun.* 22 (2018) 25–28. <https://doi.org/10.1016/j.colcom.2017.11.007>.
- [27] J.V. Milojković, Z.R. Lopičić, I.P. Anastopoulos, J.T. Petrović, S.Z. Milićević, M.S. Petrović, M.D. Stojanović, Performance of aquatic weed - Waste *Myriophyllum spicatum* immobilized in alginate beads for the removal of Pb(II), *J. Environ. Manage.* 232 (2019) 97–109. <https://doi.org/10.1016/j.jenvman.2018.10.075>.
- [28] S. Li, Z. Zeng, W. Xue, Adsorption of lead ion from aqueous solution by modified walnut shell: kinetics and thermodynamics, *Environ. Technol.* 40 (2019) 1810–1820. <https://doi.org/10.1080/09593330.2018.1430172>.
- [29] W.J. Weber, J.C. Morris, Kinetics of Adsorption on Carbon from Solution, *J. Sanit. Eng. Div.* 89 (1963) 31–60.
- [30] Z. Harrache, M. Abbas, T. Aksil, M. Trari, Thermodynamic and kinetics studies on adsorption of Indigo Carmine from aqueous solution by activated carbon, *Microchem. J.* 144 (2019) 180–189. <https://doi.org/10.1016/j.microc.2018.09.004>.
- [31] Ravi, L.M. Pandey, Enhanced adsorption capacity of designed bentonite and alginate beads for the effective removal of methylene blue, *Appl. Clay Sci.* 169 (2019) 102–111. <https://doi.org/10.1016/j.clay.2018.12.019>.
- [32] Rahmi, Ishmaturrehmi, I. Mustafa, Methylene blue removal from water using H₂SO₄ crosslinked magnetic chitosan nanocomposite beads, *Microchem. J.* 144 (2019) 397–402. <https://doi.org/10.1016/j.microc.2018.09.032>.
- [33] X. Liu, B. Cui, S. Liu, Q. Ma, Methylene Blue Removal by Graphene Oxide/Alginate Gel Beads, *Fibers Polym.* 20 (2019) 1666–1672. <https://doi.org/10.1007/s12221-019-9011-z>.
- [34] A. Nasrullah, A.H. Bhat, A. Naeem, M.H. Isa, M. Danish, High surface area mesoporous activated carbon-alginate beads for efficient removal of methylene blue, *Int. J. Biol. Macromol.* 107 (2018) 1792–1799. <https://doi.org/10.1016/j.ijbiomac.2017.10.045>.

- [35] Q. Peng, M. Liu, J. Zheng, C. Zhou, Adsorption of dyes in aqueous solutions by chitosan–halloysite nanotubes composite hydrogel beads, *Microporous Mesoporous Mater.* 201 (2015) 190–201. <https://doi.org/10.1016/j.micromeso.2014.09.003>.
- [36] K.W. Jung, B.H. Choi, M.J. Hwang, T.U. Jeong, K.H. Ahn, Fabrication of granular activated carbons derived from spent coffee grounds by entrapment in calcium alginate beads for adsorption of acid orange 7 and methylene blue, *Bioresour. Technol.* 219 (2016) 185–195. <https://doi.org/10.1016/j.biortech.2016.07.098>.
- [37] L. Liu, Y. Wan, Y. Xie, R. Zhai, B. Zhang, J. Liu, The removal of dye from aqueous solution using alginate-halloysite nanotube beads, *Chem. Eng. J.* 187 (2012) 210–216. <https://doi.org/10.1016/j.cej.2012.01.136>.
- [38] H.W. Kwak, Y. Hong, M.E. Lee, H.J. Jin, Sericin-derived activated carbon-loaded alginate bead: An effective and recyclable natural polymer-based adsorbent for methylene blue removal, *Int. J. Biol. Macromol.* 120 (2018) 906–914. <https://doi.org/10.1016/j.ijbiomac.2018.08.116>.
- [39] Z. Anfar, A. Amedlous, A.A. El Fakir, M. Zbair, H. Ait Ahsaine, A. Jada, N. El Alem, High extent mass recovery of alginate hydrogel beads network based on immobilized bio-sourced porous carbon@Fe₃O₄-NPs for organic pollutants uptake, *Chemosphere.* 236 (2019) 124351. <https://doi.org/10.1016/j.chemosphere.2019.124351>.

Chapter VI: Statistical physics modeling and thermodynamic studies for methylene blue adsorption mechanism onto an eco-friendly composite adsorbent

1. Introduction

The textile, pharmaceutical, paper, cosmetics, plastics industries produce vast amounts of effluent, containing a variety of products [1]. Even in low concentrations, these latter can be harmful to human health and the environment, especially if they are not biodegradable [2]. Moreover, some estimates suggest that over 10,000 tons of dye and coloring are used each year, with 40,000 tons of dye released into the environment each year [3]. In this context, membrane filtration [4], oxidation [5], coagulation [6], photocatalysis [7], and other biological processes have been used to decolorize these waters; however, these techniques show some drawbacks in their weak performance, in their high cost and their high secondary pollution [8]. As a consequence, adsorption remains the most used method because of its simplicity, efficiency, and low cost [9]. The synthetic cationic methylene blue (MB) dye was chosen as a test molecule in this study because of its wide range of applications, stability, high solubility (40g/L), non-biodegradability at concentrations greater than 5 mg/L, and danger in the event of accumulation in human and animal organs, where it can reduce the concentration of oxygen in the water and also affect the photosynthetic activity of plants.

According to the literature, a variety of products have been used as an adsorbent, including activated carbon [10], zeolites [11], clays [12], silica [13], and agricultural wastes [14] with the advantages and disadvantages of each other. Therefore, in this chapter, the preparation of adsorbent materials was performed using orange peels wastes as a precursor; these peels were chemically treated with phosphoric acid and then encapsulated using sodium alginate in various ratios. It is important to point out that the encapsulation was used for a variety of purposes, including obtaining a durable material with a uniform shape, improving adsorption efficiency, providing a material separable from the solution and thermally stable, approximating to an industrial application, and finally facilitating the regeneration step [15]. In addition, alginate was used as an encapsulating agent due to the negative charge of its carboxyl groups [16], which promotes the adsorption of cationic compounds.

The prepared materials were characterized using several techniques, including FTIR, XRF, SEM, TGA, and the isoelectric point. Adsorption kinetics were analyzed and fitted using the pseudo-first-order (PFO), pseudo-second-order (PSO), pseudo-nth-order (PNO), Intraparticle, and Boyd models. Furthermore, because of their simplicity and applicability [2], the two classical models of Langmuir and Freundlich were considered to analyze the obtained results from MB adsorption isotherms in order to obtain a simple interpretation for the interaction mechanism nature between MB and the prepared beads; moreover, these last two models were unsatisfactory for this aim because they cannot provide a physicochemical interpretation of the adsorption mechanism [17,18]. As a consequence of these findings, the grand canonical partition function in statistical physics was used to provide a more detailed and precise interpretation of the adsorption process [19], which can be seen from the information that was provided by the parameters obtained from the statistical physical models, such as the density of the receptor sites (N_s), the number of molecules captured by the adsorbent receptor site (n_{im}), the half-saturation concentration, adsorption energy and adsorbed amount at saturation (Q_{sat}) ... etc. In this line of thought, three statistical physical models were used such as, monolayer with single energy (MMSE), monolayer with two energies (MMTE), and double layer with two energies (DMTE). These models were considered to describe the experimental results of MB adsorption isotherms on the beads prepared at various temperatures (10, 25 and 30 °C). Moreover, the most accurate statistical physic model parameters were used to calculate, plot and evaluate the variation of internal energy, Gibbs free enthalpy, and configuration entropy to perform a thermodynamic study for MB adsorption mechanism on the prepared beads (BOP1 and BOP2).

2. Results and discussion

2.1. Material characterization

Fig. 1 depicts the isoelectric points of OP-H₃PO₄, BOP1, and BOP2. These results indicate that after encapsulation, the isoelectric point was shifted to an alkaline pH and that BOP1 had a more acidic character than BOP2, where pH_{pzc} values were 3.3, 5.4, and 6.9 for OP-H₃PO₄, BOP1, and BOP2, respectively. The micromorphology of OP-H₃PO₄, BOP1, and BOP2 is seen in Fig. 2. It is apparent that the prepared beads have a spherical shape with slight deformations that can be developed during the drying step; these images

also show a heterogeneous dispersion of the components and a porous structure, which facilitates and promotes dyes adsorption [20].

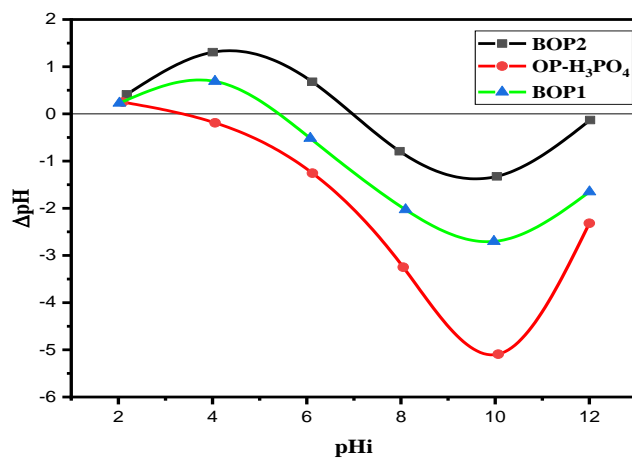


Figure 1. Isoelectric points of OP-H₃PO₄, BOP1 and BOP2.

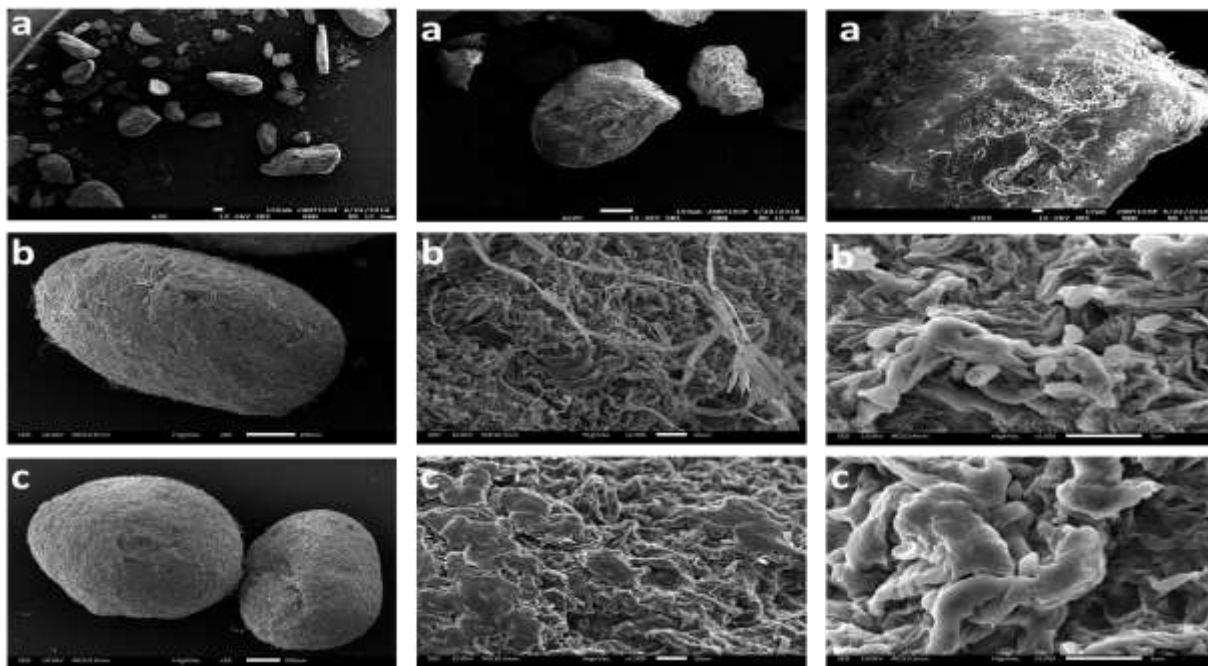


Figure 2. SEM images of OP-H₃PO₄ (a), BOP1 (b) and BOP2 (c).

The infrared spectra of raw orange peels (ROP), treated (OP-H₃PO₄), and encapsulated (BOP1 and BOP2) are shown in Fig. 3. It is evident from these spectra that after acid treatment and encapsulation, some changes occurred; the intensity of some peaks increased, others decreased, and some peaks disappeared. Otherwise, the observed similar peaks are collected in Table 1. The comparison between ROP and OP-H₃PO₄ spectra led to conclude that phosphoric acid had chemically well modified the structure of ROP. Moreover, the spectra of BOP1 and BOP2 showed very similar peaks with small peaks at

1019, 1045, and 1097 cm^{-1} , which can be attributed to the vibration modes of C–O, C–O–H, and C–C on the alginate carbohydrate rings [21].

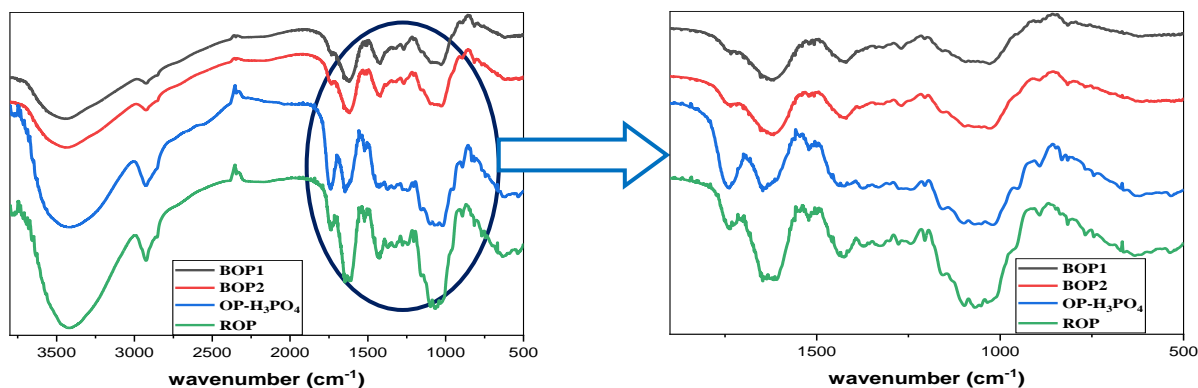


Figure 3. Infrared spectra for ROP, OP-H₃PO₄, BOP1 and BOP2.

Table1: Observed similar peaks from FTIR analysis of ROP, OP-H₃PO₄, BOP1 and BOP2.

Suggested attribution	ROP	OP-H ₃ PO ₄	BOP1	BOP2
C-O-C stretching [22]	1020	1013	1020	1020
Cellulosic compounds [23]	1065	1046	1030	1030
C=C of the aromatic rings [24]	1432	1430	1422	1432
C=C and symmetric COO ⁻	1632	1638	1620	1620
-CH _{Alph}	2922	2922	2922	2922
-O-H, NH and COOH	3433	3433	3433	3433

Wavenumber (cm^{-1})

Thermogravimetric analysis of ROP, OP-H₃PO₄, BOP1, and BOP2 was carried out at temperatures ranging from 30 to 780 °C; the obtained curves are shown in Fig. 4. These findings show that the loss of water molecules and the degradation of volatile substances [25] occurred between 30 and 200 °C for BOP and between 30 and 230 °C for ROP and OP-H₃PO₄; the four materials showed, therefore, thermal stability in these first stages, with mass losses of about 10% for OP-H₃PO₄, BOP, and 16% for ROP. Otherwise, the second stage was characterized by an intense mass loss phase between 200 and 400 °C, which may be attributed to the degradation of cellulose [23] on the one hand, and the alginate degradation by breaking its skeleton [26,27] on the other hand. Finally, the last stage was observed between 400 °C and the end of the analysis, characterized by the C-O and C-H

bands cracking or by the transformation of the carbonaceous material formed in the previous phases [27,28]. Furthermore, the TGA curves show that the degradation of BOP was less strong compared to ROP and OP-H₃PO₄, indicating that the sodium alginate had improved the thermal stability of treated orange peels, and the mass losses were 90.45, 75.91, 74.19, and 74.28 for ROP, OP-H₃PO₄, BOP1, and BOP2 respectively.

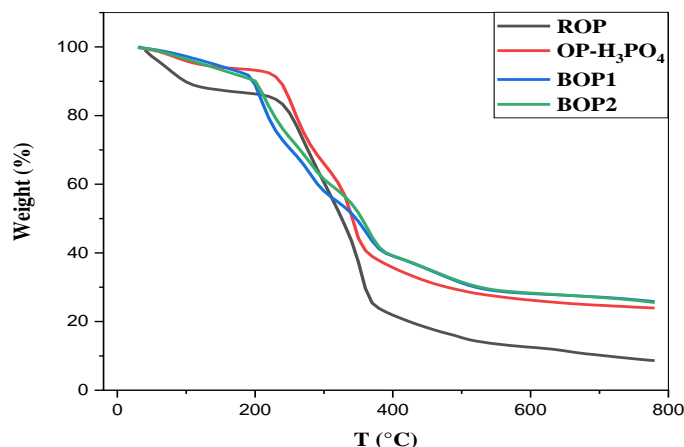


Figure 4. Thermogravimetric analysis of ROP, OP-H₃PO₄, BOP 1 and BOP2.

Table 2 shows the results of the XRF analysis of the ROP, OP-H₃PO₄, BOP1, and BOP2, with the major compounds listed in percentages. A quick comparison of the phosphorus percentage shows that it was raised after chemical treatment, which can be attributed to the incorporation of H₃PO₄ in the ROP structure. Otherwise, the presence of chlorine and calcium in the BOP composition confirmed that sodium alginate encapsulation was efficient.

Table 2: XRF analysis of ROP, OP-H₃PO₄, BOP1 and BOP2.

Element (%)	ROP	OP-H ₃ PO ₄	BOP1	BOP2
C	48.7	46.5	38.7	40.6
O	50.4	52.7	54.7	54.3
Al	0.046	0.096	0.028	0.036
Si	0.041	0.121	0.044	0.040
P	0.031	0.063	0.007	0.010
Cl	--	--	0.040	0.033
Ca	0.347	0.048	6.22	4.73
Zn	0.038	0.029	0.062	0.071
Others	0.397	0.443	0.199	0.180

2.2. Adsorption isotherm

In an adsorption phenomenon, the equilibrium data can be represented as a curve called the adsorption isotherm which can define the adsorbent-dye relationship to provide information on the nature of the adsorption process [29]. Furthermore, Fig. 5 illustrates the adsorption isotherms of MB on BOP at varying temperatures. These findings indicate that as the temperature rises, characterizing the exothermicity of the adsorption process, the adsorption potential of MB on BOP decreases. In addition, for the temperatures 10, 25, and 30 °C, the adsorption amounts were 765.82, 612.58, and 508.90 mg/g for BOP1 and 677.30, 523.51, and 400.14 mg/g for BOP2. Consequently, both materials had good performances. The results obtained from the modeling of adsorption isotherms by applying the Langmuir and Freundlich models are shown in Fig. 6, and the constants of each model are collected in Table 3. It is clear that the Freundlich model was not appropriate to describe our experimental results. The constants obtained show good determining factors regarding the Langmuir model, but the calculated quantities were a little far from those found experimentally. As a result, both classical models were not appropriate for describing the experimental results, so statistical modeling by using some physical models appears relevant.

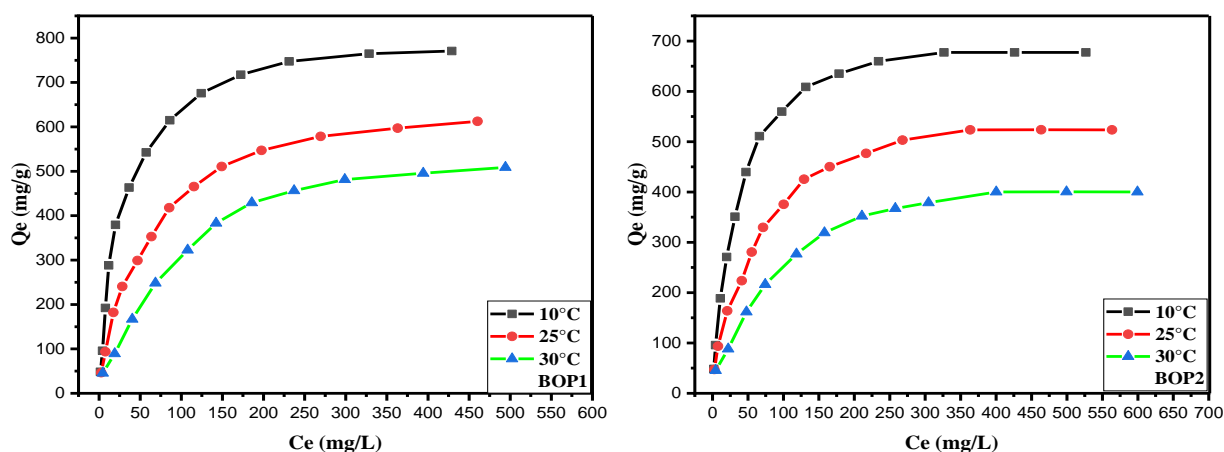


Figure 5. MB adsorption isotherms on BOP at varying temperatures

Chapter VI: Statistical physics modeling and thermodynamic studies for methylene blue adsorption mechanism onto an eco-friendly composite adsorbent

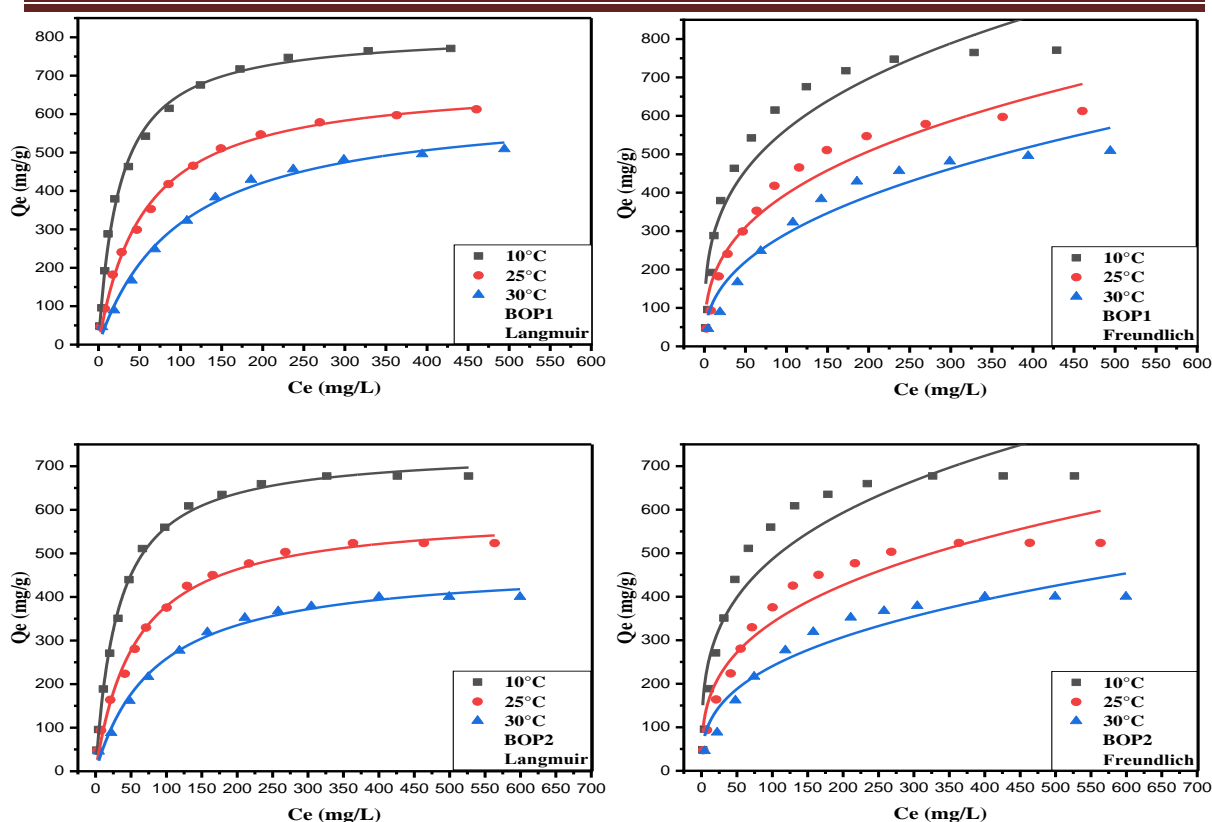


Figure 6. Langmuir and Freundlich modeling for MB adsorption isotherms onto BOP1 and BOP2 at various temperatures.

Table 3: Langmuir and Freundlich modeling's parameters for MB adsorption on BOP at various temperatures

Materials	Models	Parameters	10 °C	25 °C	30 °C
BOP1	Langmuir	Q_{exp} (mg/g)	765.82	612.58	508.90
		Q_m (mg/g)	816.76	690.54	633.18
		K_L (L/mg)	0.039	0.018	0.009
		R^2	0.996	0.997	0.993
	Freundlich	n_F	3.28	2.81	2.41
		K_F (mg/g)(L/mg) ^{1/n}	138.93	76.89	43.40
		R^2	0.899	0.928	0.928
		BOP2	Langmuir	Q_{exp} (mg/g)	677.30
Q_m (mg/g)	739.27			596.39	476.74
K_L (L/mg)	0.031			0.017	0.012
R^2	0.997			0.993	0.992
Freundlich	n_F		3.48	3.08	2.82
	K_F (mg/g)(L/mg) ^{1/n}		129.64	76.24	46.93
	R^2		0.899	0.928	0.928

2.3. Adsorption kinetics

2.3.1. Initial concentration and time effects

The effect of time and initial concentration of MB adsorption on BOP was performed and the results are shown in Fig. 7. As observed, MB adsorption kinetics on both materials (BOP1 and BOP2) was characterized by three stages, (1) a fast phase, (2) a second slower phase, and (3) an equilibrium phase, which may be explained by the availability of active sites at the beginning of adsorption, followed by a progressive reduction in the number of free sites till saturation [30]. Furthermore, the quantity of MB adsorbed rises as the initial concentration rises, which could be related to the driving force [31]. The amounts adsorbed at equilibrium were 45.94, 91.62, and 182.05 for BOP1 and 46.21, 91.44 and 181.14 for BOP2 for 50, 100, and 200 mg/L MB, respectively.

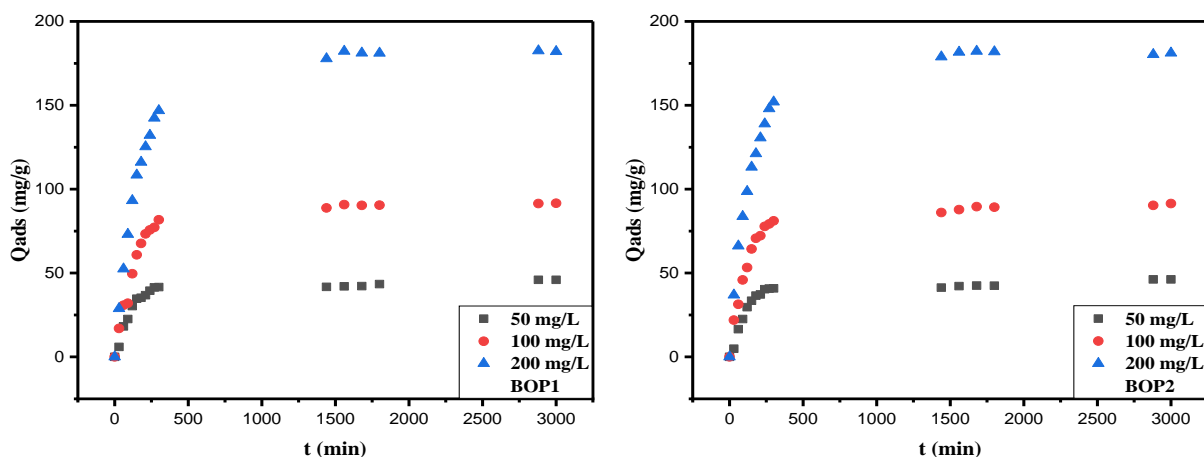


Figure 7. Time and initial concentration effects for MB adsorption on BOP1 and BOP2.

Therefore, these kinetics results were modeled using PFO, PSO, and PNO models and the curves obtained are shown in Fig. 8, and the corresponding constants are summarized in Table 4. As is well known, the best-model selection is based on a variety of criteria, citing, for example, the factor of determination R^2 (the model is more suitable if R^2 is more close to 1), the gap between the experimental and model-calculated adsorbed quantities, as well as the error function's calculated values (the model is more suitable if F error is more close to 0). As a result, all used models demonstrate that the adsorbed quantities were similar to those found experimentally regardless of the initial concentrations. Moreover, Table 4 shows on the one hand that the two models, PFO and PNO, presented rather good determination factors and low F error values compared to the PSO model (the F error values of PFO were almost the same for PNO); on the other hand, the PNO model

provided parameter values “n” that were very near to 1. So, it can be assumed that the PFO model was the most relevant to describe experimental data.

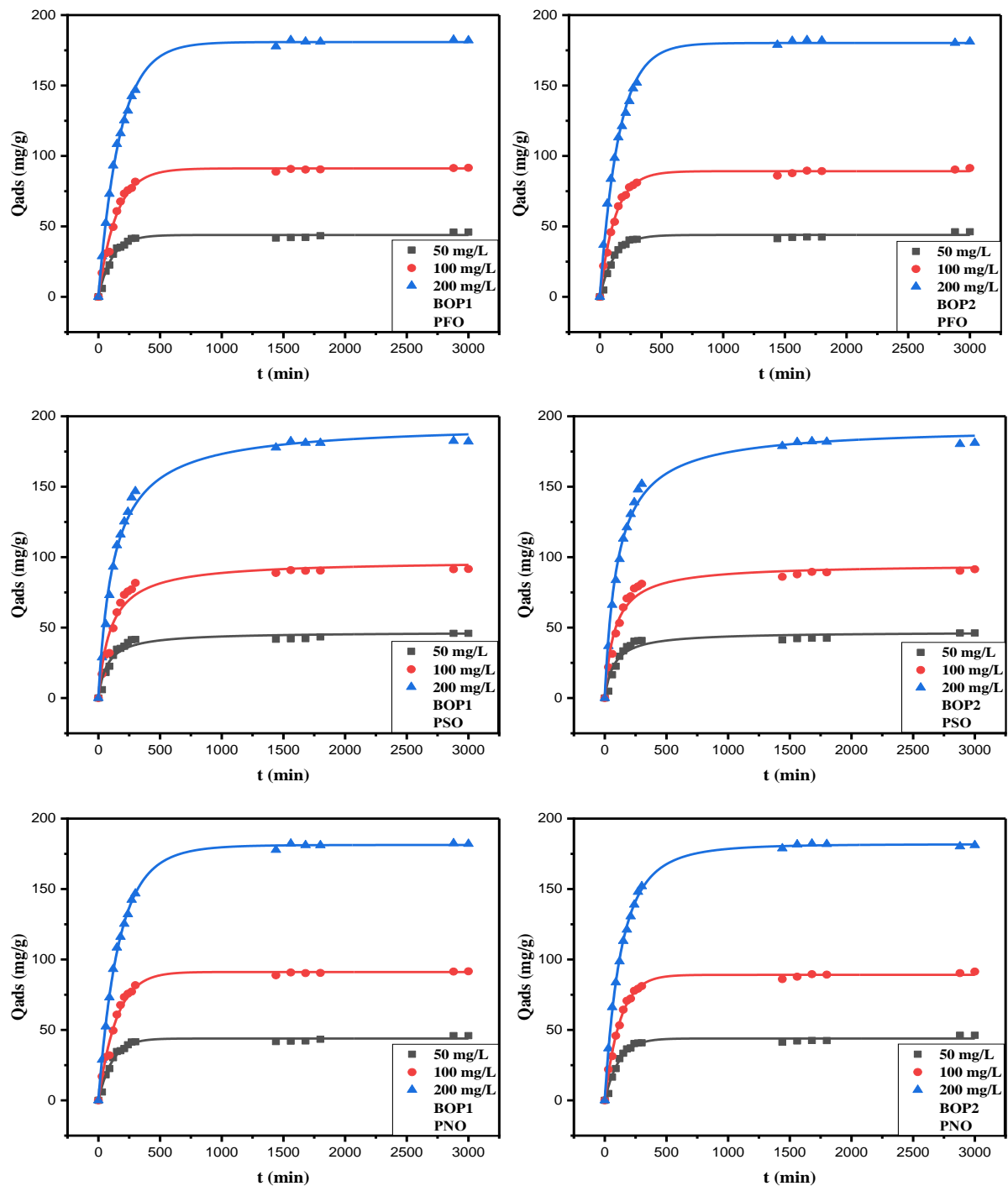


Figure 8. PFO, PSO and PNO modeling curves for MB adsorption onto BOP1 and BOP2 at different initial concentrations.

Table 4: PFO, PSO, PNO and intraparticle modeling's parameters for MB adsorption onto BOP1 and BOP2.

Materials	Models	Parameters	C ₀ (mg/L)		
			50	100	150
BOP1	PFO	Q _{exp.} (mg g ⁻¹)	45.94	91.62	182.04
		Q _{ecal.} (mg g ⁻¹)	43.92	91.18	180.86
		K ₁ (min ⁻¹)	0.009	0.007	0.006
		R ²	0.982	0.989	0.999
		F error	0.0109	0.0012	0.0016
	PSO	Q _{ecal.} (mg g ⁻¹)	46.86	97.67	195.04
		K ₂ *10 ⁴ (gm g ⁻¹ min ⁻¹)	2.95	1.02	0.14
		R ²	0.943	0.960	0.990
		F error	0.0112	0.0165	0.0178
	PNO	Q _{ecal.} (mg g ⁻¹)	43.89	91.12	181.28
		k _n (min ⁻¹) (mg g ⁻¹) ¹⁻ⁿ	0.010	0.008	0.003
		n	0.962	0.950	1.102
		R ²	0.984	0.990	0.999
	Intraparticle (First step)	F error	0.0111	0.0013	0.001
		K _{id} (mg g ⁻¹ min ^{-0.5})	4.17	6.42	10.64
		I (mg g ⁻¹)	- 15.99	- 18.98	-27.60
	Intraparticle (Second step)	R ²	0.98827	0.996	0.991
		K _{id} (mg g ⁻¹ min ^{-0.5})	2.12	2.02	1.62
I (mg g ⁻¹)		6.50	44.08	117.13	
BOP2	PFO	R ²	0.987	0.991	0.958
		Q _{exp.} (mg g ⁻¹)	46.21	91.44	181.14
		Q _{ecal.} (mg g ⁻¹)	43.95	89.21	180.18
		K ₁ (min ⁻¹)	0.009	0.008	0.006
		R ²	0.984	0.996	0.997
	PSO	F error	0.0122	0.0061	0.0013
		Q _{ecal.} (mg g ⁻¹)	46.98	95.04	192.70
		K ₂ *10 ⁴ (gm g ⁻¹ min ⁻¹)	2.81	1.31	0.50
		R ²	0.936	0.972	0.993
	PNO	F error	0.0149	0.0098	0.0159
		Q _{ecal.} (mg g ⁻¹)	43.93	89.09	181.81
		k _n (min ⁻¹) (mg g ⁻¹) ¹⁻ⁿ	0.011	0.009	0.002
		n	0.961	0.958	1.288
	Intraparticle (first step)	R ²	0.980	0.996	0.999
		F error	0.0123	0.0064	0.0009
		K _{id} (mg g ⁻¹ min ^{-0.5})	3.48	5.86	10.06
	Intraparticle (Second step)	I (mg g ⁻¹)	-11.24	-10.72	-13.67
		R ²	0.969	0.986	0.993
K _{id} (mg g ⁻¹ min ^{-0.5})		0.06	0.31	1.32	
	I (mg g ⁻¹)	39.73	74.83	129.05	
	R ²	0.805	0.959	0.999	

In addition, Fig. 9 shows that for both beads and whatever the initial concentration, the curves of the intraparticle model show three lines which do not pass through the origin (intercepts $\neq 0$); these three lines indicate that the process of MB adsorption on BOP occurred in different phases, of which the second line illustrates intraparticle diffusion which however is not the limiting step [32]. Therefore it can be assumed that the final stages of adsorption were controlled by intraparticle diffusion [33].

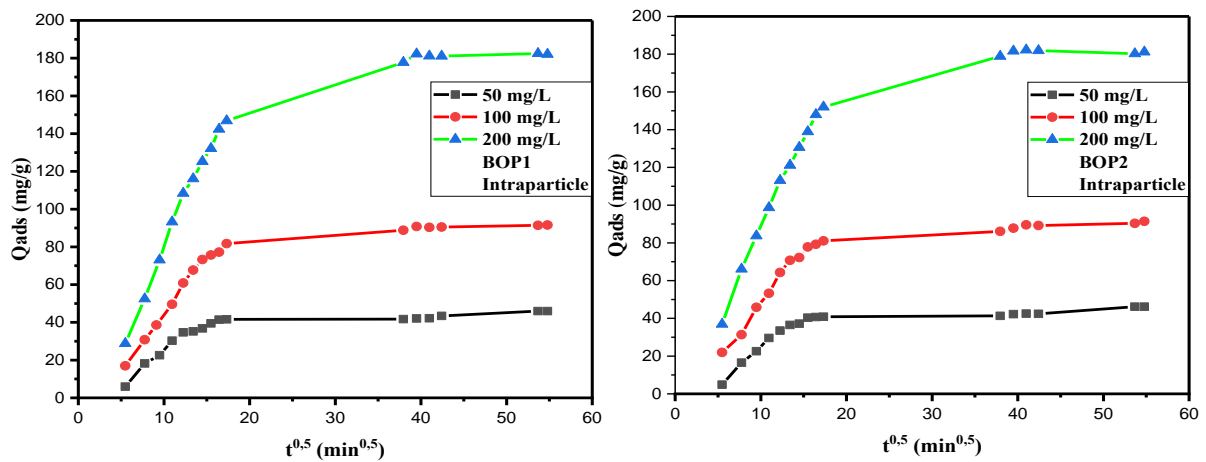


Figure 9. Intraparticle model for MB adsorption onto BOP1 and BOP2 at different initial concentrations.

Fig. 10 illustrates the results obtained from the Boyd modeling, showing linear points during the first minutes of adsorption for the two materials (BOP1 and BOP2), but do not pass through the origin. Overall, the data were not linear, suggesting that film diffusion was the limiting step rather than pore diffusion [34]. The above interpretation is compatible with the intraparticle model assumption.

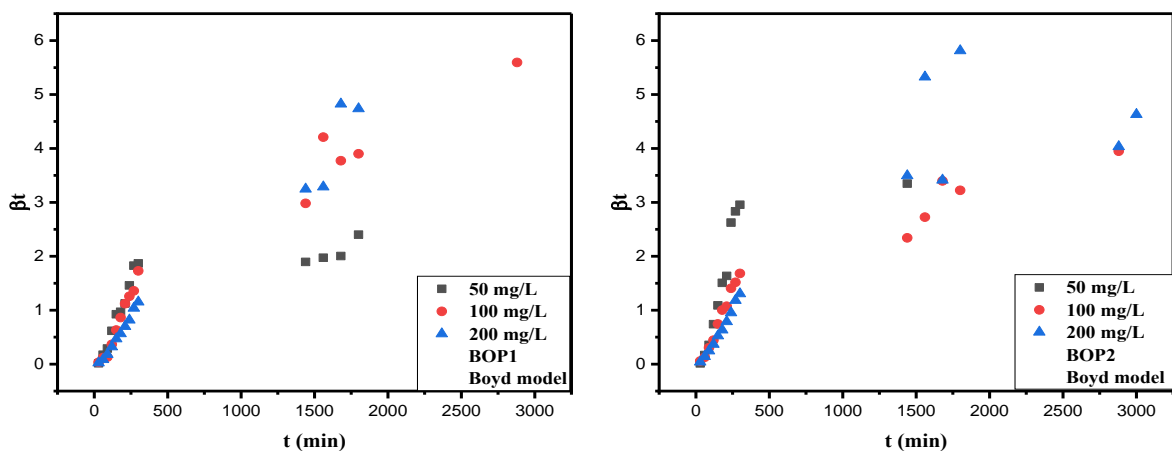


Figure 10. Boyd model for MB adsorption onto BOP1 and BOP2 at different initial concentrations.

2.4. pH effect

In general, the initial pH of the solution is an important parameter for the adsorption process since it can influence the adsorbent by changing its surface charge on the one hand. On the other hand, it can impact the adsorbate molecule through its degree of ionization or the degree of dissociation of its functional groups from the active sites [35]. Fig. 11 illustrates the initial pH effect for MB adsorption on BOP1 and BOP2. The two materials display the same shape, with curves divided into three stages. The first one is seen between pH 2 and 4, where the yield rises from 20 to 93.18 % for BOP1 and from 11 to 92.88 % for BOP2. This low yield in acidic pH may be due to electrostatic repulsion between the positive charges of the MB dye and those of the adsorbent. The second stage is observed between 4 and 10, where the adsorption quantity is quite good and almost constant for both beads; this behavior is attributed to the presence of negative charges as the pH tends towards alkaline values. Finally, the last stage between 10 and 12 is characterized by a slight decrease in yield due to MB structure modification in this interval, where the maximum wavelength shifted from 654 to 550 nm.

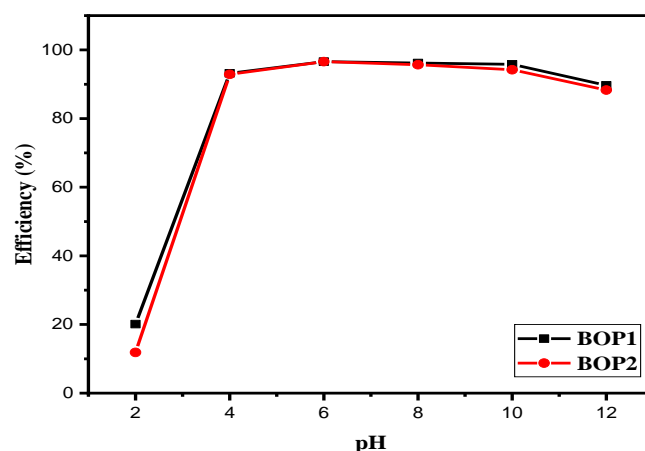


Figure 11. Initial pH effect for MB adsorption onto BOP1 and BOP2

2.5. NaCl and humic acid effects

Fig. 12 illustrates the behavior of MB adsorption in the presence of NaCl or HA. The findings show that when NaCl was added, the adsorption capacity of MB decreased because of dissolution of NaCl in Na^+ and Cl^- , which induces, on the one hand, a competitive adsorption between the Na^+ cations and the MB molecules and on the other hand, the neutralization of the MB molecules by the Cl^- ions [36]. Contrarily, the addition of HA had no effect on the adsorption performance of MB on the two materials, as seen in Fig. 12.

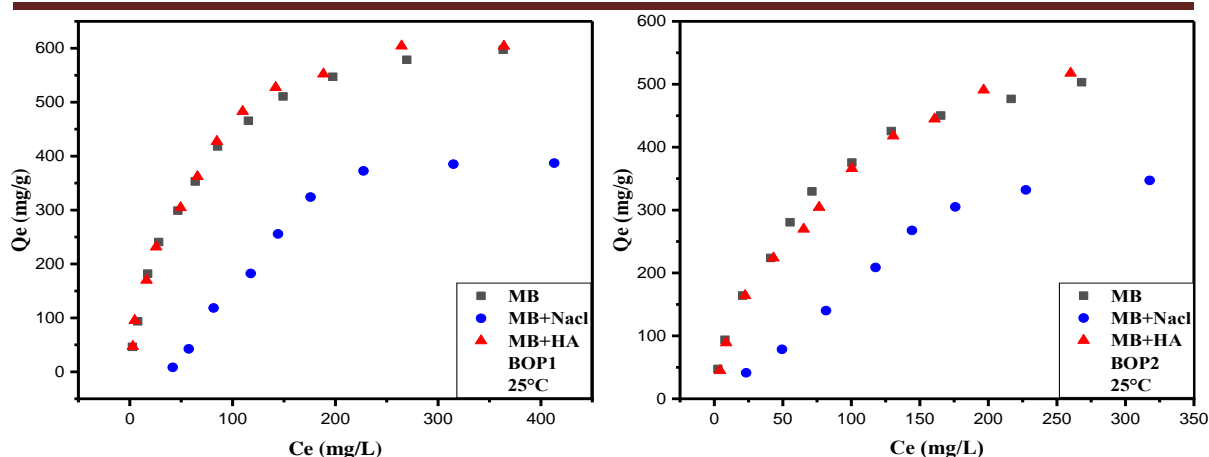


Figure 12. Ionic strength and organic compounds effects for MB adsorption onto BOP1 and BOP2 at 25°C.

2.6. Reuse of prepared beads

The regeneration tests of BOP1 and BOP2 (Fig. 13) indicate a remarkable reusability efficiency since the adsorption cycles can be repeated more than 7 times without a significant decrease in the adsorption yield. Indeed, the adsorption decrease was 5.93 % and 8.23% for BOP1 and BOP2 between the first and seventh cycles, namely a slightly higher efficiency for BOP1.

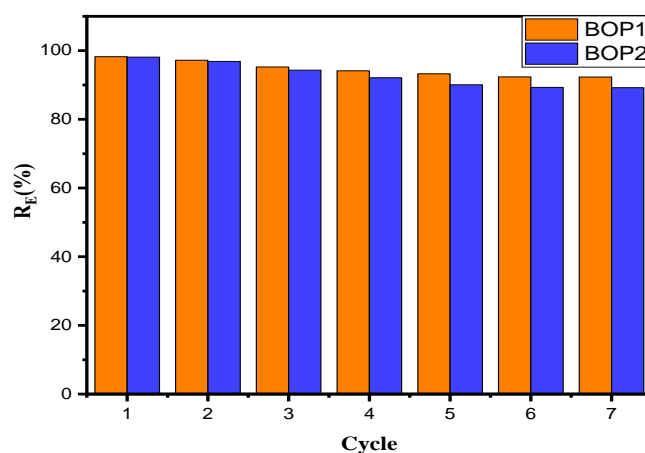


Figure 13. Regeneration efficiency of BOP1 and BOP2 at 25°C.

2.7. Statistical physical modeling

In this section, the adsorption isotherms modeling were performed using statistical physics models. As a consequence, to explain the mechanism of adsorption at the molecular level, adequate model parameters were considered to calculate, plot, and interpret thermodynamic functions such as free enthalpy, entropy, and internal energy.

2.7.1. Choosing the best model

The curves obtained from the used statistical models, namely MMSE, MMTE and DMTE, are presented in Fig. 14; the adjusted determination coefficient R^2 , F error function, and the Bayesian information criterion (BIC) values obtained from each model are summarized in Table 5. It is clear that the three models provided excellent adjusted determination coefficients (R^2), indicating that this parameter cannot be used to distinguish between the three models. Otherwise, table 5 shows that for the two materials, the second model, MMTE, offered the lowest F error and BIC values; furthermore, the BIC parameter shows that its values for the MMTE are generally greater than 10 compared to the other two models (MMSE, DMTE); as a result, it can be assumed that the MMTE is the most suitable model that can describe the experiment results.

Table 5: The comparative parameters (F error, R^2 and BIC) between the used statistical physics models.

Materials	Models	10°C			25°C			30°C		
		R^2	F error (%)	BIC	R^2	F error (%)	BIC	R^2	F error (%)	BIC
BOP1	MMSE	0.99669	0.02377	79.66	0.9977	0.05047	67.28	0.99533	0.0278	62.26
	MMTE	0.99935	0.00156	66.21	0.99945	0.03460	56.41	0.99936	0.01685	47.61
	DMTE	0.99900	0.13977	69.77	0.99805	0.11868	67.67	0.99654	0.13368	61.36
BOP2	MMSE	0.99757	0.02207	77.15	0.99288	0.04412	83.46	0.99289	0.04001	65.77
	MMTE	0.99957	0.00768	60.72	0.99886	0.00974	65.79	0.99908	0.01785	48.71
	DMTE	0.99757	0.02221	76.03	0.99412	0.11576	83.42	0.9929	0.13063	65.45

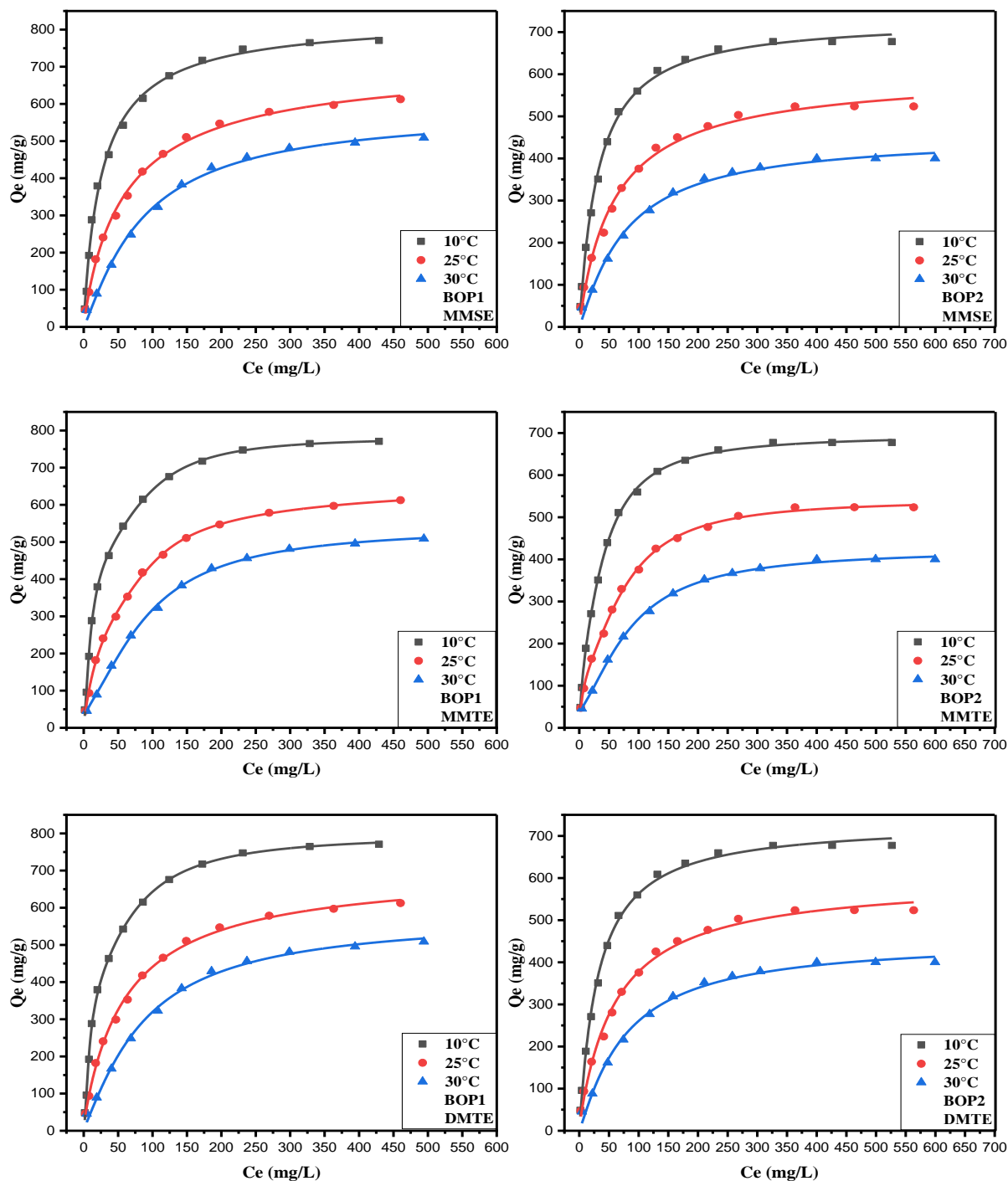


Figure 14. MMSE, MMTE, and DMTE modeling curves for MB adsorption isotherms onto BOP1 and BOP2 at different temperatures.

2.7.2. Steric interpretation for the adequate model (MMTE)

The n_{im} is one of the parameters that are essential in understanding the adsorption process since it can describe the orientation of the adsorbed molecule on the adsorbent surface [37]. As a result, three scenarios can be considered. First, if n_{im} is less than 0.5, the adsorption occurs through a multi-interaction mechanism (The MB molecule can be

adsorbed on at least two free adsorption sites) [38]; Otherwise, the MB molecule can be captured on a single and two free adsorption sites simultaneously with random and different percentages in the second scenario if n_{im} is between 0.5 and 1 [18,19]. It is worth noting that the n_{im} in the first two scenarios means that the adsorbate molecules were adsorbed parallel to the adsorbent surface [39]. In the third scenario, where n_{im} equals or exceeds 1, the adsorbate molecule is captured at a single adsorption site with an inclined or perpendicular orientation to the adsorbent surface [39,40]. Table 6 shows the variation of n_{1m} and n_{2m} as a function of temperature; these results indicate that for both materials and whatever the temperature n_{2m} is greater than n_{1m} . Furthermore, the n_{1m} has variable values ranging from 0.66 to 1.48, indicating that the MB molecules adsorption occurs in diverse types. To better understand these findings, two cases have been considered:

The first case (BOP1 at 10 °C; BOP2 at 10 and 25 °C) in which n_{1m} and n_{2m} are greater than 1: In this case, the MB molecules were adsorbed on a single site with an inclined or perpendicular orientation to the BOP surface. The second case (BOP1 at 25 and 30; BOP2 at 30 °C): the MB molecules were adsorbed simultaneously on a single and two free sites with mixed positions (parallel and perpendicular). From these results, the MB adsorption on a single free site in an inclined or perpendicular position is the dominant mode. Furthermore, physical statistical models provide more accurate values for the amount adsorbed at saturation Q_{sat} . As is well known, Q_{sat} is described by the density of the receptor sites (N_{is}) multiplied by n_{im} . It reflects BOP's ability to absorb MB; in the case of MMTE, the total Q_{sat} is given by the sum of Q_{sat1} and Q_{sat2} . The total Q_{sat} for each material at different temperatures are shown in Table 6; the obtained results demonstrate that the model's Q_{sat} values agree with Q_{exp} . Table 6 also indicates that total Q_{sat} decreases with the temperature, suggesting that the mechanism of MB adsorption on BOP is exothermic.

Table 6: Obtained parameters of the best model (MMTE) for MB isotherm adsorption onto BOP1 and BOP2 at different temperatures.

	T (°C)	n _{1m}	N _{1s} (mg/g)	n _{2m}	N _{2s} (mg/g)	C ₁ (mg/L)	C ₂ (mg/L)	Q _{sat1} (mg/g)	Q _{sat2} (mg/g)	Q _{totale} (mg/g)	Q _{exp} (mg/g)	R ²	F error (%)	BIC
B O P 1	10	1.48	346.03	2.29	117.91	10.52	93.11	511.77	269.41	781.19	767.82	0.999	0.00156	66.21
	25	0.89	658.44	3.54	25.46	44.83	97.40	587.33	90.31	677.63	612.58	0.999	0.0346	56.41
	30	0.66	131.13	1.63	278.78	5.05	92.69	86.55	455.80	542.35	508.90	0.999	0.01685	47.61
B O P 2	10	1.03	221.26	1.55	301.31	6.68	46.70	277.83	468.22	696.05	677.30	0.999	0.00768	60.72
	25	1.05	160.36	1.78	210.23	6.82	80.77	168.53	373.37	541.90	523.51	0.999	0.00974	65.79
	30	0.74	80.37	1.57	231.54	1.37	87.08	59.39	346.44	423.83	400.14	0.999	0.01785	48.71

2.7.3. Energetic interpretations

The system's adsorption energy is a crucial parameter for determining the type of interactions that occur during the process; this adsorption energy can be calculated using the following relationships (Eqs. 40 and 41) [41]:

$$C_i = C_s e^{\frac{-\Delta E_i}{RT}} \dots \dots \dots (40)$$

$$\Delta E_i = -RT \ln \left(\frac{C_i}{C_s} \right) \dots \dots \dots (41)$$

Table 7 summarizes the results of the MB adsorption energies calculations on BOP1 and BOP2 at different temperatures. This table indicates that for the two materials, $\Delta E1$ is always greater than $\Delta E2$, indicating that the first type of free active site is the most dominant. Moreover, the negative values signify that the interactions between the MB and BOP were exothermic. Based on the literature, the calculations carried out show that for the two materials, the Eads of MB were <40 kJ/mol, indicating the physisorption of the process [42] employing electrostatic interactions, dipole bond forces, and hydrophobic interactions π - π [43].

Table 7: Calculated adsorption energies from MMSE model for MB adsorption onto BOP1 and BOP2 at different temperatures.

Material	T (° C)	$\Delta E1$ (kJ/mol)	$\Delta E2$ (kJ/mol)
BOP1	10	-19.39	-13.76
	25	-16.83	-13.66
	30	-22.61	-13.77
BOP2	10	-20.46	-15.33
	25	-21.49	-14.08
	30	-25.90	-13.91

2.7.4. Thermodynamic functions calculation

The best statistical physic model (MMTE) parameters were used to conduct the calculations required to measure and plot the internal energy, Gibbs free enthalpy, and configuration entropy to perform a thermodynamic study of the MB adsorption mechanism on the two materials (BOP1 and BOP2).

2.7.4.1. Entropy

Evaluating an adsorption system's entropy configuration may provide valuable information about the order and disorder of the adsorbate. The following relationship (Eq.

28) is obtained by combining the grand canonical partition function Z_{gc} with the grand statistical potential (J) [19].

$$J = -k_B T \ln Z_{gc} = -\frac{\partial \ln Z_{gc}}{\partial \beta_s} - TS_a \dots \dots \dots (42)$$

As a result, Eq. 40 produces the following relationship (Eq. 43) [44] :

$$\frac{S_a}{k_B} = -\frac{\beta_s \partial \ln Z_{gc}}{\partial \beta_s} + \ln Z_{gc} \dots \dots \dots (43)$$

As a consequence, the second model's entropy variation as a function of the adsorbate equilibrium concentration is given by Eq. 44 [19] :

$$\frac{S_a}{k_B} = N_{1S} \left[\ln \left(1 + \left(\frac{C_e}{C_1} \right)^{n_{1m}} \right) + \frac{n_{1m} \ln \left(\frac{C_1}{C_e} \right)}{1 + \left(\frac{C_1}{C_e} \right)^{n_{1m}}} \right] + N_{2S} \left[\ln \left(1 + \left(\frac{C_e}{C_2} \right)^{n_{2m}} \right) + \frac{n_{2m} \ln \left(\frac{C_2}{C_e} \right)}{1 + \left(\frac{C_2}{C_e} \right)^{n_{2m}}} \right] \dots \dots (44)$$

Fig. 15 illustrates the evolution of entropy as a function of the equilibrium concentration. The two materials provide similar curves that can be separated into two parts: the first part was observed at low concentrations where entropy increases while the second part was seen at high concentrations where entropy decreases; this can be explained as follows: at low concentrations; MB molecules had a variety of opportunities for choosing free active sites to adsorb onto them, which leads to more disorder. However, at high concentrations, the BOP surface tends to monolayer saturation, which means that MB molecules don't have as many opportunities for being adsorbed, so the choice of free active sites was limited; as a result, the disorder decreases [45]. In general, when equilibrium is achieved, the entropy tends to zero [46], but this is not the case in our analysis, indicating that saturation had not yet been reached [47].

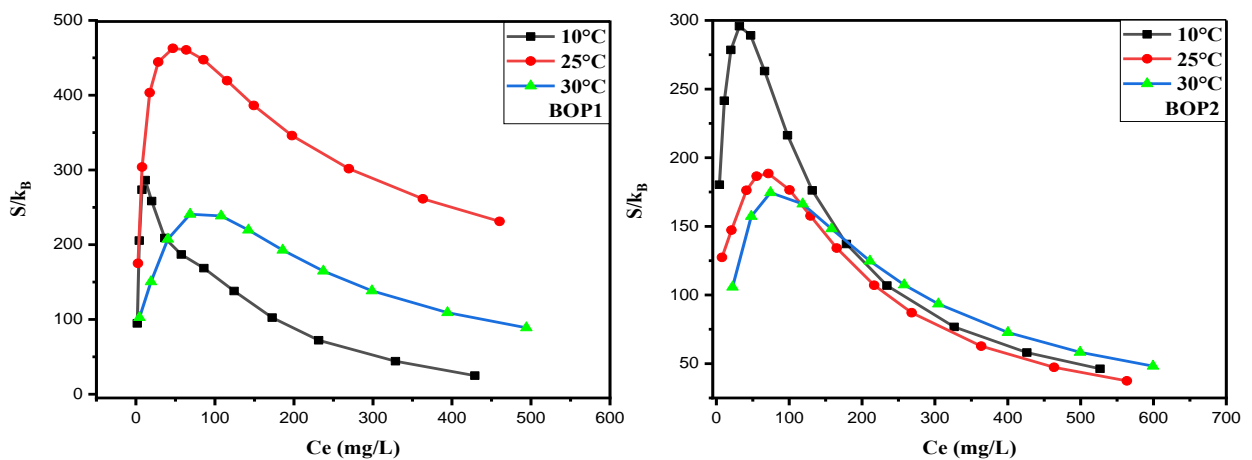


Figure 15. The evolution of entropy as a function of equilibrium MB concentrations at different temperatures for BOP1 and BOP2.

2.7.4.2. Gibbs free enthalpy

As it is known, the spontaneity of adsorption is determined by the Gibbs free enthalpy, which is presented by Eq. 45 [47] :

$$G = \mu Q \dots \dots \dots (45)$$

Where the chemical potential is given by Eq. 46 [17,48]:

$$\mu_c = k_B T \ln \left(\frac{N_s}{Z_{tr}} \right) \dots \dots \dots (46)$$

Gibbs free enthalpy as a function of the equilibrium concentration and translation partition function is given as follows (Eq.47) [44]:

$$G\beta_s = \ln \left(\frac{C_e}{Z_{tr}} \right) \left[\frac{n_{1m} N_{1s}}{1 + \left(\frac{C_1}{C_e} \right)^{n_{1m}}} + \frac{n_{2m} N_{2s}}{1 + \left(\frac{C_2}{C_e} \right)^{n_{2m}}} \right] \dots \dots \dots (47)$$

Then, the Gibbs free enthalpy for MMTE expression is given by Eq. 48 [42,49]:

$$G = k_B T \ln \left(\frac{C_e}{Z_v} \right) \left[\frac{Q_{sat1}}{1 + \left(\frac{C_1}{C_e} \right)^{n_{1m}}} + \frac{Q_{sat2}}{1 + \left(\frac{C_2}{C_e} \right)^{n_{2m}}} \right] \dots \dots \dots (48)$$

Where translation partition function per unit volume is given according to Eq. 49 [50]:

$$Z_v = \frac{Z_{gtr}}{V} = \left(\frac{2\pi m k_B T}{h^2} \right)^{3/2} \dots \dots \dots (49)$$

Fig. 16 shows the results of the Gibbs free enthalpy calculations as a function of MB concentrations at different temperatures. These results indicate that G values were negative regardless of the temperature, confirming the thermodynamic adsorption spontaneity of MB onto BOP1 and BOP2 [44,51]. Fig. 16 also shows the MB adsorption feasibility decreases with rising temperature [42], which may be due to the reduction of thermal collisions number [52].

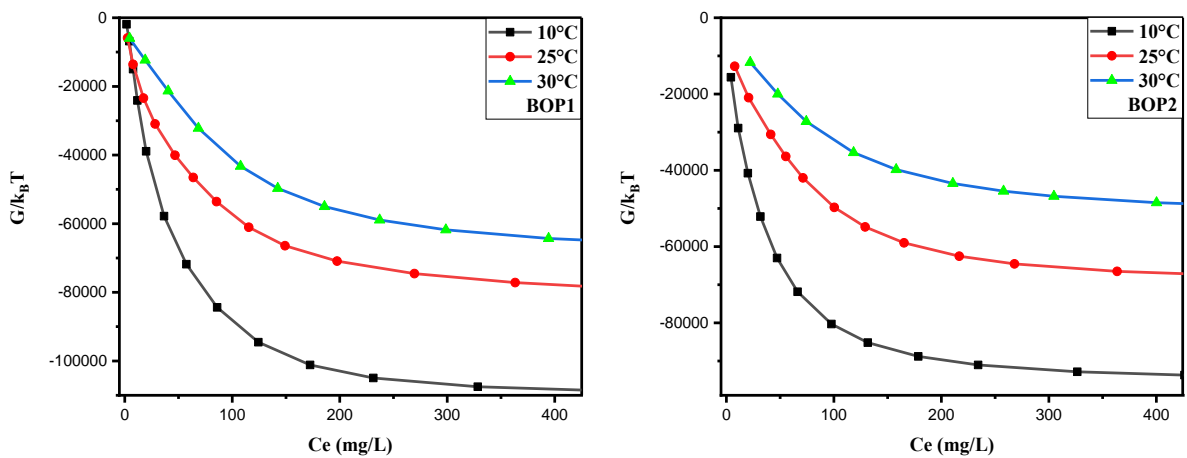


Figure 16. Gibbs free enthalpy variation as a function of equilibrium MB concentrations at different temperatures for BOP1 and BOP2.

2.7.4.3. Internal energy

The energy of an adsorption system can be described as an abstract concept developed to quantify the nature of interactions between its various components (including adsorbate-adsorbate interactions) so that it can express any type of energy that may occur in the process [45,53]. Therefore, internal energy is a key parameter for understanding the physical and chemical phenomena in this system.

The general equation of the internal energy can be described using the canonical grand partition function as follows [3] :

$$E_{int} = -\frac{\partial \ln(Z_{gc})}{\partial \beta_s} + \frac{\mu \partial \ln(Z_{gc})}{\beta_s \partial \mu} \dots \dots \dots (50)$$

Finally, the internal energy function for the monolayer model with two energies (MMTE) is given by Eq. 51 [53]:

$$E_{int} = k_B T \left[N_{1s} \frac{\ln\left(\frac{C_e}{Z_v}\right) + n_{1m} \ln\left(\frac{C_1}{C_e}\right)}{1 + \left(\frac{C_1}{C_e}\right)^{n_{1m}}} + N_{2s} \frac{\ln\left(\frac{C_e}{Z_v}\right) + n_{2m} \ln\left(\frac{C_2}{C_e}\right)}{1 + \left(\frac{C_2}{C_e}\right)^{n_{2m}}} \right] \dots \dots \dots (51)$$

Therefore, $E_{int}/k_B T$ is plotted as a function of C_e ; the results obtained are illustrated in Fig. 17

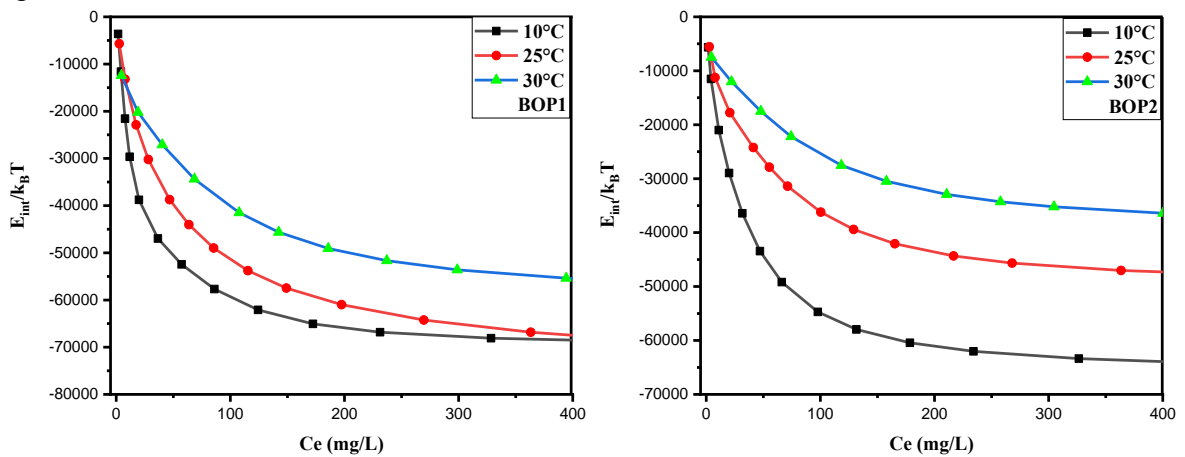


Figure 17. Internal energy variation as a function of equilibrium MB concentrations at different temperatures for BOP1 and BOP2.

It is clear that the E_{int} of the two materials are negatives, confirming the process's spontaneity [17] (in agreement with the results of Gibbs free enthalpy). Furthermore, the E_{int} values obtained can be divided into two cases. For low concentrations, the absolute values of the internal energies vary randomly with the rise of temperature. In contrast, in

the second case, the absolute values of internal energies decrease with increasing temperature, possibly due to a decrease in the thermal collisions number [54]. The two cases suggest the presence of exothermic and endothermic (at the first adsorption moments) adsorption stages [53].

3. Proposed mechanism for MB adsorption on BOP

At the end of this work, and as a result of all the obtained findings, it can be assumed that MB adsorption on BOP was spontaneous and exothermic while its mechanism can be achieved through electrostatic interactions, dipole bond forces, and hydrophobic interactions π - π , by a mixed monolayer with various ways, namely perpendicular and horizontal orientations, on a single and two free sites at the same time, but with a dominance of MB adsorption on a single free site under an inclined position to the BOP surface. Fig. 18 summarizes everything that was said about the adsorption mechanism of MB on BOP

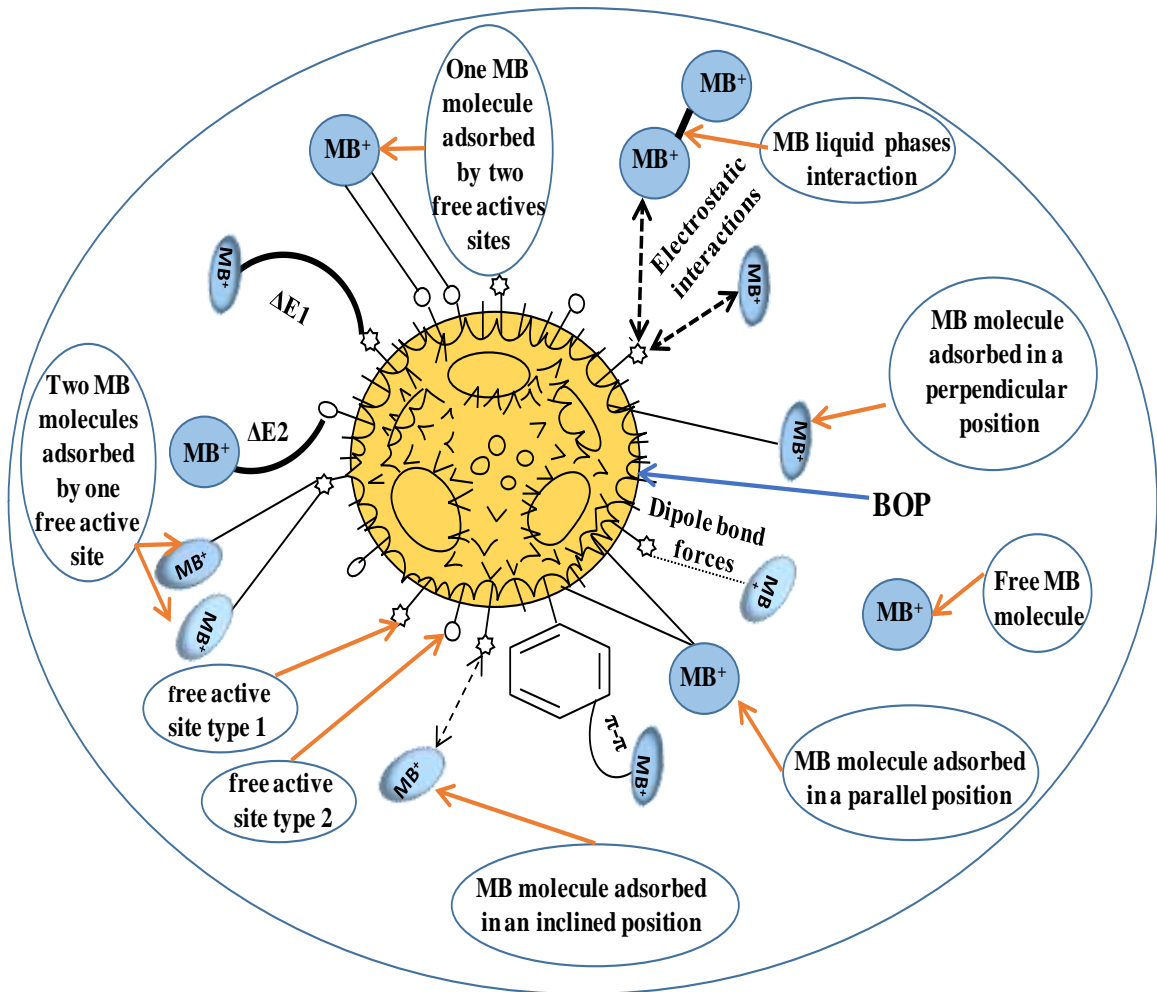


Figure 18. Proposed mechanism for MB adsorption onto BOP.

4. Conclusion

Orange peels were used as a precursor to be treated with phosphoric acid and encapsulated by sodium alginate. The modeling of the adsorption kinetics data showed that the PFO model was the most appropriate for describing the experimental results; additionally, the use of the Boyd and intraparticle models indicated the diffusion of films, rather than the diffusion of pores, was the limiting step. The isotherms of MB adsorption on prepared beads were performed over a temperature range ranging from 10 to 30°C. The experimental findings showed that the prepared beads had excellent MB adsorption performances, with adsorbed quantities of 765.82 and 677.30 mg/g for BOP1 and BOP2, respectively. Furthermore, the obtained curves were analyzed and interpreted using two classical models (Langmuir and Freundlich) and three physical models (MMSE, MMTE, DMTE) based on the grand canonical partition function in statistical physics; the findings showed that the MMTE model was the most appropriate one. The regeneration study of BOP by acidic water revealed that BOP1 and BOP2 were reusable even after the seventh cycle. Furthermore, experimental findings indicated that NaCl inhibited MB adsorption due to competition with Na⁺, while humic acid had no effect on MB adsorption. The adsorption energy measurements showed that, on the one hand, the temperature had an impact on the nature of the MB adsorption process on BOP; on the other hand, MB adsorption can be achieved through electrostatic interactions, dipole bond forces, and hydrophobic interactions π - π . Furthermore, the parameters of the best statistical physics model (MMTE) showed that MB adsorption on BOP1 and BOP2 was a mixed monolayer whose process was carried out in various ways (perpendicular and horizontal orientations, on a single and two free sites at the same time), with a dominance of MB adsorption on a single free site under an inclined position to the adsorbent surface. The best model's parameters were used to conduct the calculations required to measure and plot the internal energy, Gibbs free enthalpy, and configuration entropy to perform a thermodynamic study of the MB adsorption mechanism on BOP1 and BOP2. Negative values of free enthalpy and internal energy mean that the process of MB adsorption on BOP was spontaneous and exothermic, whereas the entropy variance indicated that order and disorder were directly related to the availability of free active sites on the BOP surface.

5. References

- [1] S.F. Azha, L. Sellaoui, M.S. Shamsudin, S. Ismail, A. Bonilla-Petriciolet, A. Ben Lamine, A. Erto, Synthesis and characterization of a novel amphoteric adsorbent

- coating for anionic and cationic dyes adsorption: Experimental investigation and statistical physics modelling, *Chem. Eng. J.* 351 (2018) 221–229. <https://doi.org/10.1016/j.cej.2018.06.092>.
- [2] L. Sellaoui, T. Depci, A.R. Kul, S. Knani, A. Ben Lamine, A new statistical physics model to interpret the binary adsorption isotherms of lead and zinc on activated carbon, *J. Mol. Liq.* 214 (2016) 220–230. <https://doi.org/10.1016/j.molliq.2015.12.080>.
- [3] L. Sellaoui, G.L. Dotto, S. Wjihi, J.O. Gonçalves, L.A.A. Pinto, A.B. Lamine, A. Erto, Thermodynamic analysis of single and binary adsorption of Food Yellow 4 and Food Blue 2 on CC-chitosan: Application of statistical physics and IAST models, *J. Mol. Liq.* 232 (2017) 499–505. <https://doi.org/10.1016/j.molliq.2017.02.103>.
- [4] H. Liu, J. Zhang, M. Lu, L. Liang, H. Zhang, J. Wei, Biosynthesis based membrane filtration coupled with iron nanoparticles reduction process in removal of dyes, *Chem. Eng. J.* 387 (2020) 124202. <https://doi.org/10.1016/j.cej.2020.124202>.
- [5] A. Muniyasamy, G. Sivaporul, A. Gopinath, R. Lakshmanan, A. Altaee, A. Achary, P. Velayudhaperumal Chellam, Process development for the degradation of textile azo dyes (mono-, di-, poly-) by advanced oxidation process - Ozonation: Experimental & partial derivative modelling approach, *J. Environ. Manage.* 265 (2020) 110397. <https://doi.org/10.1016/j.jenvman.2020.110397>.
- [6] H. Demissie, G. An, R. Jiao, T. Ritigala, S. Lu, D. Wang, Modification of high content nanocluster-based coagulation for rapid removal of dye from water and the mechanism, *Sep. Purif. Technol.* 259 (2021) 117845. <https://doi.org/10.1016/j.seppur.2020.117845>.
- [7] A. Khatri, P.S. Rana, Visible light assisted photocatalysis of Methylene Blue and Rose Bengal dyes by iron doped NiO nanoparticles prepared via chemical co-precipitation, *Phys. B Condens. Matter.* 579 (2020) 411905. <https://doi.org/10.1016/j.physb.2019.411905>.
- [8] S. Li, Z. Zeng, W. Xue, Adsorption of lead ion from aqueous solution by modified walnut shell: kinetics and thermodynamics, *Environ. Technol.* 40 (2019) 1810–1820. <https://doi.org/10.1080/09593330.2018.1430172>.
- [9] A. Mohammadi, A.H. Doctorsafaei, K.M. Zia, Alginate/calix[4]arenes modified graphene oxide nanocomposite beads: Preparation, characterization, and dye

- adsorption studies, *Int. J. Biol. Macromol.* 120 (2018) 1353–1361. <https://doi.org/10.1016/j.ijbiomac.2018.09.136>.
- [10] H. Wang, Z. Li, S. Yahyaoui, H. Hanafy, M.K. Seliem, A. Bonilla-Petriciolet, G. Luiz Dotto, L. Sellaoui, Q. Li, Effective adsorption of dyes on an activated carbon prepared from carboxymethyl cellulose: Experiments, characterization and advanced modelling, *Chem. Eng. J.* (2020) 128116. <https://doi.org/10.1016/j.cej.2020.128116>.
- [11] Y. Ji, F. Xu, W. Wei, H. Gao, K. Zhang, G. Zhang, Y. Xu, P. Zhang, Efficient and fast adsorption of methylene blue dye onto a nanosheet MFI zeolite, *J. Solid State Chem.* 295 (2021) 121917. <https://doi.org/10.1016/j.jssc.2020.121917>.
- [12] Y. Dehmani, O.E. Khalki, H. Mezougane, S. Abouarnadasse, Comparative study on adsorption of cationic dyes and phenol by natural clays, *Chem. Data Collect.* 33 (2021) 100674. <https://doi.org/10.1016/j.cdc.2021.100674>.
- [13] T. Shen, S. Mao, F. Ding, T. Han, M. Gao, Selective adsorption of cationic/anionic tritoluene dyes on functionalized amorphous silica: A mechanistic correlation between the precursor, modifier and adsorbate, *Colloids Surf. Physicochem. Eng. Asp.* 618 (2021) 126435. <https://doi.org/10.1016/j.colsurfa.2021.126435>.
- [14] R. Bushra, S. Mohamad, Y. Alias, Y. Jin, M. Ahmad, Current approaches and methodologies to explore the perceptive adsorption mechanism of dyes on low-cost agricultural waste: A review, *Microporous Mesoporous Mater.* (2021) 111040. <https://doi.org/10.1016/j.micromeso.2021.111040>.
- [15] M. Padmapriya, S.T. Ramesh, V.M. Biju, Synthesis of seawater based geopolymer: Characterization and adsorption capacity of methylene blue from wastewater, *Mater. Today Proc.* (2021). <https://doi.org/10.1016/j.matpr.2021.03.030>.
- [16] E. Alver, A.Ü. Metin, F. Brouers, Methylene blue adsorption on magnetic alginate/rice husk bio-composite, *Int. J. Biol. Macromol.* 154 (2020) 104–113. <https://doi.org/10.1016/j.ijbiomac.2020.02.330>.
- [17] A.Q. Selim, L. Sellaoui, M. Mobarak, Statistical physics modeling of phosphate adsorption onto chemically modified carbonaceous clay, *J. Mol. Liq.* 279 (2019) 94–107. <https://doi.org/10.1016/j.molliq.2019.01.100>.
- [18] M. Ben Manaa, N. Bouaziz, B. Schmaltz, F. Tran Van, A. Ben Lamine, Study of the effect of variation in temperature and pH on the adsorption process of natural Gardenia yellow dye into TiO₂ mesoporous for dye sensitized solar cells using the statistical physics formalism: Physicochemical and thermodynamic investigation,

- Microporous Mesoporous Mater. 270 (2018) 82–92.
<https://doi.org/10.1016/j.micromeso.2018.05.007>.
- [19] M. Mobarak, E.A. Mohamed, A.Q. Selim, L. Sellaoui, A.B. Lamine, A. Erto, A. Bonilla-Petriciolet, M.K. Seliem, Surfactant–modified serpentine for fluoride and Cr(VI) adsorption in single and binary systems: Experimental studies and theoretical modeling, Chem. Eng. J. 369 (2019) 333–343.
<https://doi.org/10.1016/j.cej.2019.03.086>.
- [20] L. Das, P. Das, A. Bhowal, C. Bhattacharjee, Treatment of malachite green dye containing solution using bio-degradable Sodium alginate/NaOH treated activated sugarcane bagasse charcoal beads: Batch, optimization using response surface methodology and continuous fixed bed column study, J. Environ. Manage. 276 (2020) 111272. <https://doi.org/10.1016/j.jenvman.2020.111272>.
- [21] M.A. Khan, S.M. Wabaidur, M.R. Siddiqui, A.A. Alqadami, A.H. Khan, Silico-manganese fumes waste encapsulated cryogenic alginate beads for aqueous environment de-colorization, J. Clean. Prod. 244 (2020) 118867.
<https://doi.org/10.1016/j.jclepro.2019.118867>.
- [22] B. Işık, V. Uğraşkan, Adsorption of methylene blue on sodium alginate–flax seed ash beads: Isotherm, kinetic and thermodynamic studies, Int. J. Biol. Macromol. (2020).
<https://doi.org/10.1016/j.ijbiomac.2020.11.070>.
- [23] A. Guediri, A. Bouguettoucha, D. Chebli, N. Chafai, A. Amrane, Molecular dynamic simulation and DFT computational studies on the adsorption performances of methylene blue in aqueous solutions by orange peel-modified phosphoric acid, J. Mol. Struct. (2019) 127290. <https://doi.org/10.1016/j.molstruc.2019.127290>.
- [24] I. Dalponte Dallabona, G.G. de Lima, B.I. Cestaro, I. de S. Tasso, T.S. Paiva, E.J.G. Laureanti, L.M. de M. Jorge, B.J.G. da Silva, C.V. Helm, A.L. Mathias, R.M.M. Jorge, Development of alginate beads with encapsulated jabuticaba peel and propolis extracts to achieve a new natural colorant antioxidant additive, Int. J. Biol. Macromol. 163 (2020) 1421–1432. <https://doi.org/10.1016/j.ijbiomac.2020.07.256>.
- [25] A.Ü. Metin, D. Doğan, M. Can, Novel magnetic gel beads based on ionically crosslinked sodium alginate and polyanetholesulfonic acid: Synthesis and application for adsorption of cationic dyes, Mater. Chem. Phys. 256 (2020) 123659.
<https://doi.org/10.1016/j.matchemphys.2020.123659>.

- [26] C.P. Pinheiro, L.M.K. Moreira, S.S. Alves, T.R.S. Cadaval Jr, L.A.A. Pinto, Anthocyanins concentration by adsorption onto chitosan and alginate beads: Isotherms, kinetics and thermodynamics parameters, *Int. J. Biol. Macromol.* (2020). <https://doi.org/10.1016/j.ijbiomac.2020.10.250>.
- [27] A. De Rossi, C.V.T. Rigueto, A. Dettmer, L.M. Colla, J.S. Piccin, Synthesis, characterization, and application of *Saccharomyces cerevisiae*/alginate composites beads for adsorption of heavy metals, *J. Environ. Chem. Eng.* 8 (2020) 104009. <https://doi.org/10.1016/j.jece.2020.104009>.
- [28] R. Ahmad, R. Kumar, Synthesis and Properties of Cellulose Carbon Encapsulated ZnO for Dye Removal, *J. Dispers. Sci. Technol.* 32 (2011) 737–740. <https://doi.org/10.1080/01932691.2010.480869>.
- [29] J. Kazemi, V. Javanbakht, Alginate beads impregnated with magnetic Chitosan@Zeolite nanocomposite for cationic methylene blue dye removal from aqueous solution, *Int. J. Biol. Macromol.* 154 (2020) 1426–1437. <https://doi.org/10.1016/j.ijbiomac.2019.11.024>.
- [30] A. Mokhtar, S. Abdelkrim, A. Djelad, A. Sardi, B. Boukoussa, M. Sassi, A. Bengueddach, Adsorption behavior of cationic and anionic dyes on magadiite-chitosan composite beads, *Carbohydr. Polym.* 229 (2020) 115399. <https://doi.org/10.1016/j.carbpol.2019.115399>.
- [31] B. Zhang, S. Yu, Y. Zhu, Y. Shen, X. Gao, W. Shi, J. Hwa Tay, Adsorption mechanisms of crude oil onto polytetrafluoroethylene membrane: Kinetics and isotherm, and strategies for adsorption fouling control, *Sep. Purif. Technol.* 235 (2020) 116212. <https://doi.org/10.1016/j.seppur.2019.116212>.
- [32] M.F. Oliveira, M.G.C. da Silva, M.G.A. Vieira, Equilibrium and kinetic studies of caffeine adsorption from aqueous solutions on thermally modified Verde-lodo bentonite, *Appl. Clay Sci.* 168 (2019) 366–373. <https://doi.org/10.1016/j.clay.2018.12.011>.
- [33] Y.H. Magdy, H. Altaher, Kinetic analysis of the adsorption of dyes from high strength wastewater on cement kiln dust, *J. Environ. Chem. Eng.* 6 (2018) 834–841. <https://doi.org/10.1016/j.jece.2018.01.009>.
- [34] R.A. Fideles, G.M.D. Ferreira, F.S. Teodoro, O.F.H. Adarme, L.H.M. da Silva, L.F. Gil, L.V.A. Gurgel, Trimellitated sugarcane bagasse: A versatile adsorbent for removal of cationic dyes from aqueous solution. Part I: Batch adsorption in a

- monocomponent system, *J. Colloid Interface Sci.* 515 (2018) 172–188. <https://doi.org/10.1016/j.jcis.2018.01.025>.
- [35] B.K. Nandi, A. Goswami, M.K. Purkait, Adsorption characteristics of brilliant green dye on kaolin, *J. Hazard. Mater.* 161 (2009) 387–395. <https://doi.org/10.1016/j.jhazmat.2008.03.110>.
- [36] I. Othman, M. Abu Haija, P. Kannan, F. Banat, Adsorptive Removal of Methylene Blue from Water Using High-Performance Alginate-Based Beads, *Water. Air. Soil Pollut.* 231 (2020) 396. <https://doi.org/10.1007/s11270-020-04751-3>.
- [37] L. Sellaoui, É.C. Lima, G.L. Dotto, S.L.P. Dias, A. Ben Lamine, Physicochemical modeling of reactive violet 5 dye adsorption on home-made cocoa shell and commercial activated carbons using the statistical physics theory, *Results Phys.* 7 (2017) 233–237. <https://doi.org/10.1016/j.rinp.2016.12.014>.
- [38] G.L. Dotto, L.A.A. Pinto, M.A. Hachicha, S. Knani, New physicochemical interpretations for the adsorption of food dyes on chitosan films using statistical physics treatment, *Food Chem.* 171 (2015) 1–7. <https://doi.org/10.1016/j.foodchem.2014.08.098>.
- [39] L. Sellaoui, G.L. Dotto, E.C. Peres, Y. Benguerba, É.C. Lima, A.B. Lamine, A. Erto, New insights into the adsorption of crystal violet dye on functionalized multi-walled carbon nanotubes: Experiments, statistical physics and COSMO–RS models application, *J. Mol. Liq.* 248 (2017) 890–897. <https://doi.org/10.1016/j.molliq.2017.10.124>.
- [40] I. Ben Khemis, M. Bouzid, N. Mechi, A. Ben Lamine, Statistical physics modeling and interpretation of the adsorption of enantiomeric terpenes onto the human olfactory receptor OR1A1, *Int. J. Biol. Macromol.* 171 (2021) 428–434. <https://doi.org/10.1016/j.ijbiomac.2020.12.209>.
- [41] A. Yazidi, L. Sellaoui, G.L. Dotto, A. Bonilla-Petriciolet, A.C. Fröhlich, A.B. Lamine, Monolayer and multilayer adsorption of pharmaceuticals on activated carbon: Application of advanced statistical physics models, *J. Mol. Liq.* 283 (2019) 276–286. <https://doi.org/10.1016/j.molliq.2019.03.101>.
- [42] M.K. Seliem, M. Mobarak, Cr(VI) uptake by a new adsorbent of CTAB–modified carbonized coal: Experimental and advanced statistical physics studies, *J. Mol. Liq.* 294 (2019) 111676. <https://doi.org/10.1016/j.molliq.2019.111676>.

- [43] B. Mohamed, Z. Qingyu, G. D. Moggridge, B.L. Abdelmottaleb, New insight in adsorption of pyridine on the two modified adsorbents types MN200 and MN500 by means of grand canonical ensemble, *J. Mol. Liq.* 263 (2018) 413–421. <https://doi.org/10.1016/j.molliq.2018.05.008>.
- [44] M. Mobarak, E.A. Mohamed, A.Q. Selim, F.M. Mohamed, L. Sellaoui, A. Bonilla-Petriciolet, M.K. Seliem, Statistical physics modeling and interpretation of methyl orange adsorption on high-order mesoporous composite of MCM-48 silica with treated rice husk, *J. Mol. Liq.* 285 (2019) 678–687. <https://doi.org/10.1016/j.molliq.2019.04.116>.
- [45] M. Khalfaoui, A.E. Ghali, C. Aguir, Z. Mohamed, M.H.V. Baouab, A.B. Lamine, Study on adsorption of herbicide onto functionalized cellulose extracted from *Juncus acutus* L. plant: Experimental results and theoretical modeling, *Ind. Crops Prod.* 67 (2015) 169–178. <https://doi.org/10.1016/j.indcrop.2015.01.032>.
- [46] N. Bouaziz, M. Ben Manaa, A. Ben Lamine, Physicochemical and thermodynamic investigation of hydrogen absorption and desorption in $\text{LaNi}_{3.8}\text{Al}_{1.0}\text{Mn}_{0.2}$ using the statistical physics modeling, *Results Phys.* 9 (2018) 1323–1334. <https://doi.org/10.1016/j.rinp.2018.04.035>.
- [47] A.Q. Selim, E.A. Mohamed, M.K. Seliem, Deep insights into the organic carbon role in selectivity and adsorption mechanism of phosphate and crystal violet onto low-cost black limestone: Modelling and physicochemical parameters interpretation, *Colloids Surf. Physicochem. Eng. Asp.* 580 (2019) 123755. <https://doi.org/10.1016/j.colsurfa.2019.123755>.
- [48] L. Sellaoui, H. Guedidi, S. Knani, L. Reinert, L. Duclaux, A. Ben Lamine, Application of statistical physics formalism to the modeling of adsorption isotherms of ibuprofen on activated carbon, *Fluid Phase Equilibria.* 387 (2015) 103–110. <https://doi.org/10.1016/j.fluid.2014.12.018>.
- [49] C. Briki, M. Bouzid, M.H. Dhaou, A. Jemni, A.B. Lamine, Experimental and theoretical study of hydrogen absorption by $\text{LaNi}_{3.6}\text{Mn}_{0.3}\text{Al}_{0.4}\text{Co}_{0.7}$ alloy using statistical physics modeling, *Int. J. Hydrog. Energy.* 43 (2018) 9722–9732. <https://doi.org/10.1016/j.ijhydene.2018.02.201>.
- [50] N. Bouaziz, M. Ben Manaa, F. Aouaini, A. Ben Lamine, Investigation of hydrogen adsorption on zeolites A, X and Y using statistical physics formalism, *Mater. Chem. Phys.* 225 (2019) 111–121. <https://doi.org/10.1016/j.matchemphys.2018.12.024>.

- [51] F. Dhaouadi, L. Sellaoui, H.E. Reynel-Ávila, V. Landín-Sandoval, D.I. Mendoza-Castillo, J.E. Jaime-Leal, E.C. Lima, A. Bonilla-Petriciolet, A.B. Lamine, Adsorption mechanism of Zn^{2+} , Ni^{2+} , Cd^{2+} , and Cu^{2+} ions by carbon-based adsorbents: interpretation of the adsorption isotherms via physical modelling, *Environ. Sci. Pollut. Res.* 28 (2021) 30943–30954. <https://doi.org/10.1007/s11356-021-12832-x>.
- [52] L. Sellaoui, H. Guedidi, SarraWjihi, L. Reinert, S. Knani, L. Duclaux, A.B. Lamine, Experimental and theoretical studies of adsorption of ibuprofen on raw and two chemically modified activated carbons: new physicochemical interpretations, *RSC Adv.* 6 (2016) 12363–12373. <https://doi.org/10.1039/C5RA22302D>.
- [53] F. Dhaouadi, L. Sellaoui, M. Badawi, H.E. Reynel-Ávila, D.I. Mendoza-Castillo, J.E. Jaime-Leal, A. Bonilla-Petriciolet, A.B. Lamine, Statistical physics interpretation of the adsorption mechanism of Pb^{2+} , Cd^{2+} and Ni^{2+} on chicken feathers, *J. Mol. Liq.* 319 (2020) 114168. <https://doi.org/10.1016/j.molliq.2020.114168>.
- [54] L. Sellaoui, S. Knani, A. Erto, M.A. Hachicha, A. Ben Lamine, Equilibrium isotherm simulation of tetrachlorethylene on activated carbon using the double layer model with two energies: Steric and energetic interpretations, *Fluid Phase Equilibria.* 408 (2016) 259–264. <https://doi.org/10.1016/j.fluid.2015.09.022>.

Chapter VII: A short introduction on the employment of dynamic adsorption systems using fixed and semi-fluidized beds by using BZJS1 as an adsorbent

1. Introduction

For several years and in numerous studies, adsorption has been an effective technique for water purification in batch systems. But, the question that arises is: are the obtained results in those studies applicable to real industries?

In recent years, several research teams have considered bringing their results closer to real industries by employing dynamic adsorption systems (fixed, fluidized and semi-fluidized beds); in fact, some studies have successfully eliminated various pollutants via dynamic adsorption, demonstrating the reliability of this technique for vast volumes of effluent. Furthermore, the overall perspective of adsorption turns to the continuous flow process because this strategy is the most practical technique for removing contaminants in various industries. As a result, many researchers have focused on developing adsorbents suitable for this aim, including encapsulated adsorbents.

This final chapter's objective is to develop a dynamic adsorption system in the form of a fixed bed, which is more similar to a real industry, using the best adsorbent prepared throughout this thesis, and then compare its findings to those obtained with the batch system. Furthermore, this step will allow us to evaluate the performance and benefits of our prepared beads, as well as discover and repair any problems that may occur.

Although many studies described adsorption in batch systems as an efficient process, the development of fixed-bed column adsorption techniques for water purification is highly desirable since it is an industrially viable technology for removing various pollutants from wastewater [1].

In addition, fixed-bed adsorption provides developing the continuous adsorption mode, which is suitable for large volumes of wastewater with low operating costs [2].

According to the fourth chapter, BZJS1 was the best adsorbent, with a maximum adsorbed quantity of 737.13 mg/g at ambient temperature. BZJS1 has already been characterized and well presented in that chapter; therefore, this last chapter will not discuss anything relevant to it, such as preparation methods, characterization, and so on. But, it will focus on the employment of BZJS1 in the MB dynamic adsorption process.

2. Column adsorption process

The continuous adsorption of BM on BZJS1 was carried out at room temperature (25°C) in a glass column with an internal diameter of 8 mm and a height of 600 mm. A mass of BZJS1 was introduced into the column until the desired bed height was achieved. The stabilization of the bed was performed using glass wool to avoid the beads entrainment with the solution; once the bed was ready, a solution of BM was poured from the bottom to the top using a peristaltic pump. The samples were collected at the head of the column to be analyzed in UV-visible. The fixed bed design employed in the experimental tests is shown in Fig. 1.

In general, the shape of the breakthrough curve is the essential characteristic for evaluating the dynamic behavior of the fixed-bed adsorption column. Therefore, the breakthrough curve is often plotted as the C_t/C_0 versus the continuous adsorption time (t).

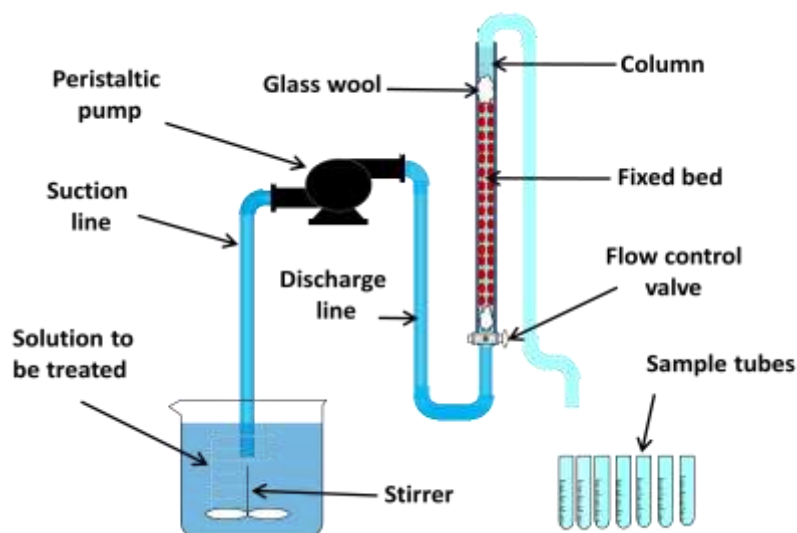


Figure1. The employed fixed bed design of MB continuous adsorption onto BZJS1.

3. Results and discussion

3.1. Bed height effect

The BZJS1 were employed at 30, 45, and 60 mm of bed height to obtain adsorption breakthrough curves at a dye inlet concentration of 100 mg/L and a flow rate of 100 ml/h. The obtained curves are presented in Fig. 2.

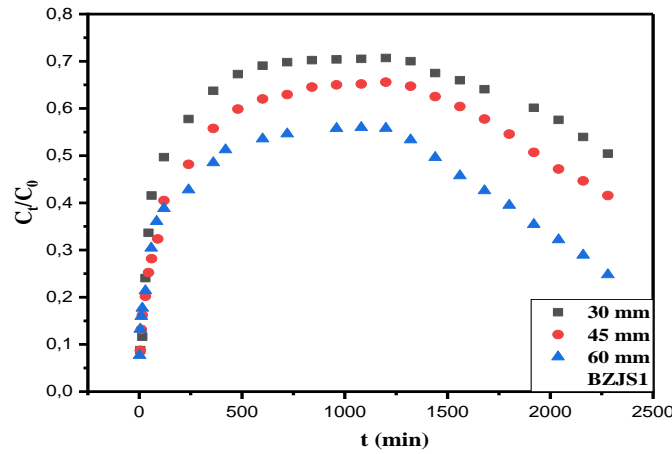


Figure 2. Bed height effect for MB dynamic adsorption on BZJS1
($C_0= 100$ mg/L, $T=25^\circ\text{C}$, $F= 100$ ml/h).

These findings show curves that are similar in shape and have three stages. The first stage provides the impression that the experiment is on the right track, but the two other stages indicate the opposite; this astonishing variation in the behavior of these curves can be related to several parameters. To understand what happened, please look at Fig. 3, which shows the relationship between the flow rate and the C/C_0 ratio at the column's outlet. As can be seen in the first hours of the experiment, everything is good (stage 1), where the C/C_0 ratio increases with time, but as time passes, the flow rate at the bed's outlet decreases, which is due to the BZJS1 beads swelling leading to its aggregation, and blocking the MB passageway and decreases the porosity of the bed; as a result, the column performances decrease (stage 2 and 3).

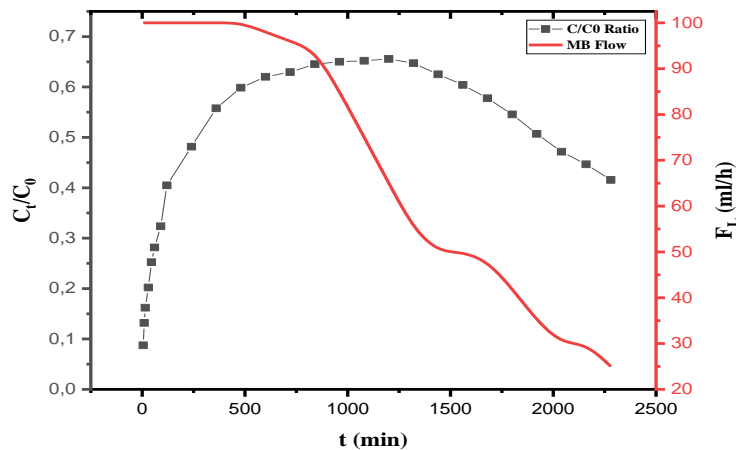


Figure 3. The relationship between the C/C_0 ratio and the BM discharge flow at column's outlet.

3.2. Proposed solutions for the fixed bed experiments

Our research team set out to find solutions and methods to solve the issues regarding the fixed bed experiments and the problem of bead swelling. Wherefore, many alternative

procedures were proposed. One solution proposed was to swell the beads in distilled water before using them, but this method did not work due to the water incorporated in the swelled beads; the second solution proposed was to fluidize the beads by increasing the MB flow.

To this purpose, the fixed bed tests have been repeated with a slight increase in the peristaltic pump's speed to facilitate bed semi-fluidization, resulting in a discharge flow of 155.4 ml/h; the initial concentrations range employed have been reduced (5 to 50 mg/L). Furthermore, the following assumptions were taken into account before performing the fluidized bed experiments [3,4]:

- BZJS1 beads are uniform in size.
- The wall effect is not taken into consideration.
- There is no solute dispersion.
- BZJS1 are uniformly distributed.
- For the solid-liquid phase, there is no gradient radial concentration in the column

3.3. Initial dye concentration effect for semi fluidized bed experiments

The initial concentrations effect on the semi-fluidized bed process was investigated using a fixed height of BZJS1 equal to 30 mm and a constant MB flow of 155.4 mL/h with initial concentrations ranging from 5 to 50 mg/L; the obtained findings are shown in Fig. 4

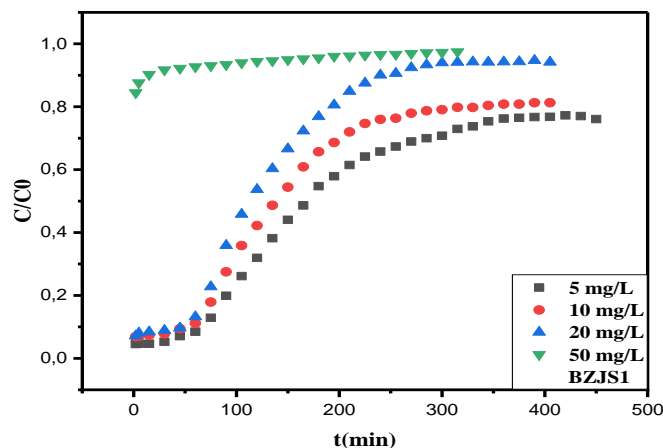


Figure 4. Initial dye concentrations effect for semi fluidized bed experiments

($F=155$ ml/h, $T= 25^{\circ}\text{C}$, $h= 30$ mm).

Fig. 4 shows two different results: for low concentrations (5, 10 and 20 mg/L), the breakthrough curve in S form is fully obvious, indicating that the semi-fluidized bed process was successful; however, the breakthrough curve for 50 mg/L concentration is not

clear. These findings indicate that operating in a semi-fluidized bed with these dimensions is more reliable for low concentrations. As a result, the column's measurements must be enlarged to treat solutions with high concentrations.

3.4. Advantages and disadvantages of MB continuous adsorption

In this part, we will provide the necessary extracted information by comparing the results obtained of dynamic and batch systems; furthermore, each process's advantages and disadvantages are presented in table1.

Table 1: Advantages and disadvantages of dynamic and batch adsorption of MB on BZJS1.

Adsorption system	Advantages	Disadvantages
Dynamic adsorption systems (fixed and semi-fluidized beds)	<ul style="list-style-type: none"> ➤ Very close to systems used in real industries. ➤ Processability of a huge amount of colored water. ➤ Auspicious results for low concentrations. ➤ The adsorption process's rapidity ➤ Ease of system installation and transition from one process to another (especially for the semi-fluidized bed). ➤ High bed porosity (especially at the first moments of the experiment) ➤ The ability to examine the evolution of low concentrations over time. 	<ul style="list-style-type: none"> ➤ Beads regeneration difficulty due to its swelling. ➤ Stiffness and blockage of the fixed Bed. ➤ The bed porosity and MB flow were both decreased when beads swelled. ➤ When switching to a semi-fluidized bed, the effectiveness for high concentrations was decreased.
Batch system	<ul style="list-style-type: none"> ➤ Ease of system installation, beads regeneration and transition from one process to another. ➤ Efficiency for high concentrations 	<ul style="list-style-type: none"> ➤ Processability of a little amount of colored water. ➤ Systems just used in laboratory scale. ➤ Examining the evolution of low concentrations through time is difficult. ➤ remarkable consumption of BZJS1

By the end of this comparison, we may conclude that the dynamic process was far more effective than the batch system, especially at low concentrations. Moreover, some enhancements should be performed to find a way to profit from each system's benefits and link them together to achieve maximum efficiency and try to improve each system's disadvantages to avoid them.

5. Conclusion

This last chapter's objective was to develop a dynamic adsorption system in the form of a fixed bed, using the best adsorbent prepared throughout this thesis, and comparing its results to those obtained in the batch system. Because chapter 4 showed that BZJS1 was the best adsorbent, it was employed to perform fixed-bed adsorption studies, revealing the beads swelling problem that resulted in bed obstruction; as a result, the fluidized bed was proposed as a solution to avoid that problem.; the semi fluidized bed process, as shown, was successful with low concentrations; however, its dimensions must be expanded to treat high concentrations. Furthermore, dynamic adsorption tests showed numerous benefits compared to batch systems, including handling massive volumes of colored water, installing quickly, and ease of transition from one process to another, etc.

6. References

- [1] P.M. Morais da Silva, N.G. Camparotto, T. de Figueiredo Neves, K.T. Grego Lira, V.R. Mastelaro, C. Siqueira Franco Picone, P. Prediger, Effective removal of basic dye onto sustainable chitosan beads: Batch and fixed-bed column adsorption, beads stability and mechanism, *Sustain. Chem. Pharm.* 18 (2020) 100348. <https://doi.org/10.1016/j.scp.2020.100348>.
- [2] N.S. Topare, S.A. Bokil, Adsorption of textile industry effluent in a fixed bed column using activated carbon prepared from agro-waste materials, *Mater. Today Proc.* 43 (2021) 530–534. <https://doi.org/10.1016/j.matpr.2020.12.029>.
- [3] S. Biswas, S. Sharma, S. Mukherjee, B.C. Meikap, T.K. Sen, Process modelling and optimization of a novel Semifluidized bed adsorption column operation for aqueous phase divalent heavy metal ions removal, *J. Water Process Eng.* 37 (2020) 101406. <https://doi.org/10.1016/j.jwpe.2020.101406>.
- [4] S. Biswas, R.K. Diwakar, I.D. Behera, B.C. Meikap, T.K. Sen, M. khiadani, Aqueous phase phenol removal from synthetic and real steel plant effluents through a batch and Semifluidized bed column operation: Experimental and model analysis, *J. Environ. Chem. Eng.* 8 (2020) 104441. <https://doi.org/10.1016/j.jece.2020.104441>.

General conclusion and prospects

The main objective of this work was to synthesize innovative materials through simple and low-cost methods and highlight the potential of the obtained materials in the depollution of wastewater effluents. In order to assess this potential, several experiments (such as material characterization, parameters effects, kinetics and equilibrium experiments) were performed. Basically, six main materials have been prepared and used as adsorbents for cationic dye removal from wastewater. Namely, ZJS-H₃PO₄, OP-H₃PO₄, BZJS1, BZJS2, BOP1 and BOP2.

The study of the adsorption of MB onto the *Ziziphus jujuba* stones treated with ortho-phosphoric acid was the subject of the third chapter. The results obtained related to adsorption kinetics, adsorption isotherms, thermodynamics and ionic strength were analyzed to explain the adsorption mode of MB onto ZJS-H₃PO₄. The study of adsorption kinetics showed that the adsorption process followed the pseudo-second-order model. Intraparticle diffusion seemed to be a significant step in the adsorption process but was not the limiting step. Moreover, the nonlinear Langmuir model was the most convincing to describe experimental data. The study of the effect of ionic strength showed that NaCl had a positive impact on adsorption. Regarding statistical models, the monolayer model was selected to describe the experimental isotherms. Furthermore, 22% of MB molecules were adsorbed by a single active site and 78% were adsorbed with two free sites. The (5–8 kJ mol⁻¹) range corresponds to physical interactions, generally electrostatic and hydrogen bonds. Moreover, the adsorption energy behavior was the same as the adsorbed saturation quantity, which confirmed that the temperature of 30 °C can be regarded as the optimum adsorption temperature of MB onto ZJS-H₃PO₄.

In the fourth chapter, raw orange peels (ROP) were used as a precursor and then modified using phosphoric acid for the preparation of our adsorbent material (OP-H₃PO₄). The results obtained showed a high adsorption potential of OP-H₃PO₄, 307.63 mg/g at 25 °C. The modeling of the adsorption kinetics showed that the pseudo-second-order model was the most reliable to describe experimental data. Moreover, the equilibrium data indicated that both Sips and Langmuir models could represent the MB uptake onto OP-H₃PO₄. The results of the ionic strength effect showed that the competition between the MB dye and the Na⁺ ions led to a decrease in the amount adsorbed. The experimental results were well correlated with the calculated quantum chemical parameters. Also,

molecular dynamics simulations indicated that the MB molecule adsorbed on the OP-H₃PO₄ (110) surface in a nearby horizontal position.

In the following chapter, the fifth, ZJS-H₃PO₄ were used to be encapsulated; however, the encapsulation by sodium alginate was used as a proposed solution to avoid problems encountered with conventional materials in powder form, such as the difficulty of regeneration. The performances of the prepared materials (BZJS1 and BZJS2) were examined in a batch system by adsorption of a cationic dye, methylene blue (MB). The results obtained confirmed that the encapsulation was efficiently carried out since the adsorption potential of the prepared beads strongly increased from 160.85 mg/g for ZJS-H₃PO₄ to 768.102 and 680.098 mg/g for BZJS1 and BZJS2 respectively at 25 °C. Furthermore, the modeling of MB adsorption isotherms showed that whatever the temperature, the Redlich Peterson model led to the most accurate fitting of experimental data. Regarding the adsorption kinetics, the nonlinear models of pseudo-first-order (PFO), pseudo-second-order (PSO), and pseudo nth order (PNO) were considered, and the PFO model was found to be the most suitable model to describe the kinetic results. In addition, the intraparticle diffusion model showed that the MB adsorption was performed in three steps, and the Boyd model suggested that film diffusion is the limiting step that controlled the MB adsorption process onto both materials. Otherwise, the effects of ionic strength and organic compounds have shown that NaCl and humic acid had a negative impact on the adsorption of MB on both materials. The temperature effect and thermodynamic parameters showed that the adsorption of MB onto BZJS1 and BZJS1 was spontaneous and exothermic. The regeneration study concluded on the reusability of the beads since the MB removal yields were 92.01 and 82.88% for BZJS1 and BZJS2, even at the sixth cycle.

In the sixth chapter, the treated orange peels (OP-H₃PO₄) were used as a precursor to be encapsulated by sodium alginate. The modeling of the adsorption kinetics data showed that the PFO model was the most appropriate for describing the experimental results; additionally, the use of the Boyd and intraparticle models indicated the diffusion of films, rather than the diffusion of pores, was 765.82 the limiting step. The isotherms of MB adsorption on prepared beads were performed over a temperature range ranging from 10 to 30°C. The experimental findings showed that the prepared beads had excellent MB adsorption performances, with adsorbed quantities of and 677.30 mg/g for BOP1 and BOP2, respectively. Furthermore, the obtained curves were analyzed and interpreted using two classical models (Langmuir and Freundlich) and three physical models (MMSE,

General conclusion and prospects

MMTE, DMTE) based on the grand canonical partition function in statistical physics; the findings showed that the MMTE model was the most appropriate one. The regeneration study of BOP by acidic water revealed that BOP1 and BOP2 were reusable even after the seventh cycle. Furthermore, experimental findings indicated that NaCl inhibited MB adsorption due to competition with Na⁺, while humic acid had no effect on adsorption. The adsorption energy measurements showed that, on the one hand, the temperature had an impact on the nature of the MB adsorption process on BOP; on the other hand, MB adsorption can be achieved through electrostatic interactions, dipole bond forces, and hydrophobic interactions π - π . Furthermore, the parameters of the best statistical physics model (MMTE) showed that MB adsorption on BOP1 and BOP2 was a mixed monolayer whose process was carried out in various ways (perpendicular and horizontal orientations, on a single and two free sites at the same time), with a dominance of MB adsorption on a single free site under an inclined position to the adsorbent surface. The best model's parameters were used to conduct the calculations required to measure and plot the internal energy, Gibbs free enthalpy, and configuration entropy to perform a thermodynamic study of the MB adsorption mechanism on BOP1 and BOP2. Negative values of free enthalpy and internal energy mean that the process of MB adsorption on BOP was spontaneous and exothermic, whereas the entropy variance indicated that order and disorder were directly related to the availability of free active sites on the BOP surface.

The seventh chapter's objective was to develop a dynamic adsorption system in the form of a fixed bed, using the best adsorbent prepared throughout this thesis, and comparing its results to those obtained in the batch system. Because chapter five showed that BZJS1 was the best adsorbent, it was employed to perform fixed-bed adsorption studies, revealing the beads swelling problem that resulted in bed obstruction; as a result, the fluidized bed was proposed as a solution to avoid that problem.; the semi fluidized bed process, as shown, was successful with low concentrations; however, its dimensions must be expanded to treat high concentrations effluents. Furthermore, dynamic adsorption tests showed numerous benefits compared to batch systems, including handling massive volumes of colored water, installing quickly, and ease of transition from one process to another, etc.

Prospects for future applications

- Finding a faster strategy to generate adsorbents in large quantities.
- Testing the effectiveness of the prepared adsorbents using real contaminated water (from valleys and industries effluents).
- Thinking of practical solutions for the pollutants' fate after adsorption or regeneration steps.
- Evaluating the prepared adsorbents' performance in a competitive adsorption process (various pollutants in the same solution).
- Apply the fixed and semi-fluidized beds systems in a pilot model with enlarged dimensions.
- Combining the batch and dynamic systems to develop a multi-stage adsorption system (for example, the batch in the first stage and the dynamic in the second stage).
- Why not collaborate with other research teams and work on wastewater treatment at the scale of our university's laboratories?

List of scientific works

International publications

1. A. Guediri, A. Bouguettoucha, D. Chebli, N. Chafai, A. Amrane, Molecular dynamic simulation and DFT computational studies on the adsorption performances of methylene blue in aqueous solutions by orange peel-modified phosphoric acid, *J. Mol. Struct.* (2019) 127290. <https://doi.org/10.1016/j.molstruc.2019.127290>.
2. A. Guediri, A. Bouguettoucha, D. Chebli, A. Amrane, The use of encapsulation as a proposed solution to avoid problems encountered with conventional materials in powder form: Application in methylene blue removal from aqueous solutions, *J. Mol. Liq.* 316 (2020) 113841. <https://doi.org/10.1016/j.molliq.2020.113841>
3. A. Guediri, A. Bouguettoucha, D. Chebli, A. Amrane, Insights on the statistical physics modeling of the methylene blue adsorption onto *Ziziphus jujuba* stones-treated ortho-phosphoric acid, **submitted to Desalination and Water Treatment, under review.**
4. A. Guediri, A. Bouguettoucha, D. Chebli, Med-K. Guediri, A. Amrane, Statistical physics modeling and thermodynamic studies for methylene blue adsorption mechanism onto an eco-friendly composite adsorbent, **submitted to Solid states sciences, under review.**
5. S. Mahmoudi, Z. Chemat-Djenni, A. Bouguettoucha, D. Chebli, A. Guediri, A. Gil, Removal of lead ions from aqueous solutions by new layered double hydroxides absorbent MgCuCaAl-LDH, **submitted to Advanced Materials Research, under revision.**

International Communications

1. A. Guediri, A. Bouguettoucha, D. Chebli, Removal of methylene blue dye from aqueous solutions by adsorption using a ziziphus jujuba stones treated with H₃PO₄, International Conference on Materials science (ICMS2018), 12-14 September, Setif 1 University (Algeria).
2. A. Guediri, A. Bouguettoucha, D. Chebli, The use of the ziziphus jujuba stones encapsulated by sodium alginate as an adsorbent of cationic dye from aqueous medium, 2^{ème} workshop international en mécanique des structures et matériaux IWMSM 2018. 17-18 December, Batna 2 University (Algeria).

List of scientific works

3. A. Guediri, A. Bouguettoucha, D. Chebli, Agricultural waste-sodium alginate composite as an adsorbent of organic dye from aqueous solution: characterization, experimental results, and modeling, First International Workshop On Environmental Engineering (IWEE'19), 15-16 September 2019, Setif 1 University (Algeria).

National Communications

1. A. Guediri, A. Bouguettoucha, D. Chebli, Application of a new composite material as adsorbent for cationic dye removal from aqueous solution: characterization, experimental results and modeling, Conférence Nationale sur la Chimie des Matériaux (CNCM 2019), 2-3 July 2019, M'hamed bougara University Boumerdes (Algeria).

Abstract

In this thesis, we are interested in synthesizing innovative materials that can be used as efficient and cost-effective adsorbents. First, the *Ziziphus jujuba* stones and orange peels were used as precursors to be treated with phosphoric acid to prepare adsorbents in powder form. Then, the two materials obtained previously (ZJS-H₃PO₄ and OP-H₃PO₄) were encapsulated using sodium alginate to obtain materials in the form of beads (BZJS and BOP). All synthesized materials were carefully characterized by different methods such as XRD, FTIR, TGA, BET, SEM, and XRF. In addition, the application of the materials obtained as adsorbents in the batch system was studied by removing basic dye methylene blue (MB). Adsorption kinetics, equilibrium studies, and the influences of different factors such as initial pH, contact time, initial concentration, ionic strength, and temperature have been explored. As a result, high adsorption capacities were obtained, confirming the efficiency of the used encapsulation process. At the end of this research, the best adsorbent of the prepared adsorbents (BZJS1) was used to employ dynamic adsorption applications (fixed and semi fluidized bed), showing interesting results.

Keywords: *Ziziphus jujuba*, orange peels, H₃PO₄, encapsulation, adsorption, batch, fixed bed, semi fluidized bed, methylene blue.

Résumé

Dans cette thèse, nous nous intéressons à la synthèse des matériaux innovants qui pourraient être utilisés comme adsorbants efficaces et rentables. D'abord, les noyaux de la *Ziziphus jujuba* et les écorces d'orange ont été utilisés comme précurseurs pour être traités par l'acide phosphorique afin de préparer des adsorbants sous forme de poudre. Ensuite les deux matériaux obtenus précédemment (ZJS-H₃PO₄ et OP-H₃PO₄) ont été encapsulés en utilisant l'alginate de sodium pour obtenir des matériaux sous forme de billes (BZJS et BOP). Tous les matériaux synthétisés ont été soigneusement caractérisés par différentes méthodes telles que DRX, IRTF, ATG, BET, MEB et XRF. De plus, l'application des matériaux obtenus comme adsorbants en system batch a été étudiée par l'adsorption de colorant basique bleu de méthylène (BM). Les cinétiques d'adsorption, les études d'équilibre aussi que l'influence de différents facteurs tels que le pH initial, le temps de contact, la concentration initiale, la force ionique et la température ont été explorés. Des capacités d'adsorption élevées ont été obtenues, confirmant l'efficacité du processus d'encapsulation utilisée. À la fin de cette étude, le meilleur adsorbant des adsorbants préparés (BZJS1) a été utilisé pour employer des applications d'adsorption dynamique (lit fixe et semi fluidisé) montrant des résultats intéressants.

Mots clés : *Ziziphus jujuba*, écorces d'orange, H₃PO₄, encapsulation, adsorption, batch, lit fixe, lit semi fluidisé, bleu de méthylène.

ملخص

في هذا البحث ، اولينا اهتماما لتوليف مواد مبتكرة يمكن استخدامها كمادة ماصة فعالة وغير مكلفة. اولاً، تم استخدام نواة *Ziziphus jujuba* وقشور البرتقال كمادة اولية لتتم معالجتها بحمض الفوسفوريك لتحضير الممتزازات في شكل مسحوق. ثم تم تغليف المادتين اللتين تم الحصول عليهما مسبقاً (ZJS-H₃PO₄ و OP-H₃PO₄) باستخدام ألجينات الصوديوم للحصول على مواد على شكل حبيبات (BZJS و BOP). تم تحديد خصائص المواد المنتجة بطرق مختلفة مثل DRX و FTIR و TGA و BET و SEM و XRF. بالإضافة إلى ذلك، تمت دراسة استخدام المواد التي تم الحصول عليها كمادة ماصة في نظام الباتش من خلال امتزاز صبغة الميثيلين الأزرق. تم دراسة حركيات الامتزاز والتوازن وتأثيرات العوامل المختلفة مثل الأس الهيدروجيني ووقت الاتصال والتركيز الأولي والقوة الأيونية ودرجة الحرارة. حيث تم الحصول على قدرات امتصاص عالية للغاية ، مما يؤكد فعالية عملية التغليف المستخدمة. في نهاية هذا البحث تم استخدام أفضل مادة ماصة من المواد الماصة المحضرة (BZJS1) لاستعمالها في تطبيقات الامتزاز الديناميكي (السرير الثابت وشبه المميع) والذي اظهر نتائج مثيرة للاهتمام.

الكلمات المفتاحية: العناب، قشر البرتقال ، H₃PO₄ ، التغليف ، الامتزاز ، باتش، سرير ثابت، سرير شبه ممييع، أزرق الميثيلين.